University of Massachusetts Medical School

eScholarship@UMMS

2019-05-13

A CNS-Active siRNA Chemical Scaffold for the Treatment of Neurodegenerative Diseases

Julia F. Alterman
University of Massachusetts Medical School

Let us know how access to this document benefits you.

A CNS-ACTIVE SIRNA CHEMICAL SCAFFOLD FOR THE

TREATMENT OF NEURODEGENERATIVE DISEASES

A Dissertation Presented

By

JULIA FRANCES ALTERMAN

Submitted To The Faculty Of The University Of Massachusetts

Graduate School Of Biomedical Sciences, Worcester,

In Partial Fulfillment Of The Requirements For The Degree Of

DOCTOR OF PHILOSOPHY

May 13, 2019

Interdisciplinary Graduate Program

A CNS-ACTIVE SIRNA CHEMICAL SCAFFOLD FOR THE

TREATMENT OF NEURODEGENERATIVE DISEASES

A Dissertation Presented

By

JULIA FRANCES ALTERMAN

This work was undertaken in the Graduate School of Biomedical Sciences

Interdisciplinary Graduate Program

Under the mentorship of

Anastasia Khvorova, Ph.D., Thesis Advisor

Miguel Sena-Esteves, Ph.D., Member of the Committee

Jonathan Watts, Ph.D., Member of the Committee

Michael Czech, Ph.D., Member of the Committee

Frank Slack, Ph.D., External Member of the Committee

Victor Ambros, Ph.D., Chair of the Committee

Mary Ellen Lane, Ph.D.,

Dean of the Graduate School of Biomedical Sciences

May13, 2019

DEDICATION

I dedicate this dissertation to my families: both nuclear

…and cytoplasmic

ACKNOWLEDGEMENTS

Science is not done in a vacuum. In fact, I believe that the best science is done collaboratively, in an environment where researchers of all different disciplines and backgrounds share ideas and formulate (or preferably conjugate…) solutions to problems as a team, drawing on the expertise of each individual.

Team Khvorova was not only the best research team I have ever worked with, but they have been my family as well. I first joined the lab as a research associate, unsure if the PhD path was the right one for me. But from the very beginning Anastasia had an enormous amount of confidence in me and quickly became my biggest fan and the greatest mentor I have ever had. From there my family only grew… Matthew Hassler, Marie Didiot, Mehran Nikan and Jasmine Abraham took be under their wings and began teaching me the ropes of oligonucleotide chemistry, cell biology, and neuroscience.

After that, we gained Soki Ly, Reka Haraszti, Andrew Coles, Anton Turanov, Maire Osborn, Loic Roux, Annabelle Biscans, Dimas Echeverria, and Bruno Godinho. We weren't just colleagues we were great friends. With heart to heart conversations, lunchtime chats, late nights with beers in the lab, paintball, lake parties, and skiing trips we were like a nerdy gang. It was during this time that my scientific knowledge also began to bloom. With many different brilliant minds and many varied expertise, I felt so lucky to be in this lab. In particular I need to acknowledge Matt and Bruno, my partners in crime in developing the Di-siRNA chemical scaffold, and Bruno and Marie, for letting me be part of their growing families. And to Annabelle, who edited this dissertation.

Then we gained Ken Yamada, Yann Thillier, and the group I like to call "the kids": Chantal Ferguson, Sarah Davis, James Gilbert, Emily Knox, Sam Hildebrand, Jacquelyn Sousa and Lorenc Vangjeli. While newer students to the lab, it quickly became clear that they were always meant to be a part of our family. They were not only thoughtful and intelligent but also funny, kind, and willing to do anything for their fellow lab mates.

And where would any of us be without Mary Beth Dziewietin.... Like a second mother to us she has not only helped with everything administrative but has generally ensured that we make it through our time here in one piece. Life in the lab would have been much more difficult and far less pleasant without her.

As our lab family grew so did our extended lab family…enter, the Khvorova lab babies; Jules, Leonor, Emma, Louise, and of course the lab dogs; have brought so much joy to all of our lives. These additions to our extended family just made all of us feel more full of love.

But my family is not limited to the Khvorova lab. So many labs at UMass supported me during my graduate studies including the Aronin Lab, the Watts lab, the Esteves lab, the Muller lab, and many more. UMass is truly a family in and of itself.

I would also like to acknowledge my classmates. When we all first started we were in the same boat. We quickly banned together and ensured that we would carry each other, not only through core, but through our entire degrees. To this day my classmates still support me and look out for me.

Last but not least, my family, Mom, Dad, Emma, and all my extended family and "feels like family" friends. They have supported me through thick and thin, in good times and bad, and I cannot thank them enough for all they have given me.

Life is a journey, and it is always nice to travel with friends.

ABSTRACT

Small interfering RNAs (siRNAs) are a promising class of drugs for treating genetically-defined diseases. Therapeutic siRNAs enable specific modulation of gene expression, but require chemical architecture that facilitates efficient *in vivo* delivery. siRNAs are informational drugs, therefore specificity for a target gene is defined by nucleotide sequence. Thus, developing a chemical scaffold that efficiently delivers siRNA to a particular tissue provides an opportunity to target any disease-associated gene in that tissue. The goal of this project was to develop a chemical scaffold that supports efficient siRNA delivery to the brain for the treatment of neurodegenerative diseases, specifically Huntington's disease (HD).

HD is an autosomal dominant neurodegenerative disorder that affects 3 out of every 100,000 people worldwide. This disorder is caused by an expansion of CAG repeats in the huntingtin gene that results in significant atrophy in the striatum and cortex of the brain. Silencing of the huntingtin gene is considered a viable treatment option for HD. This project: 1) identified a hyper-functional sequence for siRNA targeting the huntingtin gene, 2) developed a fully chemically modified architecture for the siRNA sequence, and 3) identified a new structure for siRNA central nervous system (CNS) delivery—Divalent-siRNA (Di-siRNA). Di-siRNAs, which are composed of two fully chemically-stabilized, phosphorothioate-containing siRNAs connected by a linker, support potent and sustained gene modulation in the CNS of mice and non-human primates. In mice, Di-siRNAs induced potent silencing of huntingtin mRNA and protein throughout the brain one month after a single intracerebroventricular injection. Silencing persisted for at least six months, with the degree of gene silencing correlating to guide

strand tissue accumulation levels. In Cynomolgus macaques, a bolus injection exhibited

significant distribution and robust silencing throughout the brain and spinal cord without

detectable toxicity. This new siRNA scaffold opens the CNS for RNAi-based gene

modulation, creating a path towards developing treatments for genetically-defined

neurological disorders.

TABLE OF CONTENTS

LIST OF TABLES

LIST OF FIGURES

CHAPTER I: INTRODUCTION

1.1 OLIGONUCLEOTIDES: INFORMATIONAL DRUGS

Informational drugs such as oligonucleotides are a new class of therapeutics that depend on sequence complementarity for target specificity[1]. They allow for the separation of "dianophore" from "pharmacophore" (Fig. 1.1). The pharmacophore of an informational drug is its sequence, which is responsible for targeting a specific disease-related gene, while the dianophore is the chemical scaffold that impacts distribution, retention, efficacy, potency, clearance, stability, and immunogenicity of the drug. Their advantages over conventional small molecule drugs include: (i) ease of design—rationally achieved based on sequence information and straightforward screening, leading to drug candidates within a short period of time; (ii) ability to target disease-related genes previously considered "undruggable"; and (iii) unprecedented potency and duration of effect. This dissertation focuses on the development of a new siRNA dianophore for siRNA delivery to the brain.
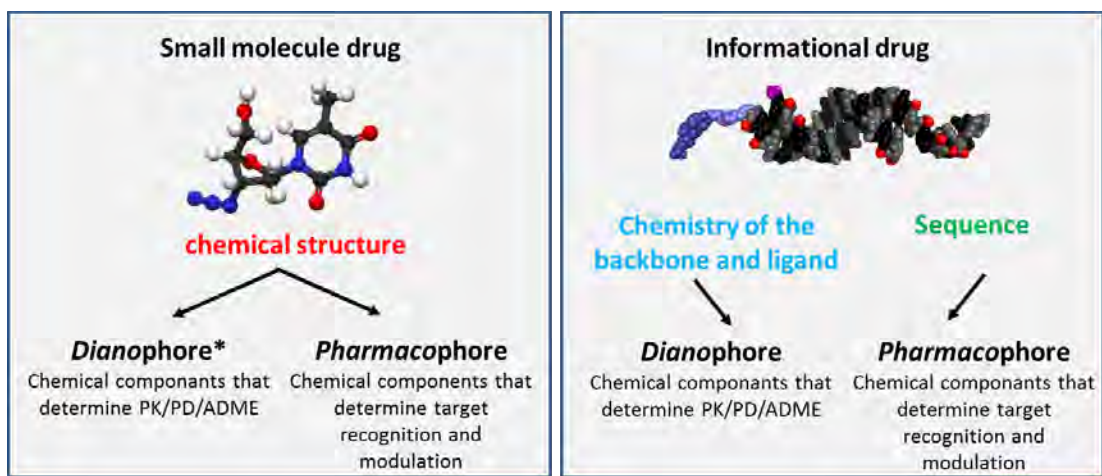
Figure 1.1 A comparison of traditional small molecules to informational drugs (This image is adapted from Nat. Biotech. 2017 and used with permission). The target specificity and pharmacokinetic, pharmacodynamics of small molecules are all encoded within the molecule's structure. Informational drugs allow for the separation of these two characteristics increasing their versatility and applicability to new diseases.

1.2 CLASSES OF OLIGONUCLEOTIDE THERAPEUTICS

There are many categories of oligonucleotide therapeutics. Each works through a different mechanism[2] and can target different nucleic acid families[3] or proteins[4], but all rely on a particular sequence to specifically influence their intended target. The two main classes of therapeutic oligonucleotides that have shown success in the clinic are antisense oligonucleotides (ASOs) and small interfering RNAs (siRNAs).

ASOs can be used to target mRNA for degradation[5], and for splice switching[6]. For the former, these molecules are typically designed as "GapmeRs", wherein a DNA gap is flanked by modified RNA nucleotides. The ASO mediated cleavage involves recognition by the protein RNAse H of a DNA/RNA hybrid formed by the binding of the GapmeR and the target mRNA[7]. The flanking regions serve to enhance binding affinity and stability when modified. For splice switching ASOs, there is no requirement for a

particular type of base chemistry[1, 8]. These oligonucleotides need only to bind tightly to the target mRNA, remain stable, and to influence splicing.

siRNAs are a newer RNA-based informational therapeutic, described by Fire and Mello in *C. elegans* in 2006[9] and subsequently shown to work in human cells[10, 11]. They are double stranded RNAs that can be recognized by the protein AGO2 in cells (Fig. 1.2)[12]. After recognition, the dissociation of the siRNA strands occurs; the passenger stand is discarded and the guide strand is retained in the RNA induced silencing complex, or RISC (Fig. 1.2)[13]. The selection of the guide strand by the RISC can be determined by the thermodynamic stability of its 5'end, with a decrease in thermodynamic stability being favored[14]. Loading of the guide strand can be encouraged by increasing AU content or by using destabilizing modifications at the 5' end. Once the passenger strand is discarded and degraded, the remaining RISC/guide strand complex is able to recognize the target mRNA complementary to the guide strand in order to cleave it with great efficiency[13]. The catalytic site, PIWI domain, in the AGO2 protein, carries out cleavage[15, 16]. Following degradation, the mRNA will no longer make its encoded protein. What makes this mechanism remarkable for therapeutic use is the long lasting and recyclable nature of RISC, which means that after cleaving one mRNA it can go on to cleave many more.
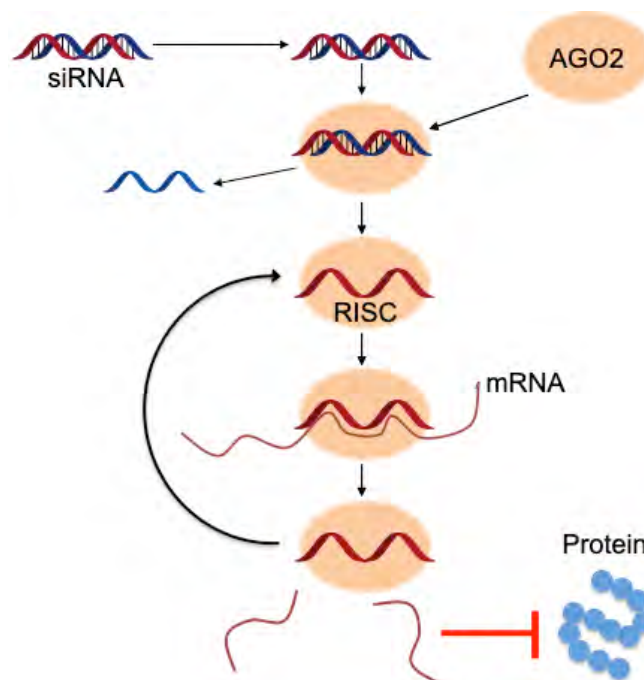
Figure 1.2 Mechanism of siRNA mediated mRNA cleavage, RNA interference (RNAi)

1.3 CHEMICAL MODIFICATION OF SIRNA

Natural RNA has limitations in its use as a therapeutic. It is hydrophilic and cannot cross the cell membrane, readily degradable by exonucleases and endonucleases[17, 18], and may elicit an immune response when delivered to the cell[19]. Over the past few decades, the scientific community has been working to overcome these obstacles by introducing chemical modifications to sugars and backbones of these molecules, as well as changing structure and adding conjugates[1]. These various modifications have led to a surge in clinically viable oligonucleotide therapeutics.

5'-Phosphate modifications	Backbone modifications	2'-Ribose modifications	
E-vinyl phosphonate	*Phosphorothioate*	*2'-Fluoro*	*2'-O-Methyl*
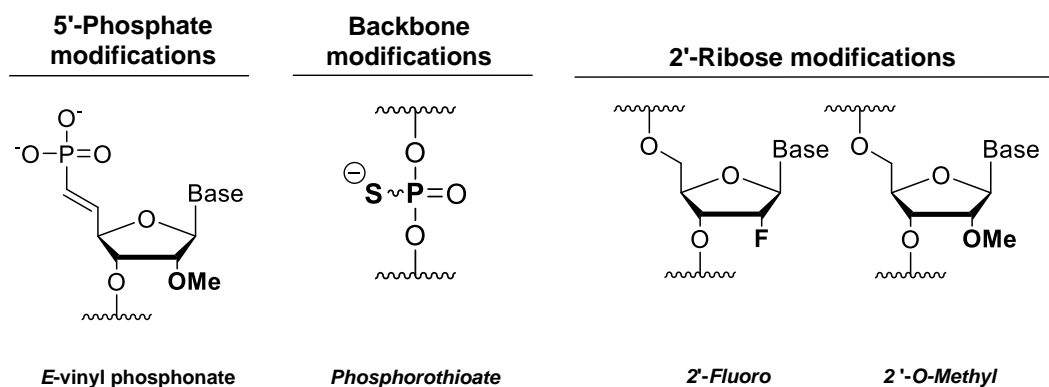
Figure 1.3 The primary modifications used for an siRNA chemical scaffold.

Starting with the sugars, 2'-*O*-Methyl (2'OMe) and 2'-Fluoro (2'F) are the most commonly used modifications for siRNA[20] (Fig. 1.3). Both are "RNA-like" with a C3'endo conformation[21, 22], and will maintain an A-form helix that is essential for them to be recognized by AGO2[23]. In addition to stabilizing the molecule against base cleavage, 2'-OMe incorporation has also been shown to prevent recognition by the immune system[24, 25].

Modifications to the phosphodiester backbone also provide exo- and endonuclease resistance. These include phosphorothioates[26], phosphorodithioates[27], and boranophosphates[28]. Phosphorothioate (PS) is the most commonly used of these modifications; it replaces one of the non-bridging oxygen atoms in the phosphodiester with a sulfur atom (Fig. 1.3), which significantly protects against nuclease attack[29]. In addition to providing stability, PS shows a high binding affinity to proteins, which allows them to associate not only with blood proteins but also with cellular membranes[30]. In fact, ASOs rely primarily on PS content for delivery and retention in tissues and all of the ASOs in the clinic contain PS linkages[5, 26, 31-34].

20

Lastly the crystal structure of RISC indicates that a phosphate at the 5'end (5'P) (Fig. 1.3) of the siRNA guide strand is essential for AGO2 recognition and thus efficiency of siRNA[23]. Therefore stabilizing the 5' phosphate can be beneficial. 5' vinyl phosphonate (5'VP) (Fig. 1.3) has been investigated to mimic the 5' terminal phosphate modification. This analog stabilizes the 5' phosphate and has been shown to enhance stability and efficacy of siRNAs in vivo[35, 36].

While these modifications abrogate many issues of instability, incorporation of the modifications can significantly affect compound efficacy and can be highly sequence specific[20]. A modified siRNA must be recognized by AGO2, must be able to disassociate from the sense strand, and must be able to recognize their target mRNA and coordinate cleavage.

For example, 2'-OMe is slightly bulkier than the natural 2'OH and is not tolerated at particular positions[20, 37]. 2'-Fluoro promotes very tight base-pairing and can lead to an enhancement of off target effects[38]. Finally, extensive PS content can lead toxicity in the form of platelet activation and potential thrombocytopenia[39, 40]. Therefore, while modifications are essential, great care must be taken to investigate tolerated chemical modification patterns.

1.4 SIRNA *IN VIVO* DELIVERY

Despite advances in sugar and backbone modifications, one main challenge that remains is how to deliver these compounds to a specific cell type or tissue of interest. Delivery of these compounds can be achieved either with formulation, including lipid nanoparticles[41], dendrimers[42], spherical nucleic acids and gold nano particles[43-46], or by

chemical conjugation. The only approved siRNA currently in the clinic, patisiran

(ONPATTRO[TM]), is partially modified and formulated within a lipid nanoparticle[41].

In the case of conjugate mediated delivery, which will be the primary focus of this

section, the N-acetylgalactosamine (GalNAc) conjugate has revolutionized the field for

liver delivery. This trivalent conjugate binds with high specificity and affinity to the

asialoglycoprotein receptor on hepatocytes[47]. This receptor is present at high

concentrations and is quickly recycled into the cell and back to the cell surface making it

an ideal target for ligand mediated siRNA delivery[48]. Indeed, there are many compounds

in the clinic today that utilize this conjugate for liver delivery[49].

While there have been many attempts to identify a ligand for targeting other

organs or cell types, finding a ligand receptor pair that has the right properties is very

difficult. Not only does the receptor have to be present in relatively high concentrations,

it also needs to recycle quickly to ensure efficient delivery of hundreds of siRNAs into

the cell. Additionally, ensuring that the ligand retains functional binding while

conjugated to a siRNA can also be very difficult. Other conjugation strategies have

included antibody conjugation (Avidity Biosciences)[50, 51] and aptamer conjugation[52-54]

but both require the development of a high affinity binding moiety and selection of

regularly recycled target receptor.

Hydrophobic conjugation is not receptor specific but takes advantage of the fact

that cells have a hydrophobic membrane, which allows these compounds to interact or

intercalate. Examples of these conjugates include polyunsaturated fatty acids[55, 56],

cholesterol[57-60], vitamins[61, 62], etc. Since they are not organ or cell type specific, they can

be used to target different organs than the liver such as the kidney, spleen, heart, muscle,

fat, adrenal glands lungs, and brain[56, 63, 64]. However, while these types of conjugates are much more versatile, their high hydrophobicity leads to a very steep gradient of diffusion away from the site of injection[58]. For organs such as the brain this means significant retention at the site of injection with little or no distribution to more distal regions of the brain and spinal cord. While this could be useful for the treatment of various glioblastomas or neuroblastomas[65] it may lead to toxicity at the site of injection, and diseases that affect the entire organ would require multiple brain injections for treatment.

1.5 ASOs in the CNS

The most advanced oligonucleotide therapeutics for delivery to the brain and spinal cord are ASOs[66, 67]. These oligonucleotides rely on phosphorothioate content to promote protein association and cellular internalization. Nusinersen (SPINRAZA®) was the first approved oligonucleotide therapeutic delivered to the central nervous system[66, 68]. This splice switching oligonucleotide has a pharmacophore targeting the SMN2 gene for the treatment of spinal muscular atrophy and a dianophore of complete PS and 2'Methoxyethyl sugar modifications[68]. Currently the dosing scheme for Nusinersen requires four loading doses followed by an additional dose every 4 months for maintenance[66]. Since Nusinersen there have been many new ASOs in the clinic including those that rely on the RNAse H mechanism for mRNA cleavage, such as C9ORF72 (Clinical Trial ID: NCT03626012) or SOD1 (Clinical Trial ID: NCT02623699) targeting for amyotrophic lateral sclerosis, TAU targeting for Alzheimer's disease (Clinical Trial ID: NCT03186989), and HTT targeting for Huntington's disease (Clinical Trial ID: NCT03342053). The most advanced ASOs in the clinic show distribution to various areas of the brain but have trouble penetrating to deeper regions of the brain including the

caudate, putamen, and hippocampus[5]. Therefore there is space in this field to improve

the versatility of informational drug delivery.

1.6 sɪRNAs ɪN ᴛʜᴇ CNS

After discovering the power of GalNAc conjugation, most siRNA efforts were

focused on liver indications leaving other organ indications to alternative oligonucleotide

groups. There are some companies that have focused efforts on local administration

(eye[59], skin[69], muscle[60]), but there is no question that liver delivery predominates the

field. The academic community continued to explore the potential for siRNA

therapeutics in the brain (Table 1.1). Attempts at natural siRNA injection are limited but

show some activity 24 hours after a single intracerebroventricular (ICV) injection with

50% silencing[70]. Due to the instability of these compounds it is not surprising that longer

term studies were not carried out. One strategy to improve distribution and silencing in

the brain is by infusing the natural siRNA over a longer period of time[71]. While infusion

did increase the overall spread of the compound, silencing was still short lived. A similar

attempt was made with repeated intranasal delivery but also yielded minimal silencing

and spread[72]. In an attempt to achieve better silencing, the DiFiglia Lab and the Sah Lab

injected partially modified siRNA conjugated to cholesterol into the brain (also

investigated in Chapter III)[57, 58, 73]. In these cases, the partial modification (PS and

2'OMe) did increase duration of effect up to one week but including hydrophobic

conjugation limited the spread to around the site of injection and did not result in major

improvements in gene silencing. At this point the field began to realize that siRNAs

require full chemical stabilization for meaningful and long-lasting siRNA *in vivo*

silencing (discussed in Chapter IV). Once full chemical stabilization was employed,

conjugate mediated delivery began to offer a much longer-term duration of effect and superior silencing[55, 56].

In the last few years there has been a boom in siRNAs being pushed towards the clinic for neuro indications, with both Dicerna Pharmaceuticals (dicerna.com), Arrowhead Pharmaceuticals (arrowhead.com) Alnylam Pharmaceuticals (alnylam.com) initiating neurodegeneration projects. In fact, recently, Alnylam Pharmaceuticals has released a side-by-side study that shows superior target silencing with their new siRNA chemical scaffold relative to ASOs[74]. However while silencing in outer brain regions persists for months in both rat and non-human primate, penetration and silencing in deeper brain regions still remains elusive.

Table 1.1 Unformulated siRNA delivery to the brain.

Disease Indication/cell type	Target	Route of administration	Chemical Modifications	Reference
Focal ischemia	MMP-9	Intracerebroventricular injection	Naked siRNA	70
Depression	SERT	Intracerebroventricular infusion	dTdT	71
Huntington's disease	HTT	Intrastriatal injection	Chol-conjugated, terminal PS	57
Oligodendrocytes	CNPase	Intraparenchymal pump	Partially 2'OMe, dT, PS	75
Oligodendrocytes	CNPase	Intraparenchymal pump	Partially 2'OMe, dT, PS, Chol	73
Depression	SERT	Intranasal infusion	Sertraline-conjugated, unmodified	72
Glioblastoma	Luciferase	Intratumoral injection	Fully modified, Chol	65
Huntington's disease	HTT	Intrastriatal injection	Fully modified, DHA	55
Huntington's disease	HTT	Intrastriatal injection	Fully modified, PC-DHA	56

MMP-9 – metallopeptidase 9, SERT – Serotonin transporter, HTT – huntingtin, CNPase – 2',3'-Cyclic-nucleotide 3'-phosphodiesterase, dT – deoxy thymine, 2'OMe – 2'*O*-methyl, PS – phosphorothioate, Chol – cholesterol conjugated, DHA – Docosahexaenoic acid conjugated, PC-DHA – phosphatidylcholine Docosahexaenoic acid conjugated

1.7 ROUTES OF ADMINISTRATION FOR CNS TARGETING

OLIGONUCLEOTIDES

When targeting the central nervous system (CNS) there are a number of additional

considerations that must be made. While simple intravenous (IV) or subcutaneous (SC)

injection into the blood stream can potentially support targeting of many other extrahepatic organs given the right conjugation strategy, targeting the brain with these routes of administration would require crossing of what is referred to as the Blood Brain Barrier (BBB)[76]. The blood brain barrier is very selective and serves to prevent potentially harmful substances in the blood from entering into the CNS. While the BBB serves a very important role, it makes delivering therapeutics to the CNS much more difficult. There have been multiple attempts to deliver oligonucleotides systemically to cross the BBB. One strategy is to use an entity that will be recognized and trafficked by the BBB. Examples include the use of rabies virus glycoprotein (RVG) and transferrin[77, 78]. Another strategy is to disrupt the BBB temporarily (e.g. by using mannitol) to allow for transport of oligonucleotide across the barrier[79]. Unfortunately repetitive disruption of the BBB could open the brain to other unwanted intruders. While some papers have shown success with these methods, direct brain injection or infusion into the CSF is currently the favored route of administration. These methods can include intraparenchymal injection[55-57], intracerebroventricular injection (ICV)[5, 80], intrathecal injection (IT) (Clinical Trial ID: NCT03342053), and intranasal delivery[72]. In the clinic the preferred route of administration is an IT injection as it is the least invasive. However there have been no side-by-side comparisons of different routes of administration of oligonucleotides to the CNS so it is unclear if an alternative route could provide enhanced distribution. Obviously, multiple brain injections are not a viable option but there is an alternative way to target a specific parenchymal region or a ventricle, by use of an Ommaya reservoir. An Ommaya reservoir is a small reservoir attached to a catheter that can be placed under the skin of the skull and a catheter can be driven down into the

lateral ventricle[81, 82]. Once healed the compound can simply be injected directly into reservoir, which could be far simpler than regular lumbar punctures, and would be less painful. This procedure has been used for cancer and pain patients and could be an alternative to regular intrathecal injections.

1.8 AN SIRNA DIANOPHORE FOR THE BRAIN

In this dissertation I describe the development of a new chemical scaffold for siRNA delivery to the brain. The first step in this project was to identify a functional sequence to a valid neurological target. Huntington's disease (HD) is an autosomal dominant neurodegenerative disorder that is caused by a CAG-repeat expansion in exon 1 of the huntingtin gene[83]. Due to the monogenicity of HD, targeting the huntingtin gene is an ideal model for testing out new CNS targeting siRNAs. This dissertation (i) identifies a functional siRNA sequence, or pharmacophore for targeting huntingtin mRNA (Chapter III), (ii) identifies a full chemical modification pattern that increases stability of the siRNA while maintaining efficacy and potency (Chapter IV), and (iii) identifies a new conjugation strategy creating a novel dianophore for siRNA delivery to the brain that results in potent and long-lasting silencing in both mice and non-human primates (Chapter V).

CHAPTER II: METHODS

2.1 HTT COMPOUND SCREEN DESIGN

We designed and synthesized a panel of 94 hsiRNA compounds (Table 3.1) targeting the human huntingtin gene. These sequences span the gene and were selected to comply with standard siRNA design parameters including assessment of GC content, specificity and low seed compliment frequency[84] elimination of sequences containing miRNA seeds, and examination of thermodynamic bias[14, 85].

2.2 OLIGONUCLEOTIDE SYNTHESIS

Oligonucleotides were synthesized using standard phosphoramidite, solid-phase synthesis conditions using a MerMade 12 (BioAutomation, Irving, Texas), Expedite DNA/RNA synthesizer, or AKTA Oligopilot 100 (GE Healthcare Life Sciences, Pittsburgh, PA). Oligonucleotides with unmodified 3′ ends were synthesized on controlled pore glass (CPG) functionalized with long-chain alkyl amine and a Unylinker® terminus (Chemgenes, Wilmington, MA). Oligonucleotides with 3' modifications were synthesized on modified solid support synthesized in house. Phosphoramidites (ChemGenes, Wilmington, MA) were prepared at 0.1M (MerMade 12) and 0.2M (AKTA) in ACN with added 15% DMF in the 2`-OMe U amidite. 5-(Benzylthio)-1H-tetrazole was used as the activator at 0.25M. Detritylations were performed using 3% trichloroacetic acid (TCA) in dichloromethane on the MerMade 12 and 3% DCA in toluene (AIC Wilmington, MA) on the AKTA Oligopilot. Capping was done with non-THF containing reagents CAP A: 20% NMI in CAN and CAP B: 20% Ac2 O, 30% 2,6-lutidine in CAN (AIC Wilmington, MA). Sulfurization was performed

with 0.1 M solution of DDTT in Pyridine (ChemGenes, Wilmington, MA) for 3 minutes. Phosphoramidite coupling times were 8 minutes for all amidites used.

2.3 DEPROTECTION

The CPG was removed from the solid phase column and air dried. 40% methylamine (16 minutes at 65°C) was used to deprotect small scale 1 umol synthesis. Large scale, 10-300 umol, was deprotected using AMA (3 hours at RT). The solution was then frozen and lyophilized to dryness. Oligonucleotides with 2′–TBDMS protecting groups were desilylated by desolving the crude oligonucleotide in DMSO followed by triethylamine trihydrofluoride and incubated for 60 min at 65°C. The triethylamine trihydrofluoride was quenched with 3M sodium acetate and precipitated with 1-butanol. The vinylphosphonate (VP) containing oligo, while still on solid support, was treated with a mixture of trimethylsilyl bromide/DMF/pyridine (1:9:0.5) for 1 hour at room temperature with gentle agitation. The CPG is then rinsed with DMF followed by of water, ACN and allowed to dry. Before being deprotected as described above.

2.4 PURIFICATION

The purification of antisense strands was performed on an Agilent 1100 series system, equipped with an Agilent PL-SAX, polymer ion exchange column, or sourceQ anion exchange resin (GE healthcare, Chicago, IL) using the following conditions, Eluent A: 20% ACN 20mM NaAc pH 8, Eluent B: 1M sodium perchlorate in 20% ACN, gradient: 0% B 2min, 35% B 12min, clean and re-equilibration to initial conditions, temperature 50°C. Purification of sense strands was performed with a PRP-C18 (Hamilton, Reno, NV), a polymer reverse phase column, using the following conditions,

Eluent A: 50 mM sodium acetate in 5% ACN, and eluent B: ACN. Gradient: 0% B 2min, 0-40% B 1min, 40-70% B 8min, clean and re-equilibration 6min. Temperature 70°C. Peaks were monitored at 280nm. The pure oligonucleotides fractions were collected, individually characterized by LCMS, combined, frozen and dried in a speedvac overnight. Oligonucleotides were re-suspended in 5% ACN, and desalted through fine Sephadex® G-25 columns (GE healthcare, Chicago, IL), and lyophilized. All reagents mentioned above were purchased form Sigma Aldrich and used as is, unless otherwise stated.

2.5 LC-MS ANALYSIS OF OLIGONUCLEOTIDES

The identity of oligonucleotides were established by LC-MS analysis on an Agilent 6530 accurate mass Q-TOF LC/MS machine using the following conditions, Buffer A: 100mM HFIP/9mM TEA in LC/MS grade water, Buffer B: 100mM HFIP/9mM TEA in LC/MS grade methanol, column: Agilent AdvanceBio oligonucleotides C18, gradient antisense: 0% B 1min, 0-30% B 8min, clean and re-equilibration 4min, gradient sense: 0% B 1min, 0-50% B 0.5min, 50-100% B 8min, clean and re-equilibration 4min, temperature: 45°C, flow rate: 0.5mL/min, UV (260nm). MS parameters, Source: ESI, ion polarity: negative mode, range: 100-3200 m/z, scan rate: 2 spectra/s, VCap: 4000, fragmentor: 180V. All reagents mentioned above were purchased form Sigma Aldrich and used as is, unless otherwise stated.

2.6 CELL CULTURE

HeLa cells (ATCC, Manassas, VA; #CCL-2) were maintained in DMEM (Cellgro, Corning, NY; #10-013CV) supplemented with 10% fetal bovine serum (Gibco,

Carlsbad, CA; #26140) and 100 U/mL penicillin/streptomycin (Invitrogen, Carlsbad, CA; #15140) and grown at 37°C and 5% CO2. Cells were split every 2 to 5 days, and discarded after fifteen passages.

Primary cytotrophoblast cells (CTB) from human placenta were a gift from Dr. S Ananth Karumanchi. CTBs were maintained in Medium 119 (Gibco, #11043) supplemented with 10% FBS (Gibco, #26140) and 100 U/mL penicillin/streptomycin (Invitrogen, #15140) at 37°C and 5% CO_2.

Human primary hepatocytes (Gibco, #HMCPUS) were thawed and plated in Cryopreserved Hepatocytes Recovery Medium (Gibco, #CM7000), consisting of Williams E Medium (Gibco, #A12176-01) supplemented with 5% fetal bovine serum, 1 μM dexamethasone in DMSO, 100 U/ml penicillin and streptomycin, 4 μg/ml human recombinant insulin, 2 mM GlutaMAX™, and 15 mM HEPES pH 7.4. Plated hepatocytes were allowed to recover for 6 h at 37°C and 5% CO2 and subsequently maintained in Williams E Medium supplemented with the Hepatocyte Maintenance Supplement Pack (Gibco, #CM4000), containing 0.1 μM dexamethasone in DMSO, 50U/ml penicillin and streptomycin, 6.25 μg/ml human recombinant insulin, 6.25 μg/ml human transferrin, 6.25 μg/ml selenous acid, 6.25 μg/ml bovine serum albumin, 6.25 μg/ml linoleic acid, 2 mM GlutaMAX™,15 mM HEPES pH 7.4, and 5 mM CaCl2 .

2.6 ANIMAL STUDIES

All experimental studies involving animals were approved by the University of Massachusetts Medical School Institutional Animal Care and Use Committee (IACUC Protocol #A-2411 and #A-2515) and performed according to the guidelines and regulations therein described.

2.7 PREPARATION OF PRIMARY NEURONS

Primary cortical neurons were obtained from FVB/NJ mouse embryos at embryonic day 15.5. Pregnant FVB/NJ females were anesthetized by intraperitoneal injection of 250 mg Avertin (Sigma, St Louis, MO; #T48402) per kg weight, followed by cervical dislocation. Embryos were removed and transferred into a Petri dish with ice-cold DMEM/F12 medium (Invitrogen, Carlsbad, CA; #11320). Brains were removed, and meninges carefully detached. Cortices were isolated and transferred into a 1.5-ml tube with pre-warmed papain solution for 25 minutes at 37°C, 5% CO_2, to dissolve tissue. Papain solution was prepared by suspending DNase I (Worthington, Lakewood, NJ; #54M15168) in 0.5 ml Hibernate E medium (Brainbits, Springfield, IL; #HE), and transferring 0.25 ml DNase I solution to papain (Worthington, Lakewood, NJ; #54N15251) dissolved in 2 ml Hibernate E medium and 1 ml Earle's balanced salt solution (Worthington, Lakewood, NJ; #LK003188). After the 25 minute incubation, papain solution was replaced with 1 mL NbActiv4 medium (Brainbits, Springfield, IL; #Nb4-500) supplemented with 2.5% FBS. Cortices were dissociated by repeated pipetting with a fire-polished, glass, Pasteur pipet. Cortical neurons were counted and plated at 1×10^6 cells per ml.

For live-cell imaging, culture plates were pre-coated with poly-L-lysine (Sigma, St Louis, MO; #P4707), and 2×10^5 cells were added to the glass center of each dish. For silencing assays, neurons were plated on 96-well plates pre-coated with poly-L-lysine (BD BIOCOAT, Corning, NY; #356515) at 1×10^5 cells per well. After overnight incubation at 37°C, 5% CO_2, an equal volume of NbActiv4 supplemented with anti-mitotics, 0.484 μL/mL of UTP Na3 (Sigma, St Louis, MO; #U6625) and 0.2402 μL/mL

of FdUMP (Sigma, St Louis, MO; #F3503), was added to neuronal cultures to prevent growth of non-neuronal cells. Half of the media volume was replaced every 48 hours until the neurons were treated with siRNA. Once the cells were treated, media was not removed, only added. All subsequent media additions contained anti-mitotics.

2.8 DIRECT DELIVERY (PASSIVE UPTAKE) OF OLIGONUCLEOTIDES

Cells were plated in DMEM containing 6% FBS at 10,000 cells per well in 96-well tissue culture plates. hsiRNA was diluted to twice the final concentration in OptiMEM (Gibco, Carlsbad, CA; #31985-088), and 50 μL diluted hsiRNA was added to 50 μL of cells, resulting in 3% FBS final. Cells were incubated for 72 hours at 37°C and 5% CO_2. Based on previous experience, we know that 1.5 μM active hsiRNA supports efficient silencing without toxicity. The primary screen for active HTT siRNAs, therefore, was performed at 1.5 μM compound, which also served as the maximal dose for *in vitro* dose response assays.

2.9 HSIRNA LIPID MEDIATED DELIVERY

Cells were plated in DMEM with 6% FBS at 10,000 cells per well in 96-well tissue culture treated plates. hsiRNA was diluted to four times the final concentration in OptiMEM, and Lipofectamine® RNAiMAX Transfection Reagent (Invitrogen, Carlsbad, CA; #13778150) was diluted to four times the final concentration (final = 0.3 μl/25 μl/well). RNAiMAX and hsiRNA solutions were mixed 1:1, and 50 μl of the transfection mixture was added to 50 μl of cells resulting in 3% FBS final. Cells were incubated for 72 hours at 37°C and 5% CO_2.

2.10 mRNA QUANTIFICATION IN CELLS AND TISSUE PUNCHES

mRNA was quantified using the QuantiGene 2.0 Assay (Affymetrix, Santa Clara, CA; #QS0011). Cells were lysed in 250 µL diluted lysis mixture composed of 1 part lysis mixture (Affymetrix, Santa Clara, CA; #13228), 2 parts H2O, and 0.167 µg/µl proteinase K (Affymetrix, Santa Clara, CA; #QS0103) for 30 minutes at 55°C.

Tissue punches (5 mg) were homogenized in 300 µl of Homogenizing Buffer (Affymetrix, Santa Clara, CA; #10642) containing 2 µg/µl proteinase K in 96-well plate format on a QIAGEN TissueLyser II (Qiagen, Valencia, CA; #85300). Samples were then incubated at 65C for 30 minutes.

NHP brains were perfused with ice-cold PBS (Fisher, BP2438) prior to sectioning. Brains were sectioned in a brain matrix into 4 mm sections. 2 mm punches were taken from various brain regions and placed in RNAlater (Sigma, R0901) for mRNA quantification.

mRNA was detected according to the Quantigene 2.0 protocol using the following probe sets: human HTT (SA-50339), human PPIB (SA-10003), mouse HTT (SB-14150), mouse GFAP (SB-14051), mouse IBA1 (SB-3027744), mouse HPRT (SB-15463), mouse PPIB (SB-10002), NHP HTT (SF-10209), NHP GFAP (SF-4228397), NHP IBA-1 (SF-4214274), and NHP HPRT (SF-10356).

Luminescence was read on a Tecan M1000.

2.11 WESTERN BLOT

Frozen tissue punches were homogenized 20 strokes on ice in 10mM HEPES pH7.2, 250mM sucrose, 1mM EDTA plus protease inhibitors (Roche #11836170001),

1mM NaF, 1mM Na3VO4. Lysates were then sonicated for 10 seconds and protein

concentration was determined using the Bradford method (BioRad #5000006).

Western blots were performed as described in reference (Keeler, AM et al. JHD 2016)[86].

Briefly, 10 µg (mouse) or 25 µg (NHP) lysates were separated by SDS-PAGE using 3-8%

Tris acetate gels (Life Technologies #EA03785BOX), transferred to nitrocellulose,

blocked in 5% milk/TBS + 0.1% Tween 20, incubated in primary antibody diluted in

blocking buffer overnight at 4C then washed and incubated in secondary antibody diluted

in blocking buffer 1 hour at RT. Blots were washed and signal was detected using Super

Signal West Pico Plus Chemiluminescent kit (Pierce #34580) and a CCD imaging system

(Alpha Innotech) or Hyperfilm ECL (GE Healthcare #28906839) and densitometry was

determined using ImageJ software (NIH). Bands were manually circled and area and

mean gray value were meaured. Total signal intensity for each band was determined by

multiplying area by mean gray value. Primary antibodies were rabbit polyclonal anti-

HTT antibody Ab1[87] (1:2000), mouse monoclonal anti-polyglutamine antibody 1C2

(1:6000, Sigma MAB1574), mouse monoclonal anti-β-tubulin (1:6000, Sigma #T8328),

rabbit polyclonal anti-GFAP (1:8000, Millipore AB5804) and rabbit monoclonal anti-

DARPP32 (1:10,000, Abcam AB40801). Secondary antibodies were peroxidase-labeled

anti-rabbit IgG (1:2500, Jackson Immunoresearch #711035152) or anti-mouse IgG

(1:5000, Jackson Immunresearch #715035150).

ApoE protein quantification:

For analysis of ApoE protein expression in mouse brain samples, WES by

ProteinSimple was used. Tissue punches were collected as above and flash-frozen and

placed at -80 C. After addition of RIPA buffer with protease inhibitors, samples were

homogenized and stored at -80C. Protein amount was determined using Bradford Assay. Samples were diluted in 0.1x sample buffer (ProteinSimple) to ~0.2-0.4 ug/ul. Anti-ApoE antibody (Abcam, 183597) was diluted 1:200 in antibody diluent (ProteinSimple) and loading control, anti-Vinculin (Invitrogen, 700062), was diluted 1:600 in antibody diluent. Assay was performed as described by ProteinSimple protocol using the 16-230 kDa plate (SM-W004).

2.12 LIVE CELL IMAGING

To monitor live cell hsiRNA uptake, cells were plated at a density of 2×105 cells per 35 mm glass-bottom dish. Cell nuclei were stained with NucBlue® (Life Technologies, Carlsbad, CA; #R37605) as indicated by the manufacturer. Imaging was performed in phenol red-free NbActiv4. Cells were treated with 0.5 µM Cy3-labeled hsiRNA, and live cell imaging was performed over time. All live cell confocal images were acquired with a Zeiss confocal microscope, and images were processed using ImageJ (1.47v) software.

2.13 STEREOTAXIC INJECTIONS

Intrastriatal injections

FVB/NJ mice (50% male and 50% female for each dose group, 6-8 weeks old) were deeply anesthetized with 1.2% Avertin (Sigma, St Louis, MO; #T48402) and microinjected by stereotactic placement into the right striatum (coordinates relative to bregma: 1.0 mm anterior, 2.0 mm lateral, and 3.0 mm ventral). For both toxicity (DARPP-32 staining) and efficacy studies, mice were injected with either PBS or artificial CSF (2 µl per striata), 12.5 µg of non-targeting hsiRNA (2 µl of 500 µM stock

per striata), 25 µg of HTT10150 hsiRNA (2 µl of 1 mM stock per striata), 12.5 µg of HTT10150 hsiRNA (2 µl of 500 µM stock per striata), 6.3 µg of HTT10150 hsiRNA (2 µl of 250 µM stock per striata), or 3.1 µg of HTT10150 hsiRNA (2 µl of 125 µM stock per striata). For toxicity studies, n=3 mice were injected per group, and for efficacy studies n=8 mice were injected per group. Mice were euthanized 5 days post-injection, brains were harvested, and three 300 µm coronal sections were prepared. From each section, a 2 mm punch was taken from each side (injected and non-injected) and placed in RNAlater (Ambion®, Carlsbad, CA; #AM7020) for 24 hours at 4°C. Each punch was processed as an individual sample for Quantigene 2.0 assay analysis (Affymetrix, Santa Clara, CA), and averaged for a single animal point.

Intracerebroventrivular injections

FVB/NJ females (8-9 weeks old) or BACHD-ΔN17 females (6 weeks old) were anesthetized using 1.2% Avertin. Single intrastriatal administrations (2 µL, per injected side) were performed as previously described in Nikan et al. 2016 2017 at the following coordinates from bregma: +1.0 mm anterior-posterior (AP), +/-2.0 mm medio-lateral (ML) and -3.0 mm dorso-ventral (DV). Single bilateral intracerebroventricular injections (5 µL, per injected side) were performed at 500 nl/min after needle placement at the following coordinates from bregma: -0.2 mm AP, ±0.8 mm ML and -2.5 mm DV. Doses of Mono-siRNA and Di-siRNA ranged between 4 nmol (50 µg) and 40 nmol (475 µg) according to the goal of the experiment.

For biodistribution studies, animals (n = 2-3/group) were euthanized at 48 hours after injection and perfused with PBS. Brains were harvested and post-fixed overnight with 10% formalin and processed for paraffin embedding. For efficacy studies, animals

(n = 6-8/group) were euthanized at different time points, including 1, 2 weeks and 1, 3, 4, 6 months after single intracranial injections. At harvesting, tissues were kept in RNA later overnight (mRNA analysis) and then stored in -80ºC, or snap frozen (western blot assessments) and stored.

2.14 FOR SYSTEMIC ADMINISTRATION OF OLIGONUCLEOTIDES

C57BL/6 or FVB/NJ (both form Jackson Laboratory) mice were intravenously injected either with phosphate buffered saline (PBS) or with different amounts of hsiRNA, resuspended in PBS, through the tail vein (IV) or SC. For *in vivo* tissue distribution C57BL/6 were injected with 10 mg/kg of hsiRNAsFLT1 and euthanized 24 hours after injection. For *in vivo* efficacy FVB/NJ mice were injected with 20 mg/kg using the same protocol. Animals were euthanized 7 days after injection and tissues were taken for microscopy or for mRNA and hsiRNA quantification (using PNA hybridization assay). Animals were euthanized 7 days after the injection and tissues were taken for mRNA quantification using QuantiGene assay[88].

2.15 IMMUNOHISTOCHEMISTRY/IMMUNOFLUORESCENCE

Organs were fixed in 10% neutral buffered formalin, embedded in paraffin, and sliced into 4 µm sections that were mounted on glass slides. Sections were deparaffinized by incubating in Xylene twice for 8 min. Sections were rehydrated in serial ethanol dilutions (100%, 95%, 80%) for 4 min each, then washed twice for two minutes with PBS.

For NeuN staining[89, 90], slides were boiled for 5 minutes in antigen retrieval buffer (10 mM Tris/ 1mM EDTA (pH 9.0)), incubated at room temperature for 20 minutes, and

then washed for 5 minutes in PBS. Slides were blocked in 5% normal goat serum in PBS

containing 0.05% Tween 20 (PBST) for 1 hour and washed once with PBST for 5

minutes. Slides were incubated with primary antibody (Millipore, Taunton, MA

MAB377, 1:1000 dilution in PBST) for 1 hour and washed three times with PBST for 5

minutes. Slides were then incubated with secondary antibody (Life Technologies,

Carlsbad, CA; #A11011, 1:1000 dilution in PBST) for 30 minutes in the dark and washed

three times with PBST for 5 minutes each. Slides were then counterstained with 250

ng/ml DAPI (Molecular Probes, Life Technologies, Carlsbad, CA; #D3571) in PBS for 1

minute and washed three times with PBS for 1 minute. Slides were mounted with

mounting medium and coverslips and dried overnight before imaging on a Leica

DM5500 microscope fitted with a DFC365 FX fluorescence camera.

For toxicity studies, injected brains were harvested after 5 days. For microglial

activation studies, brains were harvested after 6 hours or 5 days. Extracted, perfused

brains were sliced into 40 μm sections on the Leica 2000T Vibratome (Leica Biosystems,

Wetzlar, Germany) in ice cold PBS. Every 6th section was incubated with DARPP-32

(Abcam, Cambridge, United Kingdom; #40801; 1:10,000 in PBS) or IBA1 (Wako,

Osaka, Japan; #019-19741; 1:1,000 in PBS) antibody, for a total of 9 sections per brain

and 8 images per section (4 per hemisphere). IBA-1 sections were incubated in blocking

solution (5% normal goat serum, 1% bovine serum albumin, 0.2% Triton™-X-100, and

0.03% hydrogen peroxide in PBS) for 1 hour, and then washed with PBS. Sections were

incubated overnight at 4ºC in primary antibody, anti-Iba1 (polyclonal rabbit anti-

mouse/human/rat; dilution: 1:1,000 in blocking solution) (Wako, Osaka, Japan; #019-

19741). Sections were then stained with goat anti-rabbit secondary antibody (1:200

dilution) (Vector Laboratories, Burlingame, CA), followed by a PBS wash, the

Vectastain ABC Kit (Vector Laboratories, Burlingame, CA), and another PBS wash.

IBA-1 was detected with the Metal Enhanced DAB Substrate Kit (Pierce, Rockford, IL).

For DARPP32 staining, sections were washed for 3 minutes in 3% hydrogen peroxide,

followed by 20 minutes in 0.2% TritonX-100, and 4 hours in 1.5% normal goat serum in

PBS. Sections were incubated overnight at 4ºC in DARPP32 primary antibody (1:10,000

dilution) (Abcam, Cambridge, United Kingdom; #40801) made up in 1.5% normal goat

serum. Secondary antibody and detection steps were conducted as described for IBA-1

staining. DARPP-32 sections were mounted and visualized by light microscopy with 20x

objective on a Nikon Eclipse E600 with a Nikon Digital Sight DSRi1 camera (Nikon,

Tokyo, Japan). The number of DARPP-32-positive neurons was quantified manually

using the cell counter plug-in on ImageJ for tracking. Activated microglia were

quantified by morphology of IBA1-positive cells[91-94] from the same number of sections

captured with 40x objective. Counting of both IBA1 and DARPP-32 positive cells was

blinded. Coronal section images were taken with a Coolscan V-ED LS50 35mm Film

Scanner (Nikon, Tokyo, Japan).

2.16 *IN VITRO* RISC LOADING AND CLEAVAGE ASSAY

S100 cell extract from ago2−/− + Ago2 (overexpressing Ago2) MEF cells were

incubated with 50 nM chemically modified or unmodified let 7a siRNA for 30 minutes at

37°C. After 30 minutes, 100 nM of ^{32}P capped labeled RNA was incubated at 23°C for

10 minutes to measure RISC concentration. After 10 minutes, temperature was shifted to

37°C (multi-turnover condition). Cell extract, RNA labeling, and cleavage assay were

performed as previously described in: Salomon et al[12]

2.17 PNA (PEPTIDE NUCLEIC ACID) BASED ASSAY FOR DETECTION OF HSIRNA IN MOUSE TISSUES [35]

hsiRNA guide strand in tissues were quantified using PNA hybridization assay. Tissues were lysed in MasterPure™ Tissue Lysis Solution (EpiCentre®) in the presence of proteinase K (2mg/ml) (Invitrogen, #25530-049) in TissueLyser II (Quiagen) (10mg tissue in 100 µl lysis solution). Sodium dodecyl sulphate (SDS) from lysate was precipitated with KCl (3M) and pelleted at 5000 g. hsiRNA in cleared supernatant was hybridized to a Cy3-labeled PNA fully complementary to guide strand (PNABio, Thousand Oaks, CA) and injected into HPLC DNAPac® PA100 anion exchange column (Thermo Fisher Scientific Inc.) and Cy3 fluorescence was monitored and peaks integrated. Mobile phase for HPLC was 50% water 50% acetonitrile, 25 mM Tris-HCl (pH 8.5), 1mM EDTA and salt gradient was 0 to 800mM NaClO4. For the calibration curve known amounts of hsiRNAsFLT1 duplexes were spiked into the tissue lysis solution.

2.18 SYNTHESIS OF DI-SIRNA LINKER AND SOLID SUPPORT CONJUGATION
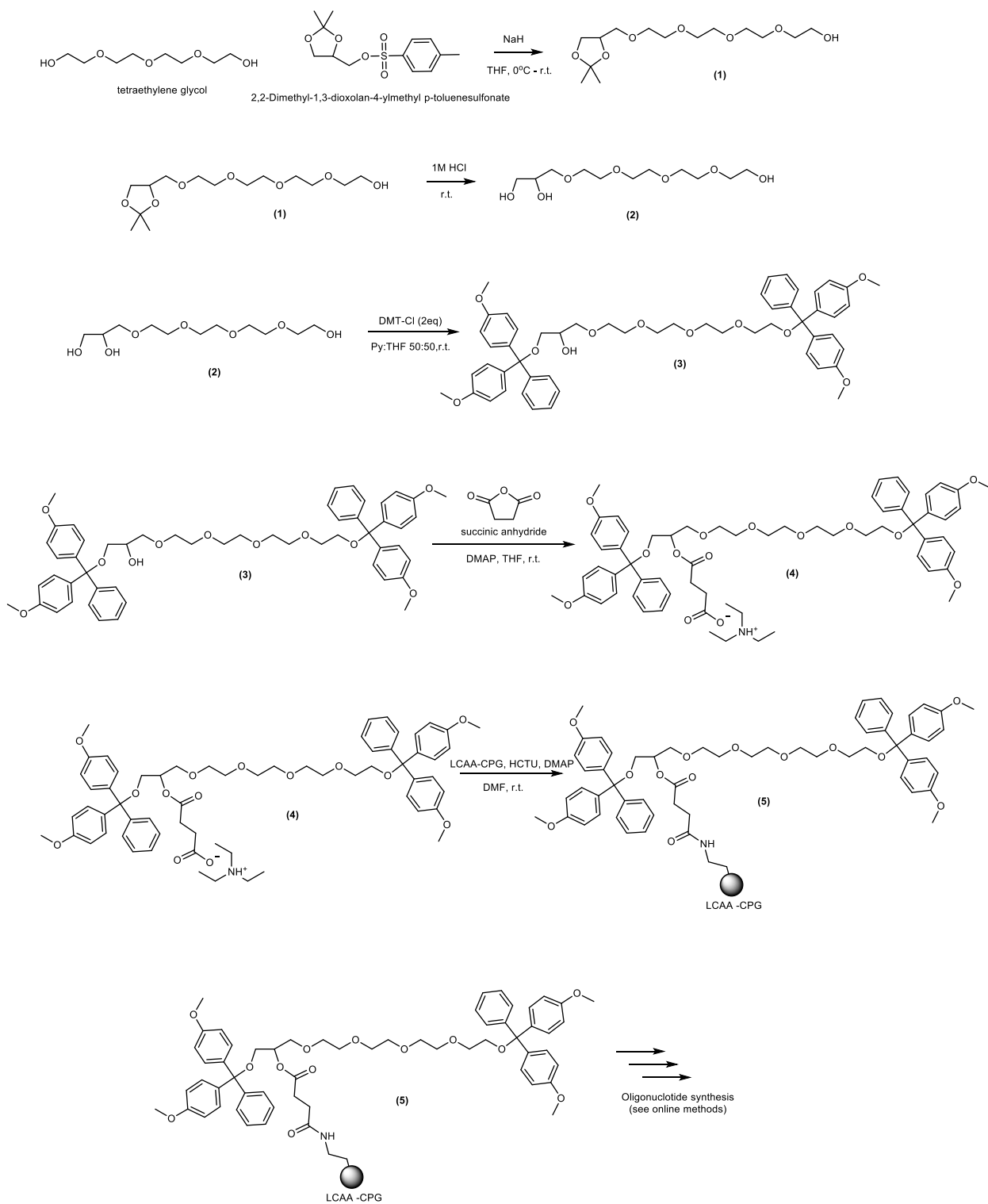
1-(2,2-dimethyl-1,3-dioxolan-4-yl)-2,5,8,11-tetraoxatridecan-13-ol **(1)**
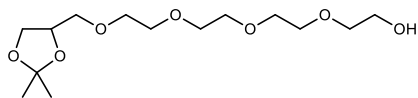
       Commercially available tetraethylene glycol (CAS: 112-60-7) (146.4g, 753.9mmol) was co-evaporated with Dry Pyridine/Toluene mixture (50:50)x2 by rotovap to remove residual water. The mixture was then dissolved in THF (700 ml) and cooled to 0°C in an ice bath with stirring. Sodium hydride, 60% dispersion in mineral oil (CAS: 7646-69-7) (4.3g, 107 mmol) was then added slowly to the cooled solution. Once hydrogen gas visibly ceased, 2,2-Dimethyl-1,3-dioxolan-4-ylmethyl p-toluenesulfonate (CAS: 7305-59-1) (30.8g, 107mmol) was added slowly. The mixture was removed from the ice bath and allowed to warm to room temperature before being refluxed for 16h under inert atmosphere. The solution was rotovapped to near dryness and the excess sodium hydride was quenched with a saturated sodium bicarbonate solution dropwise with stirring and finally extracted with chloroform x3 300ml and 10% NaCl soluiton. The organic layers were combined and dried over magnesium sulfate. The crude product was purified by flash chromatography on silica gel using hexanes/ethylacetate (75:25 to 0:100) as a colorless oil. Yield: 23g, 70.5%.

3,6,9,12-tetraoxapentadecane-1,14,15-triol **(2)**
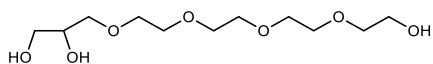
       To a solution of **(1)** in THF, equal volumn of a 1M HCl solution was added at room temperature and allowed to stir for 2h until all starting material was consumed by

TLC. The mixture was then evaporated to dryness on rotovap and then co-evaporated with 100ml (2x) dry pyridine to both remove excess water and quenched any residual HCl. The material was used directly without any further purification. MS.

1,1,19,19-tetrakis(4-methoxyphenyl)-1,19-diphenyl-2,5,8,11,14,18-hexaoxanonadecan-16-ol **(3)**
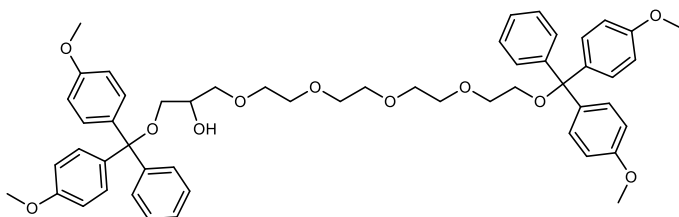
The triol **(2)** (17.2g, 64.2mmol) was then dissolved in 50:50 THF:pyridine (600ml) and triethylamine (44ml, 317mmol). To this solution solid dimethoxytrityl chloride (CAS# 40615-36-9) (43g, 126.9mmol) was added slowly over 5min. This mixture was allowed to stir at room temperature overnight (16h). By TLC all starting material was consumed (50:50 hexanes:ethylacetate). The reaction was concentrated to near dryness diluted with 600ml of ethylacetate and extracted with 5% sodium bicarbonate (x3) and once with brine (x1). The organic layer was dried over magnesium sulphate and concentrated to dryness as a yellow viscous liquid. The crude product was purified by flash chromatography on silica gel using hexanes/ethylacetate (100 to 25:75) and 1% triethylamine, in three batches as a colorless viscous oil. Yield: 42.2g, 76%.

16-((bis(4-methoxyphenyl)(phenyl)methoxy)methyl)-1,1-bis(4-methoxyphenyl)-18-oxo-1-phenyl-2,5,8,11,14,17-hexaoxahenicosan-21-oate triethylammonium salt **(4)**
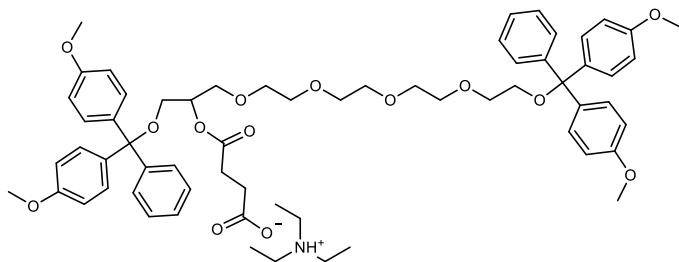
To a stirring solution of **(3)** (12.9g, 14.86mmol) in dry DCM and dry

triethylamine (3.8ml, 29.7mmol) with catalytic 4-dimethylamino pyridine (DMAP, CAS#

1122-58-3) (200mg, 1.5 mmol) dry solid succinic anhydride (CAS# 108-30-5) (2.23g,

22.3mmol) was added directly to the solution. The mixture was heated to a gentle reflux

under an inert atmosphere overnight (16h). The reaction was confirmed complete by

TLC (50:50 hexanes/ethylaceate) and concentrated to near dryness. The crude sample

was dissolved in ethylaceate and extracted with a triethylammonium bicarbonate solution

(300ml, 0.1M, pH 8) (x3) freshly prepared. The organic layer was dried over magnesium

sulfate and concentrated to dryness. The crude product was purified by flash

chromatography on silica gel quenched with triethylamine using hexanes/ethylacetate

(100 to 25:75) and 1 % triethylamine as a colorless oil. Yield: 13.1 g, 82%.

Controlled pore glass loading **(5)**
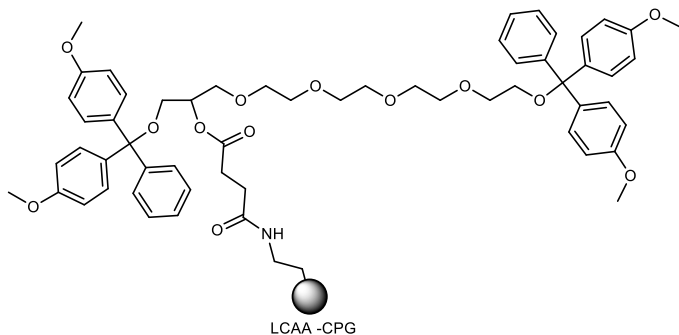
Compound (3) was dissolved in 50:50 THF/DMF along with 1.5 equivalents of HCTU (CAS# 330645-87-9) (g, mmol) and 0.1 eq of DMAP (g,mmol) and stirred until dissolved. To this solution 0.25 eq (to the amine content on the CPG) of long chain alkyl amine CPG (Chemgenes, Cat. N-5100-05) (500Å) was added and gently circulated overnight. The CPG was then filtered and rinsed first with DMF followed by DCM. The unreacted amines on the solid support were capped with an equal part mixture of CAP A (Acetic Anhydride/lutidine/ACN) CAP B (16% N-Methylimidazole in ACN). The CPG is then rinsed with ACN and diethylether and allowed to dry under reduced pressure. The loading of the support was calculated as previously described by Damha *et al*[95]. In brief: weigh CPG (5-10 mg) and treat with exactly 10 mL of 5% trichloroacetic acid in DCM in a volumetric flask. Measure absorbance at 504 nm (DMT λ max) and the amount of trityl cation determined by using extinction coefficient of 76 mL/(cm*µmol) (DMT)

2.20 STEREOTACTIC INJECTION IN NON-HUMAN PRIMATES

Cynomolgus macaques (2.5-4.5 Kg) were sedated using Ketamine (15 mg/kg), Xylazine (0.5 mg/kg) and Glycopyrolate (0.01 mg/kg), and a tracheal tube placed. Anesthesia was maintained by isoflurane 1 – 3% carried by oxygen (1 L/minute). Animals received intravenous lactate ringer solution (LRS) at a rate of 5-10 ml/kg/hr and were placed on a heating blanket. Meloxicam (0.15 mg/kg) and buprenorphine (0.01 mg/kg) were given for analgesia. Respiratory rate, end tidal CO2, body temperature, spO2 and heart rate were monitored and recorded.

Standard surgical aseptic technique was used throughout the procedure. Macaques were positioned on a stereotaxic frame for non-human primates (KOPF Model 1530M) and skin cleaned with alternating applications of betadine and alcohol. The skull was

exposed by a transverse incision and the periosteum removed from the surgical area. Based on the positioning of Bregma a burr hole (3-5 mm) was drilled using a Stryker high-speed drill (Core Powered Instrument Driver and Precision Neuro drill bit (Cat. #5820-107-530)). Real-time Cone Beam Computerized Tomography (CBCT) images were registered on pre-operative Magnetic Resonance Imaging (MRI) data sets (see details on MRI acquisition below) for determination of correct positioning of the manipulator for cannula placement. Cannula was lowered to the left lateral ventricle, 50 µL of iodohexal contrast agent was administered followed by high-resolution CBCT to confirm correct positioning of the device. FDA-approved SmartFlow™ neuroventricular cannulas (16 ga, 0.008" ID x 4 ft, MRI Interventions, Inc) were used for all intracerebroventricular (ICV) injections. Cannulas were attached to a syringe fitted in a programmable PhD Ultrapump (Harvard Apparatus).

Di-siRNAs (25 mg/750 µL) were injected at a rate of 50 µL/min for 15 minutes, and anesthesia switched to Propofol (1 mL/hour). Cannulas were withdrawn 5-10 minutes after the end of the injections. The skull was irrigated with ~50 mL of 0.9% saline and scalp sutured with absorbable sutures (3-0 or 4-0 Vicryl Rapide) in an interrupted pattern. Animals were kept under anesthesia for ~2 hours following the end of the ICV injection and were given prophylactic antibiotics (Cephazolin, IV). Macaques were returned to their home cage to recover and monitored for signs of pain and distress.

Complete Blood Counts (CBC) and a comprehensive blood chemistry panel was carried out on pre-operative blood and after 2 days (distribution study), or 15-days and 30 days post-injection (efficacy studies). For siRNA guide strand quantification, blood

samples were collected pre-operatively and at the following time points after Di-siRNA injection: 5, 15, 30 minutes, 1 and 2 hours.

At necropsy, animals where heparinized and euthanized with an intravenous injection of pentobarbital (150 mg/kg). CSF samples were immediately collected from the cisterna magna after euthanasia. Animals were then perfused with 4 L of sterile cold PBS, and tissues collected for mRNA, protein and histology.

2.19 BRAIN MAGNETIC RESONANCE IMAGING

Pre-operative and 30-day MRI scans were acquired using a Philips Achieva 3Tesla Whole Body Scanner. Animals were anesthetized as previously described and placed on a MRI-compatible stereotaxic frame in ventral recumbency (head first into the magnet). Axial T1 unenhanced spin-echo, axial T2 fast spin-echo, diffusion weighted imaging, magnetic resonance angiography and magnetization prepared rapid gradient echo sequences. In-plane resolution was 0.4 to 1mm, slice thickness 1-4mm, and 256x256 acquisition matrix. Total MR imaging time was approximately 60-90 minutes per subject. Following imaging, the animal was recovered from anesthesia and monitored in cage.

2.20 RNASEQ

Total RNA was isolated from 3 brain punches each from 4 animals per naïve and Di-siRNAHTT treated condition using Monarch® Total RNA Miniprep Kit (NEB, T2010S) following manufacturer protocol. Briefly, tissue was submerged in DNA/RNA protection reagent, homogenized by passing through a 27G hypodermic needle, and incubated for 30 minutes at 55C with proteinase K. RNA was bound to column, subjected

to on-column DNase treatment, washed, and eluted in nuclease free water. Library

preparation was performed using TruSeq® Stranded mRNA Library Prep (Illumina,

20020594) following manufacturer protocol. Single end sequencing was performed for

75 cycles on the Illumina NextSeq 500, for a total of 271.6 million reads (average of 33.9

million reads per animal).

The resulting 75nt reads were mapped to the cynomolgus macaque genome

(Macaca fascicularis 5.0) with STAR/2.5.3a. Reads mapping to annotated exons were

counted using HTseq/0.10.0 and differential expression analysis was performed with

DESeq2/1.22.2. Genes that had less than 10 reads across all samples or were only

expressed in one animal were excluded from further analyses. Seed complementary

matches and enriched 6-mers within 3' UTRs (for genes with annotated 3' UTRs in

Macaca fascicularis Ensembl 95 annotations) were identified using a custom python

script. Gene set enrichment analysis was conducted using PANTHER/14.0, conditioning

on biological process gene ontology categories.

2.21 STATISTICAL ANALYSIS

Data were analyzed using GraphPad Prism 6 software (GraphPad Software, Inc.,

San Diego, CA). Concentration-dependent IC50 curves were fitted using a log(inhibitor)

vs. response – variable slope (four parameters). The lower limit of the curve was set at

zero, and the upper limit of the curve was set at 100. For each independent mouse

experiment, the level of knockdown at each dose was normalized to the mean of the

control group (the non-injected side of the PBS or artificial CSF groups). *In vivo* data

were analyzed using a Two-way RM ANOVA with Tukey's multiple comparisons test

for dose and side of brain. Differences in all comparisons were considered significant at

P-values less than 0.05 compared with the non-targeting control (NTC) injected group. P-values reported represent significance of the entire dose group relative to NTC and are not specific to the ipsilateral or contralateral side. For microglial activation, significance was calculated using a parametric, unpaired, two-tailed t-test for comparison between dose groups, and paired t-test for comparison between ipsilateral and contralateral hemispheres within the same dose group.

CHAPTER III: HYDROPHOBICALLY MODIFIED SIRNAS SILENCE HUNTINGTIN MRNA IN PRIMARY NEURONS AND MOUSE BRAIN

3.1 PREFACE

Text and figures are reproduced from

- **Alterman, J.F.**, Hall, L.M., Coles, A.H., Hassler, M.R., Didiot, M.C., Chase, K., Abraham, J., Sottosanti, E., Johnson, E., Sapp, E. *et al.* (2015) Hydrophobically Modified siRNAs Silence Huntingtin mRNA in Primary Neurons and Mouse Brain. *Mol Ther Nucleic Acids*, 4, e266.

Anastasia Khvorova designed the study and the screen. Matthew Hassler synthesized all of the compounds. I performed all *in vitro* screening and dose responses. Lauren Hall, Marie Didiot, and I performed primary neuron experiments. Kathy Chase and Andrew Coles did mouse injections. Andrew Coles and I processed tissue samples and I did mRNA quantification. Ellen Sapp ran western blots. Emily Sottosanti, Emily Johnson , and Lauren hall counted cells. I made graphs and performed statistical analyses. Anastasia Khvorova and I wrote the manuscript.

3.2 ABSTRACT

Applications of RNA interference for neuroscience research have been limited by a lack of simple and efficient methods to deliver oligonucleotides to primary neurons in culture and to the brain. Here, we show that primary neurons rapidly internalize hydrophobically modified siRNAs (hsiRNAs) added directly to the culture medium without lipid formulation. We identify functional hsiRNAs targeting the mRNA of huntingtin, the mutation of which is responsible for Huntington's disease, and show that direct uptake in neurons induces potent and specific silencing *in vitro*. Moreover, a single injection of unformulated hsiRNA into mouse brain silences *Htt* mRNA with minimal

neuronal toxicity. Thus hsiRNAs embody a class of therapeutic oligonucleotides that enable simple and straightforward functional studies of genes involved in neuronal biology and neurodegenerative disorders in a native biological context.

3.3 INTRODUCTION

RNA interference (RNAi) is a highly efficient gene silencing mechanism in which a small interfering RNA (siRNA) binds a target mRNA, guiding mRNA cleavage via an RNA-induced silencing complex (RISC)[9, 96]. This biological phenomenon is widely used as a genetic tool in biomedical research. Advances in RNA chemistry have expanded siRNA applications toward therapeutic development, with robust efficacy seen in Phase II clinical trials for liver diseases (e.g. TTR amyloidosis)[59, 97, 98].

Despite its prevalence in biomedical research, the use of RNAi in neurodegenerative research has been limited[99]. There is a significant unmet need for simple, effective, and non-toxic siRNA delivery methods to modulate gene expression in primary neurons and brain. A range of approaches has been evaluated[100], including AAV viruses[101, 102], peptide conjugates[103], oligonucleotide formulations[104], infusion of naked or slightly modified siRNAs[57, 105], ultrasound[106] and convection-enhanced based delivery[107]. None of these approaches has received wide acceptance due to toxicity, a requirement for extensive repetitive dosing, and/or limited spatial distribution. Lipofection and electroporation of siRNAs are challenging in primary neurons due to low transfection efficiencies and their extreme sensitivity to external manipulation[108]. Delivery of siRNA precursors (Lentiviruses and AAV) has been used successfully, but viral transduction cannot readily be turned off and requires extensive formulation and

experimental optimization to achieve reproducible, non-toxic silencing in neuronal cells [109-114].

In this study, we describe the delivery, distribution, and silencing capacity of hydrophobically modified siRNAs (hsiRNAs) in primary neurons and in mouse brain. hsiRNAs are siRNA-antisense hybrids containing numerous chemical modifications (see Fig. 3.1 and Table 3.1 for exact chemical composition of compounds used) designed to promote bio-distribution and stability while minimizing immunogenicity. As a model for our studies, we silenced the huntingtin (*Htt*) gene, the causative gene in Huntington's disease (HD). HD is an autosomal dominant neurodegenerative disorder caused by a toxic expansion in the CAG repeat region of the huntingtin gene leading to a variety of molecular and cellular consequences. Tetrabenazine, the only FDA-approved therapy for HD, seeks to alleviate disease symptoms but does not treat the actual problem: the gain of toxic function caused by mutant *Htt*. Recent studies suggest that transient neuronal knockdown of *Htt* mRNA can reverse disease progression without compromising normal cellular function *in vivo*[5]. At present, RNA interference via siRNA or ASO is one of the most promising therapeutic approaches for transient *Htt* mRNA silencing.

We performed a screen of hsiRNAs targeting *Htt* mRNA and identified multiple functional compounds. We showed that primary neurons internalize hsiRNA added directly to the culture medium, with membrane saturation occurring by one hour. Direct uptake in neurons induces potent and long-lasting silencing of *Htt* mRNA for up to three weeks *in vitro* without major detectable effects on neuronal viability. Additionally, a single injection of unformulated (without cationic lipid or AAV formulation) *Htt* hsiRNA into mouse brain silences *Htt* mRNA with minimal neuronal toxicity.

Efficient gene silencing in primary neurons and *in vivo* upon direct administration of unformulated hsiRNA represents a significant technical advance in the application of RNAi to neuroscience research, enabling technically achievable genetic manipulation in a native, biological context.

3.4 RESULTS

3.4.1 HSIRNAS ARE EFFICIENTLY INTERNALIZED BY PRIMARY NEURONS

Hydrophobically modified siRNA (hsiRNA) is an asymmetric compound composed of a 15-nucleotide modified RNA duplex with a single-stranded 3′ extension on the guide strand (Fig. 3.1a, Table 3.1)[115, 116]. Pyrimidines in the hsiRNA are modified with 2′-*O*-methyl (passenger strand) or 2′-fluoro (guide strand) to promote stability, and the 3′ end of the passenger strand is conjugated to a hydrophobic teg-Chol (tetraethylene glycol cholesterol) to promote membrane binding and association[59]. The single-stranded tail contains hydrophobic phosphorothioate linkages and promotes cellular uptake by a mechanism similar to that of antisense oligonucleotides[117]. The presence of phosphorothioates, ribose modifications, and a cholesterol conjugate contribute to overall hydrophobicity and are essential for compound stabilization and efficient cellular internalization.

Table 3.1 hsiRNA sequences, chemical modification patterns, and efficacy

Gene	Position	Sense Strand	Antisense Strand	M. musculus	M. mulatta	Huntingtin mRNA Expression (% control)	Passive Uptake (IC50)	Lipid-Mediated Uptake (IC50)
HTT	1214	mG.mG.mU.mU.mU.A.mU.G.A.A.mC.mU.G#mA#mA.tegChol	PmU.fU.fC.A.G.fU.fU.fC.A.fU.A.A.mA.fC#fC#fU#G#G#mA#C	yes	yes	34.3	197.4	N/A
HTT	1218	mU.mA.mU.G.A.A.mC.mU.G.A.mC.G.mU#mU#mA.tegChol	PmU.A.A.fC.G.fU.fC.A.G.fU.fU.fC.A.fU#A#A#mA#fC#fC#U		yes	44.8	293.2	N/A
HTT	1219	mA.mU.G.A.A.mC.mU.G.A.mC.G.mU.mU#mA#mA.tegChol	PmU.fU.A.A.fC.G.fU.fC.A.G.fU.fU.fC.A#fU#A#A#mA#fC#C		yes	29.6	163.6	0.052
HTT	1257	mA.mA.mU.G.mU.mU.G.mU.G.A.mC.mC.G#mG#mA.tegChol	PmU.fC.fC.G.G.fU.fC.A.fC.A.A.fC.A.fU#fU#G#fU#G#G#U		yes	28.5	156.7	N/A
HTT	1894	mU.mA.G.A.mC.G.G.mU.A.mC.mC.G.A#mC#mA.tegChol	PmU.G.fU.fC.G.G.fU.A.fC.fC.G.fU.fC.fU#A#A#fC#A#fC#A		yes	23.7	95.53	0.047
HTT	1907	mC.mA.A.mC.mC.A.G.mU.A.mU.mU.mU.G#mG#mA.tegChol	PmU.fC.fC.A.A.mA.fU.A.fC.fU.G.G.fU.fU#G#fU#fC#G#G#U		yes	39.3	217.9	N/A
HTT	2866	mU.mG.mC.mU.mC.A.A.mU.A.A.mU.G.mU#mU#mA.tegChol	PmU.A.A.fC.A.fU.fU.A.fU.fU.G.A.mG.fC#A#fC#fU#fC#G#U		yes	35.3	191.7	0.091
HTT	4041	mU.mC.mC.mU.G.mC.mU.mU.mU.A.G.mU.mC#mG#mA.tegChol	PmU.fC.G.A.fC.fU.A.A.mA.G.fC.A.G.mG#A#fU#fU#fU#fC#A	yes	yes	53.5	765.7	N/A
HTT	4049	mU.mA.G.mU.mC.G.A.mG.A.A.mC.mC.A#mA#mA.tegChol	PmU.fU.fU.G.G.fU.fU.fC.fU.fC.G.A.fC.fU#A#A#mA#G#fC#A	yes	yes	41.2	217.8	N/A
HTT	5301	mA.mG.mU.A.mC.mU.mU.mC.A.A.mC.G.mC#mU#mA.tegChol	PmU.A.G.fC.G.fU.fU.G.A.mA.G.fU.A.fC#fU#G#fU#fC#fC#C			36.6	230.2	0.081
HTT	6016	mU.mU.mC.A.G.mU.mC.mU.mC.G.mU.mU.G#mU#mA.tegChol	PmU.A.fC.A.A.fC.G.A.mG.A.fC.fU.G.A#mA#fU#fU#G#fC#C		yes	26.4	147.9	N/A
HTT	6579	mC.mU.A.G.mC.mU.mC.mC.mC.A.mU.G.mC.mU#mU#mA.tegChol	PmU.A.A.mG.fC.A.fU.G.G.mA.G.fC.fU.A#G#fC#A#G#mG#C		yes	28.3	89.8	0.055
HTT	8603	mC.mU.G.mC.G.mU.G.A.A.mC.A.mU.mU#mC#mA.tegChol	PmU.G.A.mA.fU.G.fU.fU.fC.A.fC.G.fC.A#G#fU#G#G#mG#C	yes	yes	40.0	236.1	N/A
HTT	10125	mC.mU.mC.A.G.G.A.mU.mU.mU.A.A.A#mA#mA.tegChol	PmU.fU.fU.fU.fU.A.A.mA.fU.fC.fC.fU.G.A#mG#A#A#mG#A#A		yes	31.1	158.7	0.059
HTT	10146	mA.mU.A.mU.mC.A.G.mU.A.A.A.G.A#mG#mA.tegChol	PmU.fC.fU.fC.fU.fU.fU.A.fC.fU.G.A.fU.A#fU#A#A#fU#fU#A	yes	yes	25.9	217.7	0.05
HTT	10150	mC.mA.G.mU.A.A.A.mG.A.G.A.mU.mU#mA#mA.tegChol	PmU.fU.A.A.fU.fC.fU.fC.fU.fU.fU.A.fC.fU#G#A#fU#A#fU#A	yes	yes	28.6	82.2	0.004
HTT	424	mC.mA.G.mC.mU.A.mC.mC.A.A.G.A.A#mA#mA.tegChol	PmU.fU.fU.fU.fC.fU.fU.G.G.fU.A.G.fC.fU#G#A#mA#A#G#U		yes	67.4	N/A	N/A
HTT	456	mC.mU.G.A.mC.A.A.mU.A.mU.G.mU.G#mA#mA.tegChol	PmU.fU.fC.A.fC.A.fU.A.fU.fU.G.fU.fC.A#G#mA#fC#A#A#U		yes	51.5	N/A	N/A
HTT	522	mG.mG.mC.A.mU.mC.G.mC.mU.A.mU.G#mA#mA.tegChol	PmU.fU.fC.fC.A.fU.A.G.fC.G.A.fU.G.fC#fC#fC#A#A#G#mA#A		yes	68.2	N/A	N/A
HTT	527	mC.mG.mC.mU.A.mU.G.G.mA.A.	PmU.A.A.mA.G.fU.fU.fC.fC.A.f		yes	45.5	N/A	N/A

		mC.mU.mU#mU#mA.tegChol	U.A.G.fC#G#A#fU#G#fC#C					
HTT	878	mU.mG.A.mC.A.A.mU.G.A.mA.A.mU.mU#mA#mA.tegChol	PmU.fU.A.A.fU.fU.fU.fC.A.fU.fU.G.fU.fC#A#fU#fU#fU#G#C		yes	64.8	N/A	N/A
HTT	879	mG.mA.mC.A.A.mU.G.A.mA.A.mU.mU.A#mA#mA.tegChol	PmU.fU.fU.A.A.fU.fU.fU.fC.A.fU.fU.G.fU.fC#A#fU#fU#fU#G		yes	51.5	N/A	N/A
HTT	908	mC.mU.mU.mC.A.mU.A.G.mC.G.A.A.mC#mC#mA.tegChol	PmU.G.G.fU.fU.fC.G.fC.fU.A.fU.G.A.mA#G#G#fC#fC#fU#U		yes	99.6	N/A	N/A
HTT	1024	mA.mU.G.mU.G.mC.mU.mC.mU.mU.A.G#mC#mA.tegChol	PmU.G.fC.fC.fU.A.A.mG.A.G.fC.A.fC.A#fU#fU#fU#A#G#U		yes	52.9	N/A	N/A
HTT	1165	mU.mG.A.mC.A.A.G.mG.A.A.mA.G.A#mA#mA.tegChol	PmU.fU.fU.fC.fU.fU.fU.fC.fC.fU.fU.G.fU.fC#A#fC#fU#fC#fC#G			77.0	N/A	N/A
HTT	1207	mU.mU.G.mU.mC.mC.A.G.G.mU.mU.mU.A#mU#mA.tegChol	PmU.A.fU.A.A.mA.fC.fC.fU.G.G.mA.fC.A#A#mG#fC#fU#G#C	yes	yes	109.5	N/A	N/A
HTT	1212	mC.mA.G.G.mU.mU.mU.A.mU.G.A.A.mC#mU#mA.tegChol	PmU.A.G.fU.fU.fC.A.fU.A.A.mA.fC.fC.fU#G#G#mA#fC#A#A	yes	yes	74.9	N/A	N/A
HTT	1217	mU.mU.A.mU.G.A.A.mC.mU.G.A.mC.G#mU#mA.tegChol	PmU.A.fC.G.fU.fC.A.G.fU.fU.fC.A.fU.A#A#mA#fC#fC#fU#G		yes	104.0	N/A	N/A
HTT	1220	mU.mG.A.A.mC.mU.G.A.mC.G.mU.mU.A#mC#mA.tegChol	PmU.G.fU.A.A.fC.G.fU.fC.A.G.fU.fU.fC#A#fU#A#A#mA#C		yes	83.9	N/A	N/A
HTT	1223	mA.mC.mU.G.A.mC.G.mU.mU.A.mC.A.mU#mC#mA.tegChol	PmU.G.A.fU.G.fU.A.A.fC.G.fU.fC.A.G#fU#fU#fC#A#fU#A		yes	92.2	N/A	N/A
HTT	1227	mA.mC.G.mU.mU.A.mC.A.mU.mC.A.mU#mC#mA.tegChol	PmU.G.fU.A.fU.G.A.fU.G.fU.A.A.fC.G#fU#fC#A#G#fU#U		yes	81.4	N/A	N/A
HTT	1229	mG.mU.mU.A.mC.A.mU.mC.A.mU.A.mC.A#mC#mA.tegChol	PmU.G.fU.G.fU.A.fU.G.A.fU.G.fU.A.A#fC#G#fU#fC#A#G		yes	82.2	N/A	N/A
HTT	1260	mG.mU.mU.G.mU.G.A.mC.mC.G.mG.A.G#mC#mA.tegChol	PmU.G.fC.fU.fC.fC.G.G.fU.fC.A.fC.A.A#fC#A#fU#fU#G#U		yes	108.4	N/A	N/A
HTT	1403	mU.mA.mU.mU.G.mU.G.G.A.A.mC.mU.mU#mA#mA.tegChol	PmU.fU.A.A.mG.fU.fU.fC.fC.A.fC.A.A.fU#A#fC#fU#fC#fC#C		yes	138.6	N/A	N/A
HTT	1470	mA.mA.A.G.mU.G.mC.mU.mC.mU.mU.A.G#mG#mA.tegChol	PmU.fC.fC.fU.A.A.mG.A.G.fC.A.fC.fU.fU#U#G#fC#fC#fU#U	yes	yes	85.6	N/A	N/A
HTT	1901	mU.mA.mC.mC.G.A.mC.A.A.mC.mC.A.G#mU#mA.tegChol	PmU.A.fC.fU.G.G.fU.U.G.fU.fC.G.G.fU#A#fC#fC#G#fU#C		yes	81.4	N/A	N/A
HTT	1903	mC.mC.G.A.mC.A.A.mC.mC.A.G.mU.A#mU#mA.tegChol	PmU.A.fU.A.fC.fU.G.G.fU.fU.G.fU.fC.G#G#fU#A#fC#fC#G		yes	72.7	N/A	N/A
HTT	2411	mC.mU.A.mC.A.mU.mC.G.A.mU.mC.A.mU#mG#mA.tegChol	PmU.fC.A.fU.G.A.fU.fC.G.A.fU.G.fU.A#G#fU#fU#fC#A#A		yes	53.0	N/A	N/A
HTT	2412	mU.mA.mC.A.mU.mC.G.A.mU.mC.A.mU.G#mG#mA.tegChol	PmU.fC.fC.A.fU.G.A.fU.fC.G.A.fU.G.fU#A#G#fU#fU#fU#fC#A		yes	57.1	N/A	N/A
HTT	2865	mG.mU.G.mC.mU.mC.A.A.mU.A.A.mU.G#mU#mA.tegChol	PmU.A.fC.A.fU.fU.A.fU.fU.G.A.mG.fC.A#fC#fU#fC#G#fU#U		yes	83.1	N/A	N/A
HTT	3801	mG.mU.mU.A.mC.A.A.mC.A.A.G.mU.A#mA#mA.tegChol	PmU.fU.fU.A.fC.fU.fU.G.fU.fU.G.fU.A.A#fC#A#G#mG#A#C		yes	48.9	N/A	N/A
HTT	4040	mA.mU.mC.mC.mU.G.mC.mU.mU.mU.A.G.mU#mC#mA.tegChol	PmU.G.A.fC.fU.A.A.mA.G.fC.A.G.mG.A#fU#fU#fU#fC#A#G	yes	yes	56.2	N/A	N/A

57

HTT	4048	mU.mU.A.G.mU.mC.G.A.mG.A.A. mC.mC#mA#mA.tegChol	PmU.fU.G.G.fU.fU.fC.fU.fC.G. A.fC.fU.A#A#mA#G#fC#A#G	yes	yes	72.2	N/A	N/A
HTT	4052	mU.mC.G.A.mG.A.A.mC.mC.A.A. mU.G#mA#mA.tegChol	PmU.fU.fC.A.fU.fU.G.G.fU.fU.f C.fU.fC.G#A#fC#fU#A#A#A	yes	yes	90.8	N/A	N/A
HTT	4055	mA.mG.A.A.mC.mC.A.A.mU.G.A. mU.G#mG#mA.tegChol	PmU.fC.fC.A.fU.fC.A.fU.fU.G.G .fU.fU.fC#fU#fC#G#A#fC#U	yes	yes	37.2	N/A	N/A
HTT	4083	mC.mA.A.mC.A.A.mU.mU.G.mU. mU.G.A#mA#mA.tegChol	PmU.fU.fU.fC.A.A.fC.A.A.fU.fU. G.fU#G#A#mA#fC#A#C		yes	91.7	N/A	N/A
HTT	4275	mA.mA.mC.A.mU.G.G.mU.G.mC. A.G.G#mC#mA.tegChol	PmU.G.fC.fC.fU.G.fC.A.fC.fC.A .fU.G.fU#fU#fC#fU#fC#A	yes	yes	77.2	N/A	N/A
HTT	4372	mC.mA.A.G.A.A.mC.mC.G.mU. G.mC#mA#mA.tegChol	PmU.fU.G.fC.A.fC.G.G.fU.fU.f C.fU.fU#G#fU#G#A#fC#A		yes	44.5	N/A	N/A
HTT	4374	mA.mA.G.A.A.mC.mC.G.mU.G.m C.A.G#mA#mA.tegChol	PmU.fU.fC.fU.G.fC.A.fC.G.G.f U.fU.fC.fU#fU#G#fU#G#A		yes	97.5	N/A	N/A
HTT	4376	mG.mA.A.mC.mC.G.mU.G.mC.A. G.A.mU#mA#mA.tegChol	PmU.fU.A.fU.fC.fU.G.fC.A.fC.G .G.fU#fC#fU#fU#fU#G#U		yes	64.1	N/A	N/A
HTT	4425	mC.mC.mU.mC.mU.mU.G.mU.mU .A.mU.A.A#mA#mA.tegChol	PmU.fU.fU.A.fU.A.A.fC.A.A. mG.A.G#mG#fU#fU#fC#A#A	yes	yes	44.6	N/A	N/A
HTT	4562	mU.mG.G.mC.mU.mU.mU.G.mU. A.mU.mU.G#mA#mA.tegChol	PmU.fU.fC.A.A.fU.A.fC.A.A.mA .G.fC.fC#A#A#fU#A#A#A		yes	102.1	N/A	N/A
HTT	4692	mG.mG.A.A.mU.mU.mC.mC.mU. A.A.A.A#mU#mA.tegChol	PmU.A.fU.fU.fU.U.A.G.mG.A. A.fU.fC#fC#A#A#fU#G#A	yes	yes	53.8	N/A	N/A
HTT	4721	mU.mG.G.mC.A.mU.mC.A.mU.G. G.mC.mC#mA#mA.tegChol	PmU.fU.G.G.fC.fC.A.fU.G.A.fU. G.fC.fC#A#fU#fC#A#fC#A		yes	124.2	N/A	N/A
HTT	5200	mC.mC.mC.A.G.mU.mC.A.A.mC. mU.G.A#mA#mA.tegChol	PmU.fU.fU.fC.A.G.fU.fU.G.A.fC .fU.G.G#mG#A#A#mA#fU#C		yes	43.8	N/A	N/A
HTT	5443	mA.mG.mC.A.G.mC.A.A.mC.A.m U.A.mC#mU#mA.tegChol	PmU.A.G.fU.A.fU.G.fU.fU.G.fC. fU.G.fC#fU#fC#A#fC#fU#C		yes	48.9	N/A	N/A
HTT	5515	mG.mA.A.mU.G.mU.mU.mC.mC. G.G.A.G#mA#mA.tegChol	PmU.fU.fC.fU.fC.fC.G.G.mA.A. fC.A.fU.fU#fC#fC#A#G#mA#C	yes	yes	62.0	N/A	N/A
HTT	8609	mG.mA.A.mC.A.mU.mU.mC.A.mC .A.G.mC#mC#mA.tegChol	PmU.G.G.fC.fU.G.fU.G.A.mA.f U.G.fU.fU#fC#A#fC#G#fC#A	yes	yes	47.4	N/A	N/A
HTT	10130	mG.mA.mU.mU.mU.A.A.A.A.mU. mU.mU.A#mA#mA.tegChol	PmU.fU.fU.A.A.mA.fU.fU.fU.fU. A.A.mA.fU#fC#fC#fU#G#A#G		yes	49.6	N/A	N/A
HTT	10134	mU.mA.A.A.A.mU.mU.mU.A.A.mU .mU.A#mU#mA.tegChol	PmU.A.fU.A.A.fU.fU.A.A.mA.fU .fU.fU.A#A#mA#fU#fC#C	yes	yes	113.7	N/A	N/A
HTT	10142	mA.mA.mU.mU.A.mU.A.mU.mC.A .G.mU.A#mA#mA.tegChol	PmU.fU.fU.A.fC.fU.G.A.fU.A.fU .A.A.fU#fU#A#A#mA#fU#U	yes	yes	78.0	N/A	N/A
HTT	10169	mA.mA.mC.G.mU.A.A.mC.mU.mC .mU.mU.mU#mC#mA.tegChol	PmU.G.A.mA.A.G.mA.G.fU.fU. A.fC.G.fU#fU#A#A#mA#A#U		yes	69.0	N/A	N/A
HTT	10182	mC.mU.A.mU.G.mC.mC.mC.G.m U.G.mU.A#mA#mA.tegChol	PmU.fU.fU.A.fC.A.fC.G.G.mG.f C.A.fU.A#G#mA#A#A#mG#A	yes	yes	100.1	N/A	N/A
HTT	10186	mG.mC.mC.mC.G.mU.G.mU.A.A. A.G.mU#mA#mA.tegChol	PmU.fU.A.fC.fU.fU.fU.A.fC.A.f C.G.G.mG#fC#A#fU#A#G#A		yes	83.5	N/A	N/A
HTT	10809	mA.mG.mU.mC.A.G.G.A.G.A.G.m	PmU.G.fC.A.fC.fU.fC.fU.fC.fC.f			101.7	N/A	N/A

58

		U.G#mC#mA.tegChol	U.G.A.fC#fU#A#A#mA#A#G				
HTT	11116	mU.mG.G.G.mU.A.mU.mU.G.A.A. mU.G#mU#mA.tegChol	PmU.A.fC.A.fU.fU.fC.A.A.fU.A.f C.fC.fC#A#A#mA#A#fC#A		90.0	N/A	N/A
HTT	11129	mU.mG.G.mU.A.A.G.mU.G.G.A.G .G#mA#mA.tegChol	PmU.fU.fC.fC.fU.fC.fC.A.fC.fU.f U.A.fC.fC#A#fC#A#fU#fU#C		105.9	N/A	N/A
HTT	11134	mA.mG.mU.G.G.A.G.G.A.A.A.mU. G#mU#mA.tegChol	PmU.A.fC.A.fU.fU.fU.fC.fC.fU.f C.fC.A.fC#fU#fU#A#fC#fC#A		85.1	N/A	N/A
HTT	11147	mU.mU.G.G.A.A.mC.mU.mC.mU. G.mU.G#mC#mA.tegChol	PmU.G.fC.A.fC.A.G.mA.G.fU.f U.fC.fC.A#fC#A#fU#fU#U		109.9	N/A	N/A
HTT	11412	mU.mG.A.G.G.mA.G.G.mC.mC.m C.mU.mU#mA#mA.tegChol	PmU.fU.A.A.mG.G.G.fC.fC.fU.f C.fC.fU.fC#A#A#mA#fC#A#U		122.0	N/A	N/A
HTT	11426	mA.mG.G.G.A.A.G.mC.mU.A.mC. mU.G#mA#mA.tegChol	PmU.fU.fC.A.G.fU.A.G.fC.fU.fU .fC.fC.fC#fU#fU#A#A#mG#G	yes	106.3	N/A	N/A
HTT	11443	mA.mU.A.A.mC.A.mC.G.mU.A.A. G.A#mA#mA.tegChol	PmU.fU.fU.fC.fU.fU.A.fC.G.fU. G.fU.fU.A#fU#A#A#fU#fU#C		91.7	N/A	N/A
HTT	11659	mU.mA.mC.A.mU.mU.mU.mU.G.mU.A .A.G.A#mA#mA.tegChol	PmU.fU.fU.fC.fU.fU.A.fC.A.A.m A.fU.G#A#A#mA#fC#A#U		80.7	N/A	N/A
HTT	11666	mG.mU.A.A.G.mA.A.A.mU.A.A.m C.A#mC#mA.tegChol	PmU.G.fU.G.fU.fU.A.fU.fU.fU.f C.fU.A#fC#A#A#mA#mA#fU#G		98.5	N/A	N/A
HTT	11677	mC.mA.mC.mU.G.mU.G.A.A.mU. G.mU.A#mA#mA.tegChol	PmU.fU.fU.A.fC.A.fU.fU.fC.A.f C.A.G.fU#G#fU#fU#A#fU#U		87.8	N/A	N/A
HTT	11863	mG.mA.G.mC.mU.mC.A.mU.mU. A.G.mU.A#mA#mA.tegChol	PmU.fU.fU.A.fC.fU.A.A.A.fU.G.A. mG.fC.fU#fC#A#fU#A#fU#U		77.4	N/A	N/A
HTT	11890	mC.mA.mC.G.mC.A.mU.A.mU.A. mC.A.mU#mA#mA.tegChol	PmU.fU.A.fU.G.fU.A.fU.A.fU.G. fC.G.fU#G#G#mG#fU#G#A		114.3	N/A	N/A
HTT	11927	mG.mA.mC.A.mC.A.mU.mC.mU.A .mU.A.A#mU#mA.tegChol	PmU.A.fU.fU.A.fU.A.G.mA.fU. G.fU.G.fU#fC#fU#A#fU#A#U		113.3	N/A	N/A
HTT	11947	mC.mA.mC.A.mC.A.mC.mC.mU. mC.mU.mC.A#mA#mA.tegChol	PmU.fU.fU.G.A.mG.A.G.mG.fU .G.fU.G.fU#G#fU#G#fU#A#A		99.8	N/A	N/A
HTT	12163	mU.mA.mU.mC.A.mU.G.mU.mU. mC.mC.mU.A#mA#mA.tegChol	PmU.fU.fU.A.G.mG.A.A.fC.A.f U.G.A.fU#A#A#mA#G#fU#C		70.7	N/A	N/A
HTT	12218	mG.mC.A.A.A.mU.G.mU.G.A.mU. mU.A#mA#mA.tegChol	PmU.fU.fU.A.A.fU.fC.A.fC.A.fU. fU.fU.G#fC#A#A#fC#A#A		115.3	N/A	N/A
HTT	12223	mU.mG.mU.G.A.mU.mU.A.A.mU. mU.mU.G#mG#mA.tegChol	PmU.fC.fC.A.A.mA.fU.fU.A.A.f U.fC.A.fC#A#fU#fU#fU#G#C		114.6	N/A	N/A
HTT	12235	mG.mG.mU.mU.G.mU.mC.A.A.G. mU.mU.mU#mU#mA.tegChol	PmU.A.A.mA.A.fC.fU.fU.G.A.fC .A.A.fC#fC#A#A#mA#fU#U		108.3	N/A	N/A
HTT	12279	mU.mU.mU.mC.mC.mU.G.mC.mU .G.G.mU.A#mA#mA.tegChol	PmU.fU.A.fC.fC.A.G.fC.A.G. mG.A.A#mA#fC#A#A#A		83.9	N/A	N/A
HTT	12282	mC.mC.mU.G.mC.mU.G.G.mU.A. A.mU.A#mU#mA.tegChol	PmU.A.fU.A.fU.fU.A.fC.fC.A.G. fC.A.G#mG#A#A#mA#A#C		89.9	N/A	N/A
HTT	12297	mG.mG.G.A.A.A.G.A.mU.mU.mU. mU.A#mA#mA.tegChol	PmU.fU.fU.A.A.mA.A.fU.fC.fU.f U.fU.fC.fC#fC#G#A#fU#A#U		82.9	N/A	N/A
HTT	12309	mA.mA.mU.G.A.A.A.mC.mC.A.G. G.G#mU#mA.tegChol	PmU.A.fC.fC.fC.fU.G.G.fU.fU.f U.fC.A.fU#fU#A#A#mA#A#U		73.4	N/A	N/A

HTT	12313	mA.mA.A.mC.mC.A.G.G.G.mU.A.G.A#mA#mA.tegChol	PmU.fU.fU.fC.fU.A.fC.fC.fC.fU.G.G.fU.fU#fU#fC#A#fU#fU#A			89.8	N/A	N/A
HTT	12331	mU.mU.G.G.mC.A.A.mU.G.mC.A.mC.mU#mG#mA.tegChol	PmU.fC.A.G.fU.G.fC.A.fU.fU.G.fC.fC.A#A#mA#fC#A#A#U			109.9	N/A	N/A
HTT	13136	mC.mA.G.mU.mU.G.mU.mU.mU.mC.mU.A.A#mG#mA.tegChol	PmU.fC.fU.fU.A.G.mA.A.A.fC.A.A.fC.fU#G#A#mG#G#G#G			113.2	N/A	N/A
HTT	13398	mG.mA.mC.G.A.G.A.G.A.mU.G.mU.A#mU#mA.tegChol	PmU.A.fU.A.fC.A.fU.fC.fU.fC.fU.fC.G.fU#C#A#G#fU#fC#C			102.1	N/A	N/A
HTT	13403	mG.mA.G.A.mU.G.mU.A.mU.A.mU.mU.mU#mA#mA.tegChol	PmU.fU.A.A.mA.fU.A.fU.A.fC.A.fU.fC.fU#fC#fU#fC#G#fU#C			84.1	N/A	N/A
HTT	13423	mU.mA.A.mC.mU.G.mC.mU.G.mC.A.A.A#mC#mA.tegChol	PmU.G.fU.fU.fU.G.fC.A.G.fC.A.G.fU.fU#A#A#mA#A#A#A			124.8	N/A	N/A
HTT	13428	mG.mC.mU.G.mC.A.A.A.mC.A.mU.mU.G#mU#mA.tegChol	PmU.A.fC.A.A.fU.G.fU.G.fU.fU.fU.G.fC.A.G#fC#A#G#fU#fU#A			114.1	N/A	N/A
HTT_ um	10150	mA.mU.A.U.C.A.G.U.A.A.A.G.A.G.A.U.U.A.A.U.U	P.U.U.A.A.U.C.U.C.U.U.U.A.C.U.G.A.U.A.U.U.U	yes	yes	N/A	N/A	0.013
HTT_ Cy3	10150	Cy3-mC.mA.G.mU.A.A.A.mG.A.G.A.mU.mU#mA#mA.tegChol	PmU.fU.A.A.fU.fC.fU.fC.fU.fU.f U.A.fC.fU#G#A#fU#A#fU#A	yes	yes	28.6	82.2	0.004
PPIB	437	mC.mA.A.A.mU.mU.mC.mC.A.mU.mC.G.mU#mG#mA.tegChol	PmU.fC.A.fC.G.A.fU.G.G.mA.A.fU.fU.fU#G#fC#fU#G#U#U	yes	yes			
NTC	N/A	mA.mC.A.A.A.mU.A.mC.G.A.mU#mU#mA.tegChol	PmU.A.A.fU.fC.G.fU.A.fU.fU.fU.GU#mC#A#A#mU#mC#A			102.0	N/A	N/A

Detailed sequence, chemical modification patterns, and efficacy of hsiRNAs. Huntingtin accession number - NM_002111 .6, PPIB accession number - NM_009693.2. Chemical modifications are designated as follows. "." – phosphodiester bond, "#" – phosphorothioate bond, "m" – 2'-*O*-methyl, "f" – 2'-Fluoro, no prefix – ribonucleotide, "P" – 5' Phosphate, "tegChol" – tetraethylene glycol (teg)-cholesterol, um – unmodified. All sequences are homologous to human huntingtin. IC50 calculated as described in materials and methods.
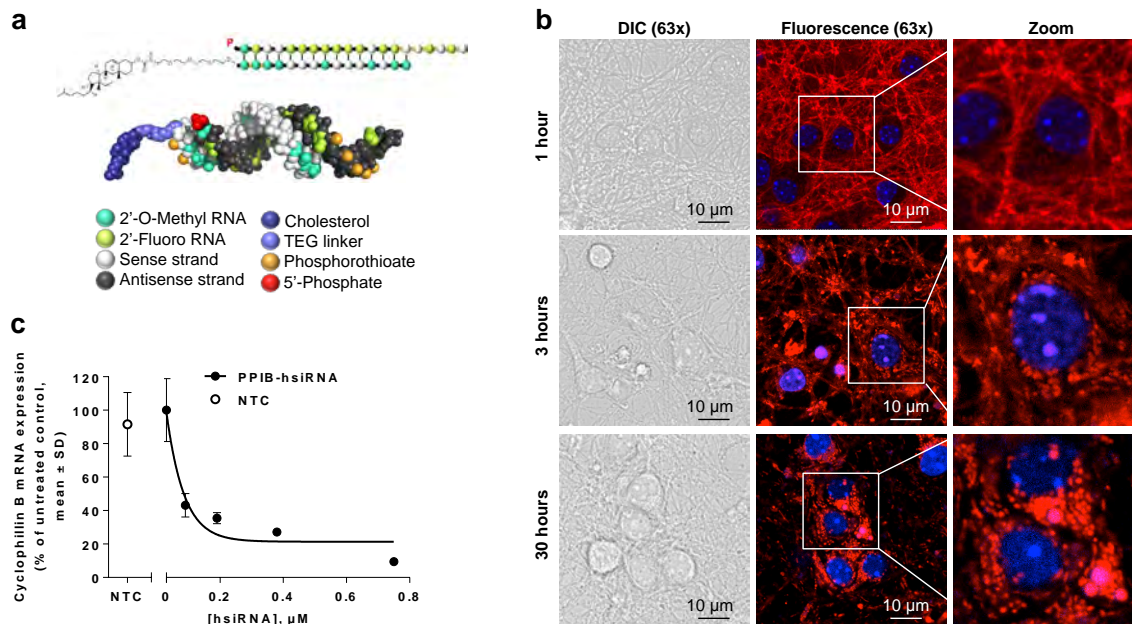
Figure 3.1 hsiRNAs are efficiently internalized by primary cortical neurons.
(**a**) Schematic structure of hsiRNAs. A double stranded oligonucleotide with single stranded, phosphorothioated tale. 2'-*O*-methyl and 2'-Fluoro modifications, conjugated to teg-chol. (**b**) Fluorescent images of primary cortical neurons incubated with 0.5 µM Cy3-PPIB hsiRNA (red). Nuclei counterstained with Hoechst dye (blue), imaged on Zeiss confocal microscope, 63x. A 10 µm scale bar is shown. Images are representative, results confirmed in 5 separate experiments. (**c**) Primary cortical neurons incubated for 72 hours with hsiRNA targeting *Ppib* at concentrations shown. Level of *Ppib* mRNA was measured using QuantiGene® (Affymetrix) normalized to housekeeping gene, *Htt*, presented as percent of untreated control (n=3 wells, mean ± SD). NTC – non-targeting control (0.75 µM). Graph is representative, results confirmed in 3 separate experiments.

Previous studies have shown that hydrophobically modified siRNAs bind to a wide range of cells and is readily internalized without the requirement for a transfection reagent[59, 118, 119]. Here, we evaluated whether asymmetric hydrophobically modified siRNAs are efficiently internalized by primary neurons. We found that, when added to the culture medium, Cy3-labeled hsiRNAs rapidly associated with primary cortical neurons (Fig. 3.1b). These Cy3-labeled hsiRNAs were observed in every cell in the culture, demonstrating efficient and uniform uptake. Initially hsiRNAs mainly associate with neuritis (within 1 hour, Fig. 3.1b) and, over time, accumulate in the cell bodies (3-30

hours, Fig. 3.1b). Treatment of primary neurons with a previously identified hsiRNA targeting Ppib[59, 118] (encodes cyclophilin B) reduced target mRNA levels by 90%, further supporting that the observed compound internalization results in potent gene silencing (Fig. 3.1c).

3.4.2 IDENTIFICATION OF HSIRNAS THAT SILENCE HUNTINGTIN MRNA

Robust uptake and efficacy observed with hsiRNAs in primary cortical neurons encouraged us to identify functional compounds that target *Htt* mRNA, the single gene responsible for the development of Huntington's disease. The hsiRNA extensive chemical scaffold[59, 118] is essential for stability, minimization of innate immune response[25, 120], and cellular internalization but imposes significant restrictions on sequence space by potentially interfering with the compound's RISC-entering ability. To maximize the likelihood of identifying functional HTT hsiRNAs and to evaluate the hit rate for this type of chemistry, we designed (using conventional criteria described in Materials & Methods) and synthesized hsiRNAs targeting 94 sites across the human *HTT* mRNA (Table 3.1). The panel of hsiRNAs was initially screened for efficacy in HeLa cells by adding hsiRNA directly to the culture medium (without lipofection or electroporation) to a final concentration of 1.5 μM and evaluating impact on levels of *HTT* and housekeeping (Ppib) gene mRNA expression using the QuantiGene® (Affymetrix) assay. At this concentration, 24 hsiRNAs reduced *HTT* mRNA levels to less than 50% of control levels, including 7 hsiRNAs that reduced *HTT* mRNA levels below 30% of control (Fig. 3.2a). Unlike unmodified siRNA libraries, creating a library with extensive 2'-*O*-methyl and 2'-fluoro modifications introduces additional constraints on sequence selection. As a result, hit rates for modified siRNA screens are lower than

that seen for conventional unmodified siRNA[121-124]. Functional hsiRNAs targeted sites distributed throughout the mRNA, except the distal end of the 3′ UTR, which later was shown to be part of the alternative HTT gene isoform[125] not expressed in HeLa cells (data not shown). Discounting the ~32 hsiRNAs targeting long 3′ UTR sites absent from the HTT isoform in HeLa cells, almost 40% of hsiRNAs showed some level of activity at 1.5 µM, demonstrating that the evaluated chemical scaffold is well tolerated by the RNAi machinery and a functional compound can be easily identified against a wide range of targets.
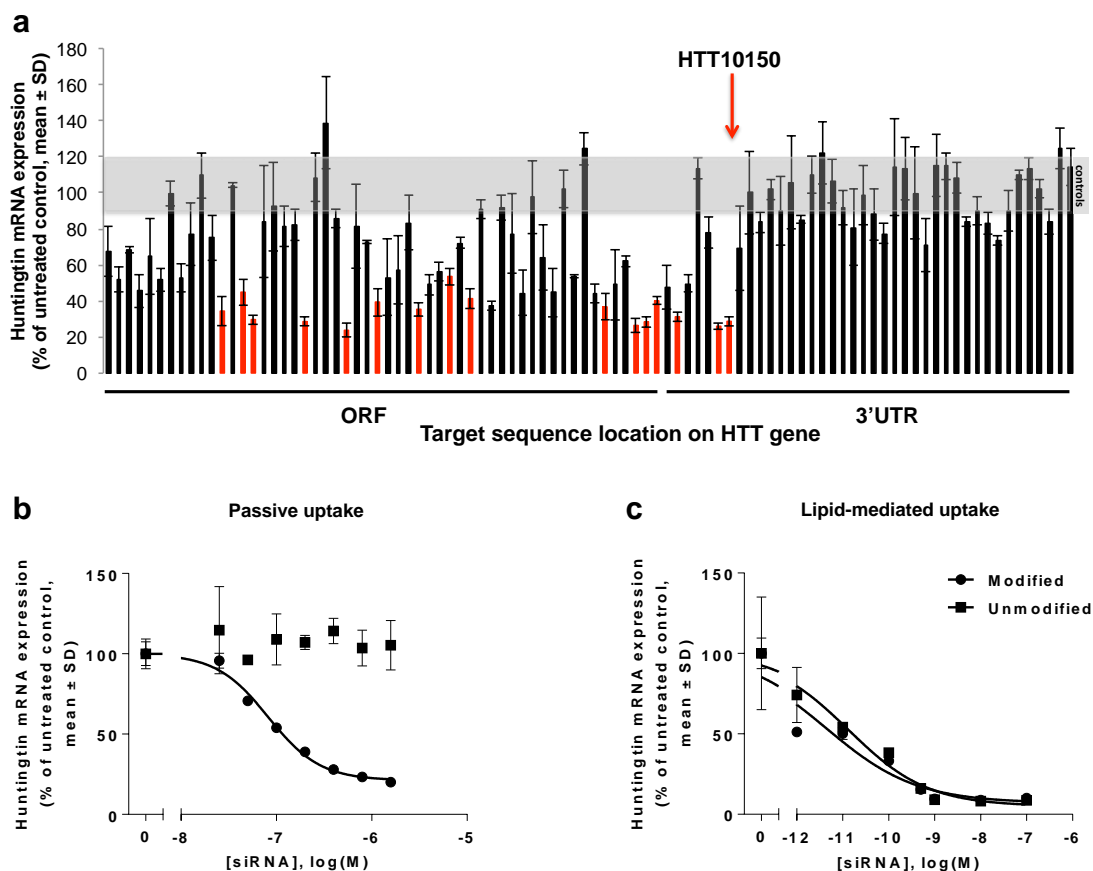
Figure 3.2 Systematic screen identifies functional hsiRNAs targeting huntingtin mRNA.
(a) Huntingtin mRNA levels in HeLa cells treated for 72 hours with 94 hsiRNAs (1.5 µM) were quantified using QuantiGene® and normalized to the housekeeping gene PPIB. Data are presented as percent of untreated control (n=3 wells, mean ± SD). Grey area represents range of huntingtin mRNA levels encompassing untreated and non-targeting hsiRNA controls. Red bars indicate compounds selected for further analysis. Compound sequence, chemical composition and level of silencing are shown in Table 3.1. Graph is representative, results confirmed in 2 separate experiments. (b,c) Dose-response analysis of huntingtin mRNA levels in HeLa cells treated with HTT10150 hsiRNA (circles) or unmodified siRNA (squares) added to culture medium in the absence (modified HTT10150 IC50 = 82.2 nM) (b), or presence (modified HTT10150 IC50 = 0.004 nM, unmodified HTT10150 IC50 = 0.013 nM) (c), of cationic lipids for 72 hours. Huntingtin mRNA was measured as described in a (n=3 wells, mean ± SD). IC50 values were calculated as described in Materials and Methods and are presented in Table 3.1. Graph is representative, results for modified siRNA confirmed in 3 separate experiments (in both absence and presence of cationic lipids), results for unmodified siRNA confirmed in 2 separate experiments (in both absence and presence of cationic lipids).

Half-maximal inhibitory concentrations (IC50) for passive uptake of hsiRNAs ranged from 82 to 766 nM (Table 3.1, Fig. 3.3). In lipid-mediated delivery, eight of the most active hsiRNAs had IC50 values ranging from 4 to 91 pM (Table 3.1). The best clinically active siRNAs are usually characterized by IC50 values in the low pM range[126]. An ability to identify highly potent compounds with low picomolar IC50 values suggests that the hsiRNA chemical scaffold does not interfere with siRNA biological activity for certain sequences. The most potent hsiRNA targeting position, 10150 (HTT10150), and an unmodified conventional siRNA version of HTT10150 showed similar IC50 values in lipid mediated delivery (4 pM and 13 pM respectively, Fig. 3.2c), further confirming that the hsiRNA chemical scaffold does not interfere with RISC loading or function. Only the modified hsiRNA, and not the unmodified version, silenced *HTT* mRNA by passive uptake (Fig. 3.2b). Thus, the chemical scaffold described here does not interfere with RISC assembly and is sufficient to support unformulated compound uptake and efficacy. HTT10150 was used for subsequent studies.

a Passive uptake

b Lipid-mediated uptake
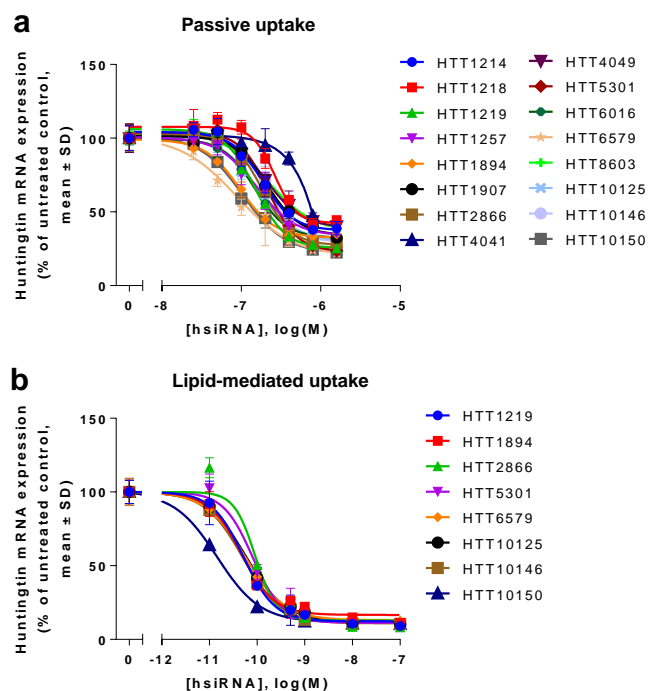
Figure 3.3 Active hsiRNAs silence huntingtin mRNA in a concentration dependent manner in HeLa cells. Level of huntingtin mRNA was measured using QuantiGene® (Affymetrix) at 72 hours normalized to housekeeping gene, PPIB (cyclophillin B), and presented as percent of untreated control (n=3 wells, mean ± SD). NTC – non-targeting control. (**a**) Dose response of 16 active sequences in passive uptake (no cationic lipid formulation). (**b**) Dose response of 8 selected sequences in lipid-mediated uptake (using Invitrogen Lipofectamine® RNAiMAX Transfection Reagent).

3.4.3 POTENT AND SPECIFIC SILENCING WITH UNFORMULATED HSIRNAS IN PRIMARY NEURONS

HTT10150 induced a concentration dependent silencing at 72 hours and one week after unformulated addition to either primary cortical or primary striatal neurons isolated from FVB/NJ mice (Fig. 3.4a). At 1.25 µM, HTT10150 induced maximal silencing, reducing both *Htt* mRNA levels and HTT protein levels by as much as 70% and 85%, respectively (Fig. 3.4a,b, and c for original westerns).
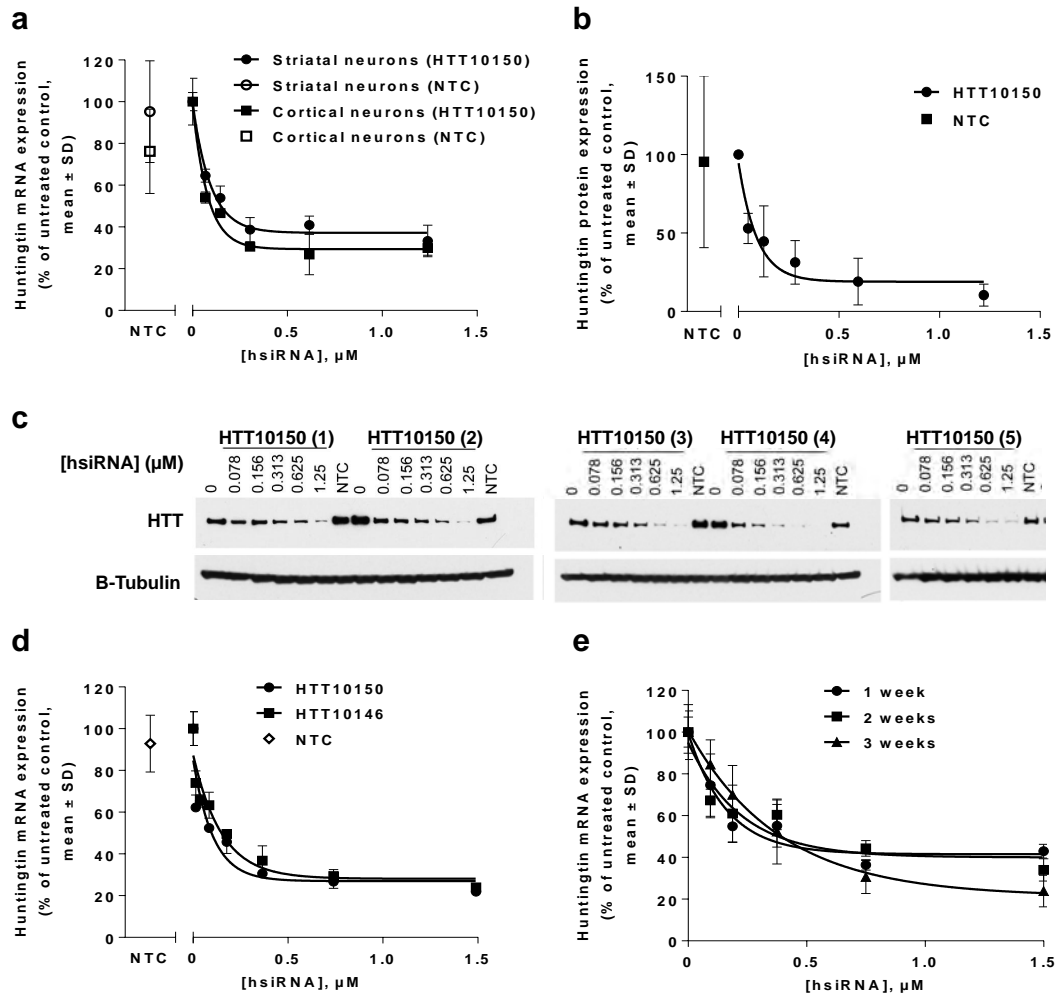
Figure 3.4 HTT10150 shows dose-dependent silencing of huntingtin by passive uptake in primary neurons.
(**a**) Huntingtin mRNA levels in primary striatal (black) or cortical (gray) neurons one week after treatment with the indicated concentrations of HTT10150. Huntingtin mRNA levels were normalized to *Ppib* mRNA. Data are expressed as percent of untreated control (n=3 wells, mean ± SD). NTC – non-targeting control (1.25 μM). (**b**) Huntingtin protein levels in primary neurons one week after treatment with the indicated concentrations of HTT10150. Huntingtin and β-tubulin proteins were quantified by densitometry of western blots, and huntingtin protein levels were normalized to β-tubulin. Data are expressed relative to the level of huntingtin protein in untreated control cells. (n=5 neuronal preparations from separate pups, mean ± SD). NTC – non-targeting control (1.25 μM). Graph of silencing in primary cortical neurons after one week is representative, results confirmed in 5 separate experiments. (**c**) Original western blots from graph in **b**. Primary cortical neurons were cultured from 5 individual pups (#1-5) and incubated with HTT10150 at concentrations shown for one week. Huntingtin protein levels were detected by Western Blot using antibody AB1 (Huntingtin 1-17). NTC – non-targeting control.

HTT10150 hsiRNA did not affect the expression levels of housekeeping controls

(Ppib and Tubb1, Fig.3.4c) or the overall viability of primary neuronal cells, as measured

by the alamarBlue assay, up to a 3 µM concentration (Fig. 3.5). Similar results were

obtained with another hsiRNA targeting *Htt* mRNA (Fig. 3.4d), supporting that the

observed phenomena is not unique to HTT10150. These experiments, in conjugation with

the results seen from targeting Ppib (Fig. 3.1c), indicate that a diversity of genes and

target sequences can be silenced by hsiRNAs in primary neurons simply upon direct

addition of compounds into cellular media.
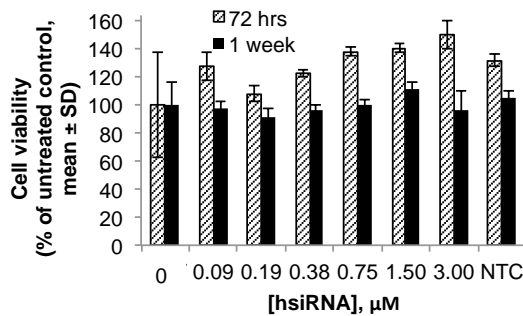
Figure 3.5 HTT10150 does not affect primary cortical neuron viability. Cell viability was tested using alamar Blue ® (Life Technologies) after incubation of HTT10150 and non-targeting control with primary cortical neurons for 72 hours and one week. Data presented as percent of untreated control (n=3 wells, mean ± SD). NTC – non-targeting control.

Since loaded RISC has a typical half-life of weeks[110], silencing is expected to be

long lasting in non-dividing cells. To evaluate duration of silencing after a single

HTT10150 treatment of primary cortical neurons, *Htt* mRNA levels were measured at

one-, two-, and three-week intervals (Fig. 3.4e). A single treatment with hsiRNA induced

Htt silencing that persisted for at least 3 weeks, the longest time that primary cortical

neurons can be maintained in culture. Together, these data demonstrate that hsiRNAs are

a simple and straightforward approach for potent, specific, non-toxic, and long-term

modulation of gene expression in primary neurons *in vitro*.

3.4.4 HSIRNA DISTRIBUTION *IN VIVO* IN MOUSE BRAIN AFTER INTRASTRIATAL INJECTION

Having shown that hsiRNAs effectively silence their targets in primary neurons *in vitro*, we sought to evaluate the ability of HTT10150 to silence *Htt* mRNA in the mouse brain *in vivo*. The distribution of HTT10150 was evaluated in perfused brain sections prepared 24 hours after intrastriatal injection with 12.5 µg Cy3-labeled hsiRNA in artificial cerebral spinal fluid (ACSF). We observed a steep gradient of fluorescence emanating from the injection site and covering most of the ipsilateral striatum (Fig. 3.6a,b), while no fluorescence was visually detectable in the contralateral side of the brain. In high magnification images of the ipsilateral side, hsiRNAs appeared preferentially associated with the tissue matrix and fiber tracts. In addition, efficient internalization was observed in a majority of cell bodies (Fig. 3.6c,d). Consistent with *in vitro* studies, we observed Cy3-labeled hsiRNA in neuronal processes and as punctae in the perinuclear space of multiple cell types, including NeuN-positive neurons[89, 90] (Fig. 3.6d,e). In summary, a single intrastriatal injection delivers hsiRNA to neurons in the striatum of the injected side.
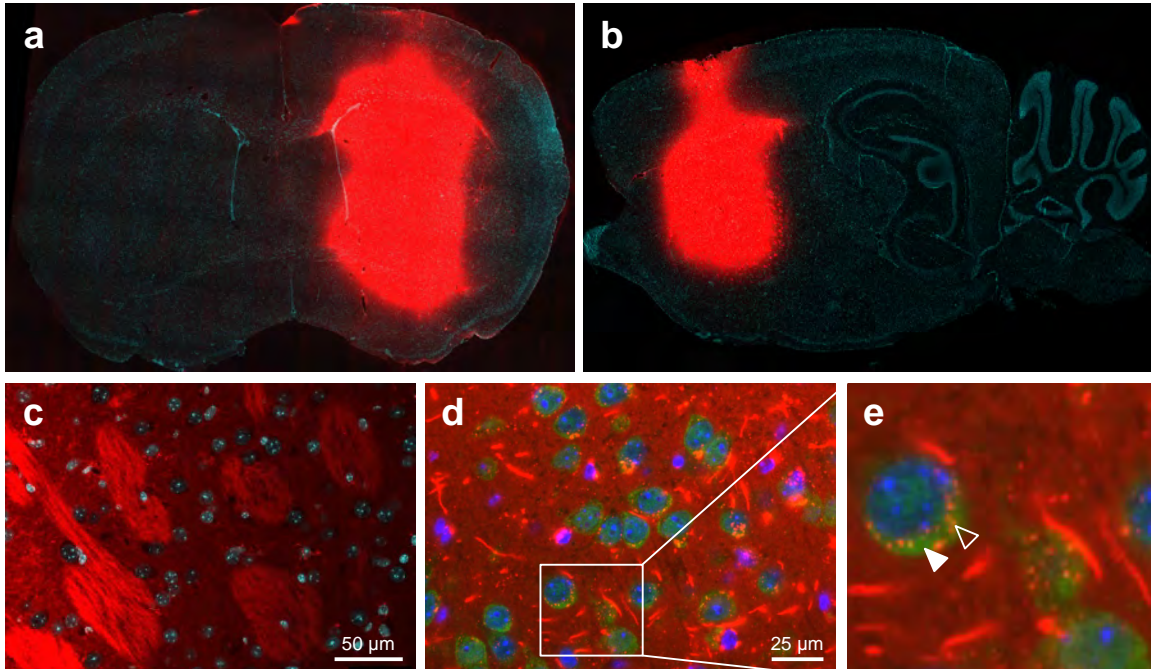
Figure 3.6 A single intrastriatal injection of HTT10150 is localized to neurons and fiber tracts ipsilateral to the injection site after 24 hours.
25 µg CY3-HTT10150 (red) was unilaterally injected into the striatum of WT (FVB/NJ) mice. Brains were collected after 24 hours, paraffin imbedded, and sectioned. (a) Tiled image of coronal brain section (16x). Majority of HTT10150 is localized at site of injection with sharp gradient of diffusion. (b) Tiled image of sagittal brain section (16x), injected side. (c), Image of coronal brain section (40x), injected side. (d) Image of coronal brain section (60x), injected side, with NeuN stained neurons. (e) NeuN stained neurons from injected side (60x) zoomed in. Solid arrow, NeuN staining. Open arrow, Cy3-HTT10150 punctae in perinuclear space. Images are representative, results confirmed in 2 separate experiments.

3.4.5 HSIRNA EFFECTIVELY SILENCES *HTT IN VIVO* WITH MINIMAL CYTOTOXICITY OR IMMUNE ACTIVATION

To measure HTT10150 efficacy *in vivo*, we performed dose-response studies in wild type FVB/NJ mice injected intrastriatally with 3.1, 6.3, 12.5, or 25 µg of HTT10150. As controls, we injected mice with a non-targeting control hsiRNA (NTC), artificial cerebrospinal fluid (ACSF), or PBS. In punch biopsies taken from the ipsilateral and

contralateral striatum, HTT10150 reduced *Htt* mRNA levels in a dose-dependent manner
(Fig. 3.7a).
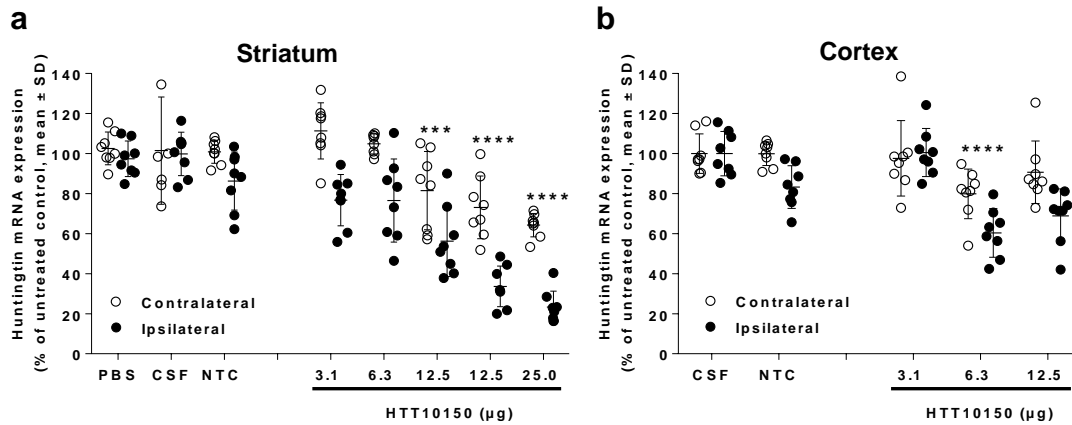
Figure 3.7 HTT10150 effectively silences huntingtin mRNA ipsilateral to the site of injection.
HTT10150 was unilaterally injected into the striatum of WT (FVB/NJ) mice (2 μl). Mice
were sacrificed at 5 days. Brains were sliced into 300 μm sections and six - 2mm punch
biopsies of the striatum (a) and cortex (b) were collected from both ipsilateral and
contralateral sides.   Level of huntingtin mRNA was measured using QuantiGene®
(Affymetrix) normalized to housekeeping gene, Ppib (cyclophillin B), and presented as
percent of untreated control (n=8 mice, mean ± SD, 3 biopsies per region). P values are
all calculated for each dose group relative to NTC by Two-way RM ANOVA: 25 μg
striatum p<0.0001, 12.5 μg striatum p<0.0001, p=0.0002, 6.3 μg cortex p=0.0009. NTC –
non-targeting control.

This experiment was repeated several times with similar results. The *Htt* mRNA

was significantly reduced in the ipsilateral side of striatum in all experiments. We

observed robust dose-dependent silencing with up to 77% (one way Anova, p<0.0001)

reduction in *Htt* mRNA expression levels at the highest dose. Interestingly we observe

statistically significant, but less pronounced silencing in the contralateral striatum and the

cortex (Fig.3.7b). The silencing reaches statistical significance with both One-way and

Two-way Anova (values for Two-way Anova are presented in Fig. 3.7). While some

level of fluorescence is detectable on the contralateral side with high laser intensity, it is

very close to the tissue auto-fluorescence and thus is not reported here. While the

phenomenon of potential transport across hemispheres can be investigated further, it is

clear that the level of silencing is at least correlative to the sharp gradient of diffusion

from the injection site.

Finally, *Htt* mRNA silencing was observed with HTT10150 but not with NTC or

ACSF (Fig. 3.7). In addition, the HTT10150 did not affect expression of several

housekeeping genes (PPIB, HPRT). In combination, this is indicative of *Htt* mRNA

silencing being caused by HTT10150 hsiRNA.

Nucleic acids, including siRNAs, are potent stimulators of the innate immune

response[127], but extensive chemical modifications, like 2′-*O*-methyl, are found to

suppress the immunostimulatory effects of siRNAs *in vitro* and *in vivo*[91]. To assess innate

immune response activation by hsiRNAs *in vivo*, we quantified IBA1-positive microglial

cells in brain sections from mice injected with 12.5 μg HT10150 or artificial CSF. IBA-1

is specific to microglial cells and is up-regulated following injury to the brain, allowing

us to distinguish between resting and activated microglia[92-94]. In the case of a major

innate immune response, an increase of 200-300% in total microglia is typical[128]. Total

microglia counts showed only a 25% increase in the ipsilateral striatum at five days post

injection indicating a lack of any major inflammatory response (Fig. 3.8). Thus the

observed activation is relatively minor, but reaches statistical significance, indicating

some level of response.
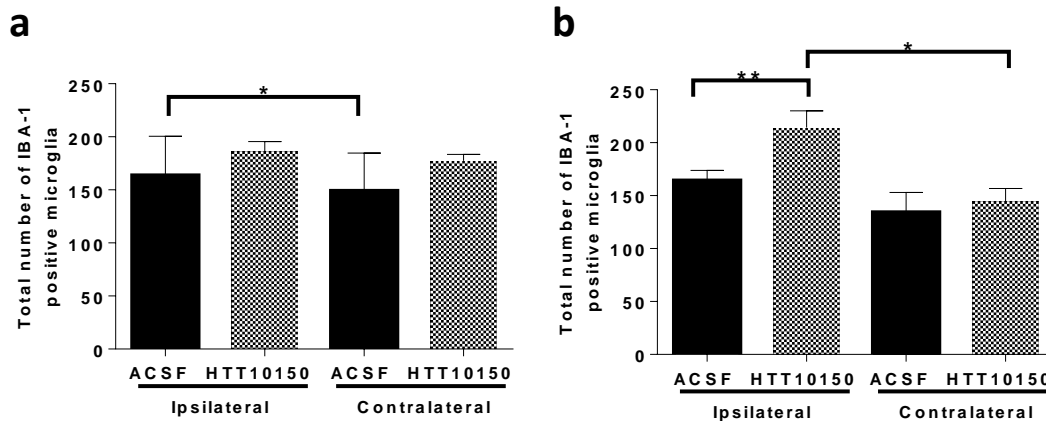
Figure 3.8 HTT10150 causes a slight increase in total resting microglia 5 days post injection.
HTT10150 was unilaterally injected into the striatum of FVB/NJ mice. Brains were collected 6 hours and 5 days post injection, fixed, sectioned, and stained with antibodies against IBA-1. Total microglia were quantified 6 hours (a) and 5 days (b) post-injection of ACSF (n=6 mice, mean ± SD) (a), n=4 mice, mean ± SD (b)), and 12.5 µg HTT10150 (n=3 mice, mean ± SD (a,b)). For (a), P values calculated by paired t-test, t=2.915, df=5: ACSF ipsilateral vs ACSF contralateral p=0.0332. For (b), P values calculated by unpaired t-test (between groups), t=5.272, df=5: ACSF vs HTT10150 ipsilateral p=0.0033; and by paired t-test (between ipsilateral and contralateral sides within the same group), t=4.845, df=2: HTT10150 ipsilateral vs contralateral p=0.0401. Images are representative, results confirmed in separate images of all injected brains.

Levels of innate immune response might be more pronounced immediately following compound administration. To assess the level of stimulation in more detail, we separately evaluated the number of activated and resting microglia at both 6 hours and 5 days post- injection. At 6 hours post-injection we observed a significant increase in the number of activated microglia in the injected side of the brain with both ACSF and HTT10150. The injection event itself causes trauma and induces a major increase in activated microglia (nine fold) compared to the contralateral side of the brain (Fig. 3.8b)[57, 129]. In the presence of HTT10150, the number of activated microglia was additionally increased two fold compared to ACSF, indicating enhancement of trauma-

related microglia activation in the presence of oligonucleotide, although the relative contribution of the oligonucleotide to the trauma related induction is minor. HTT10150-treated mice also showed some elevation of activated microglia in the contralateral striatum 6 hours post injection (Fig. 3.9b), however, after 5 days, all changes in number of microglia in the contralateral side of the brain disappeared (Fig. 3.9c, Fig. 3.9a for representative images), suggesting that HTT10150-dependent activation of microglia in the contralateral striatum is transient.
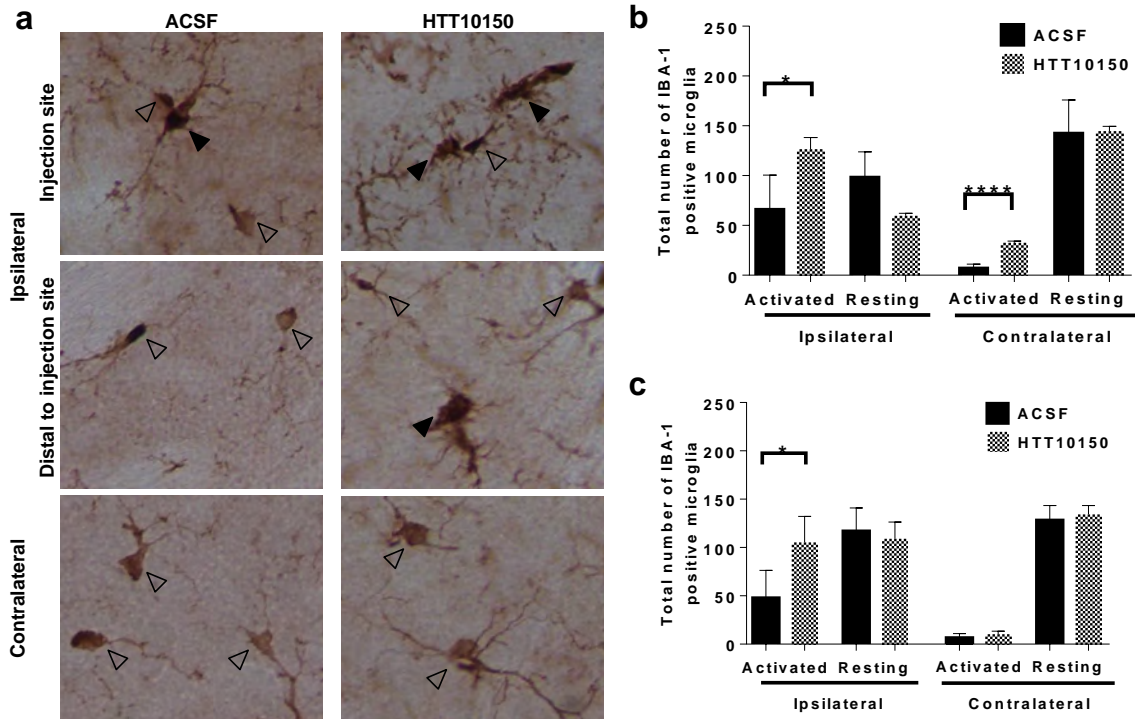
Figure 3.9 HTT10150 shows a two-fold increase in microglial activation at the site of injection.

HTT10150 was unilaterally injected into the striatum of WT (FVB/NJ) mice. Brains were collected after 6 hours (b) and 5 days (a, c) fixed, sectioned, and stained with antibodies against IBA-1. (a) Representative images of activated (black arrow) and resting (open arrow) after injection of 12.5 µg HTT10150 and ACSF 5 days post injection, 40x magnification. (b) Quantification of activated and resting microglia 6 hours post-injection of ACSF (n=6 mice, mean ± SD) and 12.5 µg HTT10150 (n=3 mice, mean ± SD). P values calculated by unpaired t-test, t=9.996, df=7: ACSF vs HTT10150 activated microglia ipsilateral striatum p=0.0239. ACSF vs HTT10150 activated microglia contralateral striatum p<0.0001. (c) Quantification of activated and resting microglia 5 days post-injection of ACSF (n=4 mice, mean ± SD) and 12.5 µg HTT10150 (n=3 mice, mean ± SD). Images are representative, results confirmed in separate images of all injected brains. P values calculated by unpaired t-test, t=2.700, df=5: ACSF vs HTT10150 activated microglia ipsilateral striatum p=0.0428.

Despite the mild immune stimulation in the brains of animals injected with

HTT10150, we did not observe any overall significant reduction of DARPP-32, an

established marker for striatal neuron viability[130] (Fig. 3.10).
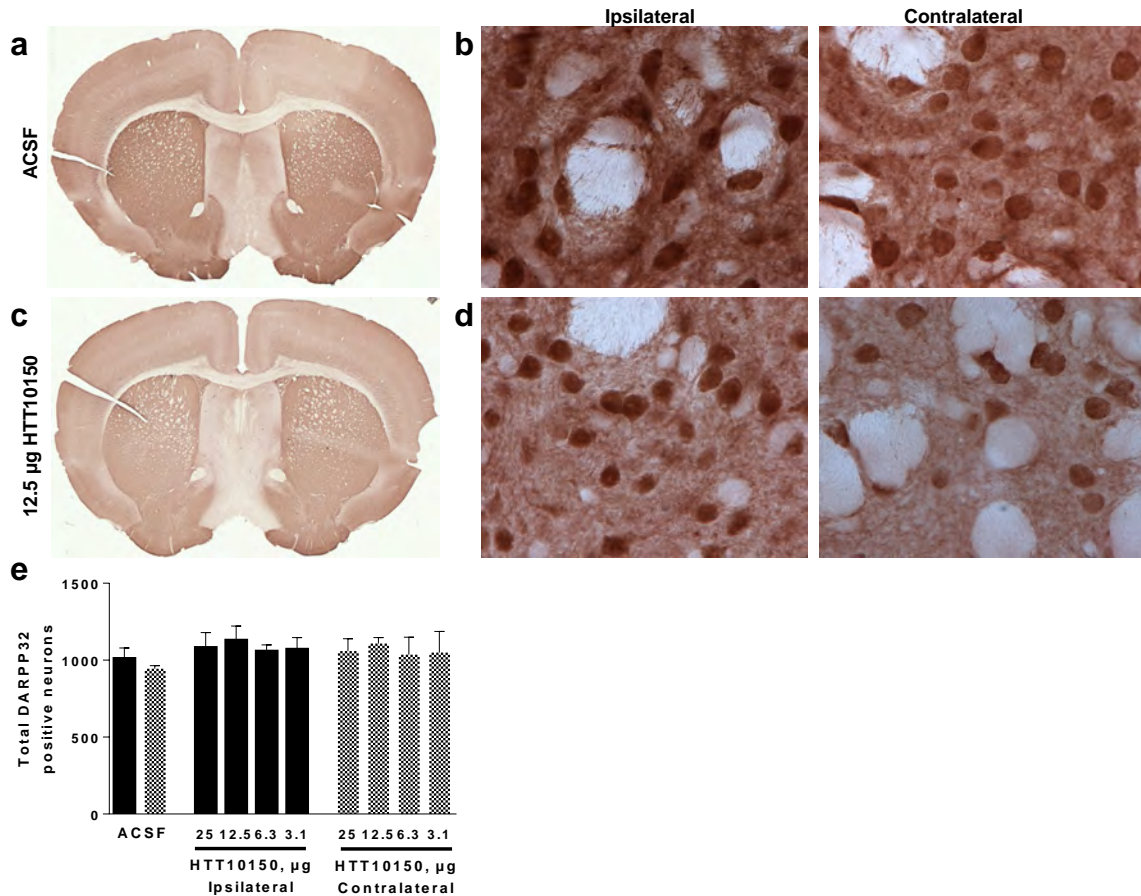
Figure 3.10 HTT10150 shows no toxicity in DARPP-32 positive neurons around the site of injection.
HTT10150 was unilaterally injected into the striatum of WT (FVB/NJ) mice. Brains were collected after 5 days, fixed, sectioned, and stained with antibodies against DARPP-32 (a-d). Representative image of striatum after injection of ACSF, full brain scan and 60x magnification (a,b) or 12.5μg HTT10150, full brain scan and 60x magnification (c,d). (a) Quantification of DARPP-32 positive neurons (n=3 mice, mean ± SD). Images are representative, results confirmed in separate images of all injected brains.

The only observed effect was at a small area directly around the injection site in animals treated with 25 μg HTT10150 (Fig. 3.11). Taken together, our data shows that a single intrastriatal injection of hsiRNA induces potent gene silencing with a mild immune response and minimal neuronal toxicity *in vivo*.
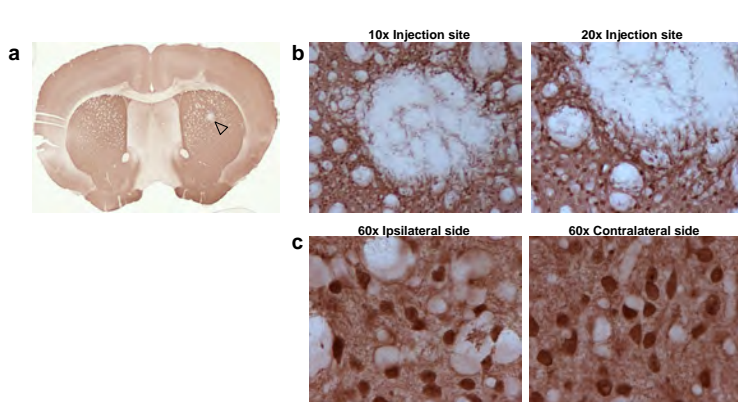
Figure 3.11 HTT10150 shows limited toxicity at the site of injection at the 25 μg dose. HTT10150 was unilaterally injected into the striatum of FVB/NJ mice. Brains were collected after 5 days, fixed, sectioned, and stained with antibodies against DARPP-32. Representative image of striatum after injection of 25 μg, full brain scan (a), 10x and 20x magnification at injections site (b), and 60x magnification directly adjacent to injection site, and contralateral to injection site (c). Images are representative, results confirmed in separate images of all injected brains.

3.5 DISCUSSION

Achieving simple, effective, and non-toxic delivery of synthetic oligonucleotides to primary neurons and brain tissue represents a challenge to the use of RNAi as a research tool and therapeutic for neurodegenerative diseases like HD[100]. We have shown that hsiRNAs elicit potent and specific silencing of *Htt* mRNA in primary neurons in culture with minimal toxicity at effective doses, while the non-targeting control hsiRNA has no effect on *Htt* or housekeeping mRNA levels. These data taken together suggests that hsiRNAs are both sequence specific and on target. Additionally, we do not see knockdown of housekeeping genes following treatment with HTT10150, suggesting that HTT silencing by this compound is both sequence specific and on target. Interestingly, the level of silencing is more pronounced on the protein level (>90%) compared to the mRNA level (>70%). The mRNA plateau effect is reproducible and is specific to *Htt* mRNA, as housekeeping genes like PPIB can be silenced by 90%. One potential explanation is that some fraction of huntingtin mRNA is translationally inactive and poorly accessible by RNAi machinery. We are continuing to investigate this

77

phenomenon. Silencing in primary neurons persists for multiple weeks after a single administration, consistent with the expected half-life of active RISC[131]. Moreover, efficient intracellular delivery of hsiRNAs does not require the use of lipids or viral packaging.

Currently, the most impressive *in vivo* modulation of *Htt* mRNA expression is demonstrated with 2'-O-methoxyethyl (MOE) GapmeR antisense oligonucleotides (ASO). A single injection of 50 µg of ASO or infusion of around 500 µg results in potent and specific *Htt* mRNA silencing in mouse and marked improvement in multiple phenotypic endpoints[5, 132-134]. However, MOE GapmeR ASOs are not readily commercially available making them inaccessible for the majority of academic labs.

Here, we show *Htt* mRNA silencing in the ipsilateral striatum and cortex, two brain areas significantly affected in HD disease progression, with a single intrastriatal injection of 12.5-25 µg. As a considerably reduced level of silencing was observed on the contralateral side of the brain, bilateral injections might be necessary to promote equal gene silencing in both hemispheres.

The limited distribution profile observed *in vivo* restricts immediate adoption of this technology for use in larger brains and eventually as a therapeutic for neurodegenerative disease. Tissue distribution can be improved by tailoring the chemical scaffold (e.g. number and type of sugar modifications, position of phosphorothioate linkages) or by changing the conjugation moiety to promote receptor-mediated cellular internalization. Formulation of hsiRNA in exosomes, exosome-like liposomes, or shielding the compounds with PEG may also provide an alternative strategy to improve tissue distribution[135, 136].

Here, we identify an active siRNA sequence targeting Huntington's disease and describe a class of self-delivering therapeutic oligonucleotides capable of targeted, non-toxic, and efficient *Htt* silencing in primary neurons and *in vivo*. This chemical scaffold can be specifically adapted to many different targets to facilitate the study of neuronal gene function *in vitro* and *in vivo*. The development of an accessible strategy for genetic manipulation in the context of a native biological environment represents a technical advance for the study of neuronal biology and neurodegenerative disease.

CHAPTER IV: COMPARISON OF FULLY AND PARTIALLY CHEMICALLY-MODIFIED SIRNA IN CONJUGATE-MEDIATED DELIVERY *IN VIVO*

4.1 PREFACE

Text and figures are reproduced from

- Hassler MR*, Turanov AA*, **Alterman JF***, Coles AH, Haraszti RA, Osborn MF, Godinho BM, Lo A Rajakumar A, Golebiowski D, Echeverria D, Nikan M, Salomon WE, Davis SM, Morrissey DV, Sena-Esteves M, Zamore PD, Karumanchi SA, Moore MJ, Aronin N, Khvorova A. Comparison of fully and partially chemically-modified siRNA in conjugate-mediated delivery *in vivo*. NAR, 2018. ***These authors contributed equally to this work.**

Anastasia Khvorova, Matthew Hassler, Anton Turanov, and I conceived of the project.

Matthew Hassler and I designed the sequences. Matthew Hassler and Dimas Echeverria

synthesized all of the compounds. Andrew Coles and Anton Turanov did injections.

Maire Osborn, Sarah Davis, Anton Turanov, and I contributed to *in vitro* dose responses.

Wes Salomon did Ago2 loading and turnover experiments. Reka Haraszti ran the PNA

assay. Anton Turanov and I processed *in vivo* tissue samples, and graphed and analyzed

the data. Matthew Hassler, Anton Turanov, Anastsia Khvorova and I wrote the

manuscript.

4.2 ABSTRACT

Small interfering RNA (siRNA)-based drugs require chemical modifications

and/or formulation to promote stability, minimize innate immunity, and enable delivery

to target tissues. Partially modified siRNAs (up to 70% of the nucleotides) provide

significant stabilization *in vitro* and are commercially available; thus are commonly used

to evaluate efficacy of bio-conjugates for *in vivo* delivery. In contrast, most clinically-

advanced non-formulated compounds, using conjugation as a delivery strategy, are fully

chemically modified (100% of nucleotides). Here we compare partially and fully

chemically modified siRNAs in conjugate mediated delivery. We show that fully

modified siRNAs are retained at 100x greater levels in various tissues, independently of

the nature of the conjugate or siRNA sequence, and support productive mRNA silencing.

Thus, fully chemically stabilized siRNAs may provide a better platform to identify novel

moieties (peptides, aptamers, small molecule) for targeted RNAi delivery.

4.3 INTRODUCTION

A variety of chemical modification patterns have been explored to improve

siRNA stability[123], ranging from the simple introduction of a dTdT overhang to highly

complicated patterns that remove the chemical nature of RNA[137]. Commonly used,

commercially available scaffolds include modification of every other nucleotide[138] or all

pyrimidines in a given sequence[139]. These "conventional" modification patterns

substantially enhance siRNA stability *in vitro*[140] and block innate immune activation *in*

vivo[25].

Partially modified siRNAs have been extensively used to study the impact of

conjugates on siRNA distribution and *in vivo* efficacy. A wide range of conjugate

modalities have been tested: steroids[141], lipids[142], folate[143], vitamins[62], aptamers[54], and

antibodies[51] all demonstrating only marginal efficacy. All of these conjugates were

evaluated in the context of naked or partially modified siRNA, miRNAs, and antisense

oligonucleotides.

A recent breakthrough in conjugate-mediated delivery was the development of the

triple N-acetylgalactosamine (GalNAc) conjugated siRNA[144, 145], which drives efficient,

receptor-mediated uptake into hepatocytes. The GalNAc-conjugated siRNAs were fully modified using an advanced version of an alternating 2′–fluoro, 2′–O–methyl pattern first described in 2005[138]. Additionally, in the context of single stranded RISC entering oligonucleotides chemical stabilization was shown to be absolutely essential for *in vivo* efficacy[145, 146]. Recently, fine-tuning of the chemical stabilization pattern, including increases in the 2′–O–methyl content, incorporation of additional phosphorothioates[145] and 5' phosphate stabilization[147-149] have been shown to even further enhance long-term efficacy of conjugated siRNAs.

Here we systematically compare the distribution, tissue accumulation, and efficacy of partially and fully modified siRNA scaffolds and show that full chemical stabilization of siRNA is preferred for *in vivo* applications, independently of the siRNA sequence or the nature of the conjugate used.

4.4 RESULTS

4.4.1 FULL CHEMICAL STABILIZATION ENABLES EFFICIENT CONJUGATE-MEDIATED SIRNA EFFICACY *IN VITRO*.

To compare the impact of fully or partially modified scaffolds on conjugate-mediated distribution and silencing *in vivo*, we used asymmetric, cholesterol-modified siRNAs as a model (Fig. 4.1a).
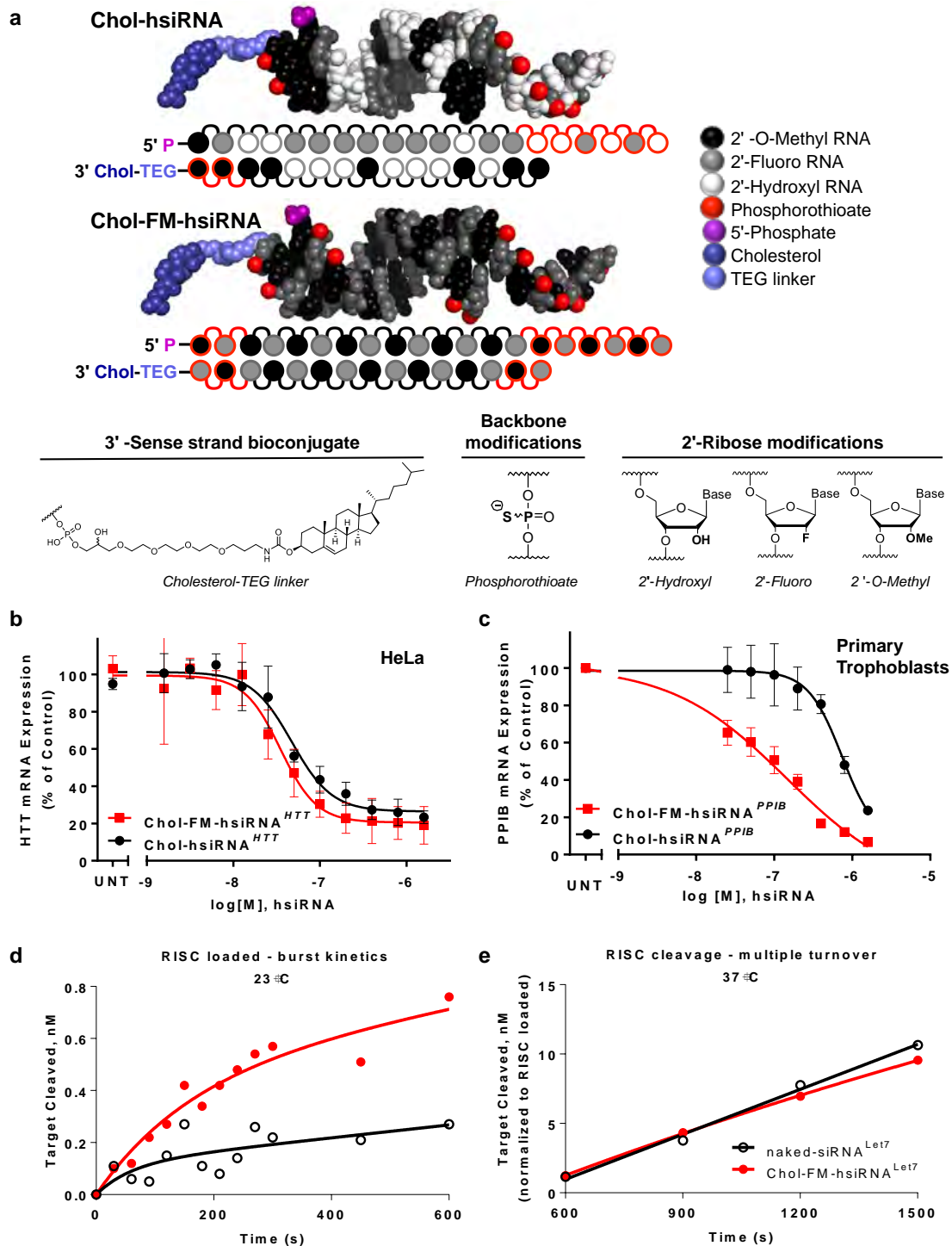
Figure 4.1 Chemical composition and cellular efficacy of fully modified hsiRNAs.
(**a**) Chemical structure, modification pattern, and molecular model of partially (hsiRNA)
and fully modified (FM-hsiRNA) hydrophobic siRNA. (**b,c**) Comparison of hsiRNA and
FM-hsiRNA activity *in vitro*. HeLa (**b**) or primary cytotrophoblasts (**c**) were incubated
with hsiRNA or FM-hsiRNA at concentrations shown for one week. mRNA levels were
measured using QuantiGene® (Affymetrix) normalized to housekeeping gene (human

Ppib for (**b**) and human *Ywhaz* for (**c**)), and presented as percent of untreated control (n=3, mean ± SD). UNT – untreated cells. (**d,e**) Preferential RISC loading of fully modified hsiRNA. (**d**) Concentration of loaded RISC with unmodified, naked-siRNA[Let7], or FM-hsiRNA[Let7] (**e**) Multiple turnover cleavage rate normalized to amount of loaded RISC with unmodified, naked-siRNA[Let7], or FM-hsiRNA[Let7].

The asymmetric design, termed hsiRNAs (15-nucleotide sense strand with a 3′-conjugate and 20-nucleotide guide strand) lowers the melting temperature of the double-strand region, to facilitate the dissociation of the non-cleavable modified sense strand from the RNA-Induced Silencing Complex (RISC) during loading. RISC loading can occur through passenger strand cleavage[150] or dissociation. Full chemical modification of the passenger strand blocks the cleavage pathway, leaving dissociation as the only functional alternative for RISC loading. This makes Tm of the fully chemically stabilized duplex one of the primary activity-limiting factors. The relative impact of asymmetric duplex configuration on compound efficacy is sequence dependent. Fig. 4.2a,b shows the activity of two siRNA sequences in the context of either the conventional symmetric (20-mer-20-mer) or asymmetric (15-mer-20-mer) duplex configuration. For the siRNA targeting HTT there is no difference between the two configurations, whereas for the siRNA targeting sFLT1, reduction in duplex length substantially improves compound efficacy. The single-strand region of the guide strand contains phosphorothioate linkages[26], providing additional stabilization and enhancing cellular internalization[151]. This chemical scaffold has been extensively characterized including mechanism of trafficking, clearance kinetics, systemic and local delivery[1, 35, 55, 56, 58, 59, 151, 152].
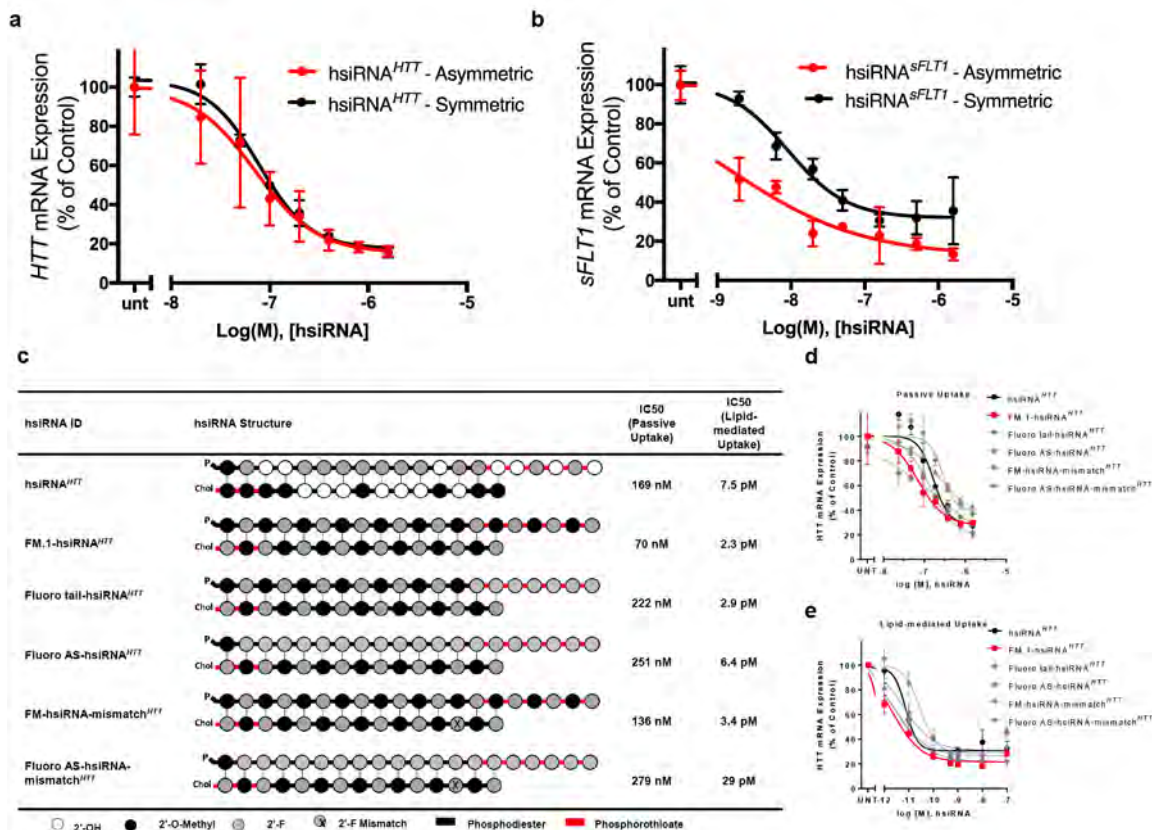
Figure 4.2 A comparison of symmetric and asymmetric siRNAs *in vitro* and screen of alternative FM-hsiRNAHTT patterns.
(a, b) The effect of duplex chemical configuration on siRNA activity is sequence dependent. HeLa cells were treated in the absence of cationic lipids with asymmetric and symmetric siRNAs targeting both HTT and sFLT1. HTT expression was measured using QuantiGene 2.0 (Affymetrix), normalized to the housekeeping gene HPRT and sFLT1 expression was measured using a luciferase reporter assay (c) Representative images of alternative modification patterns and their corresponding IC50s. IC50s calculated as described in Materials and Methods. Cells treated for 72 hours with compound in the (d) absence (e) or presence of cationic lipids. HTT mRNA was measured using QuantiGene 2.0 (Affymetrix), normalized to the housekeeping gene PPIB. All data is expressed as percent of untreated control . (n=3 wells, mean ± SD). UNT – untreated cells.

Cholesterol conjugation to partially modified hsiRNAs results in robust cellular uptake *in vitro* and potent local silencing *in vivo*[58, 59], but marginal systemic efficacy. Thus, cholesterol-conjugated siRNAs provide a good starting point to evaluate the impact of extensive chemical stabilization on conjugate-mediated hsiRNA delivery.

Using a previously identified, partially modified hsiRNA sequence targeting

huntingtin (Htt) mRNA[58], we synthesized and tested a panel of fully modified hsiRNAs

(FM-hsiRNAs) based on previously reported patterns[137, 138]. Though several

configurations were functional, an alternating 2′–O–methyl, 2′–fluoro pattern, with a

chemically monophosphorylated, 2′–O–methyl–modified uridine (U) at position 1, and a

2′-fluoro modified nucleotide at position 14 of the guide strand performed the best (Fig.

4.1a, Fig. 4.2c and Table 4.1). An alternating pattern with a 2′–fluoro in position 1 of the

guide strand reduced silencing activity (data not shown), likely due to placement of 2′–

O–methyl groups in positions 2 and 14, which negatively affects potency in the context

of heavily modified duplexes[153]. 5′ -Chemical phosphorylation of the guide strand was

performed, as terminal 2′–O–methylated U is not as good a substrate for intracellular

kinases as natural RNA. We also added two phosphorothioate linkages to both 5′ and 3′

ends of the sense and guide strands to provide additional resistance to exonucleases.

Figure 4.1a shows the modification patterns and PyMol structure models of the

conventionally modified hsiRNA and the most active fully modified hsiRNA (FM-

hsiRNA).

Table 4.1 hsiRNA sequences and chemical modification patterns

siRNA ID	Gene	Accession number	Targeting Position	Sense	Antisense	Conjugate
Chol-hsiRNA^{HTT}	HTT	NM_002111.6	10150	mC.mA.G.mU.A.A.A.mG.A.G.A.mU.mU#mA#mA	PmU.fU.A.A.fU.fC.fU.fC.fU.fU.fU.A.fC.fU#G#A#fU#A#fU#A	Teg-cholesterol
Chol-FM.1-hsiRNA^{HTT}	HTT	NM_002111.6	10150	fC.mA.fG.mU.fA.mA.fA.mG.fA.mG.fA.mU.fU#mA#fA#	PmU.fU.mA.fA.mU.fC.mU.fC.mU.fU.mU.fA.mC.fU#mG#fA#mU#fA#mU#fA	Teg-cholesterol
Chol-Fluoro tail-hsiRNA^{HTT}	HTT	NM_002111.6	10150	fC.mA.fG.mU.fA.mA.fA.mG.fA.mG.fA.mU.fU#mA#fA#	PmU.fU.mA.fA.mU.fC.mU.fC.mU.fU.mU.fA.mC.fU#fG#fA#fU#fA#fU#fA	Teg-cholesterol

86

Chol-Fluoro AS-hsiRNA[HTT]	HTT	NM_002111.6	10150	fC.mA.fG.mU.fA.mA. fA.mG.fA.mG.fA.mU .fU#mA#fA#	PmU.fU.fA.fA.fU.fC.fU.fC.fU.fU .fU.fA.fC.fU#fG#fA#fU#fA#fU#f A	Teg-cholesterol
Chol-FM.1-mismatch-hsiRNA[HTT]	HTT	NM_002111.6	10150	fC.mA.fU.mU.fA.mA. fA.mG.fA.mG.fA.mU .fU#mA#fA#	PmU.fU.mA.fA.mU.fC.mU.fC.m U.fU.mU.fA.mC.fU#mG#fA#mU #fA#mU#fA	Teg-cholesterol
Chol-Fluoro AS-mismatch-hsiRNA[HTT]	HTT	NM_002111.6	10150	fC.mA.fU.mU.fA.mA. fA.mG.fA.mG.fA.mU .fU#mA#fA#	PmU.fU.fA.fA.fU.fC.fU.fC.fU.fU .fU.fA.fC.fU#fG#fA#fU#fA#fU#f A	Teg-cholesterol
Chol-FM-hsiRNA[HTT]	HTT	NM_002111.6	10150	fC#mA#fG.mU.fA.m A.fA.mG.fA.mG.fA. mU.fU#mA#fA	PmU#fU#mA.fA.mU.fC.mU.fC. mU.fU.mU.fA.mC#fU#mG#fA# mU#fA#mU#fA	Teg-cholesterol
Chol-hsiRNA[sFLT1]	sFLT1	NM_0011599 20	2283	mG.mA.mU.mC.mU. mC.mC.A.A.A.mU.m U.mU#mA#mA	PmU.A.A.A.fU.fU.fU.G.G.mA.G. A.fU.fC#fC#G#A#G#A#G	Teg-cholesterol
Chol-FM-hsiRNA[sFLT1]	sFLT1	NM_0011599 20	2283	fG#mG#fA.mU.fC.m U.fC.mC.fA.mA.fA.m U.fU#mU#fA	PmU#fA#mA.fA.mU.fU.mU.fG. mG.fA.mG.fA.mU#fC#mC#fG# mA#fG#mA#fG	Teg-cholesterol
Chol-hsiRNA[PPIB]	PPIB	NM_009693.2	437	mC.mA.A.A.mU.mU. mC.mC.A.mU.mC.G. mU#mG#mA#	PmU.fC.A.fC.G.A.fU.G.G.mA.A. fU.fU.fU#G#fC#fU#G#U#U	Teg-cholesterol
Chol-FM-hsiRNA[PPIB]	PPIB	NM_009693.2	437	fC#mA#fA.mA.fU.m U.fC.mC.fA.mU.fC.m G.fU#mG#fA	PmU#fC#mA.fC.mG.fA.mU.fG. mG.fA.mA.fU.mU#fU#mG#fC# mU#fG#mU#fU	Teg-cholesterol
GalNAc-hsiRNA[HTT]	HTT	NM_002111.6	10150	mC.mA.G.mU.A.A.A. mG.A.G.A.mU.mU# mA#mA	PmU.fU.A.A.fU.fC.fU.fC.fU.fU.f U.A.fC.fU#G#A#fU#A#fU#A	GalNAc
GalNAc-FM-hsiRNA[HTT]	HTT	NM_002111.6	10150	fC#mA#fG.mU.fA.m A.fA.mG.fA.mG.fA. mU.fU#mA#fA	PmU#fU#mA.fA.mU.fC.mU.fC. mU.fU.mU.fA.mC#fU#mG#fA# mU#fA#mU#fA	GalNAc
siRNA[HTT]	HTT	NM_002111.6	10150	mA.mU.A.U.C.A.G.U .A.A.A.G.A.G.A.U.U. A.A.U.U	PU.U.A.A.U.C.U.C.U.U.U.A.C.U .G.A.U.A.U.U.U	none
DHA-hsiRNA[sFLT1]	sFLT1	NM_0011599 20	2283	mG.mA.mU.mC.mU. mC.mC.A.A.A.mU.m U.mU#mA#mA	PmU.A.A.A.fU.fU.fU.G.G.mA.G. A.fU.fC#fC#G#A#G#A#G	DHA
DHA-FM-hsiRNA[sFLT1]	sFLT1	NM_0011599 20	2283	fG#mG#fA.mU.fC.m U.fC.mC.fA.mA.fA.m U.fU#mU#fA	PmU#fA#mA.fA.mU.fU.mU.fG. mG.fA.mG.fA.mU#fC#mC#fG#m A#fG#mA#fG	DHA
DHA-FM-hsiRNA[PPIB]	PPIB	NM_009693.2	437	fC#mA#fA.mA.fU.m U.fC.mC.fA.mU.fC.m G.fU#mG#fA	PmU#fC#mA.fC.mG.fA.mU.fG. mG.fA.mA.fU.mU#fU#mG#fC# mU#fG#mU#fU	DHA
v**Chol-hsiRNA**[PPIB]	PPIB	NM_009693.2	437	mC.mA.A.A.mU.mU. mC.mC.A.mU.mC.G. mU#mG#mA#	VmU.fC.A.fC.G.A.fU.G.G.mA.A .fU.fU.fU#G#fC#fU#G#U#U	Teg-cholesterol
v**Chol-FM-hsiRNA**[PPIB]	PPIB	NM_009693.2	437	fC#mA#fA.mA.fU.m U.fC.mC.fA.mU.fC.m G.fU#mG#fA	VmU#fC#mA.fC.mG.fA.mU.fG. mG.fA.mA.fU.mU#fU#mG#fC# mU#fG#mU#fU	Teg-cholesterol
v**Chol-hsiRNA**[HTT]	HTT	NM_002111.6	10150	mC.mA.G.mU.A.A.A. mG.A.G.A.mU.mU# mA#mA	VmU.fU.A.A.fU.fC.fU.fC.fU.fU.f U.A.fC.fU#G#A#fU#A#fU#A	Teg-cholesterol
v**Chol-FM-hsiRNA**[HTT]	HTT	NM_002111.6	10150	fC#mA#fG.mU.fA.m A.fA.mG.fA.mG.fA. mU.fU#mA#fA	VmU#fU#mA.fA.mU.fC.mU.fC. mU.fU.mU.fA.mC#fU#mG#fA# mU#fA#mU#fA	Teg-cholesterol

[v]**Chol-hsiRNA**[sFLT1]	sFLT1	NM_0011599 20	2283	mG.mA.mU.mC.mU. mC.mC.A.A.A.mU.m U.mU#mA#mA	VmU.A.A.A.fU.fU.fU.G.G.mA.G .A.fU.fC#fC#G#A#G#A#G	Teg-cholesterol
[v]**Chol-FM-hsiRNA**[sFLT1]	sFLT1	NM_0011599 20	2283	fG#mG#fA.mU.fC.m U.fC.mC.fA.mA.fA.m U.fU#mU#fA	VmU#fA#mA.fA.mU.fU.mU.fG. mG.fA.mG.fA.mU#fC#mC#fG# mA#fG#mA#fG	Teg-cholesterol
PNA[PPIB]	PPIB	NM_009693.2	437	A*A*C*A*G*C*A* A*A*T*T*C*C*A*T *C*G*T*G*A		CY3 -(OO)-
PNA[HTT]	HTT	NM_002111.6	10150	T*A*T*A*T*C*A*G *T*A*A*A*G*A*G* A*T*T*A*A		CY3 -(OO)-
PNA[sFLT1]	sFLT1	NM_0011599 20	2283	C*T*C*T*C*G*G*A *T*C*T*C*C*A*A* A*T*T*T*A		CY3 -(OO)-

Chemical modifications are designated as follows. "." – phosphodiester bond, "#" – phosphorothioate bond, "m" – 2'-*O*-methyl, "f" – 2'-Fluoro, no prefix – ribonucleotide, "P" – 5' Phosphate, , "V" – 5' Vinyl phosphonate, "teg-cholesterol" – tetraethylene glycol (teg)-Cholesterol, GalNAc – trivalent N-Acetylgalactosamine, (OO) – O-linker (PNA Bio), DHA – docosahexaenoic acid

The FM-hsiRNA pattern supported similar or improved silencing when applied to previously identified functional siRNAs targeting Htt, Ppib, sFlt1, Tie2[154], Plk1, and Sod1 mRNAs (Fig. 4.1b,c, Fig 4.2, 4.3 and data not shown).
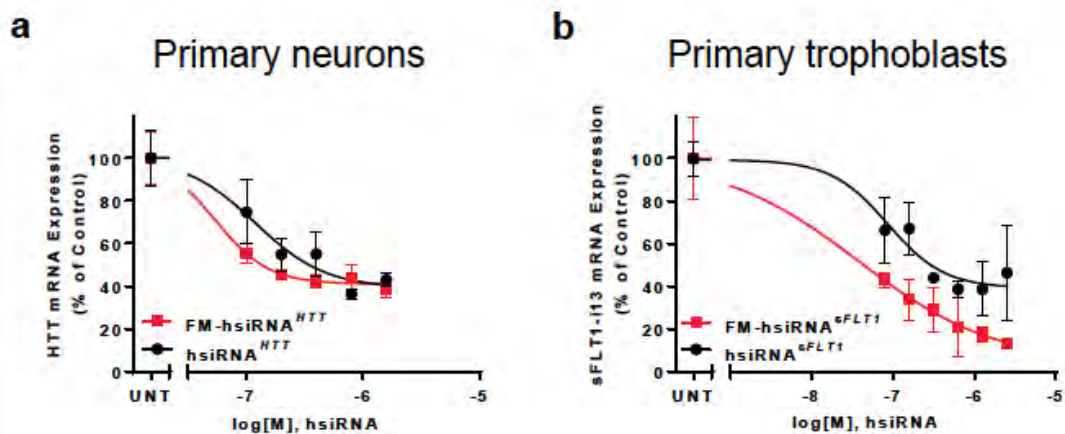
Figure 4.3 Comparison of hsiRNA and FM-hsiRNA activity cultured cells.
Primary neurons (a) or primary cytotrophoblasts (b) were incubated with hsiRNA or FM-hsiRNA at concentrations shown for one week.mRNA levels were measured using QuantiGene® (Affymetrix) normalized to housekeeping gene (mouse PPIB for (a) and human Ywhaz for (b)), and presented as percent of untreated control (n=3, mean $\pm$ SD). UNT – untreated cells.

Moreover, FM-hsiRNAs improved silencing in cultured primary neurons and primary trophoblasts, adherent and suspension cell types, respectively, the latter of which are notoriously difficult to transfect by conventional methods[109, 155]. The activity improvement provided by full chemical stabilization was more pronounced in the non-adherent primary trophoblasts where cholesterol mediated uptake is generally slower (Fig. 4.1c). When directly compared to an unmodified, unconjugated siRNA, Chol-FM-hsiRNA showed significantly enhanced efficacy following passive uptake (IC50 of 33.5 nM) while naked siRNA is inactive. However, both compounds showed comparable

potency (IC50 of 3.5 nM for siRNA and 0.9 nM FM-hsiRNA) following lipid

transfection, further confirming that full modification is compatible with RISC function

in cells (Fig. 4.4).
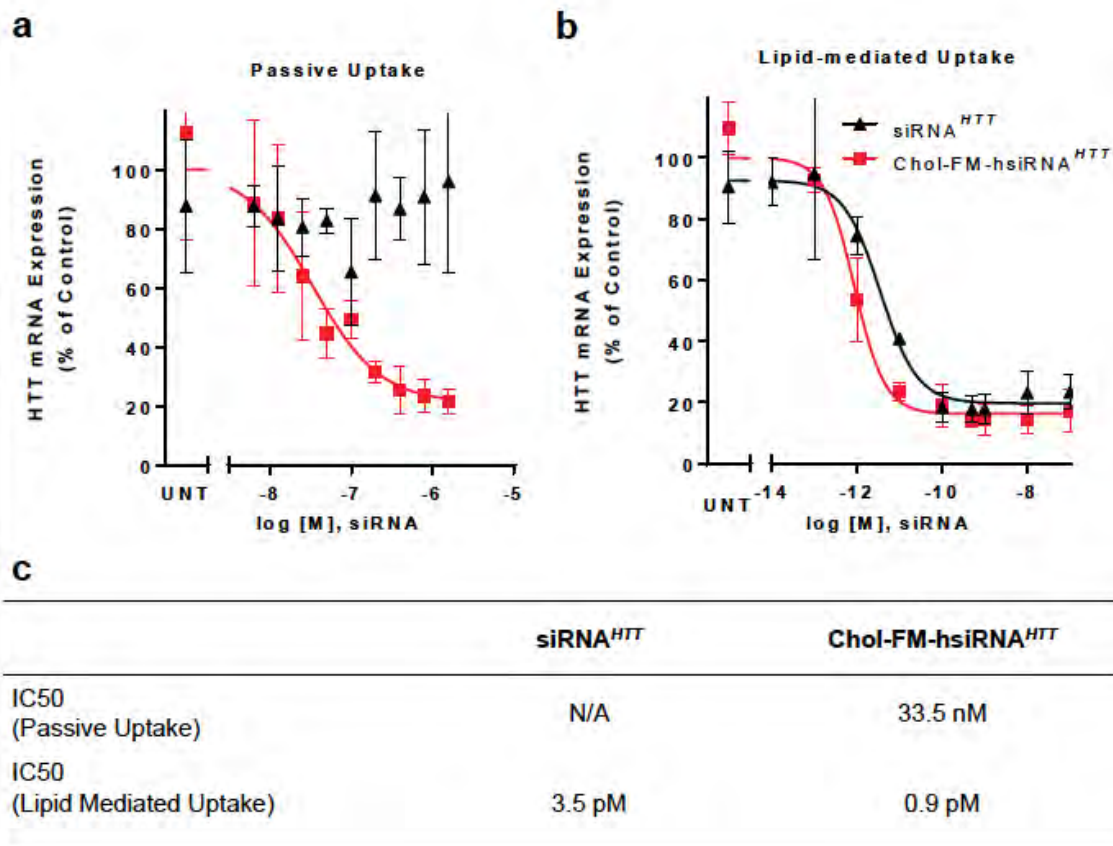
Figure 4.4 Full chemical modification is essential for unassisted cellular delivery and does not compromise siRNA RISC entry.
HeLa Cells treated for 72 hours with compound in the (a) absence or (b) presence of cationic lipids. Htt mRNA was measured using QuantiGene®, normalized to the housekeeping gene PPIB, and expressed as percent of untreated control. (n=3 wells, mean ± SD). UNT – untreated cells. IC50 values were calculated as described in Materials and Methods and are presented in table (c).

Similarly, fully modified GalNAc-conjugated siRNAs were more active in

primary hepatocytes than partially modified GalNAc-conjugated siRNAs (Fig. 4.5),

indicating that improvement in potency is not specific to the nature of the conjugate or

the cell type treated.
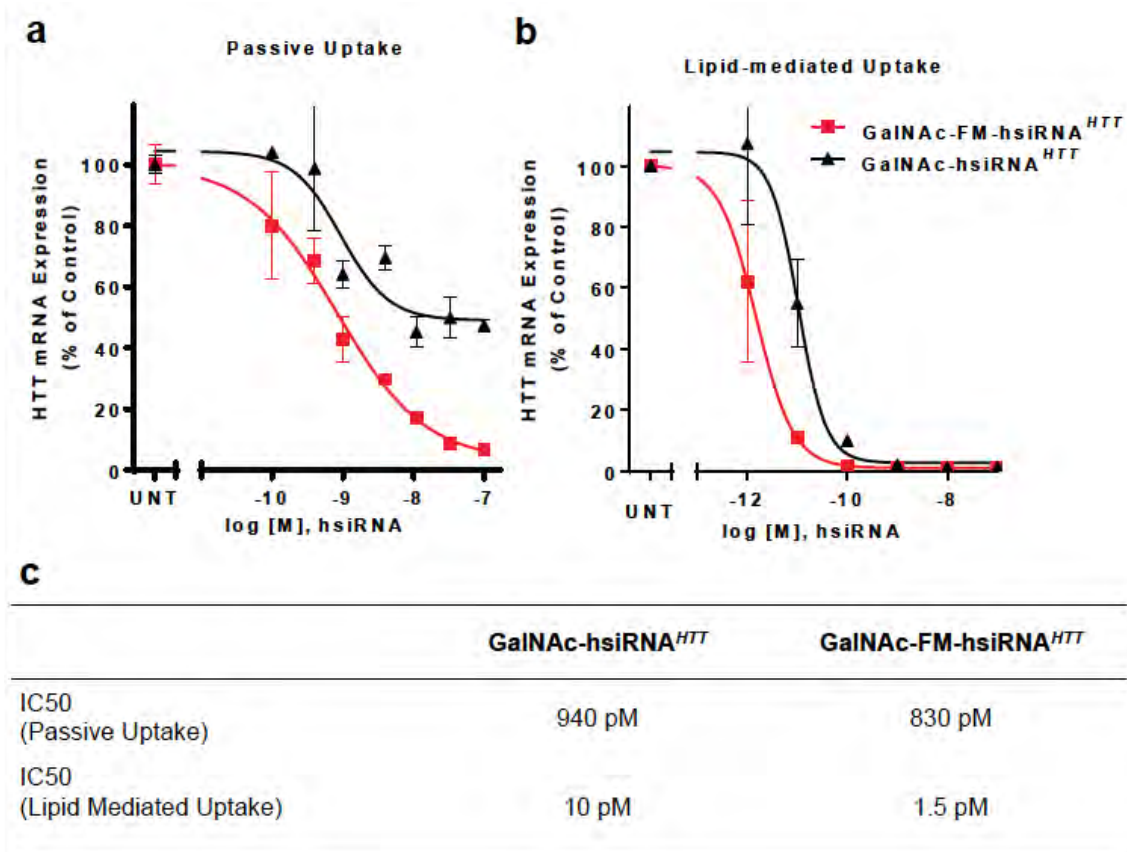
Figure 4.5 Full chemical modification enhances GalNAc-mediated mRNA silencing in human primary hepatocytes.
Cells treated for 72 hours with compound in the (a) absence or (b) presence of cationic lipids. Htt mRNA was measured using QuantiGene®, normalized to the housekeeping gene Ppib, and expressed as percent of untreated control. (n=3 wells, mean ± SD). UNT – untreated cells. IC50 values were calculated as described in Materials and Methods and are presented in table (c).

4.4.2 FULLY CHEMICALLY MODIFIED SIRNAS ARE EFFICIENTLY LOADED INTO RISC COMPLEX

The loading and cleavage rates of FM-hsiRNA were compared to a completely non-modified Let-7 siRNA in a loading and cleavage assay described earlier[156]. The FM-hsiRNA loaded almost three times more RISC complex compared to the naked siRNA

91

(Fig. 4.1d), which is likely associated with the enhanced stability of FM-hsiRNA. Once the loaded RISC was under multiple turnover conditions (37°C), the *in vitro* cleavage rates of both the FM-hsiRNA and the non-modified oligo were similar (after normalizing to equal numbers of loaded RISC) (Fig. 4.1e). Thus, full modification does not interfere with the ability of the tested oligonucleotide to be recognized by, and functionally load the RISC complex.

4.4.3 COMPARISON OF PARTIALLY AND FULLY CHEMICALLY MODIFIED SIRNAS IN CONJUGATE-MEDIATED SYSTEMIC DELIVERY.

Both partially modified (e.g., all pyrimidines) and fully modified siRNAs have increased stability *in vitro* (from minutes to days in 50% serum) over non-modified siRNAs[138, 139]. *In vivo*, however, oligonucleotides are exposed to an aggressive nuclease environment that cannot be adequately mimicked *in vitro*. Thus the stability of partially and fully modified siRNAs might be quite different from one another *in vivo*. To compare the distribution of partially modified and fully modified hsiRNAs *in vivo*, we administered 10 mg/kg of Cy3-labeled Chol (cholesterol)-hsiRNA and Chol-FM-hsiRNA by intravenous (IV) or subcutaneous (SC) injection (Fig. 4.6a,b). Twenty-four hours after injection, we harvested tissues from mice and visualized the siRNA distribution by fluorescence microscopy. Injection of partially modified Cy3-Chol-hsiRNA resulted in minimal levels of fluorescence, observed only in liver and kidney. By contrast, injection of Cy3-Chol-FM-hsiRNA resulted in intense accumulation of fluorescence in tissues throughout the body, including liver, kidney, spleen, fat, and skin (Fig. 4.6a, b and Data not shown).
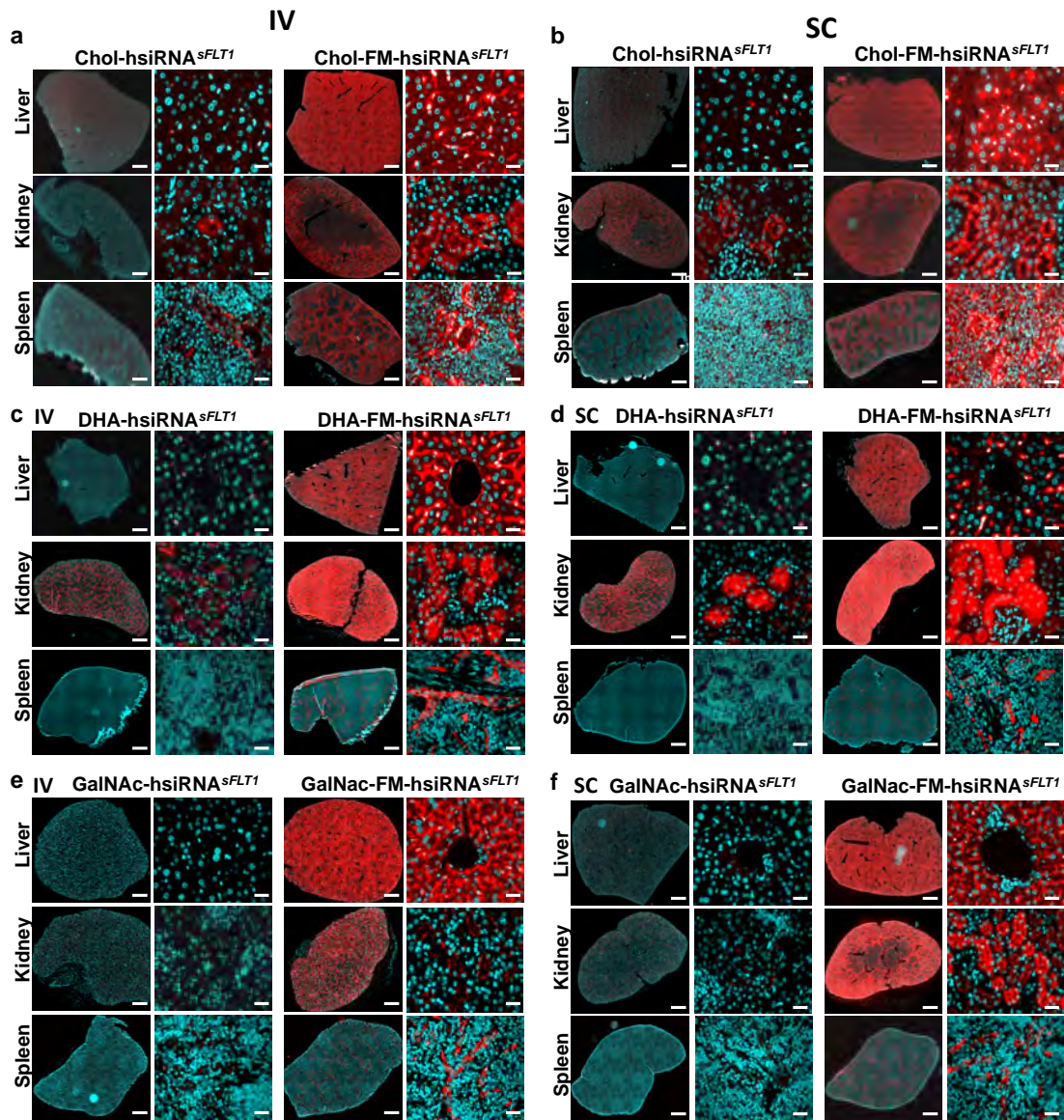
Figure 4.6 Systemically administered fully modified hsiRNA shows enhanced tissue distribution.

Tissue distribution of Cy3-Chol-hsiRNA^{sFLT1} and Cy3-Chol-FM-hsiRNA^{sFLT} after 10 mg/kg intravenous (IV) tail vein injection (**a**) or 10 mg/kg subcutaneous (SC) injection (**b**). Tissue distribution of Cy3-DHA-hsiRNA^{sFLT1} and Cy3-DHA-FM-hsiRNA^{sFLT} after 10 mg/kg intravenous (IV) tail vein injection (**c**) or 10 mg/kg subcutaneous (SC) injection (**d**). Tissue distribution of Cy3-GalNAc-hsiRNA^{sFLT1} and Cy3-GalNAc-FM-hsiRNA^{sFLT} after 10 mg/kg intravenous (IV) tail vein injection (**e**) or 10 mg/kg subcutaneous (SC) injection (**f**). Cy3-hsiRNA (red), nuclei stained with DAPI (blue). For every chemistry the left panels are tiled tissue images (scale bar – 1 mm) and the right panels are higher magnification tissue images (scale bar – 25 uM). Image is representative.

To evaluate whether a significant enhancement in retention upon full chemical stabilization is not specific to the cholesterol conjugate, we evaluated two other conjugates with potential for tissue delivery: Docosahexaenoic acid (DHA)[150], and GalNAc[144]. The fully modified and partially modified GalNAc and DHA conjugate compounds were synthesized and their tissue distribution evaluated 24 hours post IV and SC injection (Fig. 4.6 c-f). As with cholesterol, we observed a substantial increase in compound tissue accumulation with the FM-hsiRNA, independently of the nature of the conjugate. It is important to notice that changing the conjugate resulted in a change in tissue distribution profile, which could only be visualized in the context of fully modified hsiRNA.

To insure that qualitative robust difference observed in fluorescence distribution between partially and fully modified hsiRNAs is not an artifact of tissue processing or presence of the fluorescent label, we used a PNA hybridization-based assay[152, 157] to evaluate the accumulation of these compounds quantitatively. This method allows for the detection of intact guide strands present in tissue biopsies and is not dependent on the presence of the fluorescent label.

Figure 4.7 shows the quantification data for the three different conjugates (Cholesterol, DHA, and GalNAc) attached to fully and partially modified hsiRNA scaffolds injected SC and IV.
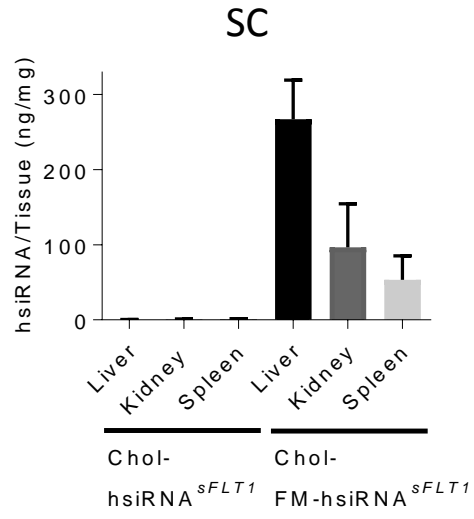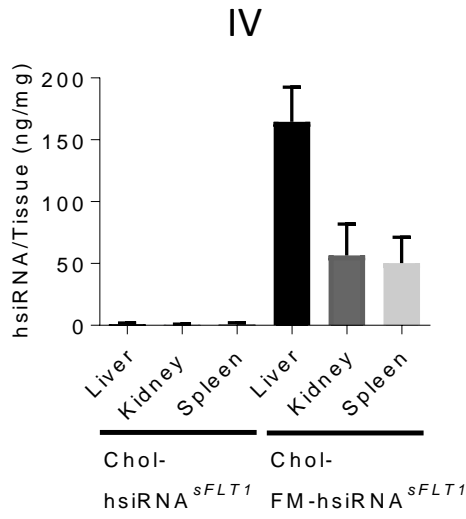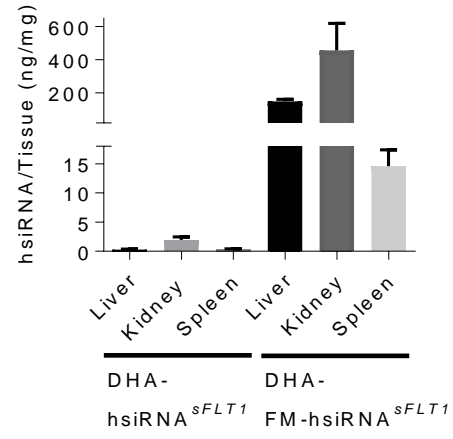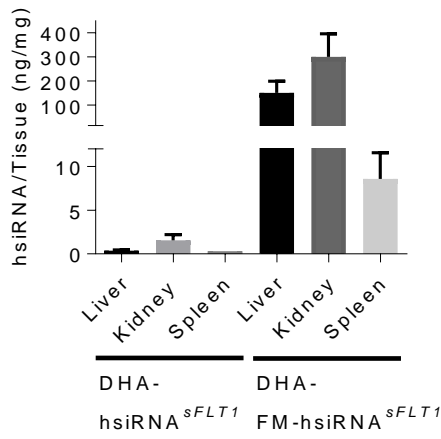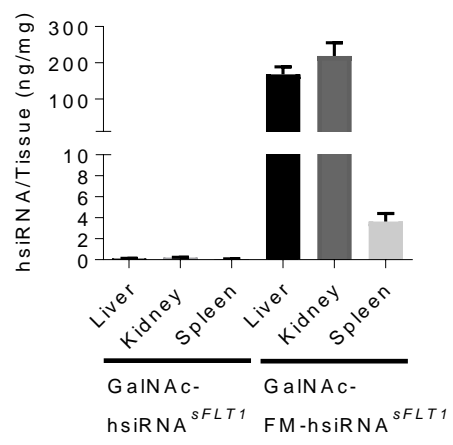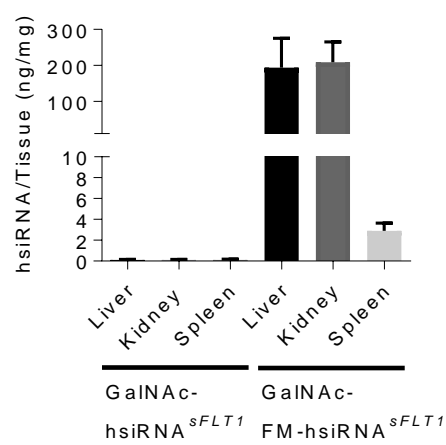
Figure 4.7 Systemic administration of fully modified hsiRNAs shows enhanced tissue accumulation
Guide strand tissue quantification by PNA hybridization-based assay in tissues from Figure 4.6. Guide strand quantification of Cy3-Chol-hsiRNA^{sFLT1} and Cy3-Chol-FM-hsiRNA^{sFLT} after 10 mg/kg intravenous (IV) tail vein injection (a) or 10 mg/kg subcutaneous (SC) injection (b). Guide strand quantification of Cy3-DHA-hsiRNA^{sFLT1} and Cy3-DHA-FM-hsiRNA^{sFLT} after 10 mg/kg intravenous (IV) tail vein injection (c) or 10 mg/kg subcutaneous (SC) injection (d). Guide strand quantification of Cy3-GalNAc-hsiRNA^{sFLT1} and Cy3-GalNAc-FM-hsiRNA^{sFLT} after 10 mg/kg intravenous (IV) tail vein injection (e) or 10 mg/kg subcutaneous (SC) injection (f). Data presented as mean ± SD (n=3 mice).

In all cases, independently of the route of administration, or the type of conjugate, over 100x tissue accumulation was observed of fully chemically modified siRNAs relative to the partially chemically modified siRNAs. FM-hsiRNA guide strands accumulated to relatively high levels, 20-200 ng/mg in liver, kidney, and spleen (Fig. 4.6 b,c). Consistent with the imaging data, the tissue distribution profile was effected by the type of conjugate used, with cholesterol preferentially accumulating in liver (~ 150 ng/mg), DHA in kidney (300-400 ng/mg) and GalNAc in both liver and kidney (~200 ng/mg). While cholesterol and DHA show distribution to tissues beyond the liver and kidney, such as the spleen, skin, and fat (data not shown), GalNAc distribution was effectively exclusive to liver and kidney (Fig. 4.6e,f). Hence, full chemical stabilization significantly enhances conjugate-mediated tissue accumulation independent of the conjugate nature, or route of administration, and is heavily reliant on the full chemical modification of the siRNA.

4.4.4 FULL CHEMICAL STABILIZATION ENABLES PRODUCTIVE SILENCING *IN VIVO*.

The poor accumulation and retention of partially modified hsiRNAs is consistent with published studies showing that systemic silencing by partially modified siRNA lipophilic conjugates requires repetitive delivery with high doses (50 to 80 mg/kg)[142]. Consistently, when cholesterol-conjugated partially modified hsiRNA was delivered systemically at 2x50 mg/kg dose levels we were unable to detect silencing, even in the liver, a primary tissue where cholesterol modified siRNAs distribute.

To confirm that significant FM-hsiRNA tissue accumulation results in functional gene silencing, we evaluated silencing efficiency in the liver and the kidney. For this experiment, we selected the following targets: Ppib, a commonly used housekeeping gene expressed in all cell types, Htt, a key target in Huntington's Disease, also expressed in all cell types, and sFlt1 (soluble fms-like tyrosine kinase 1 or VEGFR1), which is primarily expressed in endothelial cells and kidney proximal tubules epithelia, where Chol-FM-hsiRNAs tend to accumulate (Fig. 4.6 a, b).

We, and others, have recently demonstrated that chemical stabilization of the 5' phosphate of the guide strand increases *in vivo* efficacy of siRNA conjugates[35, 36, 149]. Thus for evaluation of targeted gene silencing *in vivo*, partially and fully modified siRNA scaffolds were synthesized with a 5'-(E)-VP (vinyl phosphonate). Animals were injected with 20 mg/kg of fully and partially modified hsiRNAs. The level of targeted gene expression was evaluated a week post injection using the QuantiGene® Assay. We also injected a non-targeting control (NTC), compounds of the same chemical composition but not targeting the intended mRNA, and PBS (phosphate buffered saline) as controls.

For all three genes tested, injection of controls resulted in no significant changes in gene expression. In contrast, all three genes were significantly silenced in liver after injection of a fully chemically stabilized variant (Fig. 4.9 a-c).
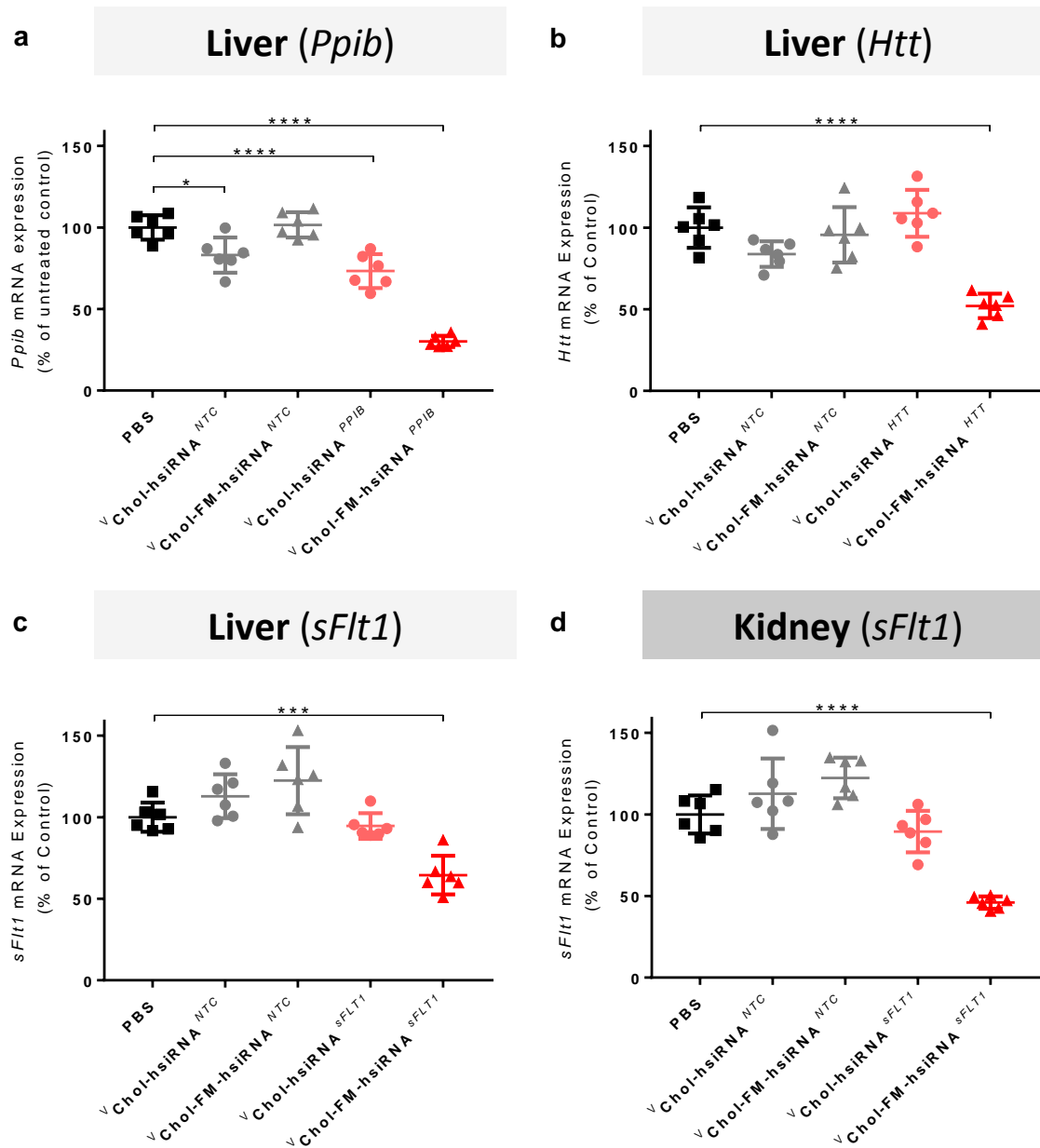
Figure 4.8 Fully modified hsiRNAs are more efficacious than partially modified hsiRNAs following systemic administration.
(a, b, c) Quantification of target *(Ppib, Htt, sFlt1,* respectively*)* mRNA silencing in liver 7 days after SC administration of cholesterol-conjugated VhsiRNA*NTC*, VFM-hsiRNA*NTC*, VhsiRNA*Target*, VFM-hsiRNA*Target* at 20 mg/kg. **(d)** Quantification of *Ppib* mRNA silencing in kidney 7 days after SC administration of cholesterol-conjugated VhsiRNA*NTC*, VFM-hsiRNA*NTC*, VhsiRNA*sFLT1*, VFM-hsiRNA*sFLT1* at 20 mg/kg. FVBNj mice (n=6 per group). mRNA levels were measured with QuantiGene® (Affymetrix) assay. *Htt*, *Ppib*, and *sFlt1* mRNA levels normalized to housekeeping gene, *Hprt*. All data presented as percent of PBS treated control. All error bars represent mean ± SD. *, P<0.05, ***, *P*<0.001; ****, *P*<0.0001 as calculated by One Way ANOVA with Tukey's test for multiple comparisons. NTC – non-targeting control.

The same phenomenon was observed in kidney, where sFlt1 was significantly

downregulated by Chol-FM-hsiRNAs (Fig. 4.10d). In both liver and kidney partially

modified hsiRNA did not support efficient silencing. The degree of silencing varies from

target to target and is likely due to differences in cell types and levels of target mRNA

expression. While distribution and efficacy are significantly enhanced by full chemical

modification, injection of cholesterol, DHA and GalNAc-conjugated, fully chemically

modified, siRNAs were well tolerated at the doses injected, with animals showing no

observable adverse events or changes in blood chemistry (data not shown).

To confirm that this phenomenon also holds true with local delivery, both

hsiRNA^{HTT} and FM-hsiRNA^{HTT} were injected unilateral into the brain striatum. FM-

hsiRNA showed not only greater potency (Fig. 4.11a) but also maintains silencing for up

to 4 weeks (Fig. 4.11b).
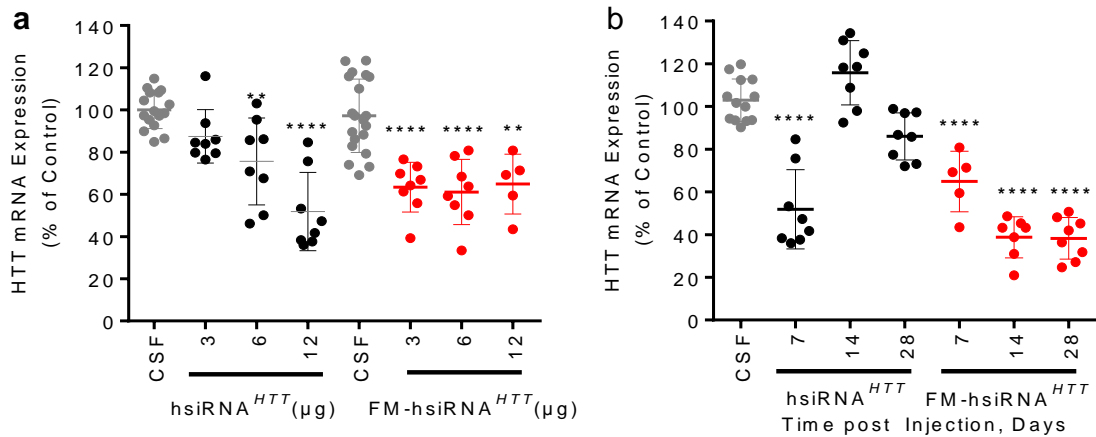
Figure 4.9 Fully modified hsiRNAs are more efficacious than partially modified hsiRNAs following intrastriatal injection.
(a) Quantification of *Htt* mRNA silencing in brain 7 days after intrastriatal administration of cholesterol-conjugated hsiRNA[HTT], FM-hsiRNA[HTT] **(b)** Quantification of *Htt* mRNA silencing in brain at different timepoints. FVBNj mice. mRNA levels were measured with QuantiGene® (Affymetrix) assay. mRNA levels normalized to housekeeping gene, *Hprt*. All data presented as percent of PBS treated control. All error bars represent mean ± SD. *, $P<0.05$, **, $P<0.01$, ***, $P<0.001$; ****, $P<0.0001$ as calculated by One Way ANOVA with Tukey's test for multiple comparisons.

This confirms that full chemical stabilization enables both siRNA tissue accumulation and productive silencing.

4.5 DISCUSSION

Here we have compared partially and fully chemical modified siRNA scaffolds in conjugate mediated delivery *in vitro* and *in vivo*. We have utilized a simple siRNA scaffold, utilizing an alternating 2′-fluoro, 2′-*O*-methyl modification[138] pattern in the context of an asymmetric siRNA. We have shown that full chemical modification does not interfere with RISC assembly and target cleavage *in vitro* and supports the activity of previously identified, functional siRNA sequences in cell culture. In fact, this chemical configuration supports efficient RISC loading (similar or better than non-modified RNA

duplex) and target cleavage *in vitro*, allows productive RISC assembly and function in cells and *in vivo* in animals.

Historically, extensive chemical modifications of siRNAs were shown to negatively impact siRNA efficacy, resulting only in a small fraction of functional, naked siRNAs being successfully converted to modified scaffolds[123, 158, 159]. The two major contributors to modification-related negative impact on silencing activity are modifications forcing the nucleic acid into a suboptimal geometry (both for loading and target cleavage) and/or making the duplex too stable, interfering with guide strand loading[150]. Indeed, complete modification of the guide strand with 2′-fluoro resulted in almost three-fold drop in silencing efficacy *in vitro*. Both, 2′-fluoro and 2′-*O*-methyl modifications favor the C3′-endo ribose conformation, but 2′-fluoro modifications slightly over-wind the duplex and 2′-*O*-methyl slightly under-wind the RNA duplex. In addition, 2′-fluoro modification is more hydrophobic and thus might contribute to enhancement in cellular uptake and *in vivo* distribution[160]. Alternating these two types of modifications supports formation of an A-form helical structure, the geometry required for guide strand-based positioning of the targeted mRNA into the cleavage center of RISC[161]. This is consistent with the recently published crystal structure of fully modified guide strand showing ability to adopt variety of confirmations[23] Alternating 2′-fluoro and 2′-*O*-methyl modifications on both strands pairing 2′-fluoro on one strand with 2′-*O*-methyl on the other weakens the modification-induced thermodynamic gain[137, 138] and reduces the sequence related biases. The shorter (15-nucleotide) duplex region will also help to promote release of the non-cleavable sense strand, alleviating a major thermodynamic limiting step in RISC assembly with fully modified, FM-hsiRNAs[161].

Our findings suggest that RISC assembled with the asymmetric fully modified-siRNA is as effective as RISC assembled with non-modified siRNAs (Fig. 4.1d, e) and potentially load more efficiently. This modification pattern can be applied to previously validated siRNA sequences, as the Htt and Ppib sequences used in this study were originally discovered using a partially modified scaffold. By switching the sequence to the fully modified pattern we effectively reduced the IC50 by almost 2.5x *in vitro*. We are in a process of evaluating the exact impact of these chemistries on RISC assembly and cleavage kinetics using single molecule approaches[12].

Interestingly, the relative impact of full chemical modification on *in vitro* efficacy was significantly less pronounced than *in vivo*. Similar effects have been seen for 5' phosphate stabilization where *in vitro*, 5′-vinyl phosphate and 5′ phosphate hsiRNAs show similar efficacy, while *in vivo* phosphate stabilization clearly enhances efficacy[35]. It is likely that in the harsh biological environment of systemic delivery, chemical stabilization impact on efficacy is much more pronounced than *in vitro* or upon local delivery.

Systemically administered FM-hsiRNAs accumulate in tissues throughout the body, including liver, kidney, spleen, fat, and skin. As expected, all oligonucleotides, including lipophilic conjugated siRNAs[119, 142] preferentially accumulated in the liver and silencing of the target genes was observed in those tissues. Additionally, significant levels of compound accumulated in the kidneys and spleen (Fig. 4.2a-d and Fig. 4.3), but importantly the substantial differences observed between the fully and partially modified siRNAs were not dependent on the nature of the conjugates themselves but rather the modification pattern of the siRNA.

The increase in tissue accumulation (50-250 ng/mg) by full chemical modification was observed with different conjugates, but it was predominantly the nature of conjugate that had an impact on tissue distribution profile. This is consistent with a recently published paper demonstrating that cholesterol modified siRNAs can silence genes in muscle, although dose levels necessary to achieve this effect were high (50mg/kg)[60]. DHA-conjugates accumulate to a higher extent in the kidneys, indicating that changing the nature of the conjugate can be used as a strategy to alter tissue distribution. Interestingly, with GalNac-hsiRNAs we observed similar distribution between kidneys and liver, specifically after SC administration. This was surprising, as GalNAc internalization is believed to be dependent on ASGPR (asialoglycoprotein receptor) overexpressed in hepatocytes. It is possible that partial kidney delivery is due to the presence of the single stranded phosphorothioated tail or the oversaturation of the ASGPR receptors at the dose levels used in this study (10 mg/kg).

With increased accumulation we observed an increase in productive silencing. However, the level of silencing was not directly proportional to the increase in siRNA tissue accumulation. It is well understood that for both antisense and siRNAs a significant fraction of internalized compounds is trapped nonproductively and different cells accumulate oligonucleotides to different degrees. This phenomenon is the subject of active investigation.

While the nature of the conjugate clearly effected tissue accumulation, these effects can be observed only in the context of a fully chemically modified scaffold. This demonstrates that some previously discarded or dismissed siRNA conjugates evaluated in

the context of partially or non-modified siRNAs might have served as viable delivery

strategies and may be worth retesting in the context of a fully modified pattern.

CHAPTER V: DIVALENT-SIRNAS: AN ADVANCED CHEMICAL SCAFFOLD FOR POTENT AND SUSTAINED MODULATION OF GENE EXPRESSION IN THE CNS.

5.1 PREFACE

Text and figures are reproduced from

Matthew Hassler, Bruno Godinho, Anastasia Khvorova, and I conceived of this project.

Matthew Hassler, Dimas Echeverria, and Loic Roux synthesized the compounds. Bruno Godinho and I did all of the mouse surgeries and tissue processing with help from Emily Knox. Bruno and I did the mouse mRNA processing, and Ellen Sapp did all of the HTT western blots. Chantal Ferguson did the APOE western blot and we both processed the monkey tissue. Robert King did the MRI. Paul Yan and Athma Pai did the RNAseq. All remaining authors contributed to large animal studies. I performed the majority of data analysis and statistical analysis. Bruno Godinho, Matthew Hassler, Chantal Ferguson, Anastasia Khvorova and I wrote the manuscript.

5.2 ABSTRACT

Small interfering RNAs (siRNAs) are a promising class of drugs for treating genetically-defined diseases. Therapeutic siRNAs enable simple and specific modulation of gene expression, but require chemical architecture that facilitates efficient *in vivo*

delivery. Here we describe an siRNA scaffold—Divalent-siRNA (Di-siRNA)—that supports potent and sustained gene silencing in the central nervous system (CNS) of mice and non-human primates, following a single injection into cerebrospinal fluid. Di-siRNAs are composed of two fully chemically stabilized, phosphorothioate containing siRNAs connected by a linker. In mice, Di-siRNAs induced potent silencing of huntingtin (causative gene in Huntington's disease) mRNA and protein throughout the brain one month after injection. Silencing persisted for at least six months, with the degree of gene silencing correlating to guide strand tissue accumulation levels. In Cynomolgus macaques, a bolus injection of 25 mg Di-siRNA exhibited significant distribution and robust silencing throughout the brain and spinal cord without detectable toxicity and minimal off-targeting effects. Broad distribution and efficacy of Di-siRNA likely depends on the cooperative binding of phosphorothioate-driven cellular interactions and its large size, contributing to favorable pharmacokinetic properties. This new siRNA architecture opens the CNS for RNAi-based gene modulation, creating a path towards developing treatments for genetically-defined neurological disorders.

5.3 INTRODUCTION

Oligonucleotide therapeutics are an emerging class of drugs that enable potent and efficient modulation of gene expression *in vivo*. Unlike traditional small molecules and biologics, oligonucleotides are informational drugs, meaning that they are designed using the informational sequences (RNA and DNA) present within the cell[1]. The development of a chemical architecture that enables robust, productive, and non-toxic delivery to a particular tissue is a prerequisite for therapeutic oligonucleotide intervention.

Antisense oligonucleotides (ASOs) and small interfering RNAs (siRNAs) are the two most clinically advanced oligonucleotide modalities for modulating mRNA expression. While both platforms work effectively in liver[162, 163], applications of ASOs have been expanded to the central nervous system (CNS)[5], with one drug approved[66] and several others undergoing clinical evaluation (Clinical Trial ID: NCT03342053). The broad distribution of ASOs, both systemically and within the CNS, is primarily driven by phosphorothioate (PS) backbone modifications[26], which facilitate cellular uptake via mechanisms that are not fully understood[164]. PS modifications are also critical for clinically-advanced siRNA configurations[37, 165]. However, siRNAs are large, negatively-charged, and double-stranded, and thus require additional modifications—formulation[166] or chemical conjugation[55, 56, 58, 167]—for meaningful *in vivo* delivery.

The development of the multivalent N-acetylgalactosamine (GalNAc) ligand[144] was a breakthrough for siRNAs[37, 145] in liver applications. GalNAc-conjugated siRNAs have been shown to provide long-term hepatic retention and functional silencing—a single subcutaneous (SC) injection can support more than 12 months of efficacy[168, 169]. Importantly, the clinical success of GalNAc as an siRNA conjugate was possible only after its development as a trivalent ligand in the context of extensive chemical stabilization of the siRNA[47]. This may be due, in part, to cooperative binding—a biological phenomenon that enables favorable binding kinetics through multivalent interactions[170].

Despite multiple attempts over the last few decades to expand siRNA functionality beyond the liver and into the CNS, its distribution and efficacy in this tissue remains limited. Even with continuous, monthly administration of siRNAs into the non-

human primate brain, distribution and efficacy remain near the site of compound infusion[5, 58].

Here we describe a new chemical scaffold—divalent, fully chemically stabilized, PS-containing siRNAs (Di-siRNAs)—which provide widespread distribution and sustained gene silencing in rodent and NHP brain after a single administration into cerebrospinal fluid (CSF).

5.4 RESULTS

5.4.1 CHEMICAL ARCHITECTURE AND SYNTHESIS OF DI-VALENT, FULLY CHEMICALLY MODIFIED SIRNAS.

Full chemical stabilization of siRNAs is essential for conjugate-mediated delivery[37]. We utilize fully chemically stabilized asymmetric siRNAs that have a 20-base guide strand and 15-base passenger strand. All terminal backbones and the protruding 3' end of the guide strand are fully phosphorothioated, resulting in PS modifications to 13 out of 35 phosphate linkages (~40% PS content) (Fig. 5.1a). When conjugated to hydrophobic ligands like cholesterol[58], docosahexaenoic acid (DHA)[55], or DHA with a phosphocholine head group[56], the siRNA scaffold is internalized by cells[151] and retained near the brain injection site, where it induces specific gene silencing. Unconjugated, siRNAs exhibit minimal brain retention and distribution (Fig. 5.1b).

a Mono-siRNA

c Di-siRNA

Legend:
- ● 2'-OMe
- ● 2'-F
- ○ Phosphorothioate
- ○ Phosphodiester
- ★ Cy3 fluorescent label
- ◆ 5' Vinyl phosphonate

b siRNA / Nuclei

d

e PBS / Di-siRNA

f Di-siRNA / Nuclei

g Striatum

h Cortex

Hipp – Hippocampus
Thal – Thalamus
Str – Striatum
PC – Posterior cortex
MC – Medial cortex

i HTT Protein Expression (% of Control)

PBS | ^{V}Di-siRNA^{NTC} 475 µg | ^{V}Di-siRNA^{HTT} 60 µg | ^{V}Di-siRNA^{HTT} 475 µg

j ApoE Protein Expression (% of Control)

PBS | ^{V}Di-siRNA^{NTC} 475 µg | ^{V}Di-siRNA^{APOE} 475 µg

Figure 5.1 A divalent siRNA chemical configuration improves distribution and retention and supports significant silencing after a single injection in the mouse brain.
a. Schematic of the chemical structure of Mono-siRNA. b. Biodistribution of Cy3-labeled Mono-siRNA 48 hours after a single intrastriatal injection of 50 µg. c. Schematic of the chemical structure of Di-siRNA. d. Biodistribution of Cy3-labeled Di-siRNA 48 hours after a single intrastriatal injection of 50 µg. e. Image of whole mouse brain injected with Di-siRNA (top – PBS, bottom – Di-siRNA). f. Di-siRNA distributes throughout mouse the brain after a bilateral injection of 475 µg (237 µg/ventricle) into the lateral ventricles. Tiled fluorescent images taken 48 hours post injection. (g,h) High resolution images of Di-siRNA distribution to various regions of the mouse brain: g. Striatum, h. Cortex. i. Scale bar – 50 µm. Di-siRNA silences huntingtin (HTT) protein at two different doses in multiple brain regions 1 month after bilateral ICV injection.   All statistics are One-Way ANOVA with Dunnett's multiple comparisons test. All results compared to PBS control. Hipp: $F_{(3,17)} = 31.92$, HTT 60µg ****$P<0.0001$, HTT 457µg ****$P<0.0001$. Thal: $F_{(3,17)} = 16.875$, HTT 60µg ***$P=0.0003$, HTT 457µg ***$P=0.0002$. Str: $F_{(3,17)} = 33.38$, HTT 60µg ****$P<0.0001$, HTT 457µg ****$P<0.0001$. PC: $F_{(3,17)} = 12.64$, HTT 457µg ***$P=0.0001$. MC: $F_{(3,17)} = 53.58$, HTT 60µg ***$P=0.0003$, HTT 475 µg ****$P<0.0001$. PBS: n=6, NTC n=5, HTT 60 µg: n=5, HTT 475 µg: n=5. Mean ± SD. NTC – non-targeting control. j. Di-siRNA silences apolipoprotein E (APOE) protein 1 month after bilateral ICV injection.   All statistics are One-Way ANOVA with Dunnett's multiple comparisons test. All results compared to PBS control. Hipp: $F_{(2,14)} = 1.991$, ****$P<0.0001$. Thal: $F_{(2,14)} = 4.283$, ****$P<0.0001$. Str: $F_{(2,15)} = 4.781$, ****$P<0.0001$. PC: $F_{(2,14)} = 6.618$, ****$P<0.0001$. PBS: n=6. NTC Mean ± SD. NTC – non-targeting control.

For ASOs, the most advanced CNS-active scaffold utilizes a mixed backbone configuration with ~70-80% PS content. This modification maintains efficacy and distribution while reducing the risk of toxic phenotypes[39, 171] that can be associated with high PS content. Increasing the PS content of individual siRNA duplexes to 80% can limit RNA-induced silencing complex (RISC) efficacy[172, 173] and will increase toxicity[174, 175]. We examined whether a multi-valent approach— specifically, cooperative interactions between two partially PS-modified siRNAs—could enhance siRNA distribution and efficacy in the CNS.

We synthesized the divalent siRNA (Di-siRNA) compound using a functionalized solid support (Fig. 5.2), which allowed for parallel growth of two oligonucleotides. As a

result, two sense strands are covalently connected at their 3'end through a tetra-ethylene glycol (TEG) linker.
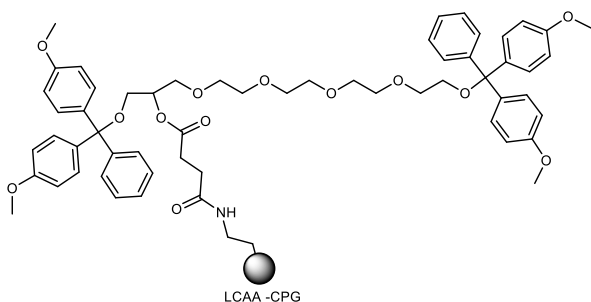
Figure 5.2 Structure of Di-valent solid support used in the synthesis of Di-siRNA.
Di-trityl protected support separated by a tetraethylene glycol spacer, attached through a succinate linker to long chain alkyl amine (LCAA) derivatized solid support.

Use of the polymeric spacer was necessary to limit steric hindrance during synthesis and functional knockdown. Annealing of the passenger strand to two identical 20-base guide strands formed a ~ 27 kD compound (Fig. 5.1c). Mono- and Di-siRNAs show comparable *in vitro* IC50 values (Fig. 5.3), suggesting that the linkage of two molecules did not compromise RISC loading.
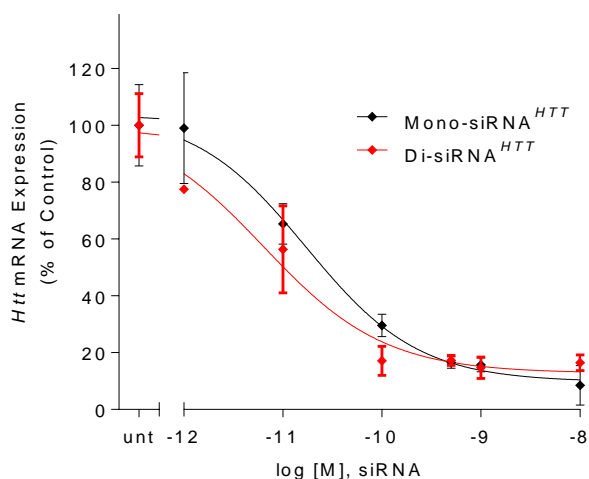
Figure 5.3 Mono-siRNA and Di-siRNA show similar gene silencing efficiency after lipid mediated delivery.
siRNAs were formulated in RNAiMax and delivered to HeLa cells at varying concentrations for 72 hours. All graphs are mean ± SD.

The sequences and chemical configuration of all compounds used in this study are shown in Table 5.1.

Table 5.1 Table of siRNAs sequences and chemical modification patterns.

Name	Gene	Acession #	Position	Sense strand	Antisense strand
Di-siRNA^{HTT}-0 PS	HTT	NM_002111.6	10150	Cy3-(fC)(mA)(fG)(mU)(fA)(mA)(fA)(mG)(fA)(mG)(fA)(mU)(fU)(mA)(fA)-DIO	P(mU)(fU)(mA)(fA)(mU)(fC)(mU)(fC)(mU)(fU)(mU)(fA)(mC)(fU)(mG)(fA)(mU)(fA)(mU)(reverse dT)
Di-siRNA^{HTT}-16 PS	HTT	NM_002111.6	10150	Cy3-(fC)#(mA)#(fG)(mU)(fA)(mA)(fA)(mG)(fA)(mG)(fA)(mU)(fU)#(mA)#(fA)-DIO	P(mU)#(fU)#(mA)(fA)(mU)(fC)(mU)(fC)(mU)(fU)(mU)(fA)(mC)(fU)(mG)(fA)(mU)(fA)#(mU)#(fA)
Di-siRNA^{HTT} (-26PS)	HTT	NM_002111.6	10150	Cy3-(fC)#(mA)#(fG)(mU)(fA)(mA)(fA)(mG)(fA)(mG)(fA)(mU)(fU)#(mA)#(fA)-DIO	P(mU)#(fU)#(mA)(fA)(mU)(fC)(mU)(fC)(mU)(fU)(mU)(fA)(mC)#(fU)#(mG)#(fA)#(mU)#(fA)#(mU)#(fA)
^{v}Di-siRNA^{HTT}-no Cy3	HTT	NM_002111.6	10150	(fC)#(mA)#(fG)(mU)(fA)(mA)(fA)(mG)(fA)(mG)(fA)(mU)(fU)#(mA)#(fA)-DIO	V(mU)#(fU)#(mA)(fA)(mU)(fC)(mU)(fC)(mU)(fU)(mU)(fA)(mC)#(fU)#(mG)#(fA)#(mU)#(fA)#(mU)#(fA)
^{v}Di-siRNA^{HTT}	HTT	NM_002111.6	10150	Cy3-(fC)#(mA)#(fG)(mU)(fA)(mA)(fA)(mG)(fA)(mG)(fA)(mU)(fU)#(mA)#(fA)-DIO	V(mU)#(fU)#(mA)(fA)(mU)(fC)(mU)(fC)(mU)(fU)(mU)(fA)(mC)#(fU)#(mG)#(fA)#(mU)#(fA)#(mU)#(fA)
^{v}Di-siRNA^{PPIB}	PPIB	NM_009693.2	437	Cy3-(fC)#(mA)#(fA)(mA)(fU)(mU)(fC)(mC)(fA)(mU)(fC)(mG)(fU)#(mG)#(fA)-DIO	V(mU)#(fC)#(mA)(fC)(mG)(fA)(mU)(fG)(mG)(fA)(mA)(fU)(mU)#(fU)#(mG)#(fC)#(mU)#(fG)#(mU)#(fU)
Di-siRNA^{NTC}	N/A	N/A	N/A	Cy3-(fU)#(mG)#(fA)(mC)(fA)(mA)(fA)(mU)(fA)(mC)(fG)(mA)(fU)#(mU)#(fA)-DIO	P(mU)#(fA)#(mA)(fU)(mC)(fG)(mU)(fA)(mU)(fU)(mU)(fG)(mU)#(fC)#(mA)#(fA)#(mU)#(fC)#(mA)#(fU)
^{v}Di-siRNA^{NTC}	N/A	N/A	N/A	Cy3-(fU)#(mG)#(fA)(mC)(fA)(mA)(fA)(mU)(fA)(mC)(fG)(mA)(fU)#(mU)#(fA)-DIO	V(mU)#(fA)#(mA)(fU)(mC)(fG)(mU)(fA)(mU)(fU)(mU)(fG)(mU)#(fC)#(mA)#(fA)#(mU)#(fC)#(mA)#(fU)
Monoi-siRNA^{HTT}	HTT	NM_002111.6	10150	Cy3-(fC)#(mA)#(fG)(mU)(fA)(mA)(fA)(mG)(fA)(mG)(fA)(mU)(fU)#(mA)#(fA)-Teg	P(mU)#(fU)#(mA)(fA)(mU)(fC)(mU)(fC)(mU)(fU)(mU)(fA)(mC)#(fU)#(mG)#(fA)#(mU)#(fA)#(mU)#(fA)
^{v}Di-siRNA^{ApoE}	ApoE	NM_00969	1134	(mA)#(mA)#(fC)(mA)(mU)(mC)(fC)(mA)(fU)(mA)(fU)(mC)(fC)#(mA)#(mA)-DIO	V(mU)#(fU)#(mG)(fG)(fA)(fU)(mA)(fU)(mG)(fG)(mA)(fU)(mG)(fU)#(mU)#(fG)#(mU)#(mU)#(mG)#(fC)
^{v}Di-siRNA^{NTC}	N/A	N/A	N/A	(mU)#(mG)#(fA)(mC)(fA)(mA)(fA)(mU)(fA)(mC)(mG)(mA)(fU)#(mU)#(mA)-DIO	V(mU)#(fA)#(mA)(fU)(fC)(fG)(mU)(fA)(mU)(fU)(mU)(fG)(mU)#(fC)#(mA)#(fA)#(mU)#(mC)#(mA)#(fU)
PNA^{HTT}	HTT	NM_002111.6	10150	T*A*T*A*T*C*A*G*T*A* A*A*G*A*G*A* T*T*A*A	

Detailed sequence, chemical modification patterns, and efficacy of siRNAs. Chemical modifications are designated as follows, "#" –phosphorothioate bond, "*" – peptide bond, "m" – 2'-*O*-methyl, "f" – 2'-Fluoro, "P" – 5' Phosphate, "V" – 5' Vinylphosphonate. "DIO" – Di-siRNA, Teg – tetraethylene glycol.

5.4.2 DI-SIRNA SHOWS WIDESPREAD RETENTION IN THE MOUSE BRAIN FOLLOWING AN INTRA-PARENCHYMAL INJECTION.

Intra-parenchymal injection of Cy3-labeled Di-siRNAs significantly enhanced distribution and retention in the mouse brain compared to Cy3-labeled monovalent siRNAs (Fig. 5.3d), supporting the idea that a cooperative interaction between two partially PS-modified siRNAs is sufficient for widespread brain retention. In all experiments, the dose of injected compounds (Mono- vs Di-siRNA) was defined by guide strand concentration. Thus, each injection contained equal amounts of fluorescent dye and active duplex that was independent of valency status (i.e. Di-siRNA injection includes half the number of molecules compared to the Mono-siRNA injection).

To evaluate if the observed enhancement in brain retention translates into functional gene silencing, we synthesized Di-siRNA targeting huntingtin (*Htt*) mRNA using a previously identified siRNA sequence targeting a sequence conserved in mouse, non-human primate, and human (Chapter III)[58]. Huntingtin is the causative gene in Huntington's disease (HD) and its modulation is considered to be a viable clinical strategy for HD treatment[5]. Intra-striatal injection of Di-siRNA^{HTT} in wild type mice resulted in potent down-regulation of *Htt* mRNA (between 50-75%) in the striatum and cortex at two doses (10 and 50 µg) two weeks after injection (Fig. 5.4a).
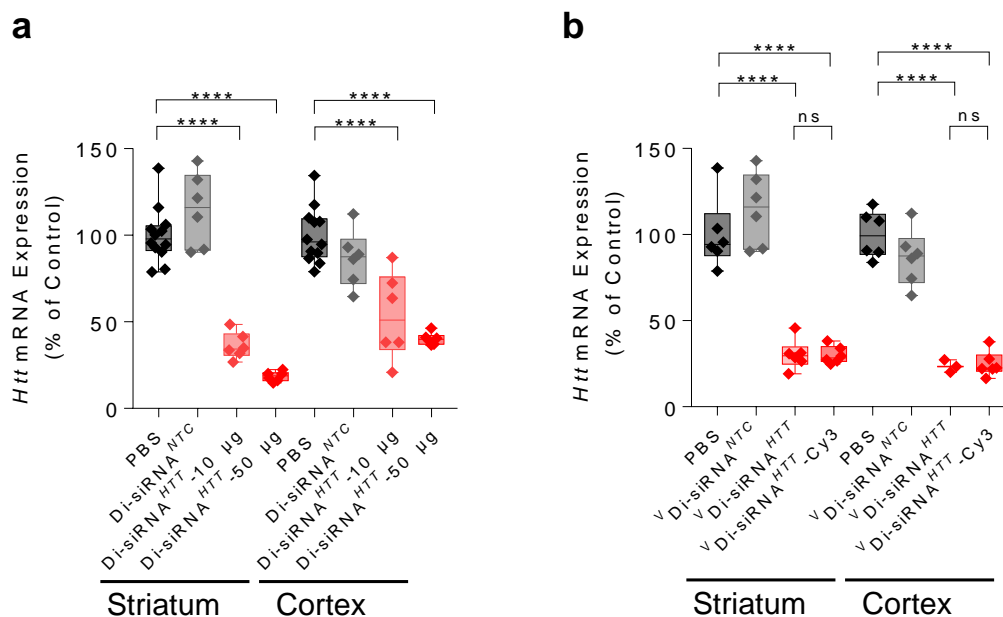
Figure 5.4 Di-siRNAs work in a dose dependent manor and do not require Cy3 conjugation for activity.

a. Di-siRNA shows significant Htt mRNA silencing (% of control) at 10 μg and 50 μg doses 2 weeks after a single intrastriatal injection. Statistics calculated by One-Way ANOVA with Dunnet's correction for multiple comparisons. All results compared to PBS control. Striatum: $F_{(3,26)} = 71.86$, ****$P<0.0001$; Cortex: $F_{(3,26)} = 21.67$, ****$P<0.0001$. PBS (n = 12), NTC (n=6), 10 μg (n=6) and 50 μg (n=6). b. Cy3-labelling has minimal impact in Di-siRNA efficacy after a single intrastriatal injection of 50 μg. Statistics calculated by One-Way ANOVA with Tukey's correction for multiple comparisons. All results compared to PBS control. Striatum: $F_{(3,20)} = 49.41$, ****$P<0.0001$. Cortex: $F_{(3,17)} = 55.36$, ****$P<0.0001$. n=6 for each group, except for Di-siRNA in cortex n=3.

Since Cy3 potentially can alter oligonucleotide retention and distribution, we compared Cy3-labeled and non-labeled Di-siRNA*HTT* efficacy following an intra-parenchymal injection into the striatum. Both compounds show similar levels of silencing in cortex and striatum (~ 80% silencing, p < 0.0001, Fig. 5.4b). The non-targeting control (NTC) oligonucleotide of the same chemical configuration did not impact target gene expression (Fig. 5.4a-b). Thus, the observed silencing activity was specific to the Htt targeting sequence.

To confirm that PS content is essentially contributing to observed efficacy, we synthesized Di-siRNA^{HTT} variants containing fewer and no PS backbones (Fig. 5.5a). Reduction of number of PS modification led to a reduction in silencing efficacy, and the complete removal of PS modification fully abolished activity (Fig. 5.5b) after IS injection in mice. Thus, the observed efficacy of Di-siRNA^{HTT} is phosphorothioate mediated, a mechanism that is likely shared with traditional antisense oligonucleotides.
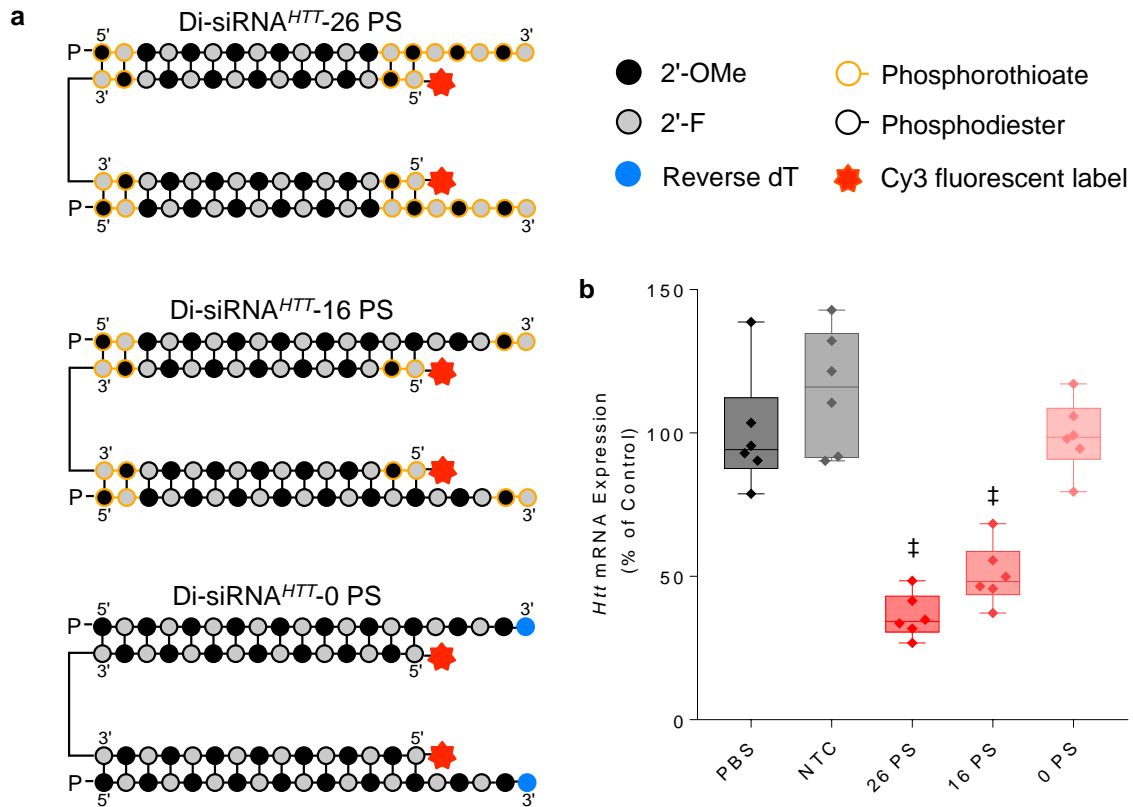
Figure 5.5 Di-siRNA efficacy is phosphorothioate content dependent.
Wild-type mice received a single intrastriatal injection of injection of 12.5 μg (237 μg/ventricle) Di-siRNA. a. Schematic of varying phosphorothioate containing Di-siRNAs. b. mRNA scilencing of various PS containing Di-siRNAs reduces efficacy in the striatum 2 weeks after an intrastriatal injection. Statistics calculated by One-Way ANOVA with Dunnetrs's correction for multiple comparisons. All results compared to PBS control. $F(4,25) = 1.294$, ****$P<0.0001$.

5.4.3 DI-SIRNA EXHIBITS BROAD DISTRIBUTION AND PRODUCTIVE SILENCING IN THE MOUSE BRAIN AFTER A BOLUS CSF INJECTION.

To evaluate CSF-driven brain distribution of Cy3-Di-siRNA, we injected 475 μg intracerebroventricularly (ICV) into the lateral ventricles of mice. Forty-eight hours after the injection, the mouse brain was uniformly pink to the naked eye (Fig. 5.1e), indicating broad distribution. Microscopy confirmed the initial observation (Fig. 5.1f). Di-siRNAs distributed to all regions of the brain—from the prefrontal cortex to the cerebellum. High magnification images show accumulation in the vast majority of neurons (Fig. 5.1g,h). Intracellular distribution followed a perinuclear localization pattern that is characteristic of oligonucleotides[151].

Broad distribution of Di-siRNA*HTT* supported productive silencing (measured two weeks post injection) in all brain regions, including prefrontal, medial and posterior cortices, striatum, hippocampus, thalamus, hypothalamus, cerebellum, brain stem and cervical, thoracic, and lumbar sections of the spinal cord (Fig. 5.6). To quantitatively evaluate guide strand accumulation, we used a PNA hybridization assay, which provides quantitative accumulation data and does not depend on the presence of a fluorescent label[157]. Analysis (Fig. 5.6a) confirmed the visual and microscopy-based observations of broad Di-siRNA distribution, and correlated with *Htt* mRNA (Fig. 5.6b) and HTT protein (Fig. 5.6c,d) silencing.

PFC –Prefrontal cortex   HT – Hypothalamus
MC – Medial cortex   Cer – Cerebellum
PC – Posterior cortex   BS – Brain stem
Str – Striatum   Cerv – Cervical spinal cord
Hipp – Hippocampus   Thor –Thoracic spinal cord
Thal – Thalamus   Lum – Lumbar spinal cord
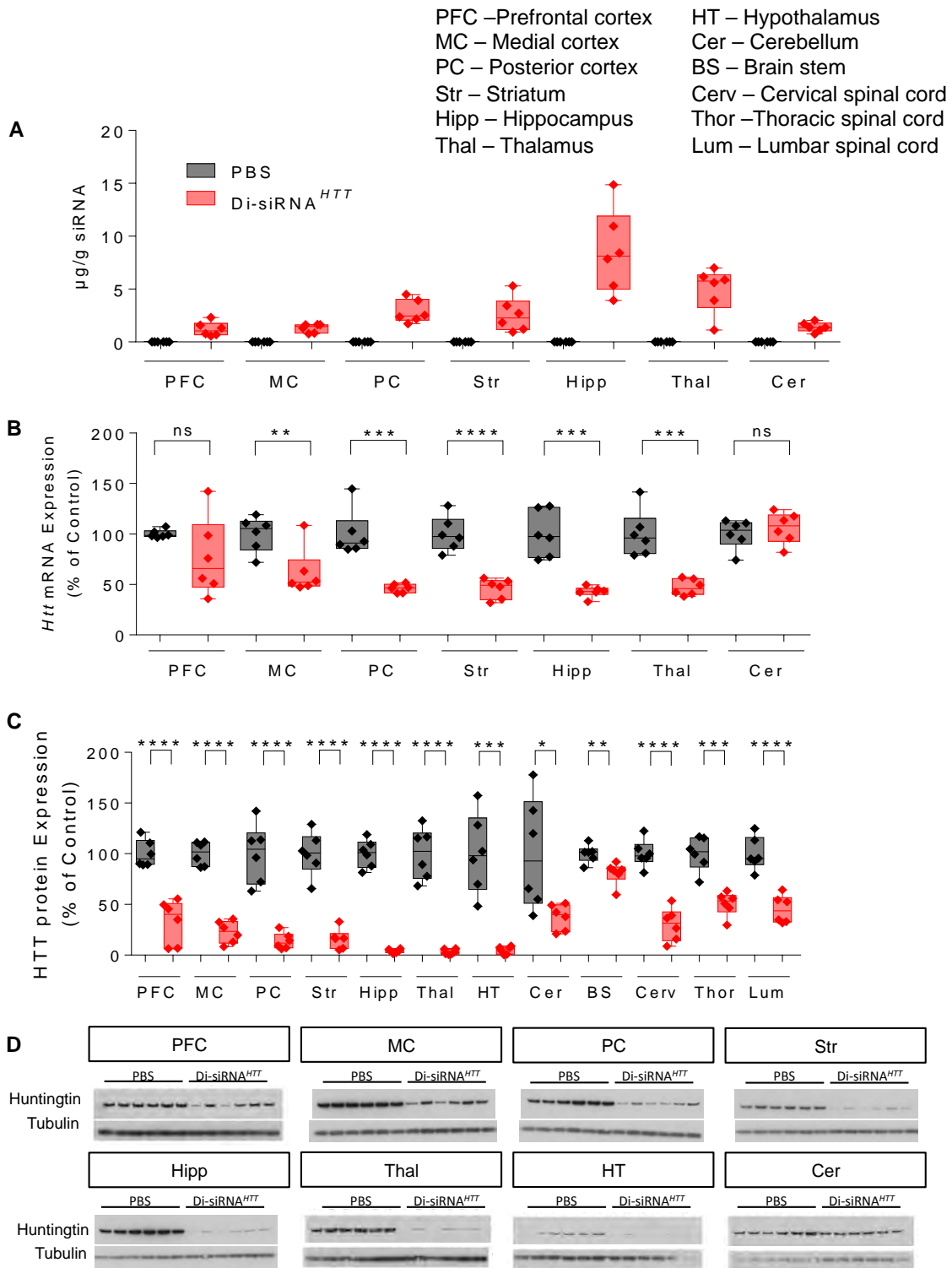
Figure 5.6 Di-siRNAs silence huntingtin throughout the brain and spinal cord of mice two weeks after a single ICV injection.
Wild-type mice received a single bilateral ICV injection of 475 µg (237 µg/ventricle) Di-siRNA. Data was collected two weeks post injection. a. siRNA guide strand accumulation (µg/g). b. Huntingtin (*Htt*) mRNA silencing (% of control). All statistics are two-tailed unpaired t-tests. MC: t=3.917, df=10, **P=0.0095. PC: t=5.677, df=10, ***P=0.0002. Str: t=6.663, df=10, ****P<0.0001. Hipp: t=5.948, df=10, ***P=0.001. Thal: t=5.312, df=10, ***P=0.0003. n=6/group. c. Huntingtin (HTT) protein silencing (% of control). PFC: t=6.439, df=10, ****P<0.0001. MC: t=11.78, df=10, ****P<0.0001. PC: t=6.972, df=10, ****P<0.0001. Str: t=8.726, df=10, ****P<0.0001. HIPP: t=16.9, df=10, ****P<0.0001. Thal: t=9.356, df=10, ****P<0.0001. HT: t=5.9, df=10, ***P=0.0002. Cer: t=2.706, df=10, *P=0.0221. BS: t= 3.335, df=10, **P=0.0076. Cerv: t=8.032, df=10, ****P<0.0001. Thor: t=5.918, df=10, ***P=0.0001. Lumb: t=6.275, df=10, ****P<0.0001. n=6/group. d. Western blots from representative brain regions (used for quantification in (c)). n=6/group.

Next, we compared the efficacy of two different Di-siRNA^{HTT} doses—60 and 475 µg—one month after injection in wild type mice (Fig. 5.7).
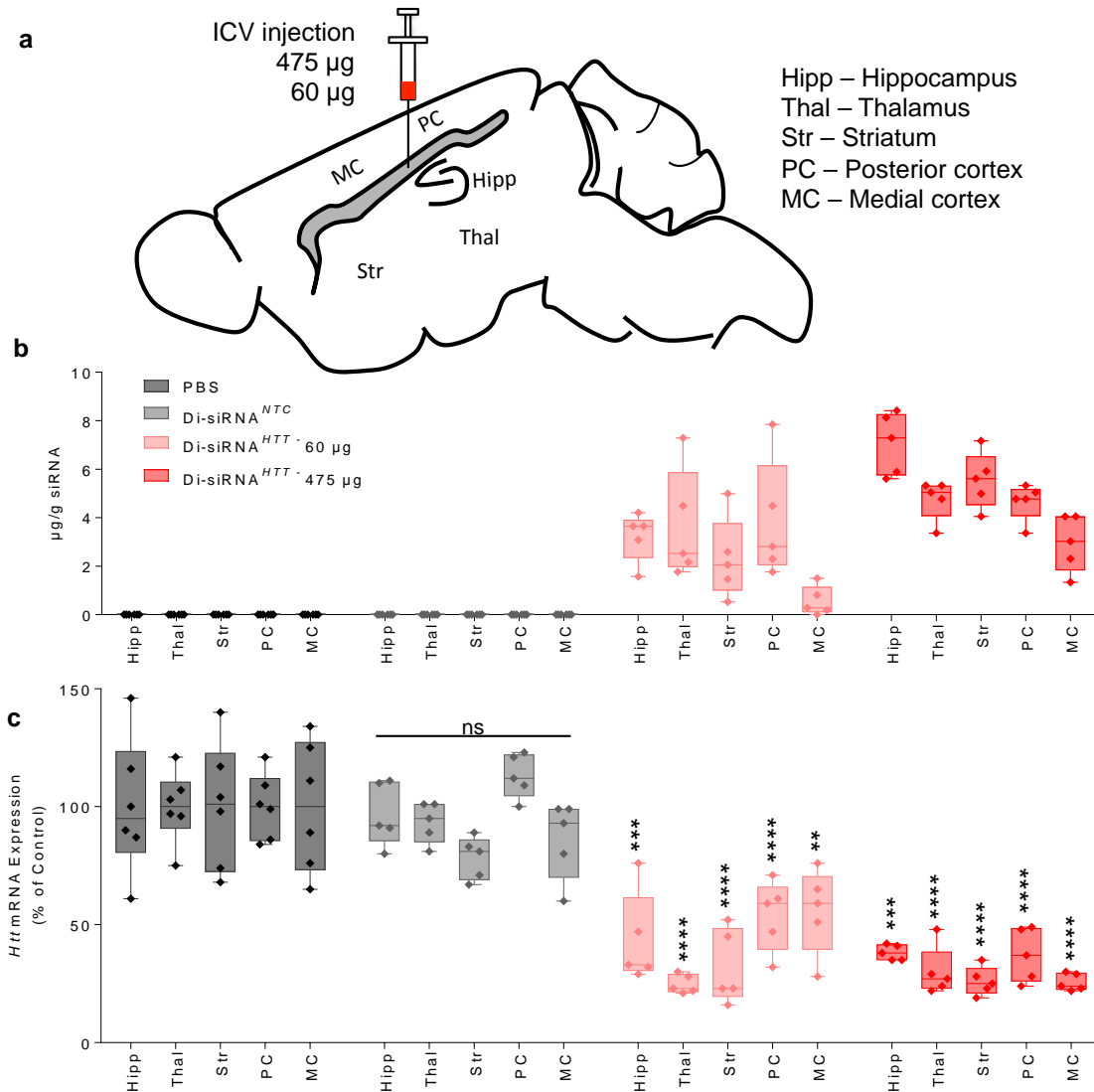
Figure 5.7 Di-siRNA shows widespread guide strand accumulation and mRNA silencing one month after a single ICV injection.
Wild-type mice received a single bilateral ICV injection of 475 µg (237 µg/ventricle), 60 µg (30 µg per ventricle), or NTC Di-siRNA. a. Schematic of experiment. b. Guide strand accumulation (µg/g). c. Huntingtin (*Htt*) mRNA silencing (% of control). n=5-6 mice/group. Mean ± SD. NTC – non-targeting control. All statistics calculated by One-Way ANOVA with Dunnet's correction for multiple comparisons. All results compared to PBS control. Hipp: $F_{(3,17)} = 15.45$, HTT 60µg ***P=0.0005, HTT 457µg ***P=0.0002. Thal: $F_{(3,17)} = 74.57$, HTT 60µg ****P<0.0001, HTT 457µg ***P<0.0001. Str: $F_{(3,17)} = 23.58$, HTT 60µg ****P<0.0001, HTT 457µg ****P<0.0001. PC: $F_{(3,17)} = 41.86$, HTT 60µg ****P<0.0001, HTT 457µg ****P<0.0001. MC: $F_{(3,17)} = 15.83$, HTT 60µg **p=0.0039 , HTT 457µg ****P<0.0001. PBS: n=6, NTC n=5, HTT 60 µg: n=5, HTT 475 µg: n=5. Mean ± SD. NTC – non-targeting control.

The higher dose resulted in approximately a two-fold maximum increase in guide

strand tissue retention and a wider distribution (0.1 to 4 µg/g at 60 µg; 2-8 µg/g at 475 µg

dose, Fig. 5.7b). The higher dose silenced HTT protein below level of detection (p <

0.0001) throughout the brain (Fig. 5.1i; Fig. 5.8).
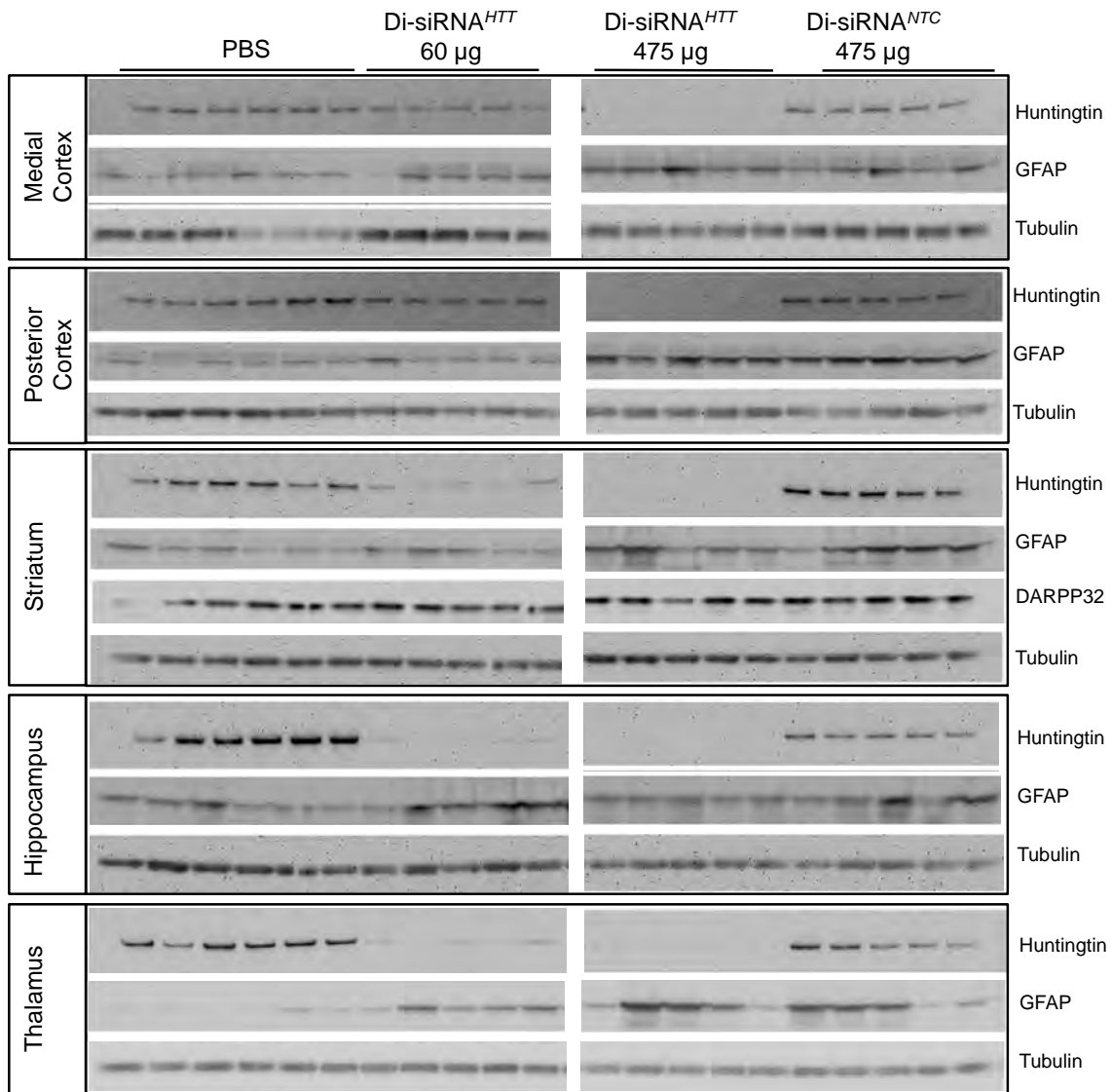
Figure 5.8 Di-siRNA silences huntingtin protein one month after a single ICV injection.
Wild-type mice received a single bilateral ICV injection of Di-siRNA. Original western blot graphically represented in Figure 5.1d. PBS n=6, 60 µg n=5, 475 µg n=5, NTC n=5.

The lower dose was highly efficacious in the hippocampus, thalamus, and striatum, showing 80-99% silencing (p < 0.0001, p < 0.001, p < 0.0001, respectively). In the cortical areas located away from the site of injection, efficacy was reduced. This observation is consistent with the relatively lower guide strand accumulation measured in these regions. NTC and PBS groups showed no difference in HTT expression level. NTC was used as a control for all subsequent experiments (Fig. 5.1i).

5.4.4 DI-SIRNA CHEMICAL SCAFFOLD IS APPLICABLE FOR SILENCING OF MULTIPLE GENES IN THE CNS.

The base sequence of the siRNA determines its target, but the chemical architecture of the oligonucleotide determines pharmacokinetics and tissue delivery. Therefore, we decided to evaluate the efficacy of the Di-siRNA scaffold containing sequences targeting other mRNAs in the CNS. Indeed, Figure 5.9 shows potent silencing (65-85%, p < 0.0001) of another target, Cyclophilin B (Ppib) upon intrastriatal injection. The NTC control had no activity, demonstrating that silencing was specific to the PPIB-targeting sequence.
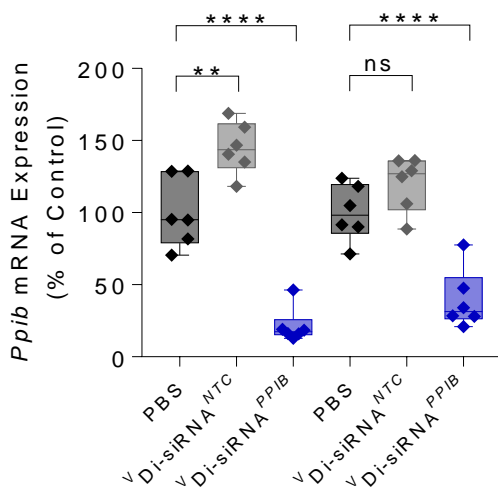
Figure 5.9 The Di-siRNA scaffold can be applied to alternative sequences after a single intrastriatal injection of 50 μg. Statistics calculated by One-Way ANOVA with Dunnet's correction for multiple comparisons. All results compared to PBS control. Striatum: $F_{(2,15)} = 66.24$, ****P<0.0001, except NTC **P=0.0017; Cortex: $F_{(2,15)} = 27.08$, ****P<0.0001, except PPIB ***P=0.0002. n=6.

While the direct cause of many neurological disorders remains unclear, some have clear genetic components, in which certain genes or mutations increase risk for neurodegeneration. Apolipoprotein E (Apo E) is implicated in several neurodegenerative diseases including Alzheimer's disease and Amyotrophic Lateral Sclerosis[176-178]. We have previously identified functional siRNA sequences targeting Apo E (Ferguson et al, manuscript in preparation). To determine if Di-siRNA scaffold could be applied to another CNS-relevant target, we synthesized Di-siRNA^{ApoE} (see Table 5.1 for sequence information) and injected mice ICV with PBS and NTC as controls. Figure 5.1j (Fig. 5.10 for raw westerns) shows that, similar to HTT, a single CSF injection of Apo E targeting Di-siRNAs resulted in potent (> 95%) silencing of ApoE protein.

ApoE Hippocampus
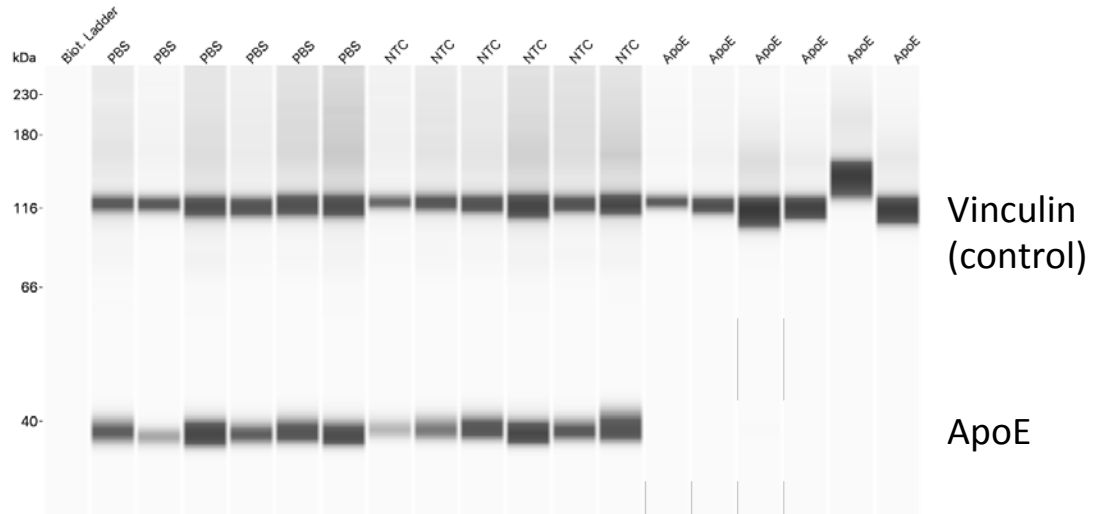
ApoE Striatum
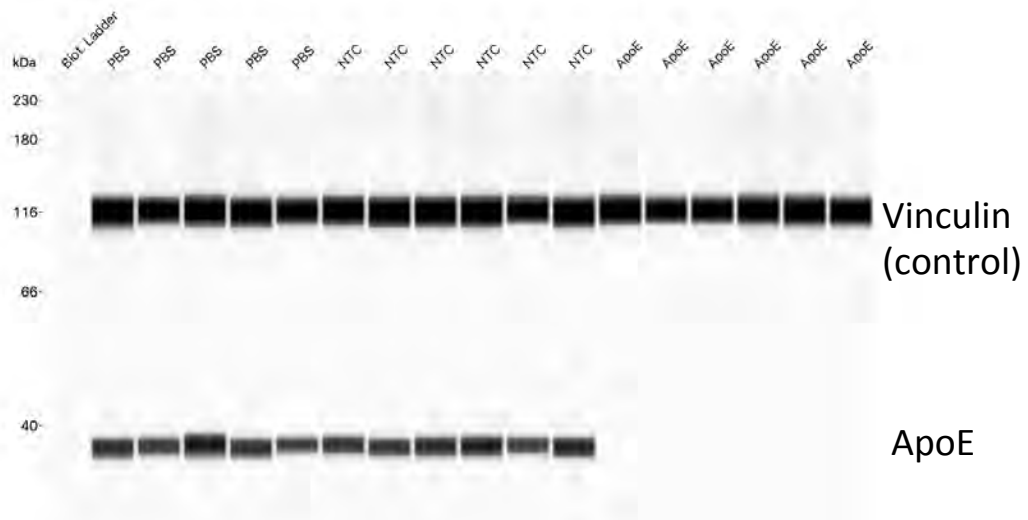
ApoE Thalamus
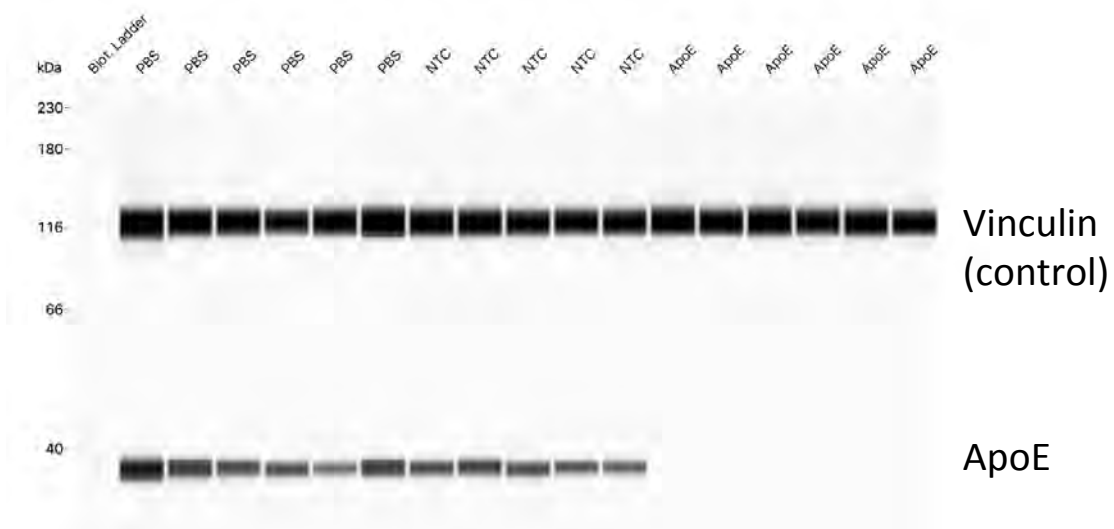
ApoE Posterior Cortex
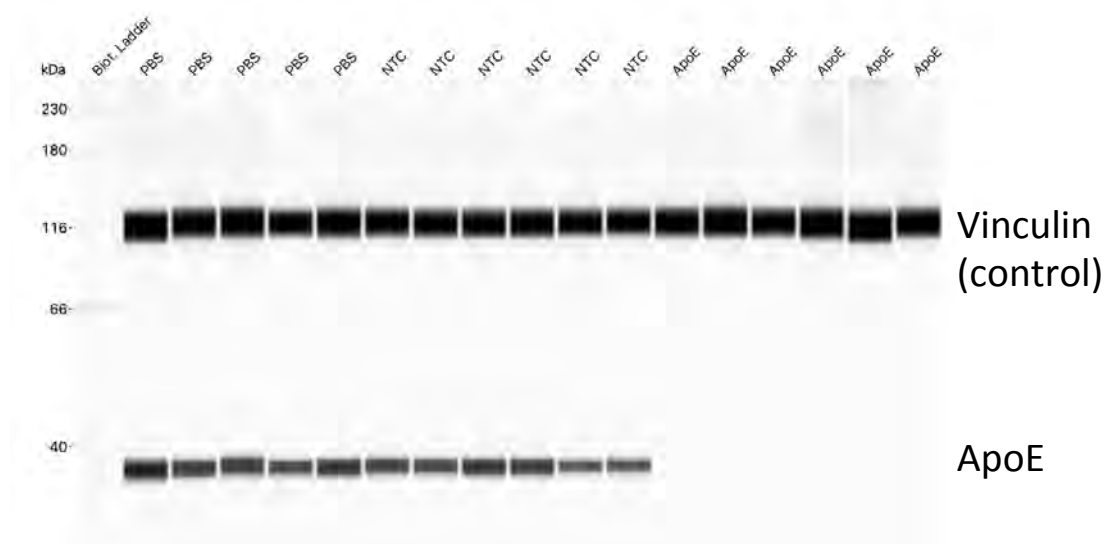
Figure 5.10 Di-siRNA silences apolipoprotein E protein one month after a single ICV injection.
Wild-type mice received a single bilateral ICV injection of Di-siRNA. Original western blot graphically represented in Figure 5.1j. n=6.

Again, NTC had no impact on ApoE expression, indicating that observed silencing is

sequence specific and not caused by the Di-siRNA chemical scaffold. In addition, the

observed protein silencing correlated well with mRNA silencing (Fig. 5.11). Thus, the

Di-siRNA chemical scaffold can be reprogrammed to modulate gene expression *in vivo*

for a number of other targets implicated in the pathogenesis of neurological conditions.
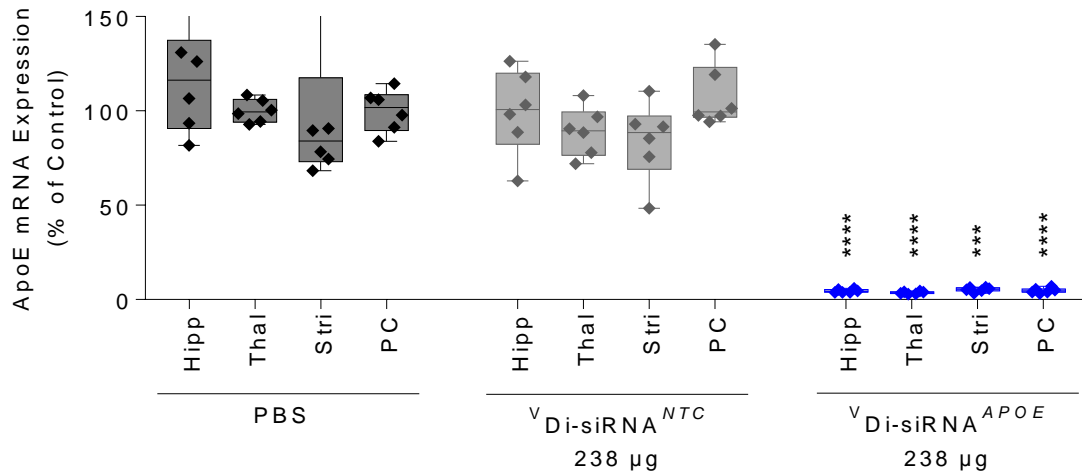
Figure 5.11 Di-siRNA silences apolipoprotein E (ApoE) mRNA 1 month after a single bilateral ICV injection of 475 μg (237 μg/ventricle).
All statistics are One-Way ANOVA with Dunnett's multiple comparisons test. All results compared to PBS control. Hipp: $F_{(2,15)} = 6.025$, ****$P<0.0001$. Thal: $F_{(2,15)} = 5.084$, ****$P<0.0001$. Str: $F_{(2,15)} = 1.382$, ***$P=0.0002$. PC: $F_{(2,15)} = 2.251$, ****$P<0.0001$. PBS: n=6. NTC Mean ± SD. NTC – non-targeting control.

5.4.5 THE DURATION OF EFFECT OF HIGH-DOSE DI-SIRNA EXCEEDS SIX MONTHS FOLLOWING A BOLUS CSF INJECTION.

To evaluate the duration of Di-siRNA efficacy, we delivered a high dose (475 μg) of Di-sRNA^{HTT} or Di-siRNA^{NTC} to mice via a single ICV injection in wild type mice. We then measured guide strand accumulation levels, *Htt* mRNA, and HTT protein in key brain regions (cortex, striatum, thalamus, hippocampus) at one, four, and six months post injection (Fig. 5.12a).
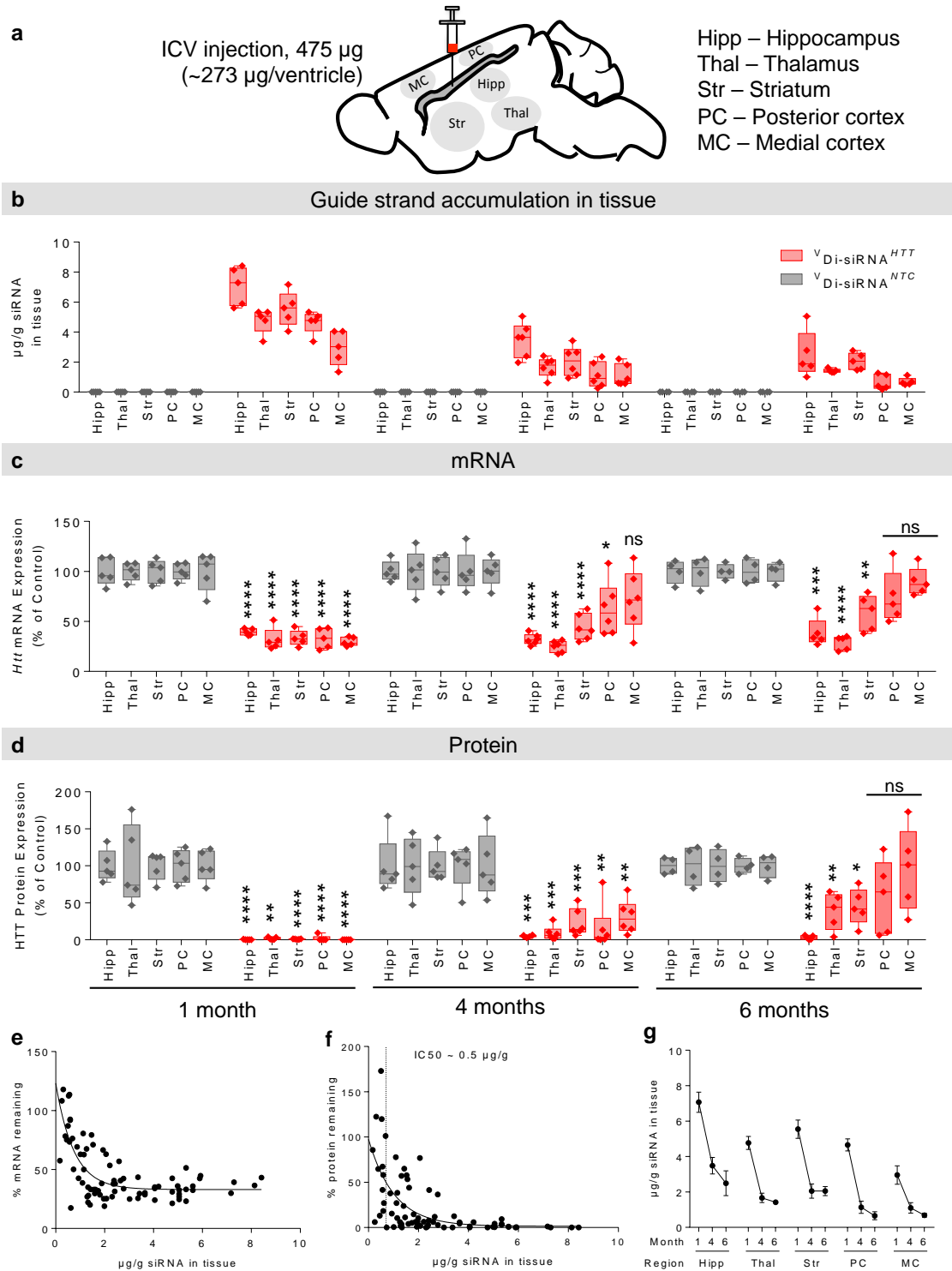
Figure 5.12 Di-siRNA efficacy is sustained for up to 6 months after a single bilateral ICV injection in the mouse brain.
Mice were injected with 475 µg siRNA (bilaterally) (237 µg/ventricle) and data was collected at 1, 4 and 6 months post injection. a. Schematic of the duration of effect study in mice. b. Guide strand accumulation (µg/g) in five brain regions. c. Huntingtin (*Htt*)

mRNA silencing (% of control) in five brain regions. All statistics are two-tailed unpaired t-tests. All results compared to NTC control. 1 month. Hipp: t=9.56, df=8, ****p<0.0001. Thal: t=10.59, df=8, ****p<0.0001. Str: t=10.63, df=8, ****p<0.0001. PC: t=11.45, df=8, ****p<0.0001. MC: t=8.082, df=8, ****p<0.0001. HTT: n=5, NTC: n=5. 4 month. Hipp: t=14.26, df=9, ****p<0.0001. Thal: t=8.577, df=9, ****p<0.0001. Str: t=6.606, df=9, ****p<0.0001. PC: t=2.561, df=9, *p=0.0306. HTT: n=6, NTC: n=5. 6 month. Hipp: t=6.998, df=7, ***p=0.0002. Thal: t=9.865, df=7, ****p<0.0001. Str: t=4.264, df=7, **p=0.0037. HTT: n=5, NTC: n=4. d. Huntingtin (HTT) protein silencing (% of control) in five brain regions. 1 month. Hipp: t=10.58, df=8, ****p<0.0001. Thal: t=14.092, df=8, **p=0.0035. Str: t=12.05, df=8, ****p<0.0001. PC: t=9.834, df=8, ****p<0.0001. MC: t=10.85, df=8, ****p<0.0001. HTT: n=5, NTC: n=5. 4 month. Hipp: t=6.117, df=9, ***p=0.0002. Thal: t=5.661, df=9, ***p=0.0003. Str: t=6.261, df=9, ***p=0.0001. PC: t=4.651, df=9, **p=0.0012, MC: t=3.46, df=9, **p=0.0072. HTT: n=6, NTC: n=5. 6 month. Hipp: t=19.01, df=7, ****p<0.0001. Thal: t=93.536, df=7, **p=0.0095. Str: t=3.479, df=7, *p=0.0103. HTT: n=5, NTC: n=4. e. Di-siRNA *Htt* mRNA silencing shows a strong correlation with siRNA guide strand accumulation. f. Di-siRNA HTT protein silencing shows a strong correlation with siRNA guide strand accumulation (IC50 ~ 0.5 µg/g). g. siRNA guide strand retention shows strong, two phase tissue clearance kinetics. The majority of the compound is cleared within the first month. Clearance slows between 4 and 6 months. Mean ± SD. NTC – non-targeting control.

Guide strand accumulation in different brain regions ranged between 2-7 µg/g at one month, 0.8-2.5 µg/g at four months, and 0.2- 1.8 µg/g at six months, suggesting relatively slow clearance (Fig. 5.12b). We also noticed that the extent of HTT protein modulation was always greater than *Htt* mRNA (> 99% vs ~70%) (Fig. 5.12c,d). This discrepancy is due to a fraction of *Htt* mRNA being localized to the nucleus, and thus more resistant to RNAi-based modulation[179]. More than 80% silencing of HTT protein was maintained at four months in all brain regions analyzed (Fig. 5.12d, Fig. 5.8, and 5.13 for raw westerns). At six months, the degree of silencing differed between brain regions: > 90% in hippocampus, ~50% in thalamus and striatum, and high variability in the cortex.
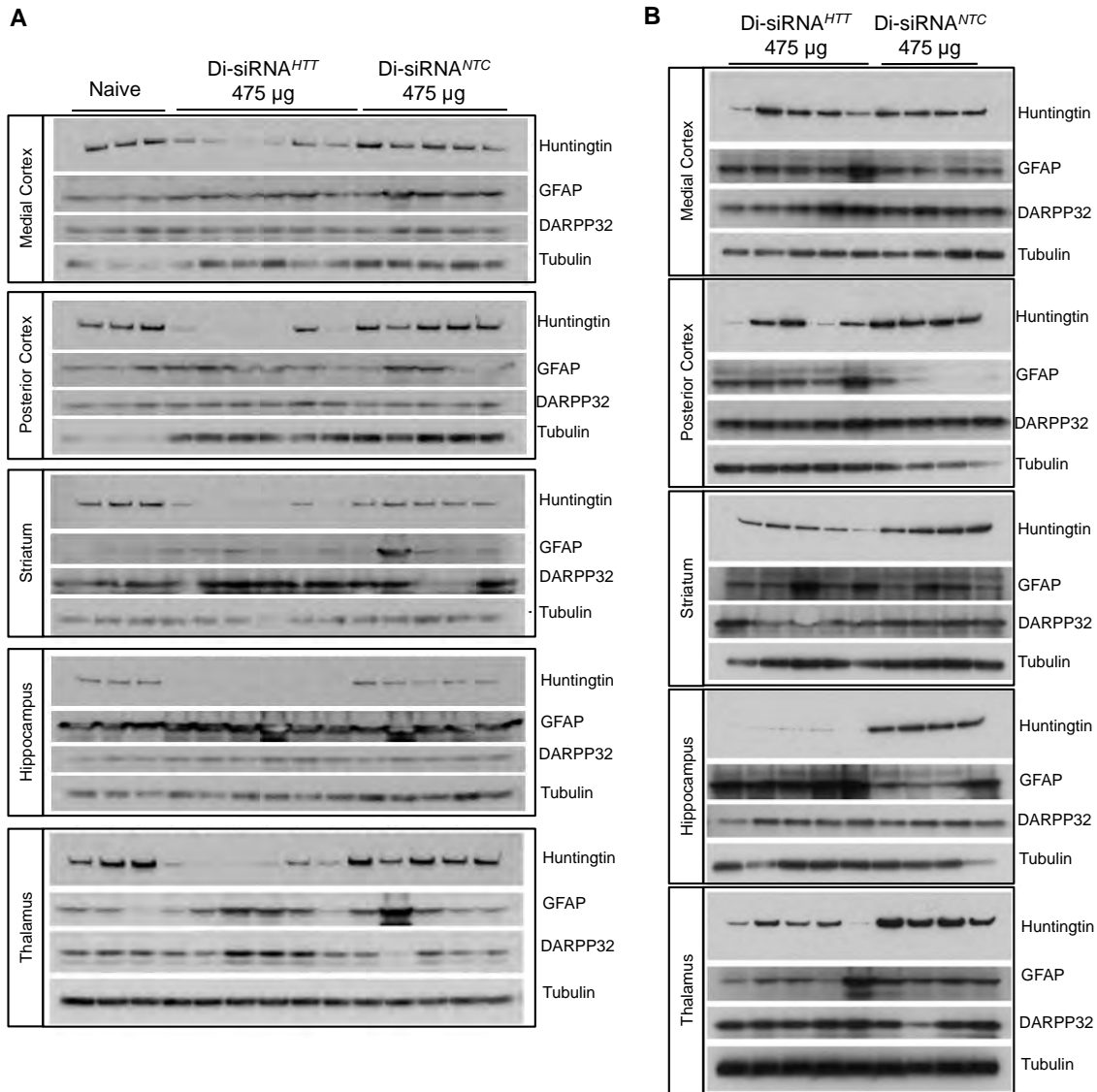
Figure 5.13 Di-siRNA shows sustained huntingtin protein silencing after a single ICV injection.
Wild-type mice received a single bilateral ICV injection of 475 µg (237 µg/ventricle) Di-siRNA.   a. Huntingtin (HTT) protein silencing at 4 months (% of control). Naïve n=3, HTT n=6, NTC n=5, b. HTT protein silencing at 6 months (% of control). HTT n=5, NTC n=4. Densitometry analysis of the original western blot graphically represented in Figure 5.12d.

5.4.6 DI-SIRNA GUIDE STRAND RETENTION IN TISSUE IS CORRELATED TO THE DEGREE OF MRNA AND PROTEIN SILENCING.

Using data from all time points in the duration of effect study, we observed strong correlations between the level of residual guide strand accumulation and the degree of *Htt* mRNA (Fig. 5.12e) and HTT protein (Fig. 5.12f) silencing. We estimate the protein silencing IC50 value to be ~0.5 µg/g and the IC90 value to be ~2 µg/g. Figure 5.12g shows guide strand clearance over time for individual brain regions. Initial (one month) hippocampal accumulation of ~7 µg/g resulted in ~2 µg/g present at 6 months. Both levels of guide strand accumulation are sufficient to silence HTT protein below the level of detection. In the cortical regions, initial accumulation at one month was 3-4 µg/g and fell below the 0.5 µg/g threshold by six months, resulting in loss of silencing in some animals. This suggests that siRNA tissue accumulation at early time points can be used to estimate duration of effect.

5.4.7 DI-SIRNA INJECTION AT DIFFERENT DOSES IS SAFE AND WELL-TOLERATED IN MICE

To evaluate overall safety and tolerability of Di-siRNA at 475 µg over 6 months, we measured DARPP32 protein expression, innate immune response activation markers, and blood biochemistry. Loss of DARPP32, an established marker for medium spiny neurons in the striatum[130], indicates neuronal death. Injection of Di-siRNA had no impact on DARPP32 expression, indicating maintenance of neuronal viability (Fig. 5.8, Fig. 5.13). To evaluate impact of Di-siRNA injection on microglia activation and gliosis we measured two well-established markers of immune stimulation, IBA-1 and GFAP. IBA-1

is located within a major histocompatibility complex and increases as a result of microglial activation[180]. GFAP is an intermediate filament protein and increases as a result of astrocyte proliferation[181]. We observed only minor changes in Iba-1 expression (< 1.5 fold from control) at both dose levels and at all three time points. At the higher dose, we observed transient activation of Gfap at one month, which was absent by four months (Fig. 5,14, 5.15).
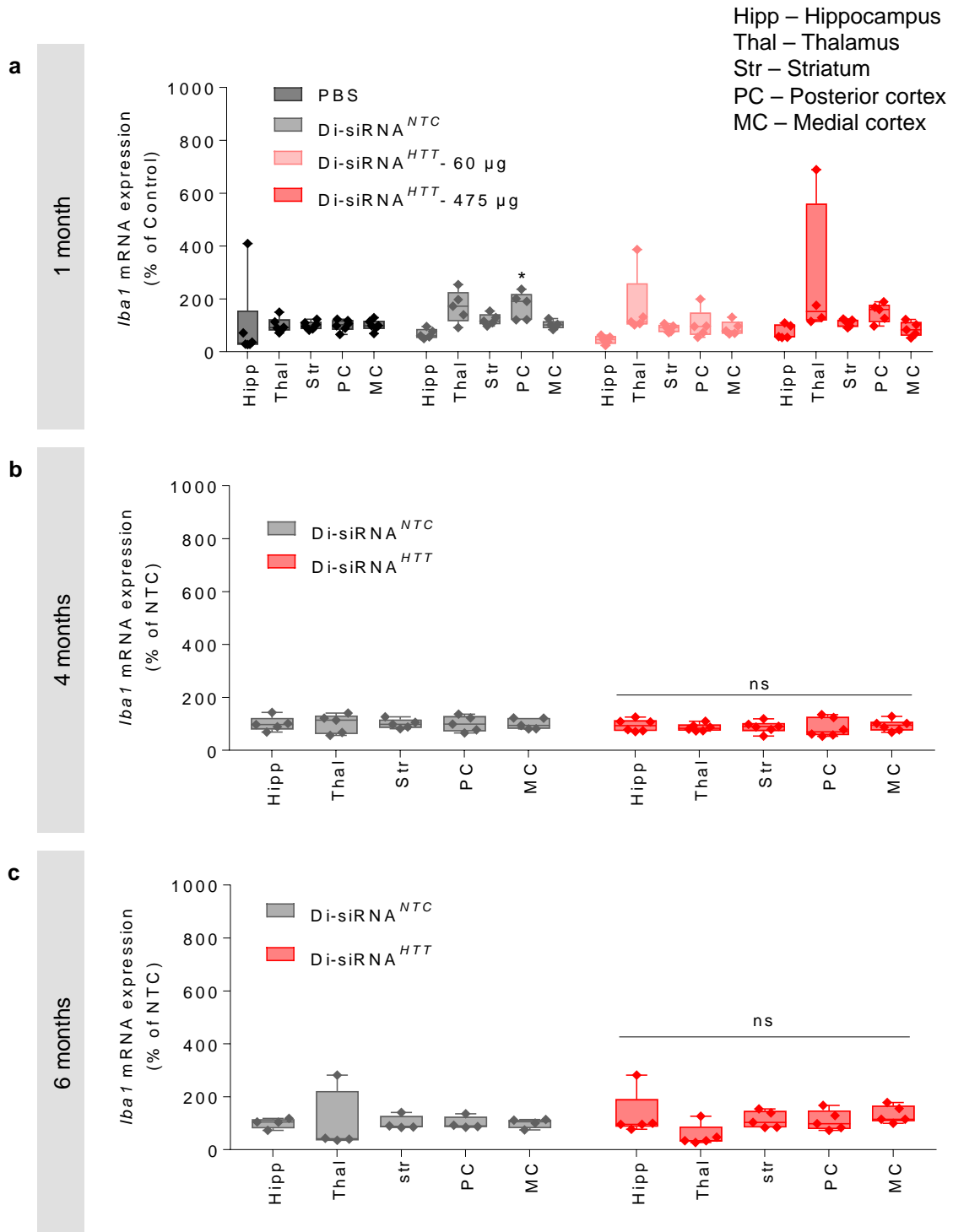
Figure 5.14 Di-siRNA does not cause Iba-1 upregulation after a single bilateral ICV injection.
Wild-type mice received a single bilateral ICV injection of 475 µg (237 µg/ventricle) Di-siRNA. a. Iba-1 mRNA expression 1 month post injection. Statistics calculated by One-Way ANOVA with Dunnet's correction for multiple comparisons. All results compared to PBS control. PC: $F_{(3,17)} = 3.715$, NTC *p=0.0275. PBS: n=6, NTC: n=5, HTT 60µg:

n=5, HTT 475µg: n=5. b. Iba-1 mRNA expression 4 months (HTT: n=6, NTC: n=5) and. c. 6 months (HTT: n=5, NTC: n=4) after injection. Statistics for 4 and 6 months calculated by two tailed unpaired t-test. All results compared to NTC control. Mean ± SD.
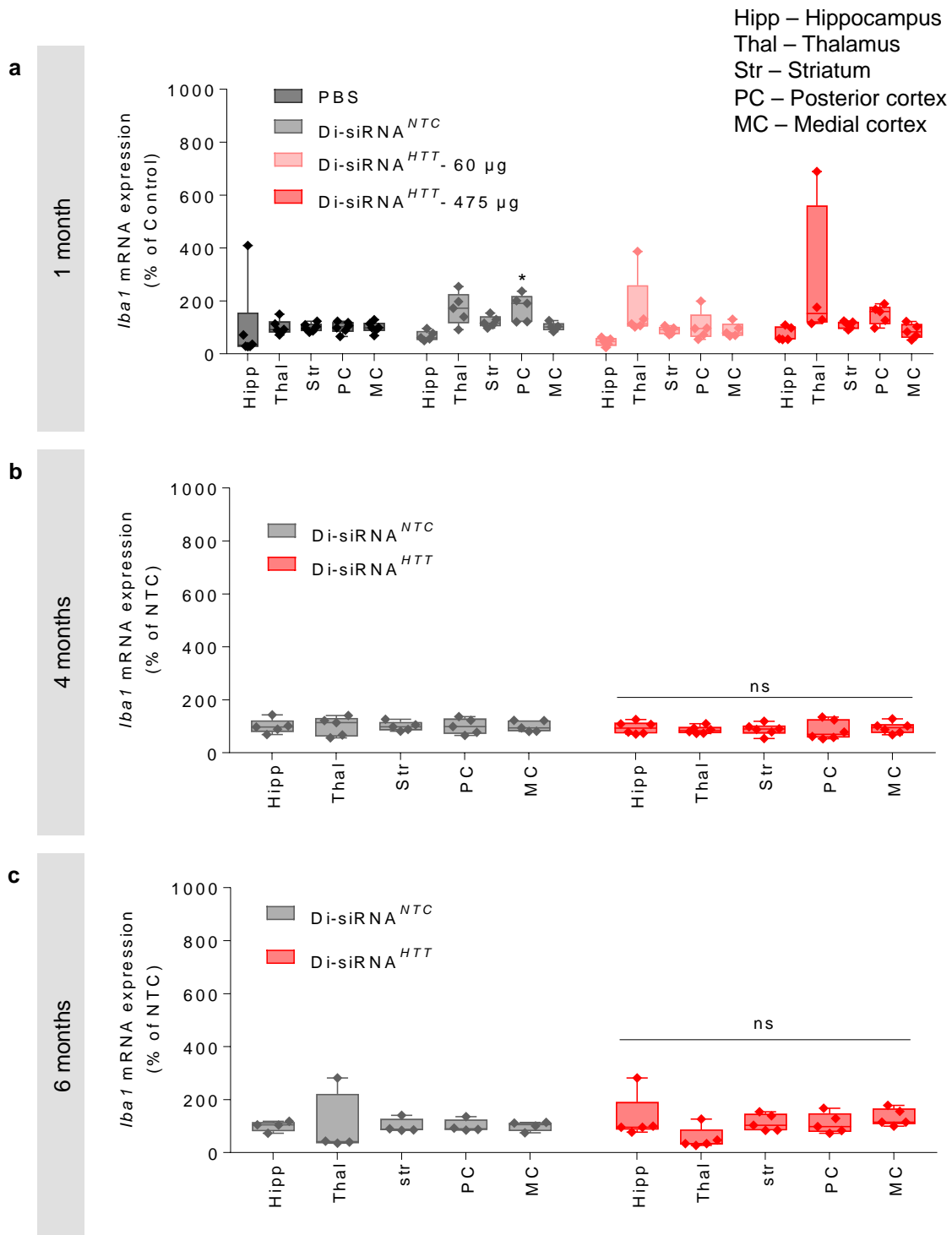
Figure 5.15 Di-siRNA causes transient Gfap mRNA up-regulation 1 month after a single ICV injection.
Wild-type mice received a single bilateral ICV injection of 475 µg (237 µg/ventricle) Di-siRNA. a. Gfap mRNA expression 1 month after injection. Statistics calculated by One-Way ANOVA with Dunnet's correction for multiple comparisons. All results compared to PBS control. Hipp: $F_{(3,17)} = 6.76$, HTT 475µg **p=0.0012. Str $F_{(3,17)} = 4.266$,

HTT475µg *p=0.0154, PC: F(3,17) = 4.287, HTT475µg *p=0.0259. (PBS: n=6, NTC: n=5, HTT 60µg: n=5, HTT 475µg: n=5). b. Gfap mRNA expression 4 months (HTT: n=6, NTC: n=5) and c. 6 month after injection (HTT: n=5, NTC: n=4). Statistics for 4 and 6 months calculated by two-tailed unpaired t-test, compared to NTC control Mean ± SD.

Additionally, a comprehensive blood chemistry panel showed no detectable changes at any time point, suggesting a systemic tolerability of Di-siRNA administration to the CNS (Fig. 5.16). Overall, Di-siRNA injection in the CSF appears to be well tolerated in mice at the doses and time points tested, supporting safe and sustained modulation of gene expression.

Test	1 month				4 months			6 months	
	PBS	NTC (475 ug)	HTT (60 ug)	HTT (475 ug)	Naive	NTC (475 ug)	HTT (475 ug)	NTC (475 ug)	HTT (475 ug)
ALB	3.3±0.77	3.4±0.19	3.9±0.13	3.5±0.27	3.5±0.23	3.6±0.16	3.6±0.17	3.8±0.17	3.6±0.18
ALP	35±12.02	24.2±15.55	24.8±12.72	26.6±15.24	57.7±5.51	28.4±24.88	46.5±7.26	28.3±12.95	36.2±20.55
ALT	99±54.07	85.6±54.27	92.8±43.86	61.2±31.96	54.3±11.02	75.4±28.61	72±23.54	61.8±19.41	120.2±143.74
AMY	744.6±95.53	746.4±80.6	837±45.78	751.8±78.3	871.7±22.12	846±149.35	888.5±52.39	926.3±56.02	950.4±40.53
TBIL	0.2±0	0.2±0.06	0.2±0	0.2±0	0.2±0	0.2±0	0.2±0	0.2±0.06	0.2±0.05
BUN	24.6±3.21	25.4±2.7	19.8±2.05	22.4±7.8	23.7±4.04	19.4±4.56	20.7±2.8	24.5±3	23.6±2.88
CA	9.2±1.17	8.4±0.33	10.2±0.41	8.5±0.52	9.8±0.31	9.8±0.47	9.6±0.29	10.1±0.29	10±0.58
PHOS	8.8±1.65	6.3±0.78	7.8±0.87	6.8±1.88	7.1±0.5	7.9±0.5	8±0.69	8.1±0.61	8±1.23
CRE	0.3±0.13	0.2±0.04	0.2±0.05	0.2±0.09	0.2±0	0.3±0.1	0.2±0	0.2±0	0.2±0
GLU	273.2±72.42	200±35.48	223.2±29.07	197.4±32.85	225±10.44	202.4±27.18	186±22.34	201±18.11	210.8±29.51
NA+	4.5±0.99	4.4±0.21	5.2±0.25	4.5±0.37	5±0.31	5±0.23	5±0.23	5.3±0.18	5.1±0.31
GLOB	1.1±0.23	1±0.11	1.2±0.13	1±0.18	1.5±0.1	1.4±0.18	1.5±0.12	1.5±0.08	1.5±0.19

Figure 5.16 Di-siRNA does not show any significant blood toxicity after a single bilateral ICV injection in mouse.
Wild-type mice received a single bilateral ICV injection of 475 µg (237 µg/ventricle) Di-siRNA. A comprehensive diagnostic blood chemistry profile of 14 biochemical markers was analyzed 30 days post-injection using a VetScan 2. 1 Month, PBS n=6, 60 µg n=5, 475 µg n=5, NTC n=5. 4 month, Naïve n=3, HTT n=6, NTC n=5. 6 months, HTT n=5, NTC n=4. Mean ± SD.

5.4.8 DI-SIRNA SILENCES BOTH WILD TYPE AND MUTANT HTT PROTEIN WITH SIMILAR EFFICIENCY.

Di-siRNA^{HTT} has perfect homology to both human and mouse *Htt* genes[58]. To evaluate the ability of Di-siRNA^{HTT} to silence mutant HTT, we measured efficacy in the BACΔN17 mouse model of HD. This HD model contains both wild type mouse HTT and mutant human HTT (97 CAG repeats) with 17 N-terminal amino acids removed[182]. At

seven weeks of age, animals were injected with 475 µg Di-siRNA targeting HTT or

NTC, or injected with PBS. Levels of HTT protein expression were evaluated at five

months of age (~three months post injection). We used a combination of two antibodies

(Ab1 and 1C2) to evaluate specific knockdown of wild type mouse and mutant human

HTT protein. The Ab1 antibody only detects wild type HTT protein, as its epitope is

located in exon 1[87]. The 1C2 antibody detects polyQ expansions[183], and thus is specific to

the mutant protein. A single injection of Di-siRNA^{HTT} showed potent down-regulation of

both mutant and wild type HTT protein (**Fig. 5.17**), with a silencing efficiency similar to

observations in wild type mice at four months post injection (**Fig. 5.12d**). This finding

suggests that Di-siRNA can be utilized for modulation of mutant and wild type HTT

expression.
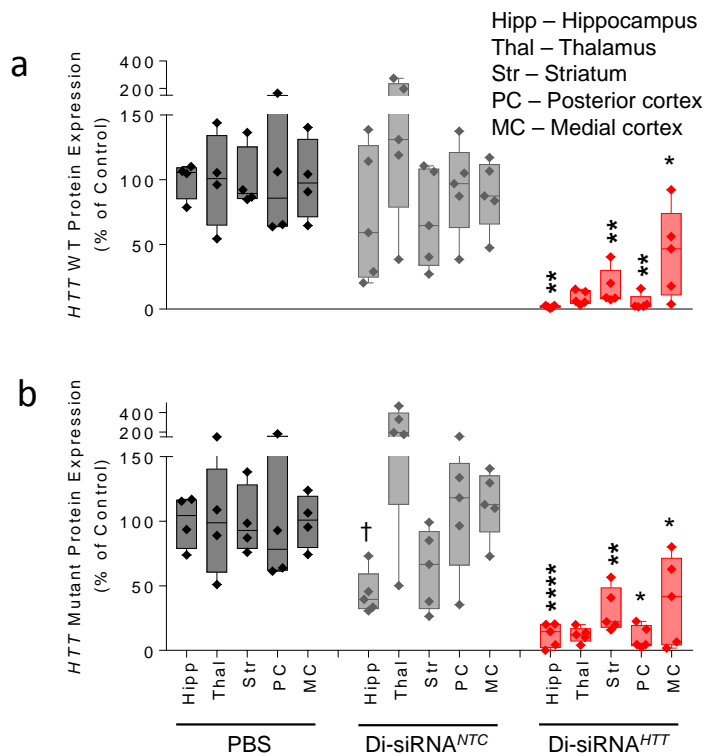
Figure 5.17 Di-siRNA silences mutant huntingtin protein in the BACHD-ΔN17 mouse model of Huntington's disease.
a. Quantification of wild type huntingtin protein silencing in BACΔN17 mice. All statistics are One-Way ANOVA with Dunnett's multiple comparisons test. Hipp: $F_{(2,11)} = 11.25$, HTT **$P=0.0017$. Str: $F_{(2,11)} = 10.67$, HTT **$P=0.0017$. PC: $F_{(2,11)} = 12.21$, HTT **$P=0.0024$. MC: $F_{(2,11)} = 4.363$, HTT *$P=0.0361$. PBS n=4, NTC n=5, HTT n=5. b. Quantification of mutant huntingtin protein silencing in BACdeltaN17 mice. All statistics are One-Way ANOVA with Dunnett's multiple comparisons test. All results compared to PBS control. Hipp: $F_{(2,11)} = 34.66$, NTC ***$P=0.0005$, HTT ****$P<0.0001$. Str: $F_{(2,11)} = 8.112$, HTT **$P=0.0037$. PC: $F_{(2,11)} = 8.6$, HTT *$P=0.0136$. MC: $F_{(2,11)} = 9.885$, HTT *$P=0.014$. PBS n=4, NTC n=5, HTT n=5. Mean ± SD. NTC – non-targeting control.

5.4.9 DI-SIRNA SHOWS WIDESPREAD DISTRIBUTION AND SUSTAINED SILENCING IN NON-HUMAN PRIMATE BRAIN.

Rodent systemic distribution is generally predictive of large mammal distribution. However, this is not necessarily the case for the CNS. Complexity of brain structure, CSF volume, rate of clearance, and the overall distance of brain regions from the CSF may contribute to oligonucleotide distribution and retention. ASO delivery to deep brain structures has been a challenge[5, 184]. Thus, we evaluated the distribution, efficacy, and

safety of a single CSF injection of Di-siRNA in the Cynomolgus macaque, whose siRNA targeting region in the *Htt* sequence is homologous to both mouse and human.

We delivered Di-siRNA^{HTT} via ICV injection, using MRI and CT to confirm needle placement in the lateral ventricle. A 25 mg dose in 750 µl of PBS was infused over 10 minutes (see Methods). Animals woke up within 15 minutes after anesthesia was discontinued, with no observable adverse events. Figure 5.18a shows a schematic of the study timeline. Forty-eight hours after unilateral injection, we observed uniform distribution throughout the non-human primate (NHP) brain, similar to mice. The injected oligonucleotide was fluorescently labeled, allowing for visual and microscopy-based distribution evaluation. The brain appeared visibly pink with no obvious difference in the degree of oligonucleotide distribution in injected vs. non-injected sides (Fig. 5.18b). Upon sectioning of the brain, we observed uniform cortical distribution with evident delivery to deep brain structures, including the striatum (caudate and putamen) and hippocampus (Fig. 5.18c). Fluorescent microscopy confirmed the visual distribution, with significant delivery to the cortex, caudate, and hippocampus.
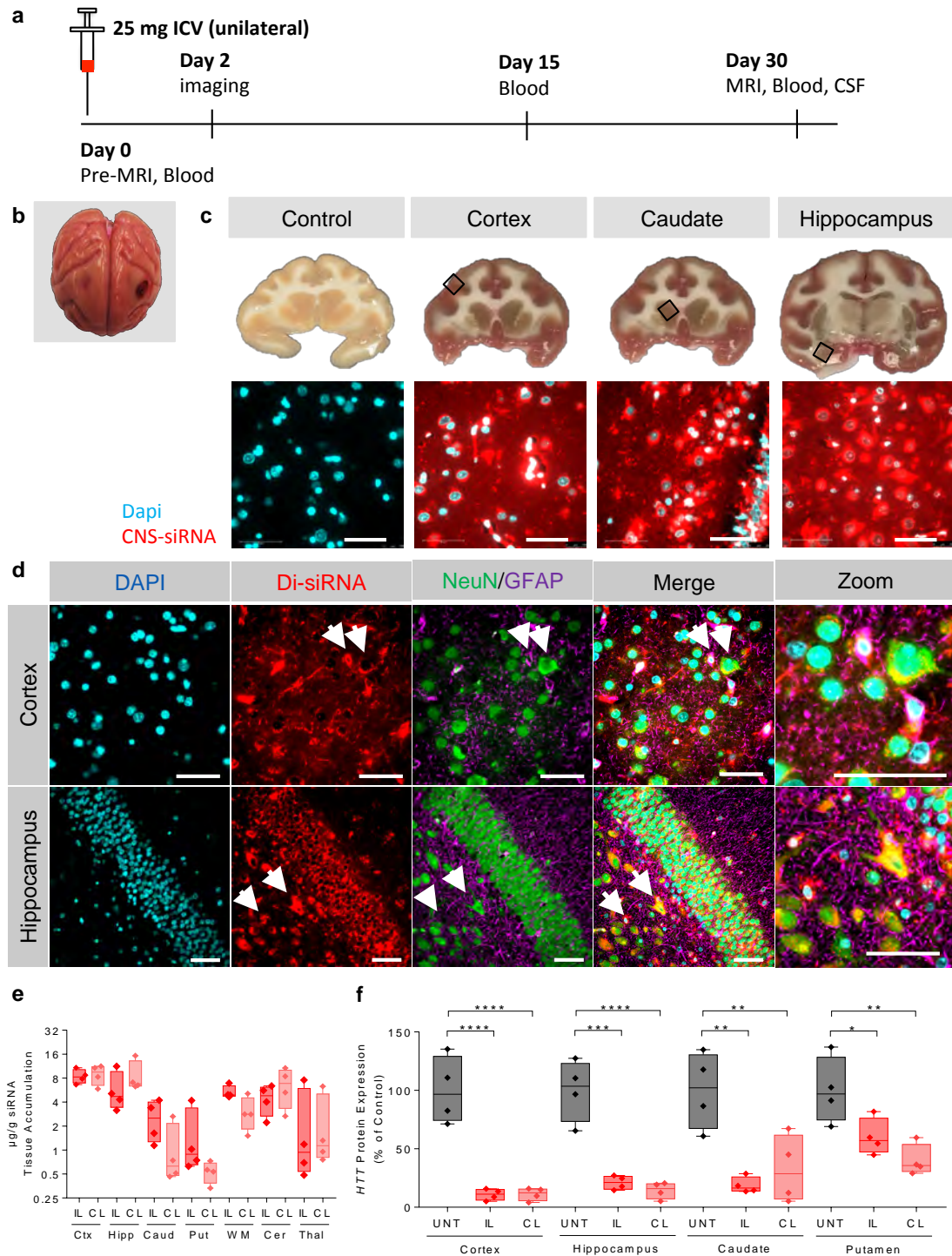
Figure 5.18 Di-siRNA shows widespread distribution, retention, and efficacy in the non-human primate brain.

Cynomolgus macaques received a unilateral ICV injection of Di-siRNAs (25 mg). Samples were collected at 48 hours for biodistribution and at 30 days for gene silencing and toxicity assessments. **a.** Schematic of NHP study. **b.** Image of whole NHP brain (left). Images of NHP brain slices (top). High-resolution fluorescent images of Di-

siRNA in various regions of the NHP brain (bottom). **c**. Immunofluorescence of the NHP cortex and hippocampus. All images acquired 48 hours after a single unilateral ICV injection of 25 mg Di-siRNA. Scale bar – 50 µm. **d.** Quantification of siRNA guide strand (n=4 treated animals, µg/g) in seven brain regions, IL – ipsilateral, CL – contralateral. **e.** Huntingtin (HTT) protein silencing (% of control) ipsilateral and contralateral sides of four brain regions. Statistics calculated by One-Way ANOVA with Dunnet's correction for multiple comparisons. All results compared to naïve control. Cortex: $F_{(2,9)} = 35.86$, ****$P < 0.0001$. Hippocampus: $F_{(2,9)} = 35.15$, ipsilateral ***$P = 0.0001$, contralateral ****$P < 0.0001$. Caudate: $F_{(2,9)} = 11.51$, ipsilateral **$P = 0.0028$, contralateral **$P = 0.0087$. Putamen: $F_{(2,9)} = 9.08$, ipsilateral *$P = 0.0385$, contralateral **$P = 0.0043$. n=4/group. 1 month (n=4 Di-siRNA treated animals, n=4 naive animals). All graphs are mean ± SD.

To evaluate any potential preference for specific cell-types, we performed immunofluorescence on sections of Di-siRNA treated NHP brains using neuron specific (NeuN)[89, 90] and glial cell specific (GFAP)[185] antibodies. We observed efficient distribution of Di-siRNA to both neurons and glial cells in the hippocampus and cortex, and observed co-localization of Di-siRNA (red) with both neurons (green) and glial cells (purple) (Fig. 5.18d).

Upon evaluation of guide strand accumulation in different NHP brain regions at one month post injection (Fig. 5.18e), we observed 1-9 µg/g guide strand accumulation, with the highest accumulation detected in the cortex (9 µg/g), hippocampus (6 µg/g), and thalamus (6 µg/g), and the lowest accumulation in the caudate (2 µg/g) and putamen (1 µg/g). Figure 5.19 shows cortical accumulation across seven slices spanning the entire brain (both ipsilateral and contralateral biopsies), confirming microscopy observations. In all NHP brain regions, guide strand accumulation level was well above the established IC50 value of ~0.5 µg/g (Fig. 5.12f).
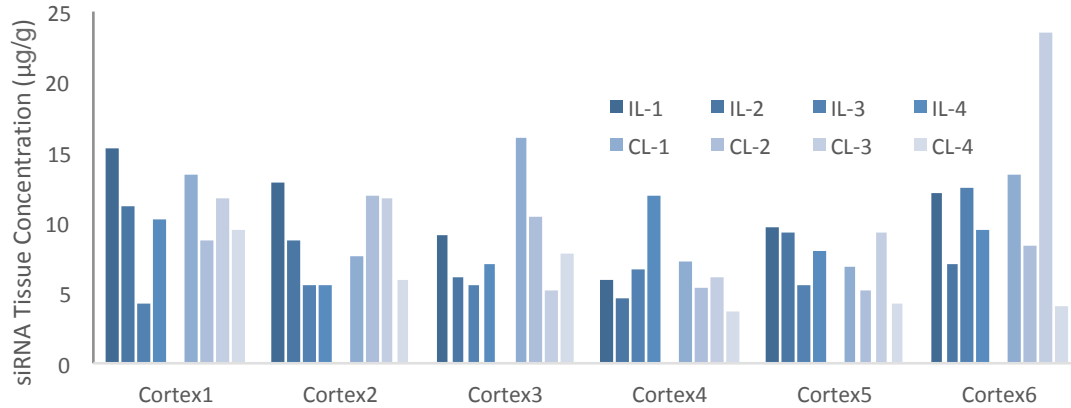
Figure 5.19 Di-siRNA support uniform cortex delivery.
Cynomolgus macaques received an ICV injection of Di-siRNAs (25 mg). siRNA accumulation was measured after 48 hours in the cortex from the anterior to the posterior of the brain. Each bar represents one animal. IL – ipsilateral. CL – contralateral.

One month following injection, we assessed HTT mRNA and protein expression in the NHP brain, to evaluate Di-siRNA^{HTT} efficacy. We observed potent modulation of mRNA expression in all brain regions, independent of the normalization control used (*PPIB* and *HPRT*), Figure 5.20).
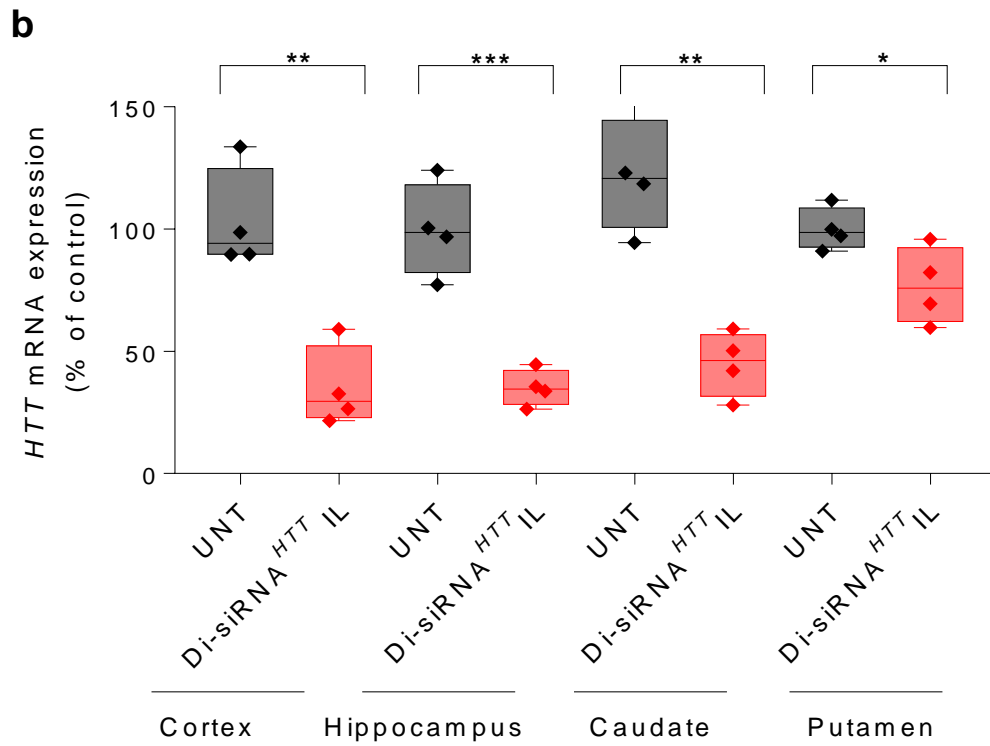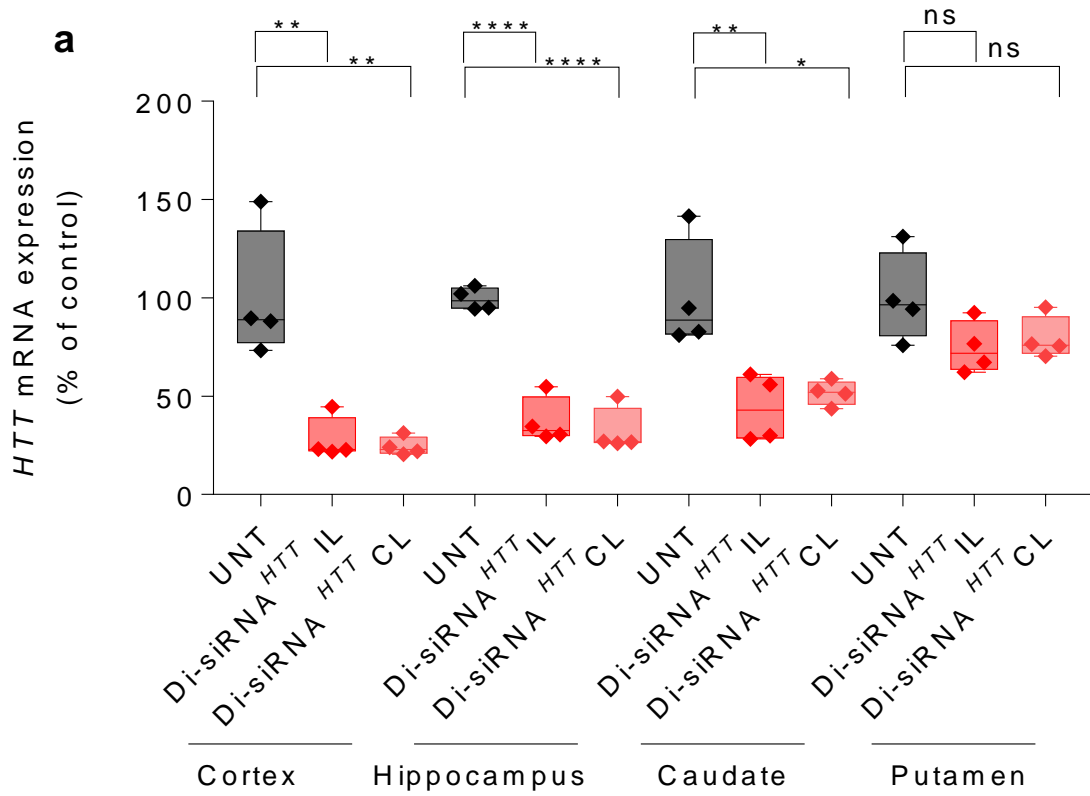
Figure 5.20 Di-siRNA significantly silences mRNA throughout the non-human primate CNS 1 month after a unilateral injection into the CSF.
Four animals treated with 25mg of Di-siRNA are compared with 4 naïve animals. a. Huntingtin (*HTT*) mRNA silencing in various regions of the NHP brain. Normalized to housekeeping gene, HPRT. All statistics are One-Way ANOVA with Dunnett's multiple comparisons test. Cortex: $F_{(2,9)} = 17.3$, ipsilateral **P=0.0014, contralateral **P=0.0011. Hippocampus: $F_{(2,9)} = 54.66$, ****P<0.0001. Caudate: $F_{(2,9)} = 9.809$, ipsilateral **P=0.005, contralateral *P=0.0119. n=4/group. b. *HTT* mRNA silencing in various regions of the NHP brain (injected side). Normalized to housekeeping gene, PPIB. All statistics are two-tailed unpaired t-tests. Cortex, t= 5.085, df=6, **P=0.0023. Hippocampus, t= 6.263, df=6, ***P=0.0008. Caudate, t=5.71, df=6, **P=0.0012. Putamen, t=2.581, df=6, *P=0.0417. n=4/group. Mean ± SD. NTC – non-targeting control.

There was no major difference in silencing between the ipsilateral and contralateral sides of the brain, which is consistent with uniform distribution. For protein silencing (Fig. 5.18f, Fig. 5.21 for raw westerns), we observed >90% silencing in cortex (p < 0.001), >80% silencing in hippocampus (p < 0.01), between 50 and 85% silencing in the caudate (p < 0.001), and ~40-70% silencing in putamen (p < 0.05). These data indicate that a single injection of Di-siRNA enables modulation of target gene expression throughout the NHP brain.
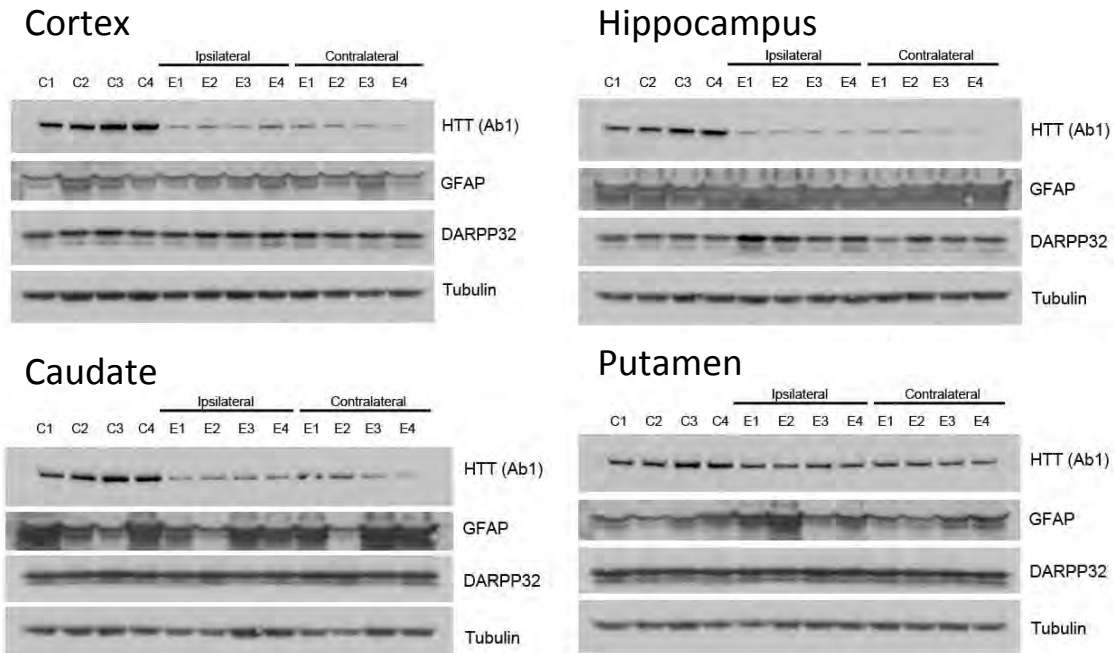
Figure 5.21 Di-siRNA shows significant silencing of huntingtin protein one month after a single injection into the lateral ventricle of the non-human primate. Cynomolgus macaques received an ICV injection of Di-siRNAs (25 mg). mRNA silencing was measured at 1 month (n=4). Densitometry analysis of original western blots graphically represented in Figure 5.18d.

5.4.10 Dɪ-sɪRNA SHOWS WIDESPREAD DISTRIBUTION AND SUSTAINED SILENCING IN NON-HUMAN PRIMATE SPINAL CORD.

The cortex and striatum are the two brain regions primarily affected in HD. However, treatment of other neurodegenerative disorders (e.g. ALS) may require gene modulation in the spinal cord. In ALS, a rapidly progressive and devastating neurodegenerative disease, dysfunction and degeneration of motor neurons is a primary driver of disease pathogenesis[186]. Consequently, we evaluated Di-siRNA distribution and efficacy throughout the spinal cord (one month post injection) (Fig. 5.22).
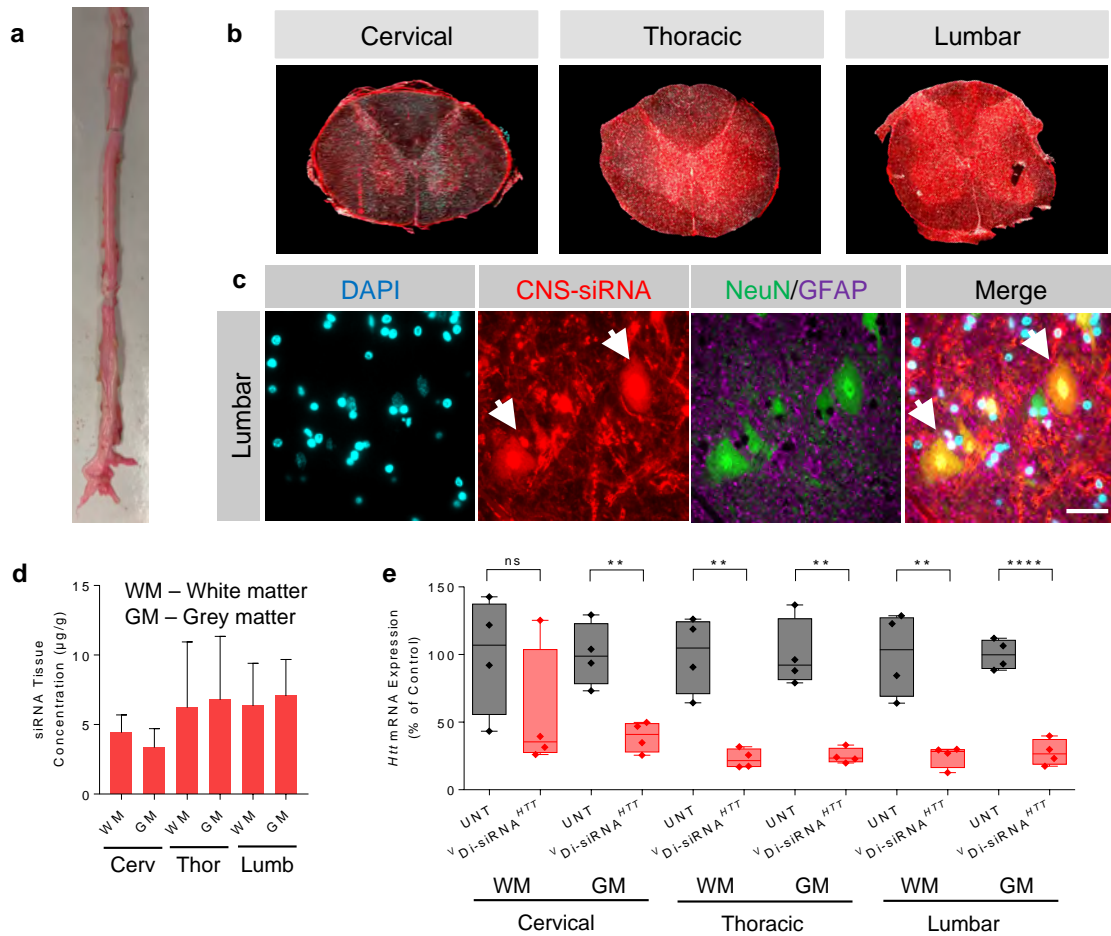
Figure 5.22 Di-siRNA shows widespread distribution, retention, and efficacy in the non-human primate spinal cord.
a. Image of the whole NHP spinal cord. b. Tiled fluorescent images of cross sections of the spinal cord at each segment c. Immunofluorescence of the NHP spinal cord (cervical, thoracic and lumbar regions). All images acquired 48 hours after a single unilateral ICV injection of 25 mg Di-siRNA. Scale bar – 50 µm. d. Quantification of siRNA guide strand (µg/g) in three spinal cord regions, both white and grey matter. e. *HTT* mRNA silencing in various regions of the NHP spinal cord. Statistics calculated by two-tailed unpaired t-test: Cervical GM: t=4.686, df=6, **P=0.0034. Thoracic WM: t= 5.278, df=6, **P=0.0019. Thoracic GM: t=5.757, df=6, **P=0.0012. Lumbar WM: t=4.69, df=6, **P=0.0034. Lumbar GM: t=9.853, df=6, ****P<0.0001. 1 month (n=4 Di-siRNA treated animals, n=4 naive animals). All graphs are mean ± SD.

We observed robust distribution to all spinal cord regions, with guide strand

accumulation ranging from 4-7 µg/g (Fig. 5.22d). Slightly higher accumulation was seen

in the lumbar compared to the cervical region. In all sections tested, we observed efficient

delivery to all cell types, including neurons. Figure 5.22c shows immunofluorescence of the ventral horn of the lumbar spinal cord segment, indicating robust delivery to lower motor neurons, easily identified morphologically by their large soma[187].

Again, the level of guide strand accumulation was sufficient for significant and potent *HTT* mRNA silencing in all regions tested ($p < 0.01$), with the exception of a single outlier in cervical white matter (Fig. 5.22e). These findings suggest that a single Di-siRNA injection supports potent and widespread gene modulation in the NHP brain and spinal cord, thus opening all regions of the CNS to RNAi based therapeutics.

5.4.11 A SINGLE INJECTION OF 25 MG OF DI-SIRNA IN NHP BRAIN DOES NOT INDUCE ANY DETECTABLE ADVERSE EVENTS.

We next looked at overall safety and tolerability of a single injection of 25 mg Di-siRNA in NHP. MRI is commonly used to look at brain inflammation and edema. MRIs were collected pre-operatively and one month following injection. There was no detectable difference between these scans, indicating that Di-siRNA injection did not cause a major inflammatory response (Fig. 5.23a). Consistent with this finding, we observed no significant up-regulation of IBA-1 and GFAP at one month post injection (Fig. 5.23b,c).
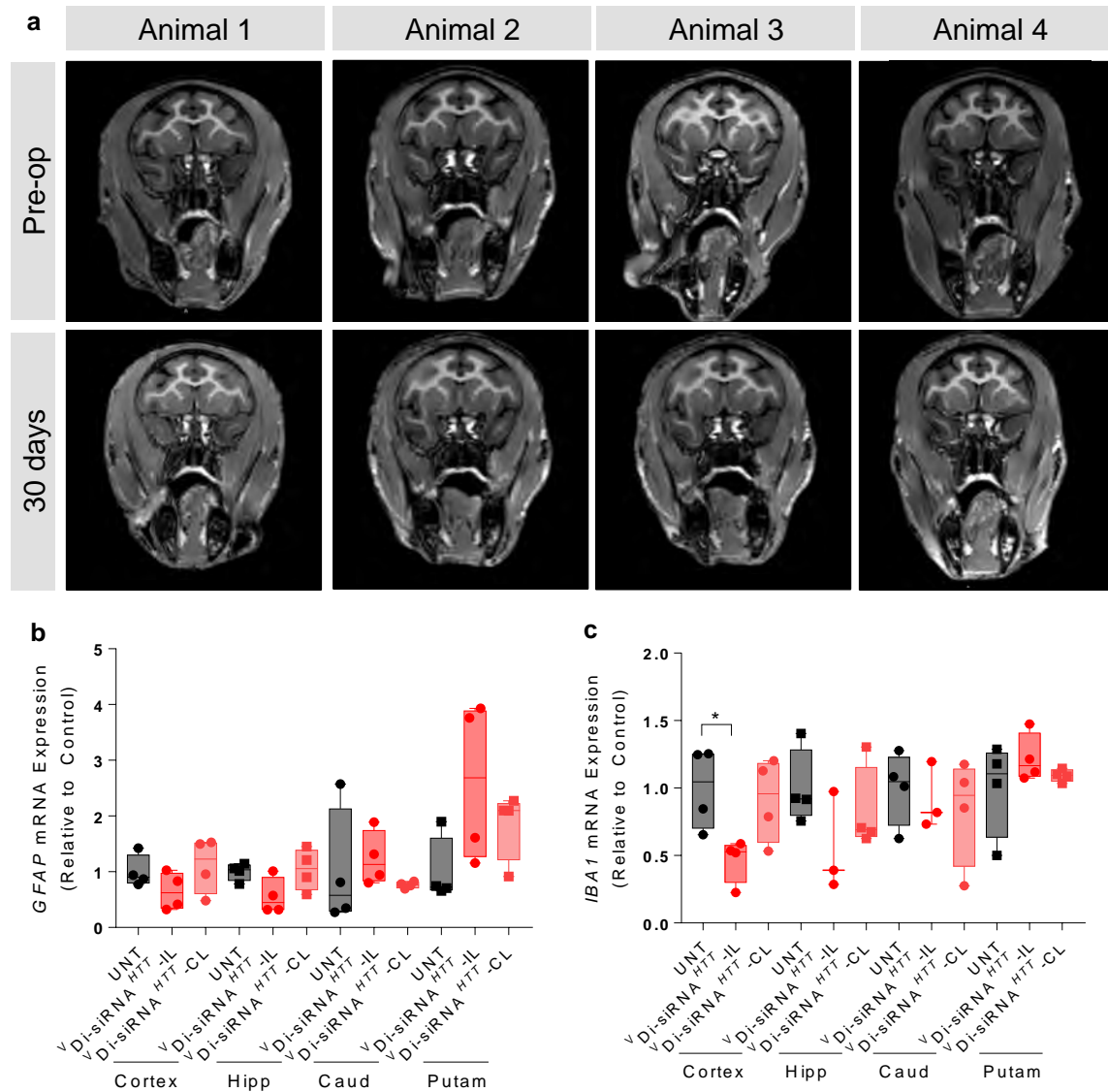
Figure 5.23 No detectable brain toxicity 1 month after a single ICV injection of Di-siRNA in pilot non-human primate studies.
Animals were all dosed with 25 mg Di-siRNA unilaterally into the lateral ventricle. a. Pre-operative and post-operative (30 days) MRI scans. b. There is no significant increase in GFAP mRNA expression 30 days after a single ICV injection.. c. There is no significant increase in IBA-1 mRNA expression 30 days after a single ICV injection. Statistics calculated by One-Way ANOVA with Dunnet's correction for multiple comparisons. All results compared to naïve control. $F(2,9) = 4.578$ iplsilateral *$P<0.0359$. n=4/group.

To determine whether there was any effect on neuronal viability, we examined two additional markers by western blot, NeuN[188] and BF-1[189]. We observed no differences between naïve and treated animals (Fig. 5.24).
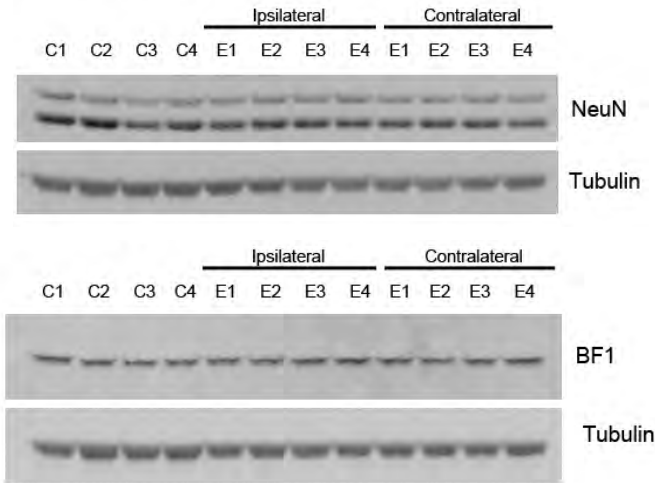
Figure 5.24 Di-siRNA does not cause cell loss in the cortex 1 month after a single ICV injection. Cynomolgus macaques received an ICV injection of Di-siRNAs (25 mg). Two neuronal markers were measured by western blot: NeuN and BF1.

In addition, we found no measurable changes in blood chemistry or cell counts (Fig. 5.25), which is particularly important because thrombocytopenia (low platelet count) has been reported as a PS-mediated rare adverse event[39, 171].

a

	Dates of the assay: Units	1312007 4-Apr Pre-op	1312007 19-Apr 15 days	1312007 3-May 30 days	1312019 3-Apr Pre-op	1312019 19-Apr 15 days	1312019 3-May 30 days	1401045 9-Apr Pre-op	1401045 23-Apr 15 days	1401045 10-May 30 days	1401401 30-Apr Pre-op	1401401 15-May 15 days	1401401 30-May 30 days
ALB	g/dL	4.5	4.7	4.5	4	4.4	4.2	3.6	4.2	3.6	4.3	4.5	4.4
ALP	U/L	381	354	406	267	288	312	231	288	260	419	420	417
ALT	U/L	36	35	39	30	28	32	29	36	26	40	45	35
AMY	U/L	318	408	359	269	295	275	238	196	193	240	222	223
TBIL	mg/dL	0.4	0.4	0.4	0.4	0.4	0.5	0.3	0.4	0.3	0.4	0.3	0.3
BUN	mg/dL	20	18	16	17	11	15	13	10	7	17	17	10
Ca2+	mg/dL	9.3	9.8	9.5	9.2	10	9.4	8.6	9	8.4	9.7	9.8	9.8
PHOS	mg/dL	7.2	5.6	5.3	6.7	5.9	7.1	7.3	4.5	6.6	6.7	5.5	4.7
Cre	mg/dL	0.9	0.7	0.8	0.8	0.3	0.9	0.9	0.7	0.7	1	0.9	0.9
GLU	mg/dL	65	59	61	112	88	81	81	68	111	95	66	86
Na+	nmol/L	140	140	141	137	141	140	142	140	140	147	140	138
K+	nmol/L	4.6	3.9	3.7	4.4	3.8	3.8	4.6	4	4	4.2	4.1	3.8
TP	g/dL	6.4	6.9	6.4	6.2	7.1	6.3	5.9	7	5.7	6.7	7.5	6.9
GLOB	g/dL	1.9	2.3	1.9	2.2	2.7	2.1	2.4	2.8	2.1	2.4	3	2.5
QC		Ok	OK	OK	OK	OK	OK	OK	OK	OK	OK	OK	OK
HEM		0	0	0	0	2+	0	0	0	0	0	2+	0
LIP		0	0	0	0	0	0	0	0	0	0	0	0
ICT		0	0	0	0	0	0	0	0	0	0	0	0

b

	Dates of the assay: Units	1312007 8-Jan Pre-op	1312007 19-Apr 15 days	1312007 3-May 30 days	1312019 8-Jan Pre-op	1312019 19-Apr 15 days	1312019 3-May 30 days	1401045 30-Nov Pre-op	1401045 23-Apr 15 days	1401045 10-May 30 days*	1401401 30-Apr Pre-op	1401401 15-May 15 days	1401401 30-May 30 days
WBC	10^9/L	13.27	15.5	14.09	9.64	15.96	9.07	5.7	2.46		6.58	15.35	14.63
LYM	10^9/L	0.26	0.25	0.16	0.01	1.27	0.01	0.2	0.04		0.1	5.73	0.25
MON	10^9/L	6.48	7.77	8.2	5.78	11.04	4.75	3.34	1.86		4.62	2.71	6.47
NEU	10^9/L	6.54	7.48	5.73	3.85	3.65	4.31	2.16	0.56		1.86	6.91	7.9
EOS	10^9/L												
BAS	10^9/L												
LYM%	%	1.9	1.6	1.2	0.1	7.9	0.1	3.5	1.7		1.5	37.3	1.7
MON%	%	48.8	50.1	58.2	60	69.2	52.4	58.6	75.7		70.2	17.6	44.3
NEU%	%	49.2	48.3	40.7	39.9	22.9	47.5	37.9	22.6		28.3	45	54
EOS%	%												
BAS%	%												
RBC	10^12/L	5.03	5.09	4.89	5.15	5.35	4.71	4.81	4.44		5.78	5.65	5.48
HGB	g/dL	13.9	14.2	13	14	14.1	12.6	13	11.3		14.4	14	13.7
HCP	%	37.4	37.83	36.78	38.93	40.11	35.93	36.81	35.1		40.1	38.77	38.33
MCV	fl	74	74	75	76	75	76	80	79		69	69	70
MCH	pg	27.7	27.8	26.5	27.1	26.3	26.8	28.1	25.5		25	24.8	25.1
MCHC	g/dL	37.3	37.5	35.2	35.9	35.2	35.1	35.2	32.2		36	36.1	35.9
RDWc	%	15.1	14.9	15.1	14.9	14.6	14.8	14.1	14.5		15.6	15.4	15.7
RDWs	fl	45.3	44.5	45.3	45.3	43.8	44.5	45.3	46.1		43	42.2	43.8
PLT	10^9/L	427	510	442	303	301	292	330	2		396	242	413
MPV	fl	7.9	7.8	7.7	8.2	9.4	7.9	9.2	6		8.7	9	8.5
PCT	%	0.34	0.4	0.34	0.25	0.28	0.23	0.31	0		0.34	0.22	0.35
PDWc	%	36.2	35.3	36.2	36.9	35.9	36.7	38	22.8		37.8	36.4	36.2
PDWs	fl	11.9	11.2	11.9	12.7	11.7	12.4	14.9	4.5		13.7	12.2	11.9
PrVP		338/342	340/344	339/342	346/349	344/348	330/335	350/354	348/352		340/344	348/352	345/349
PrVR		334/336	332/333	328/330	337/340	334/336	323/325	343/346	339/341		334/336	338/340	335/337
PrVE		0/0	0/0	0/0	0/0	0/0	0/0	0/0	0/0		0/0	0/0	0/0
WBC Lyse	ml	0.5	0.5	0.5	0.5	0.5	0.5	0.5	0.5		0.5	0.5	0.5
Lyse2	ml	0	0	0	0	0	0	0	0		0	0	0

*Sample not available

Figure 5.25 Di siRNA shows no changes in blood chemistry or cell counts.
Data collected before pre-op, 15 days and 30 days post ICV Di-siRNA injection. a.
Blood chemistry markers. b. Cell counts. N=4/group.

Finally, we sent treated and naïve NHP brain sections for independent neuropathological analysis. The summary of the report is included in Appendix A. No histopathological changes, with exception of changes resulting directly from the needle track, were identified.

Collectively, these findings suggest that a single CSF injection of Di-siRNA enables broad, potent, and safe modulation of gene expression throughout the NHP brain in the animals tested. It is important to note that the data presented is limited to a short-term, one-month study. Further evaluation of long-term safety of non-selective HTT modulation, as well as repetitive dosing of Di-siRNA, is necessary.

5.4.12 DI-SIRNA HTT MODULATES HTT EXPRESSION WITH MINIMAL OFF-TARGET EVENTS.

To determine if HTT modulation or Di-siRNA treatment had any major effect on the transcriptome, we performed genome-wide RNA sequencing (RNA-seq), comparing Di-siRNA^{HTT}-treated to naïve NHP brains. We analyzed three cortical replicates from each of 8 animals (4 naïve, 4 treated). We chose to analyze the cortex, because we observed the highest accumulation of Di-siRNA in this region; therefore, the chances of seeing off-target effects would be maximized.

We observe 52 genes with significant differential expression between treated and naïve animals, using a 1% FDR significance threshold (Figure 5.26, Table 5.2).
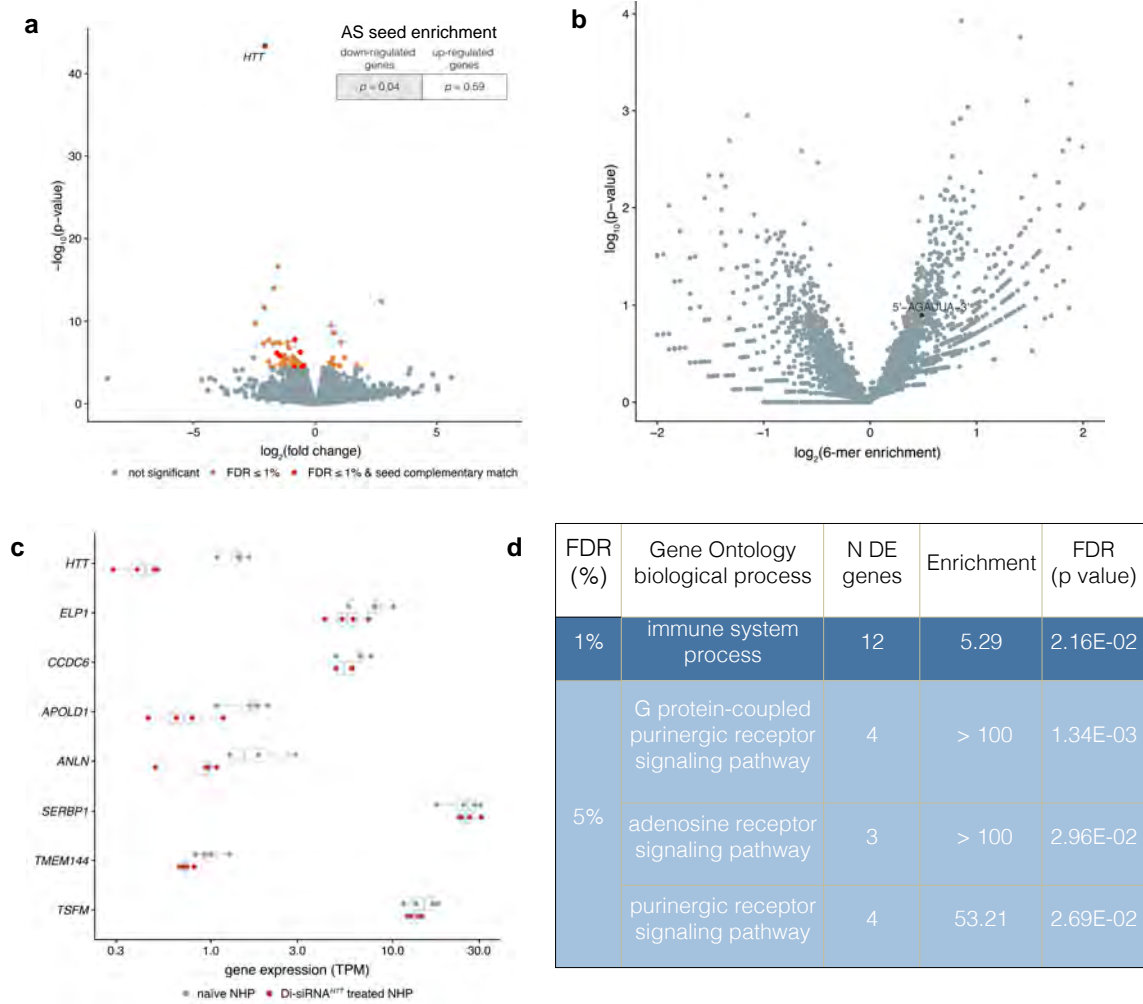
Figure 5.26 Di-siRNA shows few off-target effects genome-wide.
RNA collected from Cynomolgus macaques was subjected to RNA-sequencing to assess genome-wide patterns of differential gene expression. a. Volcano plot showing genome-wide gene expression changes in Di-siRNA[HTT] treated NHPs, with differentially expressed genes (Benjamini Hochberg FDR < 1%) in orange and differentially expressed genes with a 3' UTR seed complementary region in red. Enrichment of 3' UTR seed complementarity down- or up-regulated genes (top-right) was calculated using a Fisher's exact test. b. Volcano plot showing unbiased screen for enriched 6-mer sequences within 3' UTRs of differentially expressed gene (FDR < 1%). There are no significantly over- or under-represented sequences after Benjamini Hochberg multiple test correction. Seed complementary sequence for Di-siRNA[HTT] is indicated in black. c. Gene expression measurements (transcripts per million, x-axis) across 4 naïve NHPs (grey) and 4 Di-siRNA[HTT] treated NHPs (red) for the 8 differentially expressed genes with seed complementary regions. d. Significant gene ontology categories for differentially expressed genes with FDR < 1% and FDR < 5%.

Table 5.2 Differentially expressed genes

Ensembl_ID	Gene Symbol	log2 Fold Change	pvalue	padj	n_mismatch	Description
ENSMFAG00000036776	HTT	-2.06	4.27E-44	5.83E-40	0	huntingtin [Source:NCBI gene;Acc:102128821]
ENSMFAG00000046425	ND5	-1.52	2.14E-17	1.46E-13	NA	NADH dehydrogenase subunit 5 [Source:NCBI gene;Acc:7857747]
ENSMFAG00000034429	CSF1R	-1.68	9.88E-15	4.49E-11	2	colony stimulating factor 1 receptor [Source:NCBI gene;Acc:102124214]
ENSMFAG00000037799	HBB	2.73	3.40E-13	1.16E-09	1	hemoglobin subunit epsilon 1 [Source:NCBI gene;Acc:102136244]
ENSMFAG00000030190	SELPLG	-2.09	1.91E-12	5.20E-09	NA	selectin P ligand [Source:NCBI gene;Acc:102142477]
ENSMFAG00000044029	CX3CR1	-2.46	1.67E-10	3.80E-07	NA	C-X3-C motif chemokine receptor 1 [Source:NCBI gene;Acc:101925250]
ENSMFAG00000030038		0.66	3.32E-10	6.47E-07	3	uncharacterized LOC101866646 [Source:NCBI gene;Acc:101866646]
ENSMFAG00000031555	MICALL2	0.79	2.26E-09	3.85E-06	NA	MICAL like 2 [Source:NCBI gene;Acc:102118938]
ENSMFAG00000031963	LENG8	0.75	2.61E-09	3.95E-06	1	leukocyte receptor cluster member 8 [Source:NCBI gene;Acc:102140623]
ENSMFAG00000043210	ELP1	-0.83	1.71E-08	2.33E-05	0	elongator complex protein 1 [Source:NCBI gene;Acc:102135106]
ENSMFAG00000045718	PLD4	-1.90	2.00E-08	2.48E-05	3	phospholipase D family member 4 [Source:NCBI gene;Acc:102145104]
ENSMFAG00000033464	BBC3	1.07	3.23E-08	3.53E-05	1	BCL2 binding component 3

As expected, HTT stood out as a single outlier with the most significantly impacted mRNA levels (75% silencing, P < 10-40). With the exception of HTT, most gene expression changes were minimal. Importantly, both the level and consistency of modulation for other genes were nowhere near what was observed with HTT.

siRNA off-target effects are a major concern in development of siRNA-based therapeutics[38]. siRNA off-target effects are predominantly due to seed (position 2-7 of the guide strand) complementarity in the 3'UTR of other targets[190]. To evaluate if the observed non-HTT gene expression changes were due to off target effects of the siRNA, we looked at enrichment for seed complementarity in significantly downregulated and upregulated targets. Downregulated transcripts were slightly enriched for perfect complementarity to the guide strand seed region (P = 0.04) while no enrichment was observed in up-regulated genes (P = 0.59). No enrichment was observed for seed reverse complement. In comparison to a previous study evaluating RNA-seq in rat livers treated with siRNA, the off target effects observed here are minor[38].

To look more broadly at potential seed enrichment, we performed a novel analysis, searching all differentially expressed 3' UTRs for any combination of six nucleotides (seed length) that were overrepresented. For genes differentially expressed at a 1 % FDR, there were no significantly over-represented 6-mers and the HTT siRNA seed complement "AGAUUA" was present in the middle of distribution (Fig. 5.26b). Relaxing the differential expression threshold to 10% FDR, there were several overrepresented 6-mers, but none of them match AGAUUA (Fig. 5.27).
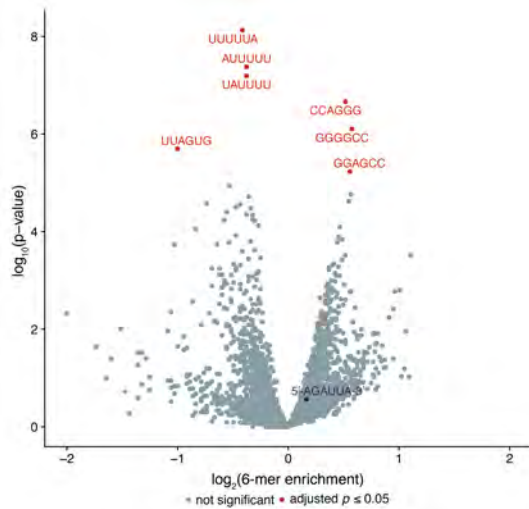
Figure 5.27 Volcano plot showing unbiased screen for enriched 6-mer sequences within 3' UTRs of differentially expressed gene (FDR < 10%). Significantly over- or under-represented sequences (Benjamini Hochberg adjusted p-value < 0.05) are in red. Seed complementary sequence for Di-siRNA*HTT* is indicated in black.

There were 7 differentially expressed genes whose 3' UTRs contain the AGAUUA seed complement. The gene expression values (transcripts per million) for individual animals are shown in Figure 5.27c. For five out of seven transcripts, the changes were minor and are likely not to be biologically significantly. Thus, there were only two potential genes, APOLD1 (~ 40% down) and ANLN (~ 20% down), that might be down-regulated due to miRNA-like off-target modulation.

Huntingtin expression is essential for embryonic development[191], but the conditional modulation of huntingtin in adult mice has very minimal phenotype[192], suggesting that non-selective modulation of HTT might be a reasonable therapeutic approach. However, HTT is involved in several cellular processes[193], generating the potential for transcriptional changes downstream of HTT silencing ("on-target effects" vs "off-target"). To determine if changes were due to "on-target effects" of HTT modulation, we performed gene ontology analyses on the differentially expressed genes. With a 1% FDR, only the "immune system processes" category was significantly enriched among differentially expressed genes, with 12 out of 576 expressed genes in this category showing differential expression.

155

With a 5% FDR, three other pathways were slightly significantly enriched (Fig. 5.26d; G-protein-coupled purinergic receptors signaling, adenosine receptor signaling and purinergic receptor signaling), with all changes being minor.

At this point, we are not able to distinguish if the observed minor transcriptional changes are of biological significance and, if so, they are due to the trauma of ICV injection itself, a consequence of month-long HTT silencing, or off-target modulation.

In general, RNA-seq analyses of Di-siRNA HTT treated NHP brains reveal a lack of major transcriptional changes (aside from HTT modulation) and minimal, if any, off-targeting activity. Thus Di-siRNA enable highly specific modulation of gene expression in the CNS.

5.5 DISCUSSION

The ability to modulate gene expression in the CNS opens up a wide range of neurological diseases to therapeutic intervention. Many different technologies are being explored for gene modulation in the CNS, including ASOs and adeno-associated virus (AAV)[5, 133, 184, 194]. Delivery of AAV via intra-parenchymal injections shows promise, with efficient HTT silencing being observed in minipig, sheep, and NHP[194-196]. However, multiple injections of AAV are required due to the limited distribution achieved upon a single injection. While this approach would eliminate the need for repetitive dosing, major technological advances in the field of AAV delivery are needed to achieve uniform silencing throughout the brain. In contrast, ASOs are the most clinically-advanced technology, with multiple compounds in different stages of clinical evaluation[197]. Recent data with HTT-targeting ASOs show ~50% modulation of soluble mutant HTT in the CSF of patients following monthly intrathecal injections (Clinical Trial ID:

NCT03342053). However, ASO delivery to deep brain structures is limited[5], with no significant HTT silencing observed in NHP caudate with multiple injections[184]. Di-valent, PS-containing, fully chemically stabilized siRNA enables wide spread distribution and efficacy after a single bolus injection in rodent and NHP brains, and offers a new approach for gene modulation in the CNS.

The broad distribution and retention of Di-siRNAs in the non-human primate brain is likely due to its large size, which may slow the rate of CSF clearance. Thus, the difference in size between ASOs (7 KD) and Di-siRNAs (27 KD) may be partially responsible for the observed difference in distribution to deep brain structures. It is possible that similar strategies might be employed to enhance deep brain delivery of other therapeutic RNA classes. The concept of branching has been explored for ASOs, specifically by IDERA Pharmaceuticals. Their approach links two first-generation ASOs (fully phosphorothioated DNA and RNA) together via the 5' ends, which results in better systemic efficacy compared to monomeric ASO variants[198].

In addition to size, the Di-siRNAs are comprised of two PS-containing siRNAs, with 26 PS modifications per molecule. Elimination of PS content in siRNA scaffold completely abolished efficacy (Fig. 5.5), suggesting that enhanced brain retention and distribution is dependent on the presence of PS modifications. The mechanism behind PS-mediated delivery is not fully understood, but multiple cell surface receptors have been recently identified that may be involved in phosphorothioated oligonucleotide uptake[164]. Optimizing PS content is currently the strategy utilized for fine-tuning ASO potency and toxicity profiles. The siRNA scaffold used in this study (13 out of 35 backbones phosphorothioated or ~40% PS content) is not sufficient to promote

significant retention for monomeric compounds. Yet, by increasing the size and linking these two compounds together, the cooperativity of weak PS-driven cellular interactions produces robust cellular uptake and retention. Increasing the percentage of PS modifications, either uniformly (i.e. every other nucleotide linkage) or strategically positioned, throughout the siRNA may interfere with RISC assembly[172, 173] and reduce tolerability. Therefore, a multi-valency approach may be preferable for achieving siRNA uptake without overt toxicity.

Mouse studies confirmed that duration of effect could be predicted based on compound tissue accumulation at earlier time points (one month). In NHPs, we observed potent silencing in all brain regions at one month after injection. Given the level of accumulation in cortex and hippocampus, silencing is expected to last 6-9 months in these regions, and as long as 2-4 months in the caudate and putamen. Therefore, repetitive injections would be necessary to maintain HTT silencing throughout the brain. While a single injection was found to be safe at one month, additional studies would be necessary to evaluate long-term safety.

Interestingly, animals with a single treatment of Di-siRNA targeting HTT show significant silencing of HTT, yet did not exhibit major transcriptional changes. There were minimal observed miRNA-like off target effects, with only two genes identified as putative candidates for minor off-target based modulation. While seed complementary sequences were slightly overrepresented in the 3' UTRs of downregulated transcripts (P = 0.04), the overall effect and overall degree of enrichment was minimal compared to previously observed off-target effects with siRNA in rat livers[38] and in cells[199]. Off-target effects were explored in cortical samples, where guide strands accumulated to more than

9 ug/g resulting in more than 90% HTT protein silencing. Significantly lower accumulation has been observed to be sufficient for target modulation, so the lack of significant off-target effects in this region is likely representative of the transcriptome changes at high guide strand concentration. It is unclear if the lack of significant off-target effects is specific to CNS regions, NHPs or these particular compounds. At this point there is no other genome-wide off-targeting data in NHPs available for comparison.

The lack of a large number of transcriptome changes at one month following potent HTT modulation is consistent with published data that elimination of HTT in adult mice has minimal phenotypes[192]. While encouraging, long-term safety studies need to be performed to conclude that non-selective potent HTT modulation is safe.

An interesting and often debated consideration is whether non-selective or single nucleotide polymorphism (SNP)-selective modulation of *Htt* expression is a better therapeutic strategy for HD. The most clinically-advanced ASO compound targeting Htt (Clinical Trial ID: NCT03342053) modulates wild type and mutant HTT non-selectively. However, there are other programs (from Wave Life Sciences and IONIS Pharmaceuticals) that enable SNP-based discrimination. An argument for a non-selective strategy is that it allows for the treatment of all HD patients with a single entity[200]. Furthermore, although HTT knockout is embryonically lethal, its elimination is well tolerated in adult mice[192]. Di-siRNA compounds deliver to most of the cortical neurons, resulting in non-selective, potent silencing of wild type and mutant HTT. The long-term safety of such widespread down-regulation must be assessed carefully.

In this paper, we characterized Di-siRNA as a new chemical scaffold that enables potent modulation of *Htt* gene expression in the CNS, independent of brain size. The

identified scaffold can be reprogrammed to silence other genes in CNS, opening CNS of

RNAi-based modulation of gene expression in CNS. Further, in depth, evaluation in

established disease models is necessary to assess the impact of Di-siRNA-mediated

silencing of HTT on disease progression. However, these findings establish a foundation

for developing a range of siRNA compounds to target genetically defined CNS disorders.

CHAPTER VI: DISCUSSION

In this dissertation I have described a new siRNA dianophore that enables both a long-lasting duration of effect of silencing as well as widespread distribution and retention in the non-human primate brain. This is the first described siRNA to show this magnitude of distribution and silencing.

ASOs are leading the field of oligonucleotide delivery to the brain[5, 133]. While siRNAs had been investigated with some local brain delivery[55-58], it was difficult to achieve widespread long-term distribution not in small part due the limitations in chemical structure and modification space[20]. siRNAs must be recognized by the AGO2 protein and their modification pattern must neither interfere with their shape nor effect their interactions with the various domains of the AGO2[23]. However given the efficiency of siRNA mediated mRNA silencing[12] it seemed important to determine if an alternative chemical scaffold could support similar delivery and efficacy with siRNAs than ASOs.

In Chapter I of this dissertation the qualities of an informational drug that uniquely allow for separation of the pharmacophore, or targeting sequence, from the dianophore[1], or chemical scaffold that supports delivery characteristics, are laid out. Therefore the first step in identifying a new dianophore is to identify an efficient pharmacophore to establish the context in which the dianophore efficiency can be assessed. In Chapter III I identify a functional siRNA sequence for targeting Huntington's disease. Partially modified cholesterol conjugated siRNA dianophore did not provide ideal distribution, silencing, or duration of effect, thus identification of this sequence acted as a jumping off point for further investigation[58].

161

At the start of this research, the standard chemistry in the field for siRNAs was partial 2'-*O*-methyl/2'fluoro modification[59]. In Chapter IV of this dissertation I describe different versions of fully modified siRNAs in the context of systemic delivery and efficacy. While other labs have published on a fully modified chemical scaffold, there has been no side-by-side comparison of retention and efficacy of partially and fully modified siRNAs in a multi-organ *in vivo* study. This research made it abundantly clear that assessing the functionality of new chemical conjugate for siRNA can only be done in the context of a fully chemically stabilized siRNA[37]. These results are confirmed by Alnylam Pharmaceuticals who have continued to improve the efficacy and potency of an individual sequence by adjusting even the pattern and position of 2'-*O*-methyl and 2'-fluoro modifications[20, 163, 165].

In my final research Chapter V I describe a new dianophore for delivery of siRNA to the brain. As I mentioned, ASOs are currently leading the field in the treatment of neurodegenerative diseases with an informational drug[5, 66]. When I joined the lab the strategy to support siRNA delivery to the brain was to synthesize a number of different hydrophobic conjugates to try to increase distribution while maintaining retention. Unfortunately these two aspects of a hydrophobic molecule are tightly linked with increased hydrophobicity leading to increased retention but decreased distribution and vice versa[58]. And while we understood at the time that ASOs rely on phosphorothioate mediated delivery to the brain it was unclear as to whether we could incorporate enough PS content into siRNAs to ensure retention without toxicity. As we brainstormed different ways of incorporating increased PS content into siRNAs (whether in the duplexed region, or in the context of an additional 3'sense PS tail) a failed conjugate

synthesis produced the Di-siRNA chemical scaffold. We were immediately intrigued by the properties of this molecule.

There are a number of possible explanations for the observed efficacy of the Di-siRNA chemical scaffold. One of the most obvious, the potentially enhanced PK properties and changes in compound clearance kinetics. Phosphorothioate content supports binding to both circulating proteins as well as cellular membrane proteins[30]. By linking two molecules together two flexible PS modified single stranded tails may be potentially increasing the opportunity for cooperative PS binding, where the presence of two PS binding opportunities is possibly increasing overall membrane association. There is another example of this phenomenon in siRNA field. The GalNAc conjugate consists of three identical N-acytalgalactosamine units, which increase the binding of this conjugate to the ASGPR receptor[47]. Studies have shown that while one unit of GalNAc can bind to the receptor and initiate internalization, the presence of additional GalNAc units significantly increases receptor binding[47]. It is possible that the cooperative interaction of the two PS tails has a similar effect, although with non-specific PS protein binding.

Another unique aspect to the Di-siRNA chemical scaffold is its size. It is known that systemically, a molecule's size affects the rate at which it is cleared. For example, the kidneys have a cutoff of approximately 70KD[201]. Where molecules <70KD are cleared by the kidney and molecules >70KD remain in circulation for a longer period of time. This phenomenon has been exploited by adding additional molecular weight to compounds in the form of PEGylation to increase overall circulating times which may lead to greater tissue exposure[202]. Similarly, the increase in size of the Di-siRNA

chemical scaffold relative to either the mono-siRNA chemical scaffold or the even smaller molecular weight of an ASO could be impacting the rate of CSF clearance, increasing the amount of time that the siRNA is exposed to various brain regions. This increased exposure could also explain the ability of Di-siRNA to penetrate to deeper regions of the brain such as the caudate and putamen. By increasing the time of circulation we may also be increasing the amount of interstitial fluid exchange allowing for deeper penetration and increased overall compound retention. ASO studies in both mouse and non-human primate require weekly dosing for one month [66], yet silencing in the non-human primate brain is not observed in deeper brain regions such as the caudate, putamen or hippocampus[184]. The observed deep brain silencing of the Di-siRNA chemical scaffold could be a result of changes in PK properties.

While the studies performed here suggest robust silencing and duration of effect that could offer significant therapeutic value, it is important to think about the potential drawbacks to such a potent non-specific down-regulation of a protein whose function is not well understood. Huntington's disease is autosomal dominant[83]. This means that there is still a wild type copy of the huntingtin gene. In mice a huntingtin knockout phenotype, while embryonic lethal, has not been shown to have any notable effects in adults[192]. However with a protein that has been implicated in so many functions[193], it is hard to know whether near complete silencing of the huntingtin gene will have an effect in adult humans. Therefor an alternative treatment could be to silence only the mutant huntingtin transcript leaving expression of the wild type transcript unaltered. There are two main differences between the mutant and the wild type transcript: one is the length of the CAG repeats[203] and the other is the presence of differing SNPs, or single nucleotide

164

polymorphisms[200]. Attempts to silence at the CAG repeats could potentially have off target effects as there are other genes that contain this repeat, but our lab and others have had success in selectively silencing at SNPs. While the potential off-target (the wild type transcript) is only different by a single nucleotide, introduction of a second mismatch or use of alternative backbone and base chemistry can increase the selectivity of the informational drug for the mutant HTT transcript. While the current clinical candidate ASO targets both the wild type and mutant huntingtin, exploring the ability to just silence a single allele is an important therapeutic question and is currently being investigated (Wave Life Sciences)[133, 204].

There has also been some evidence that it is not even the full-length transcript that is causing the disease but a truncated version (exon and intron 1) that is toxic[205]. Given that the sequence described in this dissertation targets the early 3'UTR, this informational therapeutic would not target the short fragment. In this case it would be necessary to identify a new sequence that target both the short fragment as well as the full length fragment, or potentially only the short fragment by targeting an intronic sequence. This, like SNP targeting, becomes far easier to attempt given that the dianophore for brain delivery has already been identified.

Lastly our lab has shown that huntingtin mRNA, especially in Huntington's disease exhibits significant nuclear localization[179]. While there is some evidence that siRNA can functionally silence mRNA in the nucleus, the more obvious choice for nuclear silencing is an ASO approach. It may be possible to use this branched PS scaffold discussed in this dissertation to deliver an ASO as well. Using two complementary oligonucleotides attached by a linker, the scaffold could be used to carry

two antisense oligonucleotides into cells. Different chemical modifications could adjust

the melting temperature of the duplexes to ensure disassociation. `

      With any informational drug or functional genomics study it is important to

ensure that observed effects are a result of specific silencing of the target gene and not

non-specific off target gene silencing as a result of seed complementarity with another

gene. Additionally it is important to understand whether silencing of huntingtin

specifically has any major effect on the expression levels of other proteins or transcripts.

In order to investigate off target effects we chose to do RNAseq.   To ensure that we were

investigating the most serious off target effects we looked at the cortex where we had the

most silencing.   After one month no significant off target events were observed.

However there are a number of considerations to make when extending this limited

analysis to broad assumptions of off target effects. For one, while the cortex may have

the greatest silencing, it is possible that there are other brain regions that have had more

significant off target effect than the cortex as huntingtin may play a more important role

in another brain region. Secondly, the analysis was done after one month.   Given that

the huntingtin protein has so many functions it is possible that off target effects could

accumulate and cause issue at a later date. Therefor it is important that we investigate the

effect of huntingtin lowering at later time points.

      With the identification of a new siRNA dianophore for the brain the most obvious

next question is can this scaffold be applied to alternative genetically defined

neurodegenerative disease?   This research shows that the chemical scaffold is not

sequence dependent and can be applied to alternative sequences (APOE and PPIB).

Additionally the widespread distribution achieved opens other regions of the brain for

therapeutic targeting. For example, Huntington's disease will primarily require targeting of the striatum and cortex, Alzheimer's disease requires targeting of the hippocampus and cortex, cerebellar ataxia requires targeting of the cerebellum, and ALS requires targeting of the spinal cord and lower motor neurons as well as targeting of the motor cortex. With full cortical, deep brain, and spinal cord distribution and silencing, this new chemical scaffold can potentially be applied to a wide range of neurodegenerative diseases.

Although this dissertation primarily focuses on the therapeutic applications of a new chemical scaffold it is important to note that there are many basic biological applications of such a chemical scaffold as well. For instance, applying this technology for functional genomics to understand the effect of gene or protein silencing on neurological function. At present, many of these studies are done in the context of cell culture, but cell culture is unable to recapitulate the complexities of a mouse brain or brains more complex like that of the non-human primate. Even if the studies are carried out in the brain, communication between various brain regions may be able to compensate for silencing in a single brain region which could make analysis of findings in a less robust *in vivo* study more convoluted[206].

In conclusion this dissertation has 1) Identified a potent siRNA sequence for targeting huntingtin mRNA, 2) identified a fully modified chemical scaffold that enables increased systemic accumulation as well as increased silencing in multiple organs and increased duration of effect in the brain, and 3) identified a new siRNA dianophore for brain delivery that shows not only a six month duration of effect in the mouse but supports widespread distribution retention and silencing in the non-human primate brain (Fig. 6.1). These findings suggest a possible new path towards the use of siRNAs for

widespread mRNA silencing in larger animals brains and could potentially be translated

into a robust therapeutic for a number of genetically defined neurodegenerative diseases.

Chapter III: A new pharmacophore

Chapter IV: Stabilizing the siRNA

- 2'-O-Methyl RNA
- 2'-Fluoro RNA
- 2'-Hydroxyl RNA
- Phosphorothioate
- 5'-Phosphate
- Cholesterol
- TEG linker

Informational drug

Chapter V: A new dianophore
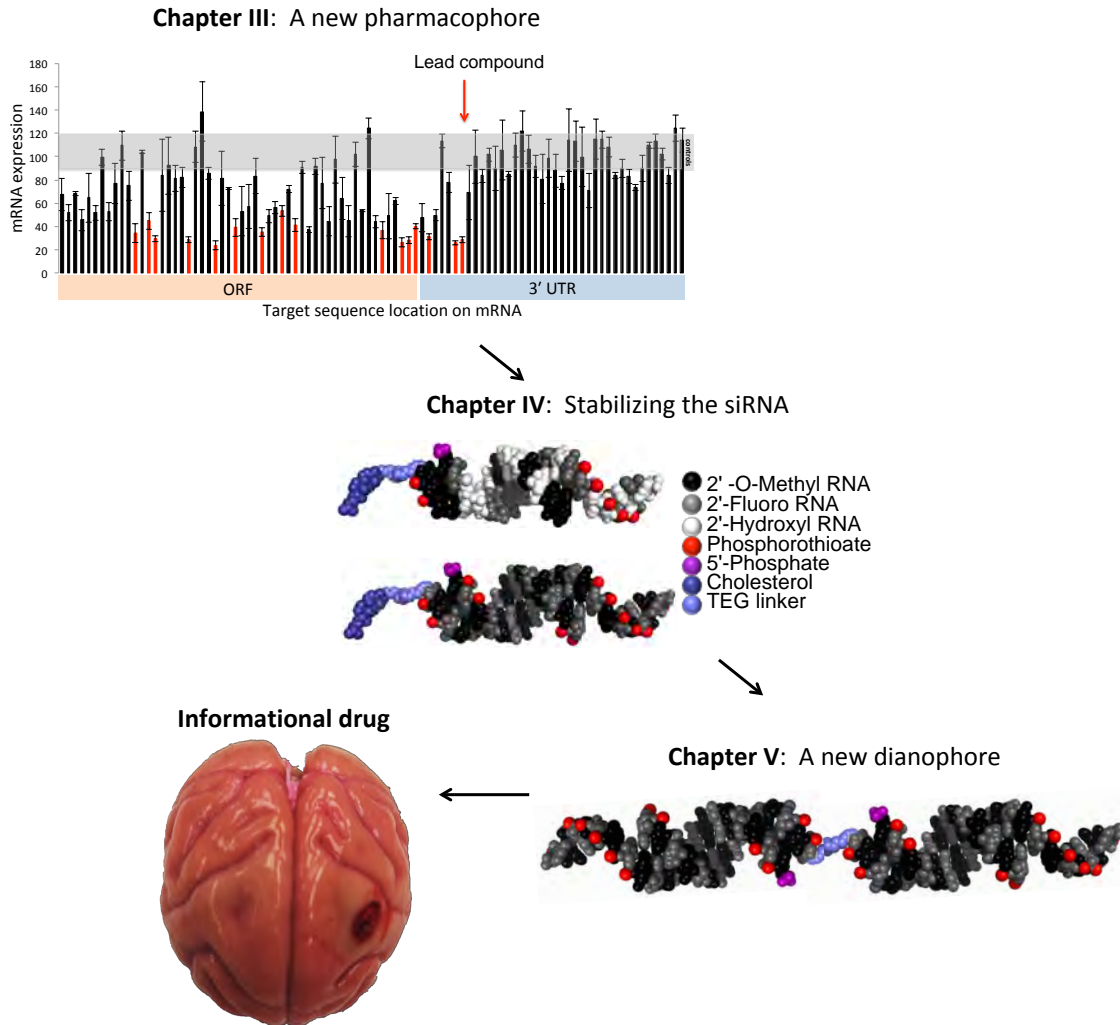
Figure 6.1 Graphical summary

APPENDICES

APPENDIX A: NON-HUMAN PRIMATE BRAIN HISTOLOGY REPORT

Test Site Reference No. 20187084

Histopathologic changes in the brain were very similar in all four monkeys and were primarily localized to the brain regions at the site of the ICV injection. These changes included the presence of an injection track; minimal to mild gliosis with gemistocytosis; minimal to mild perivascular cuffing of mononuclear cells; and minimal to mild axonal degeneration. The nature, severity and distribution of these changes is consistent with the ICV procedures employed and/or the resulting reparative processes. No evidence is present that suggests an exacerbation due to the presence of the siRNA test article.

In addition, two monkeys (Nos. 1 and 4) had mild degenerative changes focally in the superficial cerebral cortex. The nature, severity and location of these changes is consistent with effects due to the surgical procedures used for the ICV injection. In conclusion, the histopathologic changes identified, i.e., injection track, gliosis, perivascular cuffing of mononuclear cells, axonal degeneration, were localized to the immediate region of the injection and were considered related to the experimental procedures that were employed and/or the resulting reparative processes. Histopathologic changes resulting directly from the administration of the siRNA were not identified.

RESPONSIBLE PERSONNEL

Study Pathologist	James P. Morrison, DVM, DACVP
	Charles River Laboratories, Inc.
	334 South Street
	Shrewsbury, MA 01545
Test Site Management	Scott Fountain, PhD
	Charles River Laboratories, Inc.
	334 South Street
	Shrewsbury, MA 01545

INTRODUCTION

This report presents the pathology findings in Cynomolgus monkeys assigned to Study No. 20187084. The objective of this study was to evaluate the brain from four Cynomolgus macaques treated with siRNA once via ICV injection followed by 1 month recovery period.

The study was sponsored by University of Massachusetts Medical School, Worcester, MA. Julia Alterman, PhD candidate, served as the Study Monitor.

MATERIALS AND METHODS

All animals received an image guided ICV injection of a chemically modified siRNA intended to treat Huntington's Disease unilaterally on study day 1. The animals were submitted for necropsy after 1 month (Terminal Euthanasia). Necropsies were

performed by University of Massachusetts Medical School personnel. Tissues required for microscopic evaluation were trimmed, processed routinely, embedded in paraffin, and stained with hematoxylin and eosin by University of Massachusetts Medical School. Microscopic evaluation was conducted by the Study Pathologist, a board-certified veterinary pathologist on select tissues from 3 male and 1 female monkeys. Tissues were evaluated by light microscopy.

The brain trimming procedure that was employed resulted in seven transverse brain sections for evaluation. The sections were taken unilaterally from the hemisphere of the brain that received the ICV injection and included the following regions: frontal lobe, temporal lobe, frontoparietal lobe, occipital lobe, mesencephalon, cerebellum and medulla oblongata.

RESULTS AND DISCUSSIONS
Histopathology

Histopathologic changes in the brain were similar in all animals and were primarily localized to the brain region at the site of the intracerebroventricular (ICV) injection. Overall the changes were consistent with those expected from the injection procedure and evidence of an exacerbation of the changes resulting from the presence of the siRNA test article was not present.

The injection track was identified in all four monkeys within the cerebral white matter of the frontal lobe. The subanatomic location of the injection track in the sections evaluated ranged from immediately deep to the overlying cerebral cortex to immediately dorsal to the lateral ventricle. The variability in the location most likely reflects sectioning variability from small differences in the location of the trimming plane, although small variations in the site or angle of the injection could have contributed.

Histopathologically the injection track was characterized by a small, focal, circular to ovoid area in which the parenchyma was absent and replaced by small numbers of finely vacuolated macrophages/microglia. Mildly increased numbers of astroglia and microglia surrounded the injection tracks and extended into the neuroparenchyma a small distance from the track, gradually decreasing in number with increasing distance from the injection track. Small numbers of astrocytes surrounding the injection track had abundant homogenous eosinophilic cytoplasm and prominent, eccentrically placed, open faced nuclei, consistent with a gemistocytic morphology. In addition, small numbers of degenerating axons were present throughout the surrounding neuroparenchyma, characterized by scattered digestion chambers containing pyknotic debris and/or axonal spheroids. Multifocal perivascular cuffs of mononuclear inflammatory cells were scattered throughout the section and were minimal to mild in severity. These cuffs occasionally had small numbers of macrophages containing golden brown pigment, most likely representing lipofuscin.

In animals 1 and 4, minimal to mild degenerative changes were focally present in the superficial cerebral cortex, presumably near the location of the entry point through the skull. These changes included gliosis, minimal neuronal loss/degeneration, edema, mononuclear perivascular cuffing, and multifocal axonal spheroids. In animal 4, there was also a focal depression in the cerebral cortex at this location that was surrounded by mildly hyperplastic meninges. These changes are consistent with and presumably the result of minimal trauma resulting from the surgical entry though the skull.

Rare perivascular cuffs of mononuclear cells were present in other brain sections and occurred at an incidence and severity typical of non-human primates and thus are considered background findings unrelated to the injection procedure. In addition, in animal 4, a focal decrease in granule neurons was present in the cerebellar cortex. This was consistent with a developmental abnormality and is unrelated to the experimental procedures. All other findings are consistent with spontaneous changes.

In conclusion, the histopathologic changes identified (i.e., injection track, gliosis, perivascular cuffing of mononuclear cells, axonal degeneration) were localized to the immediate region of the injection and were considered related to the experimental procedures that were employed and/or the resulting reparative processes. Histopathologic changes resulting directly from the administration of the siRNA were not identified.

CONCLUSIONS

In conclusion, four cynomolgus macaques received an intracerebroventricular injection of an siRNA on study day 1. The majority of the histopathologic changes identified in the brain were localized to the immediate region of the injection and were considered related to the experimental procedures that were employed and/or the resulting reparative processes. Histopathologic changes resulting directly from the administration of the siRNA were not identified. Other findings occurred at an incidence and severity consistent with background or spontaneous change.

APPENDIX B: CO-AUTHORED PUBLICATIONS

1. **Alterman JF***, Godinho BMDC*, Hassler MR*, Echeverria D, Sapp E, Ferguson CM, Haraszti RA, Coles AH, Conroy F, Miller R, Roux L, King, RM, Gernoux G, Mueller C, Gray-Edwards HL, Moser RP, Bishop NC, Jaber SM, Gounis MJ, Sena-Esteves M, DiFiglia M, Aronin N, Khvorova A. Divalent-siRNAs: an advanced chemical scaffold for potent and sustained modulation of gene expression in the CNS. *Authors contributed equally to this work. Nat. Biotech., Submitted.

2. Turanov A*, Hassler MR*, Lo A*, Makris A*, Ashar-Patel A, **Alterman JF**, Coles AH, Haraszti RA[1], Roux L, Godinho BMDC, Echeverria D, Pears S, Iliopoulos J, Shanmugalingam R, Ogle R, Hennessy A, Karumanchi SA, Moore MJ, and Khvorova A. RNAi Modulation of Placental sFLT1 for the Treatment of Preeclampsia. *Authors contributed equally to this work. Nat. Biotech., 2018.

3. Haraszti RA, Miller R, Didiot MC, Biscans A, **Alterman JF**, Hassler MR, Roux L, Echeverria D, Sapp E, DiFiglia M, Aronin N, Khvorova A. Optimized Cholesterol-siRNA Chemistry Improves Productive Loading onto Extracellular Vesicles. Mol. Ther., 2018 26(8).

4. Godinho BMDC, Henninger N, Bouley J, **Alterman JF**, Haraszti RA, Gilbert JW, Sapp E, Coles AH, Biscans A, Nikan M, Echeverria D, DiFiglia M, Aronin N, Khvorova A. Transvascular Delivery of Hydrophobically Modified siRNAs: Gene Silencing in the Rat Brain upon Disruption of the Blood-Brain Barrier. Mol. Ther., 2018.

5. Mir A, **Alterman JF**, Hassler MR, Debacker AJ, Hudgens E, Echeverria D, Brodsky M, Khvorova A, Watts JK, Sontheimer EJ. Heavily and Fully Modified RNAs for Efficient Cas9-Mediated Genome Editing. Nat. Commun, 2018, 9:2641.

6. Hassler MR*, Turanov AA*, **Alterman JF***, Coles AH, Haraszti RA, Osborn MF, Godinho BM, Lo A Rajakumar A, Golebiowski D, Echeverria D, Nikan M, Salomon WE, Davis SM, Morrissey DV, Sena-Esteves M, Zamore PD, Karumanchi SA, Moore MJ, Aronin N, Khvorova A. Comparison of fully and partially chemically-modified siRNA in conjugate-mediated delivery *in vivo*. NAR, 2018, 46 (5), 2185-2196. *Authors contributed equally to this work.

7. **Alterman JF**, Coles AH, Hall LM, Aronin N, Khvorova K, Didiot MC. A High-Throughput Assay for mRNA Silencing in Primary Cortical Neurons With Oligonucleotide Therapeutics. Bio Protoc. 2017 Aug 20; 7(16): e2501

8. Sharma VK, Singh SK, Krishnamurthy PM, **Alterman JF**, Haraszti RA, Khvorova A, Prasad AK, Watts JK. Synthesis and biological properties of triazole-linked locked nucleic acid. Chem Commun (Camb). 2017 Aug 3;53(63):8906-8909.

9. Haraszti RA*, Roux L*, Coles AH, Turanov AA, **Alterman JF**, Echeverria D, Godinho BM, Aronin N, Khvorova A. 5′vinylphosphonate improves tissue accumulation and efficacy of conjugated siRNAs *in vivo. Nucleic Acids Res. 2017 Jul 27; 45(13): 7581–7592*. *Authors contributed equally to this work.

10. Didiot MC, Hall LM, Coles AH, Haraszti RA, Godinho BM, Chase K, Sapp E, Ly S, **Alterman JF,** Hassler MR, Echeverria D, Raj L, Morrissey DV, DiFiglia M,

Aronin N, Khvorova A. Exosome-mediated Delivery of Hydrophobically Modified siRNA for Huntingtin mRNA Silencing. Mol Ther. 2016 Oct;24(10):1836-1847.

11. Ly S, Navaroli DM, Didiot MC, Cardia J, Pandarinathan L**, Alterman JF**, Fogarty K, Standley C, Lifshitz LM, Bellve KD, Prot M, Echeverria D, Corvera S, Khvorova A. Visualization of self-delivering hydrophobically modified siRNA cellular internalization. Nucleic Acids Res. 2017 Jan 9;45(1):15-25.

12. Coles AH*, Osborn MF*, **Alterman JF**, Turanov AA, Godinho BM, Kennington L, Chase K, Aronin N, Khvorova A. A High-Throughput Method for Direct Detection of Therapeutic Oligonucleotide-Induced Gene Silencing *In Vivo*. Nucleic Acid Ther. 2016 Apr;26(2):86-92. *Authors contributed equally to this work.

13. **Alterman JF**, Hall LM, Coles AH, Hassler MR, Didiot MC, Chase K, Abraham J, Sottosanti E, Johnson E, Sapp E, Osborn MF, Difiglia M, Aronin N, Khvorova A. Hydrophobically Modified siRNAs Silence Huntingtin mRNA in Primary Neurons and Mouse Brain. Mol Ther Nucleic Acids. 2015 Dec 1;4:e266.

14. Osborn MF, **Alterman JF**, Nikan M, Cao H, Didiot MC, Hassler MR, Coles AH, Khvorova A. Guanabenz (Wytensin™) selectively enhances uptake and efficacy of hydrophobically modified siRNAs. Nucleic Acids Res. 2015 Oct 15;43(18):8664-72.

APPENDIX C: PATENTS AND PROVISIONAL PATENTS

1. Khvorova, A., Aronin, N., **Alterman, J.** Oligonucleotide Compounds for Targeting Huntingtin mRNA. US Patent US9809817, Nov 7, 2017.
2. Khvorova, A., Aronin, N., Hassler, M., **Alterman, J**. Fully Stabilized Asymmetric siRNA. US Provisional Patent Application No. 62/142,786, 4/3/2015
3. Khvorova, A., Hassler, M., **Alterman, J.** Branched Oligonucleotides. US Provisional Patent Application No. 62/289,268, 1/31/2016
4. Khvorova, A., **Alterman, J,** Hassler, M**.** Two-tailed Self-Delivering siRNA. U.S. Provisional Patent Application No. 62/523,949, 6/23/17.
5. Khvorova, A., **Alterman, J**., Davis, S., Turanov, A. O-Methyl Rich Fully Stabilized siRNA. U.S. Provisional Patent Application No. 62/721,993, 8/23/18.
6. Khvorova, A., Conroy, F., **Alterman, J.**, Pfister, E., Aronin, N., Chemically Modified Oligonucleotides Targeting SNPs.
7. Sontheimer, E., Khvorova, A., Watts, J., Mir, A., **Alterman, J.**, Hassler, M., Brodsky, M., Debacker, A. Modified Guide RNAs for CRISPR Genome Editing. U.S. Provisional Patent Application No.: 62/644,944, 3/19/18.

REFERENCES

1. Khvorova, A. & Watts, J.K. The chemical evolution of oligonucleotide therapies of clinical utility. *Nature biotechnology* **35**, 238 (2017).
2. Levin, A.A. Treating Disease at the RNA Level with Oligonucleotides. *New England Journal of Medicine* **380**, 57-70 (2019).
3. Barrangou, R. Cas9 Targeting and the CRISPR Revolution. *Science* **344**, 707-708 (2014).
4. Liu, J. et al. Recent developments in protein and cell-targeted aptamer selection and applications. *Current medicinal chemistry* **18**, 4117-4125 (2011).
5. Kordasiewicz, H.B. et al. Sustained therapeutic reversal of Huntington's disease by transient repression of huntingtin synthesis. *Neuron* **74**, 1031-1044 (2012).
6. Havens, M.A. & Hastings, M.L. Splice-switching antisense oligonucleotides as therapeutic drugs. *Nucleic acids research* **44**, 6549-6563 (2016).
7. Kurreck, J., Wyszko, E., Gillen, C. & Erdmann, V.A. Design of antisense oligonucleotides stabilized by locked nucleic acids. *Nucleic acids research* **30**, 1911-1918 (2002).
8. Bauman, J., Jearawiriyapaisarn, N. & Kole, R. Therapeutic Potential of Splice-Switching Oligonucleotides. *Oligonucleotides* **19**, 1-13 (2009).
9. Fire, A. et al. Potent and specific genetic interference by double-stranded RNA in Caenorhabditis elegans. *nature* **391**, 806 (1998).
10. Elbashir, S.M., Lendeckel, W. & Tuschl, T. RNA interference is mediated by 21- and 22-nucleotide RNAs. *Genes & development* **15**, 188-200 (2001).
11. Elbashir, S.M. et al. Duplexes of 21-nucleotide RNAs mediate RNA interference in cultured mammalian cells. *Nature* **411**, 494-498 (2001).
12. Salomon, W.E., Jolly, S.M., Moore, M.J., Zamore, P.D. & Serebrov, V. Single-molecule imaging reveals that Argonaute reshapes the binding properties of its nucleic acid guides. *Cell* **162**, 84-95 (2015).
13. Wilson, R.C. & Doudna, J.A. Molecular mechanisms of RNA interference. *Annu Rev Biophys* **42**, 217-239 (2013).
14. Khvorova, A., Reynolds, A. & Jayasena, S.D. Functional siRNAs and miRNAs Exhibit Strand Bias. *Cell* **115**, 209-216 (2003).
15. Song, J.-J., Smith, S.K., Hannon, G.J. & Joshua-Tor, L. Crystal Structure of Argonaute and Its Implications for RISC Slicer Activity. *Science* **305**, 1434-1437 (2004).
16. Liu, J. et al. Argonaute2 is the catalytic engine of mammalian RNAi. *Science* **305**, 1437-1441 (2004).
17. Layzer, J.M. et al. In vivo activity of nuclease-resistant siRNAs. *RNA* **10**, 766-771 (2004).
18. Behlke, M.A. Chemical Modification of siRNAs for In Vivo Use. *Oligonucleotides* **18**, 305-320 (2008).
19. Jensen, S. & Thomsen, A.R. Sensing of RNA Viruses: a Review of Innate Immune Receptors Involved in Recognizing RNA Virus Invasion. *Journal of Virology* **86**, 2900-2910 (2012).

20. Foster, D.J. et al. Advanced siRNA Designs Further Improve In Vivo Performance of GalNAc-siRNA Conjugates. *Molecular Therapy* **26**, 708-717 (2018).

21. Damha, M.J. et al. Properties of arabinonucleic acids (ANA & 20'F-ANA): implications for the design of antisense therapeutics that invoke RNase H cleavage of RNA. *Nucleosides Nucleotides Nucleic Acids* **20**, 429-440 (2001).

22. Zhao, X. et al. Structure variations of TBA G-quadruplex induced by 2'-O-methyl nucleotide in K+ and Ca2+ environments. *Acta Biochim Biophys Sin (Shanghai)* **46**, 837-850 (2014).

23. Schirle, N.T. et al. Structural analysis of human Argonaute-2 bound to a modified siRNA guide. *Journal of the American Chemical Society* **138**, 8694-8697 (2016).

24. Robbins, M. et al. 2'-O-methyl-modified RNAs Act as TLR7 Antagonists. *Molecular Therapy* **15**, 1663-1669 (2007).

25. Judge, A.D., Bola, G., Lee, A.C. & MacLachlan, I. Design of noninflammatory synthetic siRNA mediating potent gene silencing in vivo. *Molecular Therapy* **13**, 494-505 (2006).

26. Eckstein, F. Phosphorothioates, essential components of therapeutic oligonucleotides. *Nucleic acid therapeutics* **24**, 374-387 (2014).

27. Wu, S.Y. et al. 2′-OMe-phosphorodithioate-modified siRNAs show increased loading into the RISC complex and enhanced anti-tumour activity. *Nature Communications* **5**, 3459 (2014).

28. Hall, A.H.S., Wan, J., Shaughnessy, E.E., Ramsay Shaw, B. & Alexander, K.A. RNA interference using boranophosphate siRNAs: structure-activity relationships. *Nucleic acids research* **32**, 5991-6000 (2004).

29. Monia, B.P., Johnston, J.F., Sasmor, H. & Cummins, L.L. Nuclease resistance and antisense activity of modified oligonucleotides targeted to Ha-ras. *The Journal of biological chemistry* **271**, 14533-14540 (1996).

30. Brown, D.A. et al. Effect of phosphorothioate modification of oligodeoxynucleotides on specific protein binding. *The Journal of biological chemistry* **269**, 26801-26805 (1994).

31. Miller, C.M. et al. Stabilin-1 and Stabilin-2 are specific receptors for the cellular internalization of phosphorothioate-modified antisense oligonucleotides (ASOs) in the liver. *Nucleic Acids Res* **44**, 2782-2794 (2016).

32. Bijsterbosch, M.K. et al. In vivo fate of phosphorothioate antisense oligodeoxynucleotides: predominant uptake by scavenger receptors on endothelial liver cells. *Nucleic acids research* **25**, 3290-3296 (1997).

33. Butler, M. et al. Phosphorothioate oligodeoxynucleotides distribute similarly in class A scavenger receptor knockout and wild-type mice. *J Pharmacol Exp Ther* **292**, 489-496 (2000).

34. Benimetskaya, L. et al. Binding of phosphorothioate oligodeoxynucleotides to basic fibroblast growth factor, recombinant soluble CD4, laminin and fibronectin is P-chirality independent. *Nucleic Acids Res* **23**, 4239-4245 (1995).

35. Haraszti, R.A. et al. 5′-Vinylphosphonate improves tissue accumulation and efficacy of conjugated siRNAs in vivo. *Nucleic acids research* **45**, 7581-7592 (2017).

36. Parmar, R. et al. 5′‑(E)‑Vinylphosphonate: A Stable Phosphate Mimic Can Improve the RNAi Activity of siRNA–GalNAc Conjugates. *ChemBioChem* **17**, 985-989 (2016).
37. Hassler, M.R. et al. Comparison of partially and fully chemically-modified siRNA in conjugate-mediated delivery in vivo. *Nucleic Acids Res* **46**, 2185-2196 (2018).
38. Janas, M.M. et al. Selection of GalNAc-conjugated siRNAs with limited off-target-driven rat hepatotoxicity. *Nature Communications* **9**, 723 (2018).
39. Sewing, S. et al. Assessing single-stranded oligonucleotide drug-induced effects in vitro reveals key risk factors for thrombocytopenia. *PLoS One* **12**, e0187574 (2017).
40. Henry, S.P. et al. Assessment of the Effects of 2′-Methoxyethyl Antisense Oligonucleotides on Platelet Count in Cynomolgus Nonhuman Primates. *Nucleic Acid Therapeutics* **27**, 197-208 (2017).
41. Adams, D. et al. Patisiran, an RNAi Therapeutic, for Hereditary Transthyretin Amyloidosis. *New England Journal of Medicine* **379**, 11-21 (2018).
42. Biswas, S. & Torchilin, V.P. Dendrimers for siRNA Delivery. *Pharmaceuticals (Basel, Switzerland)* **6**, 161-183 (2013).
43. Nemati, H. et al. Using siRNA-based spherical nucleic acid nanoparticle conjugates for gene regulation in psoriasis. *Journal of Controlled Release* **268**, 259-268 (2017).
44. Guo, S. et al. Enhanced gene delivery and siRNA silencing by gold nanoparticles coated with charge-reversal polyelectrolyte. *ACS nano* **4**, 5505-5511 (2010).
45. Ding, Y. et al. Gold Nanoparticles for Nucleic Acid Delivery. *Molecular Therapy* **22**, 1075-1083 (2014).
46. Melamed, J.R., Kreuzberger, N.L., Goyal, R. & Day, E.S. Spherical Nucleic Acid Architecture Can Improve the Efficacy of Polycation-Mediated siRNA Delivery. *Molecular Therapy - Nucleic Acids* **12**, 207-219 (2018).
47. Lee, Y.C. et al. Binding of synthetic oligosaccharides to the hepatic Gal/GalNAc lectin. Dependence on fine structural features. *The Journal of biological chemistry* **258**, 199-202 (1983).
48. Willoughby, J.L.S. et al. Evaluation of GalNAc-siRNA Conjugate Activity in Pre-clinical Animal Models with Reduced Asialoglycoprotein Receptor Expression. *Mol Ther* **26**, 105-114 (2018).
49. Huang, Y. Preclinical and Clinical Advances of GalNAc-Decorated Nucleic Acid Therapeutics. *Molecular therapy. Nucleic acids* **6**, 116-132 (2017).
50. Tushir-Singh, J. Antibody-siRNA conjugates: drugging the undruggable for anti-leukemic therapy. *Expert Opin Biol Ther* **17**, 325-338 (2017).
51. Cuellar, T.L. et al. Systematic evaluation of antibody-mediated siRNA delivery using an industrial platform of THIOMAB–siRNA conjugates. *Nucleic acids research* **43**, 1189-1203 (2014).
52. Kruspe, S. & Giangrande, P.H. Aptamer-siRNA Chimeras: Discovery, Progress, and Future Prospects. *Biomedicines* **5** (2017).
53. Sivakumar, P., Kim, S., Kang, H.C. & Shim, M.S. Targeted siRNA delivery using aptamer-siRNA chimeras and aptamer-conjugated nanoparticles. *Wiley Interdiscip Rev Nanomed Nanobiotechnol* **11**, e1543 (2019).

54. McNamara II, J.O. et al. Cell type–specific delivery of siRNAs with aptamer-siRNA chimeras. *Nature biotechnology* **24**, 1005 (2006).

55. Nikan, M. et al. Docosahexaenoic acid conjugation enhances distribution and safety of siRNA upon local administration in mouse brain. *Molecular Therapy-Nucleic Acids* **5** (2016).

56. Nikan, M. et al. Synthesis and Evaluation of Parenchymal Retention and Efficacy of a Metabolically Stable O-Phosphocholine-N-docosahexaenoyl-l-serine siRNA Conjugate in Mouse Brain. *Bioconjugate chemistry* **28**, 1758-1766 (2017).

57. DiFiglia, M. et al. Therapeutic silencing of mutant huntingtin with siRNA attenuates striatal and cortical neuropathology and behavioral deficits. *Proceedings of the National Academy of Sciences* **104**, 17204-17209 (2007).

58. Alterman, J.F. et al. Hydrophobically modified siRNAs silence huntingtin mRNA in primary neurons and mouse brain. *Molecular Therapy-Nucleic Acids* **4** (2015).

59. Byrne, M. et al. Novel hydrophobically modified asymmetric RNAi compounds (sd-rxRNA) demonstrate robust efficacy in the eye. *Journal of Ocular Pharmacology and Therapeutics* **29**, 855-864 (2013).

60. Khan, T. et al. Silencing myostatin using cholesterol-conjugated siRNAs induces muscle growth. *Molecular Therapy-Nucleic Acids* **5** (2016).

61. Duan, L. et al. Target delivery of small interfering RNAs with vitamin E-coupled nanoparticles for treating hepatitis C. *Scientific reports* **6**, 24867-24867 (2016).

62. Nishina, K. et al. Efficient in vivo delivery of siRNA to the liver by conjugation of α-tocopherol. *Molecular Therapy* **16**, 734-740 (2008).

63. Osborn, M.F. et al. Hydrophobicity drives the systemic distribution of lipid-conjugated siRNAs via lipid transport pathways. *Nucleic acids research* **47**, 1070-1081 (2018).

64. Biscans, A. et al. Diverse lipid conjugates for functional extra-hepatic siRNA delivery in vivo. *Nucleic acids research* **47**, 1082-1096 (2018).

65. Osborn, M.F. et al. Efficient Gene Silencing in Brain Tumors with Hydrophobically Modified siRNAs. *Mol Cancer Ther* **17**, 1251-1258 (2018).

66. Finkel, R.S. et al. Nusinersen versus Sham Control in Infantile-Onset Spinal Muscular Atrophy. *The New England journal of medicine* **377**, 1723-1732 (2017).

67. Tabrizi, S. et al. Effects of IONIS-HTTRx in Patients with Early Huntington's Disease, Results of the First HTT-Lowering Drug Trial (CT.002). *Neurology* **90**, CT.002 (2018).

68. Hua, Y. et al. Antisense correction of SMN2 splicing in the CNS rescues necrosis in a type III SMA mouse model. *Genes & development* **24**, 1634-1644 (2010).

69. Hickerson, R.P. et al. Gene Silencing in Skin After Deposition of Self-Delivery siRNA With a Motorized Microneedle Array Device. *Mol Ther Nucleic Acids* **2**, e129 (2013).

70. Hu, Q. et al. Therapeutic application of gene silencing MMP-9 in a middle cerebral artery occlusion-induced focal ischemia rat model. *Experimental Neurology* **216**, 35-46 (2009).

71. Thakker, D.R. et al. siRNA-mediated knockdown of the serotonin transporter in the adult mouse brain. *Molecular Psychiatry* **10**, 782 (2005).

72.   Ferrés-Coy, A. et al. Therapeutic antidepressant potential of a conjugated siRNA silencing the serotonin transporter after intranasal administration. *Molecular Psychiatry* **21**, 328 (2015).

73.   Chen, Q. et al. Lipophilic siRNAs mediate efficient gene silencing in oligodendrocytes with direct CNS delivery. *J Control Release* **144**, 227-232 (2010).

74.   Milstein, S. in RNA Therapeutics (Cold Spring Harbor Laboratories; 2019).

75.   Querbes, W. et al. Direct CNS delivery of siRNA mediates robust silencing in oligodendrocytes. *Oligonucleotides* **19**, 23-29 (2009).

76.   Abbott, N.J., Patabendige, A.A.K., Dolman, D.E.M., Yusof, S.R. & Begley, D.J. Structure and function of the blood–brain barrier. *Neurobiology of Disease* **37**, 13-25 (2010).

77.   Gao, Y. et al. RVG-peptide-linked trimethylated chitosan for delivery of siRNA to the brain. *Biomacromolecules* **15**, 1010-1018 (2014).

78.   Wiley, D.T., Webster, P., Gale, A. & Davis, M.E. Transcytosis and brain uptake of transferrin-containing nanoparticles by tuning avidity to transferrin receptor. *Proceedings of the National Academy of Sciences of the United States of America* **110**, 8662-8667 (2013).

79.   Godinho, B. et al. Transvascular Delivery of Hydrophobically Modified siRNAs: Gene Silencing in the Rat Brain upon Disruption of the Blood-Brain Barrier. *Mol Ther* **26**, 2580-2591 (2018).

80.   Passini, M.A. et al. Antisense oligonucleotides delivered to the mouse CNS ameliorate symptoms of severe spinal muscular atrophy. *Science translational medicine* **3**, 72ra18-72ra18 (2011).

81.   Weiner, G.M. et al. Ommaya reservoir with ventricular catheter placement for chemotherapy with frameless and pinless electromagnetic surgical neuronavigation. *Clin Neurol Neurosurg* **130**, 61-66 (2015).

82.   Dickerman, R.D. & Eisenberg, M.B. Preassembled method for insertion of Ommaya reservoir. *Journal of Surgical Oncology* **89**, 36-38 (2005).

83.   Mangiarini, L. et al. Exon 1 of the HD gene with an expanded CAG repeat is sufficient to cause a progressive neurological phenotype in transgenic mice. *Cell* **87**, 493-506 (1996).

84.   Anderson, E., Boese, Q., Khvorova, A. & Karpilow, J. in RNAi 45-63 (Springer, 2008).

85.   Schwarz, D.S. et al. Asymmetry in the assembly of the RNAi enzyme complex. *Cell* **115**, 199-208 (2003).

86.   Keeler, A.M. et al. Cellular Analysis of Silencing the Huntington's Disease Gene Using AAV9 Mediated Delivery of Artificial Micro RNA into the Striatum of Q140/Q140 Mice. *J Huntingtons Dis* **5**, 239-248 (2016).

87.   DiFiglia, M. et al. Huntingtin is a cytoplasmic protein associated with vesicles in human and rat brain neurons. *Neuron* **14**, 1075-1081 (1995).

88.   Coles, A.H. et al. A high-throughput method for direct detection of therapeutic oligonucleotide-induced gene silencing in vivo. *nucleic acid therapeutics* **26**, 86-92 (2016).

89.   Mullen, R.J., Buck, C.R. & Smith, A.M. NeuN, a neuronal specific nuclear protein in vertebrates. *Development* **116**, 201-211 (1992).

90.   Weyer, A. & Schilling, K. Developmental and cell type‐specific expression of the neuronal marker NeuN in the murine cerebellum. *Journal of neuroscience research* **73**, 400-409 (2003).

91.   Imai, Y., Ibata, I., Ito, D., Ohsawa, K. & Kohsaka, S. A novel geneiba1in the major histocompatibility complex class III region encoding an EF hand protein expressed in a monocytic lineage. *Biochemical and biophysical research communications* **224**, 855-862 (1996).

92.   Garden, G.A. & Möller, T. Microglia biology in health and disease. *Journal of Neuroimmune Pharmacology* **1**, 127-137 (2006).

93.   Shitaka, Y. et al. Repetitive closed-skull traumatic brain injury in mice causes persistent multifocal axonal injury and microglial reactivity. *Journal of Neuropathology & Experimental Neurology* **70**, 551-567 (2011).

94.   Brown, G.C. & Neher, J.J. Inflammatory neurodegeneration and mechanisms of microglial killing of neurons. *Molecular neurobiology* **41**, 242-247 (2010).

95.   Damha, M.J., Giannaris, P.A. & Zabarylo, S.V. An improved procedure for derivatization of controlled-pore glass beads for solid-phase oligonucleotide synthesis. *Nucleic acids research* **18**, 3813-3821 (1990).

96.   Zamore, P.D. RNA interference: listening to the sound of silence. *Nature Structural and Molecular Biology* **8**, 746 (2001).

97.   Castanotto, D. & Rossi, J.J. The promises and pitfalls of RNA-interference-based therapeutics. *Nature* **457**, 426 (2009).

98.   Davidson, B.L. & McCray Jr, P.B. Current prospects for RNA interference-based therapies. *Nature Reviews Genetics* **12**, 329 (2011).

99.   Miller, V.M., Paulson, H.L. & Gonzalez-Alegre, P. RNA interference in neuroscience: progress and challenges. *Cellular and molecular neurobiology* **25**, 1195-1207 (2005).

100.   Sah, D.W. & Aronin, N. Oligonucleotide therapeutic approaches for Huntington disease. *The Journal of clinical investigation* **121**, 500-507 (2011).

101.   Boudreau, R.L. et al. Nonallele-specific silencing of mutant and wild-type huntingtin demonstrates therapeutic efficacy in Huntington's disease mice. *Molecular Therapy* **17**, 1053-1063 (2009).

102.   Ramachandran, P.S., Boudreau, R.L., Schaefer, K.A., La Spada, A.R. & Davidson, B.L. Nonallele specific silencing of ataxin-7 improves disease phenotypes in a mouse model of SCA7. *Molecular Therapy* **22**, 1635-1642 (2014).

103.   Kumar, P. et al. Transvascular delivery of small interfering RNA to the central nervous system. *Nature* **448**, 39 (2007).

104.   Huo, H. et al. Polyion complex micelles composed of pegylated polyasparthydrazide derivatives for siRNA delivery to the brain. *Journal of colloid and interface science* **447**, 8-15 (2015).

105.   Thakker, D.R. et al. Neurochemical and behavioral consequences of widespread gene knockdown in the adult mouse brain by using nonviral RNA interference. *Proceedings of the National Academy of Sciences* **101**, 17270-17275 (2004).

106.   Burgess, A., Huang, Y., Querbes, W., Sah, D.W. & Hynynen, K. Focused ultrasound for targeted delivery of siRNA and efficient knockdown of Htt expression. *Journal of controlled release* **163**, 125-129 (2012).

107. Stiles, D.K. et al. Widespread suppression of huntingtin with convection-enhanced delivery of siRNA. *Experimental neurology* **233**, 463-471 (2012).
108. Dass, C.R. Cytotoxicity issues pertinent to lipoplex‑mediated gene therapy in‑vivo. *Journal of pharmacy and pharmacology* **54**, 593-601 (2002).
109. Karra, D. & Dahm, R. Transfection techniques for neuronal cells. *Journal of Neuroscience* **30**, 6171-6177 (2010).
110. Song, H. & Yang, P.-C. Construction of shRNA lentiviral vector. *North American journal of medical sciences* **2**, 598 (2010).
111. Tomar, R.S., Matta, H. & Chaudhary, P.M. Use of adeno-associated viral vector for delivery of small interfering RNA. *Oncogene* **22**, 5712 (2003).
112. Bell, H., Kimber, W.L., Li, M. & Whittle, I.R. Liposomal transfection efficiency and toxicity on glioma cell lines: in vitro and in vitro studies. *Neuroreport* **9**, 793-798 (1998).
113. Masotti, A. et al. Comparison of different commercially available cationic liposome–DNA lipoplexes: Parameters influencing toxicity and transfection efficiency. *Colloids and Surfaces B: Biointerfaces* **68**, 136-144 (2009).
114. Zou, L. et al. Liposome-mediated NGF gene transfection following neuronal injury: potential therapeutic applications. *Gene Therapy* **6**, 994 (1999).
115. Birmingham, A. et al. A protocol for designing siRNAs with high functionality and specificity. *Nature protocols* **2**, 2068 (2007).
116. Reynolds, A. et al. Rational siRNA design for RNA interference. *Nature biotechnology* **22**, 326 (2004).
117. Geary, R.S., Norris, D., Yu, R. & Bennett, C.F. Pharmacokinetics, biodistribution and cell uptake of antisense oligonucleotides. *Advanced drug delivery reviews* **87**, 46-51 (2015).
118. Khvorova, A., Kamens, J, Samarsky, D, Woolf, T, Cardia, J (2014).
119. Soutschek, J. et al. Therapeutic silencing of an endogenous gene by systemic administration of modified siRNAs. *Nature* **432**, 173 (2004).
120. Dolga, A.M. et al. TNF‑α‑mediates neuroprotection against glutamate‑induced excitotoxicity via NF‑κB‑dependent up‑regulation of KCa2. 2 channels. *Journal of neurochemistry* **107**, 1158-1167 (2008).
121. De Paula, D., Bentley, M.V.L. & Mahato, R.I. Hydrophobization and bioconjugation for enhanced siRNA delivery and targeting. *Rna* **13**, 431-456 (2007).
122. Watts, J.K., Deleavey, G.F. & Damha, M.J. Chemically modified siRNA: tools and applications. *Drug discovery today* **13**, 842-855 (2008).
123. Watts, J.K. & Corey, D.R. Silencing disease genes in the laboratory and the clinic. *The Journal of pathology* **226**, 365-379 (2012).
124. Deleavey, G.F. & Damha, M.J. Designing chemically modified oligonucleotides for targeted gene silencing. *Chemistry & biology* **19**, 937-954 (2012).
125. Li, S.-H. et al. Huntington's disease gene (IT15) is widely expressed in human and rat tissues. *Neuron* **11**, 985-993 (1993).
126. Foster, D.J. et al. Comprehensive evaluation of canonical versus Dicer-substrate siRNA in vitro and in vivo. *Rna* (2012).
127. Marques, J.T. & Williams, B.R. Activation of the mammalian immune system by siRNAs. *Nature biotechnology* **23**, 1399 (2005).

128. Ferrazzano, P. et al. Age-dependent microglial activation in immature brains after hypoxia-ischemia. *CNS & Neurological Disorders-Drug Targets (Formerly Current Drug Targets-CNS & Neurological Disorders)* **12**, 338-349 (2013).

129. Koshinaga, M. et al. Rapid microglial activation induced by traumatic brain injury is independent of blood brain barrier disruption. *Histology and histopathology* **22**, 129-136 (2007).

130. Ouimet, C., Miller, P., Hemmings, H., Walaas, S.I. & Greengard, P. DARPP-32, a dopamine-and adenosine 3': 5'-monophosphate-regulated phosphoprotein enriched in dopamine-innervated brain regions. III. Immunocytochemical localization. *Journal of Neuroscience* **4**, 111-124 (1984).

131. Bartlett, D.W. & Davis, M.E. Insights into the kinetics of siRNA-mediated gene silencing from live-cell and live-animal bioluminescent imaging. *Nucleic acids research* **34**, 322-333 (2006).

132. Carroll, J.B. et al. Potent and selective antisense oligonucleotides targeting single-nucleotide polymorphisms in the Huntington disease gene/allele-specific silencing of mutant huntingtin. *Molecular Therapy* **19**, 2178-2185 (2011).

133. Southwell, A.L. et al. In vivo evaluation of candidate allele-specific mutant huntingtin gene silencing antisense oligonucleotides. *Molecular Therapy* **22**, 2093-2106 (2014).

134. Southwell, A.L. et al. Ultrasensitive measurement of huntingtin protein in cerebrospinal fluid demonstrates increase with Huntington disease stage and decrease following brain huntingtin suppression. *Scientific reports* **5**, 12166 (2015).

135. Alvarez-Erviti, L. et al. Delivery of siRNA to the mouse brain by systemic injection of targeted exosomes. *Nature biotechnology* **29**, 341 (2011).

136. Marcus, M. & Leonard, J. FedExosomes: engineering therapeutic biological nanoparticles that truly deliver. *Pharmaceuticals* **6**, 659-680 (2013).

137. Deleavey, G.F. et al. Synergistic effects between analogs of DNA and RNA improve the potency of siRNA-mediated gene silencing. *Nucleic acids research* **38**, 4547-4557 (2010).

138. Allerson, C.R. et al. Fully 2 '-modified oligonucleotide duplexes with improved in vitro potency and stability compared to unmodified small interfering RNA. *Journal of medicinal chemistry* **48**, 901-904 (2005).

139. Choung, S., Kim, Y.J., Kim, S., Park, H.-O. & Choi, Y.-C. Chemical modification of siRNAs to improve serum stability without loss of efficacy. *Biochemical and biophysical research communications* **342**, 919-927 (2006).

140. Czauderna, F. et al. Structural variations and stabilising modifications of synthetic siRNAs in mammalian cells. *Nucleic acids research* **31**, 2705-2716 (2003).

141. Chen, Q. et al. Lipophilic siRNAs mediate efficient gene silencing in oligodendrocytes with direct CNS delivery. *Journal of Controlled Release* **144**, 227-232 (2010).

142. Wolfrum, C. et al. Mechanisms and optimization of in vivo delivery of lipophilic siRNAs. *Nature biotechnology* **25**, 1149 (2007).

143. Dohmen, C. et al. Defined folate-PEG-siRNA conjugates for receptor-specific gene silencing. *Molecular Therapy-Nucleic Acids* **1** (2012).

144. Nair, J.K. et al. Multivalent N-acetylgalactosamine-conjugated siRNA localizes in hepatocytes and elicits robust RNAi-mediated gene silencing. *Journal of the American Chemical Society* **136**, 16958-16961 (2014).

145. Nair, J.K. et al. Impact of enhanced metabolic stability on pharmacokinetics and pharmacodynamics of GalNAc–siRNA conjugates. *Nucleic acids research* **45**, 10969-10977 (2017).

146. Yu, D. et al. Single-stranded RNAs use RNAi to potently and allele-selectively inhibit mutant huntingtin expression. *Cell* **150**, 895-908 (2012).

147. Lima, W.F. et al. Single-stranded siRNAs activate RNAi in animals. *Cell* **150**, 883-894 (2012).

148. Prakash, T.P. et al. Identification of metabolically stable 5′-phosphate analogs that support single-stranded siRNA activity. *Nucleic acids research* **43**, 2993-3011 (2015).

149. Prakash, T.P. et al. Synergistic effect of phosphorothioate, 5′-vinylphosphonate and GalNAc modifications for enhancing activity of synthetic siRNA. *Bioorganic & medicinal chemistry letters* **26**, 2817-2820 (2016).

150. Matranga, C., Tomari, Y., Shin, C., Bartel, D.P. & Zamore, P.D. Passenger-strand cleavage facilitates assembly of siRNA into Ago2-containing RNAi enzyme complexes. *Cell* **123**, 607-620 (2005).

151. Ly, S. et al. Visualization of self-delivering hydrophobically modified siRNA cellular internalization. *Nucleic acids research* **45**, 15-25 (2016).

152. Godinho, B.M. et al. Pharmacokinetic profiling of conjugated therapeutic oligonucleotides: a high-throughput method based upon serial blood microsampling coupled to peptide nucleic acid hybridization assay. *nucleic acid therapeutics* **27**, 323-334 (2017).

153. Jackson, A.L. et al. Position-specific chemical modification of siRNAs reduces "off-target" transcript silencing. *Rna* **12**, 1197-1205 (2006).

154. Dahlman, J.E. et al. In vivo endothelial siRNA delivery using polymeric nanoparticles with low molecular weight. *Nature nanotechnology* **9**, 648 (2014).

155. Dass, C.R. & Burton, M.A. Modified microplex vector enhances transfection of cells in culture while maintaining tumour‐selective gene delivery in‐vivo. *Journal of pharmacy and pharmacology* **55**, 19-25 (2003).

156. Wee, L.M., Flores-Jasso, C.F., Salomon, W.E. & Zamore, P.D. Argonaute divides its RNA guide into domains with distinct functions and RNA-binding properties. *Cell* **151**, 1055-1067 (2012).

157. Roehl, I., Schuster, M. & Seiffert, S. (Google Patents, 2011).

158. Rozema, D.B. et al. Dynamic PolyConjugates for targeted in vivo delivery of siRNA to hepatocytes. *Proceedings of the National Academy of Sciences* **104**, 12982-12987 (2007).

159. Deleavey, G.F. et al. The 5′ binding MID domain of human Argonaute2 tolerates chemically modified nucleotide analogues. *Nucleic acid therapeutics* **23**, 81-87 (2013).

160. Manoharan, M. et al. Unique Gene‐Silencing and Structural Properties of 2′‐Fluoro‐Modified siRNAs. *Angewandte Chemie International Edition* **50**, 2284-2288 (2011).

161. Schirle, N.T., Sheu-Gruttadauria, J. & MacRae, I.J. Structural basis for microRNA targeting. *Science* **346**, 608-613 (2014).
162. Østergaard, M.E. et al. Efficient Synthesis and Biological Evaluation of 5′-GalNAc Conjugated Antisense Oligonucleotides. *Bioconjugate Chemistry* **26**, 1451-1455 (2015).
163. Rajeev, K.G. et al. Hepatocyte-specific delivery of siRNAs conjugated to novel non-nucleosidic trivalent N-acetylgalactosamine elicits robust gene silencing in vivo. *Chembiochem* **16**, 903-908 (2015).
164. Crooke, S.T., Wang, S., Vickers, T.A., Shen, W. & Liang, X.H. Cellular uptake and trafficking of antisense oligonucleotides. *Nat Biotechnol* **35**, 230-237 (2017).
165. Manoharan, M. in TIDES (https://www.alnylam.com/web/assets/ALNY-ESC-GalNAc-siRNA-TIDES-May2014-Capella.pdf, 2014).
166. Coelho, T. et al. Safety and efficacy of RNAi therapy for transthyretin amyloidosis. *The New England journal of medicine* **369**, 819-829 (2013).
167. Osborn, M.F. & Khvorova, A. Improving Small Interfering RNA Delivery In Vivo Through Lipid Conjugation. *Nucleic Acid Ther* (2018).
168. Fitzgerald, K. et al. A Highly Durable RNAi Therapeutic Inhibitor of PCSK9. *The New England journal of medicine* **376**, 41-51 (2017).
169. Ray, K.K. et al. Inclisiran in Patients at High Cardiovascular Risk with Elevated LDL Cholesterol. *New England Journal of Medicine* **376**, 1430-1440 (2017).
170. Prakash, T.P. et al. Comprehensive Structure-Activity Relationship of Triantennary N-Acetylgalactosamine Conjugated Antisense Oligonucleotides for Targeted Delivery to Hepatocytes. *J Med Chem* **59**, 2718-2733 (2016).
171. Flierl, U. et al. Phosphorothioate backbone modifications of nucleotide-based drugs are potent platelet activators. *J Exp Med* **212**, 129-137 (2015).
172. Behlke, M.A. Progress towards in vivo use of siRNAs. *Mol Ther* **13**, 644-670 (2006).
173. Winkler, J., Stessl, M., Amartey, J. & Noe, C.R. Off-target effects related to the phosphorothioate modification of nucleic acids. *ChemMedChem* **5**, 1344-1352 (2010).
174. Amarzguioui, M., Holen, T., Babaie, E. & Prydz, H. Tolerance for mutations and chemical modifications in a siRNA. *Nucl. Acids Res.* **31**, 589-595 (2003).
175. Harborth, J. et al. Sequence, Chemical, and Structural Variation of Small Interfering RNAs and Short Hairpin RNAs and the Effect on Mammalian Gene Silencing. *Antisense & Nucleic Acid Drug Development* **13**, 83-105 (2003).
176. Liu, C.C., Liu, C.C., Kanekiyo, T., Xu, H. & Bu, G. Apolipoprotein E and Alzheimer disease: risk, mechanisms and therapy. *Nat Rev Neurol* **9**, 106-118 (2013).
177. Mahley, R.W., Weisgraber, K.H. & Huang, Y. Apolipoprotein E4: a causative factor and therapeutic target in neuropathology, including Alzheimer's disease. *Proc Natl Acad Sci U S A* **103**, 5644-5651 (2006).
178. Zetterberg, H., Jacobsson, J., Rosengren, L., Blennow, K. & Andersen, P.M. Association of APOE with age at onset of sporadic amyotrophic lateral sclerosis. *J Neurol Sci* **273**, 67-69 (2008).
179. Didiot, M.C. et al. Nuclear Localization of Huntingtin mRNA Is Specific to Cells of Neuronal Origin. *Cell Rep* **24**, 2553-2560 e2555 (2018).

180. Ito, D. et al. Microglia-specific localisation of a novel calcium binding protein, Iba1. *Molecular Brain Research* **57**, 1-9 (1998).
181. Achuta, V.S. et al. Tissue plasminogen activator contributes to alterations of neuronal migration and activity-dependent responses in fragile X mice. *J Neurosci* **34**, 1916-1923 (2014).
182. Gu, X. et al. N17 Modifies mutant Huntingtin nuclear pathogenesis and severity of disease in HD BAC transgenic mice. *Neuron* **85**, 726-741 (2015).
183. Herndon, E.S. et al. Neuroanatomic profile of polyglutamine immunoreactivity in Huntington disease brains. *J Neuropathol Exp Neurol* **68**, 250-261 (2009).
184. Southwell, A.L. et al. Huntingtin suppression restores cognitive function in a mouse model of Huntington's disease. *Science translational medicine* **10** (2018).
185. Takala, R.S. et al. Glial Fibrillary Acidic Protein and Ubiquitin C-Terminal Hydrolase-L1 as Outcome Predictors in Traumatic Brain Injury. *World Neurosurg* **87**, 8-20 (2016).
186. Taylor, J.P., Brown, R.H., Jr. & Cleveland, D.W. Decoding ALS: from genes to mechanism. *Nature* **539**, 197-206 (2016).
187. De Lahunta, A., Glass, E.N. & Kent, M. Veterinary Neuroanatomy and Clinical Neurology-E-Book. (Elsevier Health Sciences, 2014).
188. Lind, D., Franken, S., Kappler, J., Jankowski, J. & Schilling, K. Characterization of the neuronal marker NeuN as a multiply phosphorylated antigen with discrete subcellular localization. *J Neurosci Res* **79**, 295-302 (2005).
189. Dou, C.L., Li, S. & Lai, E. Dual role of brain factor-1 in regulating growth and patterning of the cerebral hemispheres. *Cereb Cortex* **9**, 543-550 (1999).
190. Birmingham, A. et al. 3' UTR seed matches, but not overall identity, are associated with RNAi off-targets. *Nature methods* **3**, 199-204 (2006).
191. Jeong, S.J. et al. Huntingtin is localized in the nucleus during preimplanatation embryo development in mice. *Int J Dev Neurosci* **24**, 81-85 (2006).
192. Wang, G., Liu, X., Gaertig, M.A., Li, S. & Li, X.J. Ablation of huntingtin in adult neurons is nondeleterious but its depletion in young mice causes acute pancreatitis. *Proc Natl Acad Sci U S A* **113**, 3359-3364 (2016).
193. Zuccato, C., Valenza, M. & Cattaneo, E. Molecular mechanisms and potential therapeutical targets in Huntington's disease. *Physiol Rev* **90**, 905-981 (2010).
194. Evers, M.M. et al. AAV5-miHTT Gene Therapy Demonstrates Broad Distribution and Strong Human Mutant Huntingtin Lowering in a Huntington's Disease Minipig Model. *Molecular Therapy* **26**, 2163-2177 (2018).
195. Pfister, E.L. et al. Artificial miRNAs Reduce Human Mutant Huntingtin Throughout the Striatum in a Transgenic Sheep Model of Huntington's Disease. *Hum Gene Ther* **29**, 663-673 (2018).
196. Grondin, R. et al. Six-month partial suppression of Huntingtin is well tolerated in the adult rhesus striatum. *Brain* **135**, 1197-1209 (2012).
197. Schoch, K.M. & Miller, T.M. Antisense Oligonucleotides: Translation from Mouse Models to Human Neurodegenerative Diseases. *Neuron* **94**, 1056-1070 (2017).
198. Bhagat, L. et al. Novel oligonucleotides containing two 3'-ends complementary to target mRNA show optimal gene-silencing activity. *J Med Chem* **54**, 3027-3036 (2011).

199. Malcolm, D.W., Sorrells, J.E., Van Twisk, D., Thakar, J. & Benoit, D.S. Evaluating side effects of nanoparticle-mediated siRNA delivery to mesenchymal stem cells using next generation sequencing and enrichment analysis. *Bioeng Transl Med* **1**, 193-206 (2016).

200. Pfister, E.L. et al. Five siRNAs targeting three SNPs may provide therapy for three-quarters of Huntington's disease patients. *Current biology : CB* **19**, 774-778 (2009).

201. Knauf, M.J. et al. Relationship of effective molecular size to systemic clearance in rats of recombinant interleukin-2 chemically modified with water-soluble polymers. *The Journal of biological chemistry* **263**, 15064-15070 (1988).

202. Suk, J.S., Xu, Q., Kim, N., Hanes, J. & Ensign, L.M. PEGylation as a strategy for improving nanoparticle-based drug and gene delivery. *Advanced drug delivery reviews* **99**, 28-51 (2016).

203. Fiszer, A., Mykowska, A. & Krzyzosiak, W.J. Inhibition of mutant huntingtin expression by RNA duplex targeting expanded CAG repeats. *Nucleic acids research* **39**, 5578-5585 (2011).

204. Skotte, N.H. et al. Allele-specific suppression of mutant huntingtin using antisense oligonucleotides: providing a therapeutic option for all Huntington disease patients. *PloS one* **9**, e107434-e107434 (2014).

205. Sathasivam, K. et al. Aberrant splicing of HTT generates the pathogenic exon 1 protein in Huntington disease. *Proceedings of the National Academy of Sciences of the United States of America* **110**, 2366-2370 (2013).

206. Maday, S., Twelvetrees, A.E., Moughamian, A.J. & Holzbaur, E.L.F. Axonal transport: cargo-specific mechanisms of motility and regulation. *Neuron* **84**, 292-309 (2014).